

4. SITE 583¹

Shipboard Scientific Party²

HOLE 583

Date occupied: 8 July 1982

Date departed: 10 July 1982

Time on hole: 43 hr., 49 min.

Position (latitude; longitude): 31°50.00'N, 133°51.40'E

Water depth (sea level; corrected m, echo-sounding): 4634

Water depth (rig floor; corrected m, echo-sounding): 4644

Bottom felt (rig floor; m, drill pipe): 4673

Penetration (m): 152

Number of cores: 27

Total length of cored section (m): 152

Total core recovered (m): 83.91

Core recovery (%): 55

Oldest sediment cored:

Depth sub-bottom (m): 149 (Core 26)

Nature: Hemipelagic mud

Age: late to early Quaternary

Measured velocity (km/s): $V_p = 1.42$ (in soupy sand at 126.8 m sub-bottom)

Principal results: See Summary and Conclusions section.

HOLE 583A

Date occupied: 10 July 1982

Date departed: 11 July 1982

Time on hole: 20 hr., 37 min.

Position (latitude; longitude): 31°50.18'N, 133°51.26'E

Water depth (sea level; corrected m, echo-sounding): 4618

Water depth (rig floor; corrected m, echo-sounding): 4628

Bottom felt (rig floor; m, drill pipe): 4632

Penetration (m): 54.0

Number of cores: 11

Total length of cored section (m): 54.0

Total core recovered (m): 47.8

Core recovery (%): 89

Oldest sediment cored:

Depth sub-bottom (m): 54.0

Nature: Hemipelagic mud, graded silts and sands

Age: middle to early Quaternary

Measured velocity (km/s): $V_p = 1.58$ (at 50.6 m sub-bottom)

Principal results: See Summary and Conclusions section.

HOLE 583B

Date occupied: 11 July 1982

Date departed: 12 July 1982

Time on hole: 16 hr., 44 min.

Position (latitude; longitude): 31°49.76'N, 133°51.26'E

Water depth (sea level; corrected m, echo-sounding): 4677

Water depth (rig floor; corrected m, echo-sounding): 4687

Bottom felt (rig floor; m, drill pipe): 4759

Penetration (m): 30.0

Number of cores: 6

Total length of cored section (m): 28.0

Total core recovered (m): 24.69

Core recovery (%): 88

Oldest sediment cored:

Depth sub-bottom (m): 25.0

Nature: Hemipelagic mud, inclined graded beds

Age: late Quaternary

Measured velocity (km/s): $V_p = 1.64$ (at 20 m sub-bottom)

Principal results: See Summary and Conclusions section.

¹ Kagami, H., Karig, D. E., Coulbourn, W. T., et al., *Init. Repts. DSDP*, 87: Washington (U.S. Govt. Printing Office).

² LEG 87A: Hideo Kagami (Co-Chief Scientist), Ocean Research Institute, University of Tokyo, 1-15-1 Minamidai, Nakano, Tokyo 164, Japan; Daniel E. Karig (Co-Chief Scientist), Department of Geological Sciences, Cornell University, Ithaca, New York 14853; William T. Coulbourn (Science Representative), Deep Sea Drilling Project, Scripps Institution of Oceanography, University of California at San Diego, La Jolla, California 92093 (present address: Hawaii Institute of Geophysics, University of Hawaii, 2525 Correa Road, Honolulu, Hawaii 96822); Cynthia J. Bray, Department of Geological Sciences, Cornell University, Ithaca, New York 14853; Jacques Charvet, Sciences de la Terre, ERA 601, Université d'Orléans, 45046 Orléans, France; Hajimu Kinoshita, Department of Earth Science, Faculty of Science, Chiba University, Chiba 280, Japan; Martin Lagoe, ARCO Exploration Company, Denver, Colorado 80217 (present address: Department of Geologic Science, University of Texas at Austin, Austin, Texas 78712); Thomas H. Lang, Department of Geology, Florida State University, Tallahassee, Florida 32306; Gail A. Lombardi, Graduate School of Oceanography, University of Rhode Island, Kingston, Rhode Island 02881; Neil Lundberg, Earth Sciences Board, University of California, Santa Cruz, Santa Cruz, California 95064 (present address: Department of Geological and Geophysical Sciences, Princeton University, Princeton, New Jersey 08544); Tsutomu Machihara, Technology Research Center, Japan National Oil Corporation, 3-5-5 Midorigaoka, Hamura-cho, Nishitama-gun, Tokyo 190-11, Japan; Prasanta K. Mukhopadhyay, Institut für Erdöl und Organische Geochemie (ICH-5), P.O. Box 1913, Kernforschungsanlage Jülich GmbH, D-5170 Jülich 1, Federal Republic of Germany; Alec J. Smith, Department of Geology, Bedford College, University of London, London NW1 4NS, United Kingdom; Carol L. Stein, Earth Sciences, Division 6331, Sandia National Laboratories, Albuquerque, New Mexico 87185; and Asahiko Taira, Department of Geology, Kochi University, Kochi 780, Japan (present address: Ocean Research Institute, University of Tokyo, 1-15-1 Minamidai, Nakano, Tokyo 164, Japan).

LEG 87B: Hideo Kagami (Co-Chief Scientist), Ocean Research Institute, University of Tokyo, 1-15-1 Minamidai, Nakano, Tokyo 164, Japan; Daniel E. Karig (Co-Chief Scientist), Department of Geological Sciences, Cornell University, Ithaca, New York 14853; William T. Coulbourn (Science Representative), Deep Sea Drilling Project, Scripps Institution of Oceanography, University of California at San Diego, La Jolla, California 92093 (present address: Hawaii Institute of Geophysics, University of Hawaii, 2525 Correa Road, Honolulu, Hawaii 96822); Fumio Akiba, Japan Petroleum Exploration Co., Ltd., 3-5-5 Midorigaoka, Hamura-cho Nishitama-gun, Tokyo 190-11, Japan; Cynthia J. Bray, Department of Geological Sciences, Cornell University, Ithaca, New York 14853; Jean-Paul Cadet, Sciences de la Terre, ERA 601, Université d'Orléans, 45046 Orléans, France; Jacques Charvet, Sciences de la Terre, Université d'Orléans, 45046 Orléans, France; Kantaro Fujioka, Ocean Research Institute, University of Tokyo, 1-15-1 Minamidai, Nakano, Tokyo 164, Japan; Martin Lagoe, ARCO Exploration Company, Denver, Colorado 80217 (present address: Department of Geologic Science, University of Texas at Austin, Austin, Texas 78712); Thomas H. Lang, Department of Geology, Florida State University, Tallahassee, Florida 32306; Jeremy K. Leggett, Department of Geology, Imperial College of Science and Technology, London SW7 2BP, United Kingdom; Gail A. Lombardi, Graduate School of Oceanography, University of Rhode Island, Kingston, Rhode Island, 02881; Ryo Matsumoto, Geological Institute, University of Tokyo, Hongo, Bunkyo-ku, Tokyo 113, Japan; Nobuaki Niitsuma, Institute of Geosciences, Shizuoka University, 836 Oya, Shizuoka 422, Japan; and Carol L. Stein, Earth Sciences, Division 6331, Sandia National Laboratories, Albuquerque, New Mexico 87185.

HOLE 583C

Date occupied: 12 July 1982
Date departed: 12 July 1982
Time on hole: 20 hr., 8 min.
Position (latitude; longitude): 31°49.80'N, 133°51.26'E
Water depth (sea level; corrected m, echo-sounding): 4677
Water depth (rig floor; corrected m, echo-sounding): 4687
Bottom felt (rig floor; m, drill pipe): 4759
Penetration (m): 49.0
Number of cores: 5
Total length of cored section (m): 24
Total core recovered (m): 17.87
Core recovery (%): 74
Oldest sediment cored:
 Depth sub-bottom (m): 49.0
 Nature: Hemipelagic mud, graded silts and sands on inclined bedding planes
 Age: late Quaternary
 Measured velocity (km/s): $V_p = 1.60$ (at 25 m sub-bottom)
Principal results: See Summary and Conclusions section.

HOLE 583D

Date occupied: 13 July 1982
Date departed: 16 July 1982
Time on hole: 92 hr., 33 min.
Position (latitude; longitude): 31°49.76'N, 133°51.54'E
Water depth (sea level; corrected m, echo-sounding): 4676
Water depth (rig floor; corrected m, echo-sounding): 4686
Bottom felt (rig floor; m, drill pipe): 4759
Penetration (m): 326.6
Number of cores: 29
Total length of cored section (m): 279.8
Total core recovered (m): 69.7
Core recovery (%): 25
Oldest sediment cored:
 Depth sub-bottom (m): 326.6
 Nature: Firm, bioturbated, biosiliceous, hemipelagic mud
 Age: middle Quaternary
 Measured velocity (km/s): $V_p = 1.62$ km/s (at 218 m sub-bottom) (583D-29-2, 20-25 cm)
Principal results: See Summary and Conclusions section.

HOLE 583E

Date occupied: 16 July 1982
Date departed: 18 July 1982
Time on hole: 27 hr., 5 min.
Position (latitude; longitude): 31°50.10'N, 133°51.30'E
Water depth (sea level; corrected m, echo-sounding): 4629
Water depth (rig floor; corrected m, echo-sounding): 4639
Bottom felt (rig floor; m, drill pipe): 4665
Penetration (m): 198.7
Number of cores: 5
Total length of cored section (m): 48.3

Total core recovered (m): 0.99
Core recovery (%): 2
Oldest sediment cored:
 Depth sub-bottom (m): 198.7
 Nature: Hemipelagic mud
 Age: late to early Quaternary(?)
Principal results: See Summary and Conclusions section.

HOLE 583F

Date occupied: 18 July 1982
Date departed: 23 July 1982
Time on hole: 128 hr., 4 min.
Position (latitude; longitude): 31°50.10'N, 133°51.30'E
Water depth (sea level; corrected m, echo-sounding): 4629
Water depth (rig floor; corrected m, echo-sounding): 4639
Bottom felt (rig floor; m, drill pipe): 4665
Penetration (m): 439.7
Number of cores: 30
Total length of cored section (m): 289.3
Total core recovered (m): 46.7
Core recovery (%): 16
Oldest sediment cored:
 Depth sub-bottom (m): 439.7
 Nature: Firm hemipelagic mud
 Age: early Quaternary
 Measured velocity (km/s): $V_p = 1.60$ km/s (at 421 m sub-bottom)
Principal results: See Summary and Conclusions section.

HOLE 583G

Date occupied: 28 July 1982
Date departed: 31 July 1982
Time on hole: 70 hr., 42 min.
Position (latitude; longitude): 31°50.07'N, 133°51.40'E
Water depth (sea level; corrected m, echo-sounding): 4627
Water depth (rig floor; corrected m, echo-sounding): 4637
Bottom felt (rig floor; m, drill pipe): 4663
Penetration (m): 450.7
Number of cores: 15
Total length of cored section (m): 143.4
Total core recovered (m): 62.11
Core recovery (%): 43
Oldest sediment cored:
 Depth sub-bottom (m): 450.0
 Nature: Hemipelagic mud
 Age: Quaternary
 Measured velocity (km/s): $V_p = 1.71$ (at 443 m sub-bottom)
Principal results: See Summary and Conclusions section.

BACKGROUND AND OBJECTIVES

The general background for drilling at Site 583 is broadly covered in the Background and Objectives section in the site chapter for Site 582 (this volume), because the two sites were intended to provide comparisons of structural, physical, and mechanical properties of sediments before and after the influence of subduc-

tion-related deformation. Site 583 was located on the first structural step, physiographically the deepest terrace on the inner trench slope. Site 298 was drilled on this same terrace, approximately 15 km westward, but was located further arcward, in an area where the acoustic coherence is sufficiently degraded so that no reliable seismic correlation with undeformed trench strata could be made (Ingle, Karig, et al., 1975). Moreover, Site 298 was only spot cored and did not focus on the main thrust-fold structure bounding the terrace, as was the intention at Site 583.

Two holes were planned at Site 583: a shallower safety hole and a deeper hole to address the primary scientific objectives. The initial, shallower hole was intended to probe the possibility that hydrocarbons, migrating upward from zones of greater organic maturation, might be trapped beneath the targeted thrust fault. This hole was to penetrate the thrust at a sub-bottom depth less than 300 m, presumably in a zone where gaseous hydrocarbons would be in the form of solid hydrate. If conditions in this safety hole proved favorable, a deep hole was planned to penetrate the fault near 600 m and possibly to continue to a depth near 1000 m. The logic was that, at this greater depth of fault intersection, the greater degree of lithification would result in a higher and better quality of core recovery. After the drilling of the deeper hole, we planned a logging survey to complement the lithologies observed in cores, to reveal differences between laboratory (or shipboard) and *in situ* physical properties, and to compare both the lithologic and physical properties between Sites 582 and 583.

Although the primary objective at Site 583 was to examine the mechanics of subduction-accretion processes, as explained more fully in the site chapter for Site 582 (this volume), several objectives were more specific to Site 583. In particular, holes at this site might provide information concerning the nature of sedimentation on the lower trench slope and determine the stratigraphic and structural nature of the contact, or transition, from trench to slope strata. We also hoped to date that transition in order to further define the structural evolution of the base of the inner slope and to aid in the calculations of subduction rate and distribution of deformation.

OPERATIONS

The *Glomar Challenger* steamed from Site 582 on a course of 158° at 1825Z, 7 July 1982. Underway profiling gear was streamed at 1842Z en route to Site 583. At 1901Z we changed course to 308° and passed over the beacon of Site 582. Holding steady along seismic line N55-3-1, we profiled the slope near shot point (SP) 1795 at the landward side of the Nankai Trough. Coming upslope, we changed course to 136° and arrived at the beacon of Site 582 at 2138Z. By that time we knew the area well and returned on a course of 311° to approach the proposed site, finally dropping a beacon on the bottom of the slope at 2217Z on 7 July (Fig. 1). Our preliminary site survey indicated that the reference seismic line was offset 0.3 mi. to the west and 0.6 mi. to the south of track of the *Challenger*, causing some difficulty in positioning of the site (Fig. 2A). Because of the resulting mislocation of the site, we requested the safety panel to

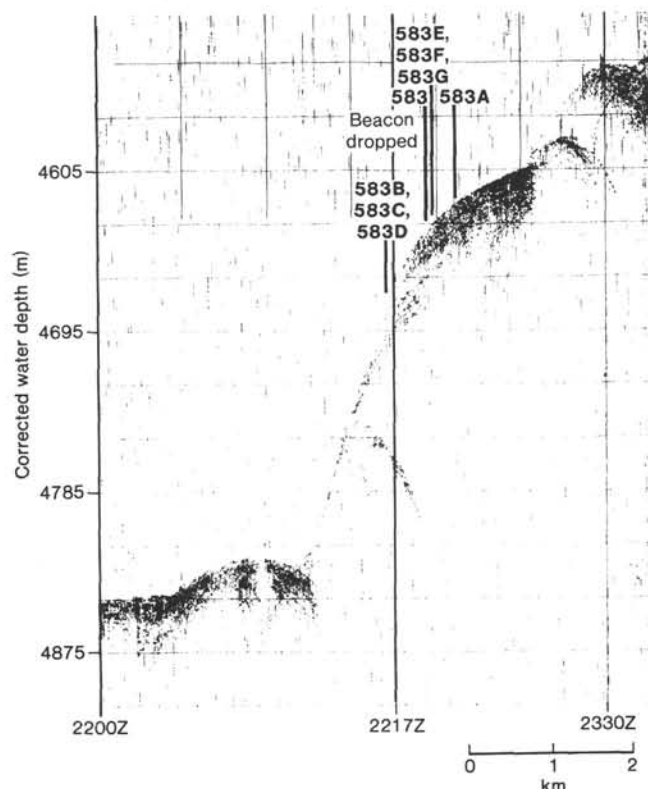


Figure 1. *Glomar Challenger* 3.5-kHz profile showing the location of Site 583.

allow movement of the proposed site to a location 250 m upslope.

While awaiting a response to our request, we offset the ship 400 m to the north-northwest, to an upslope position where a 3.5-kHz reflector indicated safer conditions for the bottom-hole assembly (BHA). The final position is 31°50'N, 133°51.4'E (Fig. 2B). Drill pipe run-in began at 2330Z with the 9.5-m hydraulic piston corer (HPC), and the first mudline core penetrated the bottom at 1231Z on 8 July (Table 1). The drill string depth was 4663 m, in contrast to a corrected precision depth recorder (PDR) depth of 4634 m. The 29 m difference is probably the result of our recording a side-echo produced from the steep slope as representative of true seafloor.

By 1225Z on 9 July, the HPC had reached 102 m sub-bottom (Core 15) and recovery was very low. The core catchers may have been held open by sand sticking in them. The recovery ratio continued to decrease, even though the 5-m-long HPC was used, beginning with Core 14. Heat flow measurements were not very successful; four measurements out of the eight attempts recorded mudline temperatures. At 0520Z on 10 July, the final core (Core 27) was retrieved from the "refusal" depth of 152 m and contained only a trace of muddy sand. Hole 583 was filled with heavy mud.

Hole 583A

After the pipe was pulled four stands above the mudline at Hole 583, the *Glomar Challenger* moved to the north-northwest and at 0745Z to 0815Z on 10 July, off-

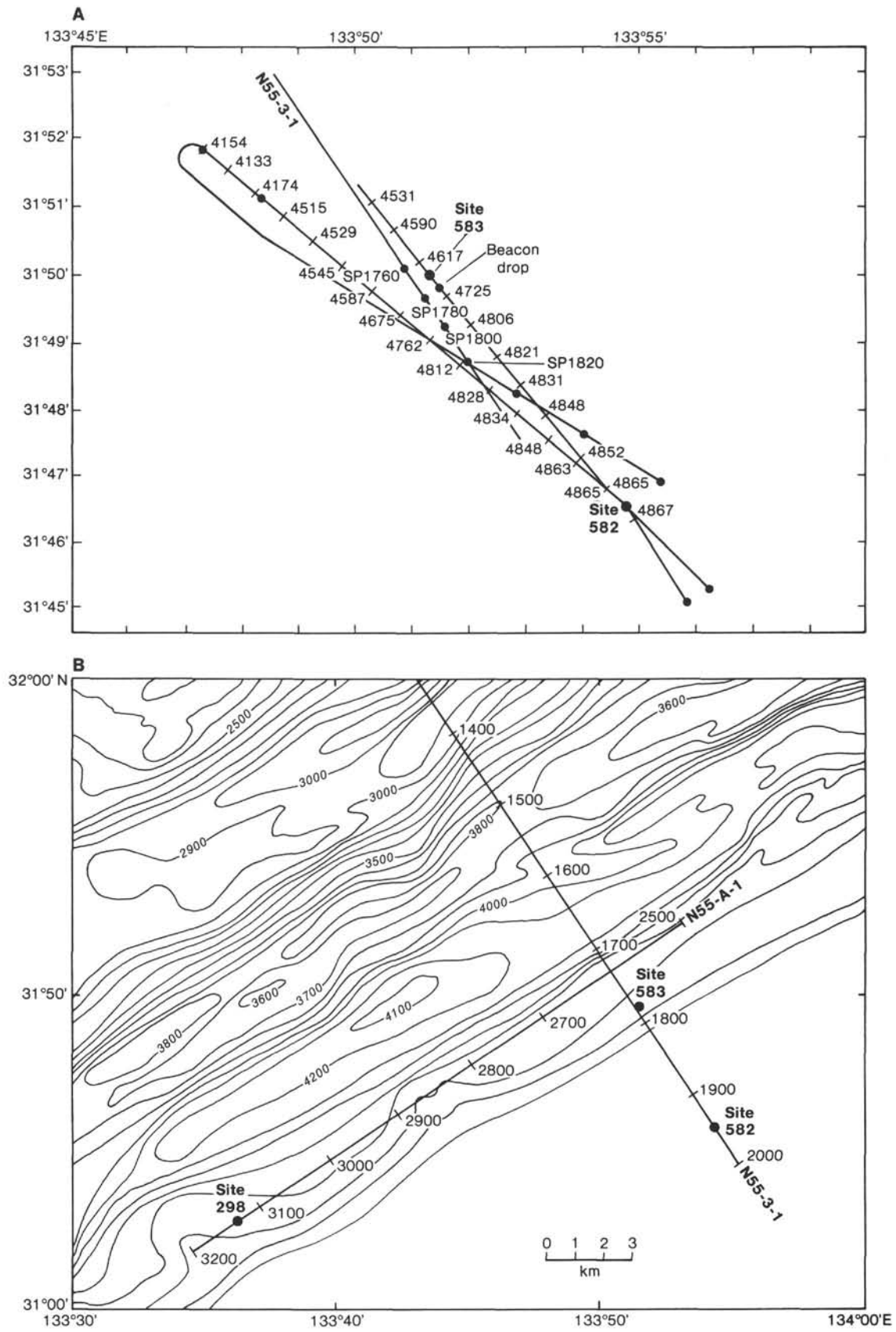


Figure 2. A. Ship's survey track showing approach to Site 583. Depths are water depths in m, SP is shot point. B. Map showing location of seismic Profiles N55-3-1 and N55-A-1 and Sites 582, 583, and 298 with respect to bathymetric features of the Nankai Trough. Numbers along profiles (1400-3200) are shot points.

Table 1. Coring Summary, Site 583.

Core	Date (1982)	Time (L) ^a	Depth from drill floor (m)	Depth below seafloor (m)	Length cored (m)	Length recovered (m)	Percent recovered
Hole 583							
1	7/8	2200	4673.0-4678.5	0-5.5	5.5	1.41	26
2	7/8	2340	4678.5-4688.0	5.5-15.0	9.5	10.06	106
3	7/9	0046	4688.0-4696.0	15.0-23.0	8.0	7.94	99
4	7/9	0605	4696.0-4705.5	23.0-32.5	9.5	9.50	100
5	7/9	0755	4705.5-4713.9	32.5-40.9	8.4	8.45	101
6	7/9	0920	4713.9-4718.9	40.9-45.9	5.0	0.30	6
7	7/9	1025	4718.9-4728.4	45.9-55.4	9.5	9.7	103
8	7/9	1145	4728.4-4735.5	55.4-62.5	7.1	7.30	102
9	7/9	1310	4735.5-4740.5	62.5-67.5	5.0	1.56	31
10	7/9	1423	4740.5-4746.5	67.5-73.5	6.0	4.09	68
11	7/9	1540	4746.5-4750.5	73.5-77.5	4.0	3.69	92
12	7/9	1650	4750.5-4760.0	77.5-87.0	9.5	0.15	2
13	7/9	1828	4760.0-4765.0	87.0-92.0	5.0	1.79	36
14	7/9	1945	4765.0-4770.0	92.0-97.0	5.0	1.51	30
15	7/9	2125	4770.0-4775.0	97.0-102.0	5.0	0.01	—
16	7/9	2240	4775.0-4780.0	102.0-107.0	5.0	0.0	0
17	7/10	0000	4780.0-4785.0	107.0-112.0	5.0	4.57	91
18	7/10	0135	4785.0-4790.0	112.0-117.0	5.0	0	0
19	7/10	0255	4790.0-4795.0	117.0-122.0	5.0	2.46	49
20	7/10	0425	4795.0-4799.0	122.0-126.0	4.0	2.82	71
21	7/10	0547	4799.0-4803.0	126.0-130.0	4.0	0.95	24
22	7/10	0725	4803.0-4808.0	130.0-135.0	5.0	0	0
23	7/10	0850	4808.0-4812.0	135.0-139.0	4.0	4.99	125
24	7/10	1010	4812.0-4816.0	139.0-143.0	4.0	Trace	—
25	7/10	1145	4816.0-4821.0	143.0-148.0	5.0	0.59	12
26	7/10	1245	4821.0-4823.0	148.0-150.0	2.0	0.52	26
27	7/10	1420	4823.0-4825.0	150.0-152.0	2.0	Trace	—
					152.0	83.91	55
Hole 583A							
1	7/10	1953	4632.0-4636.0	0-4.0	4.0	3.87	97
2	7/10	2116	4636.0-4641.0	4.0-9.0	5.0	4.89	98
3	7/10	2230	4641.0-4646.0	9.0-14.0	5.0	4.89	98
4	7/11	0010	4646.0-4651.0	14.0-19.0	5.0	4.81	96
5	7/11	0135	4651.0-4656.0	19.0-24.0	5.0	4.73	95
6	7/11	0310	4656.0-4661.0	24.0-29.0	5.0	4.32	86
7	7/11	0445	4661.0-4666.0	29.0-34.0	5.0	2.38	48
8	7/11	0615	4666.0-4671.0	34.0-39.0	5.0	5.07	101
9	7/11	0740	4671.0-4676.0	39.0-44.0	5.0	4.43	89
10	7/11	0905	4676.0-4681.0	44.0-49.0	5.0	4.62	92
11	7/11	1030	4681.0-4686.0	49.0-54.0	5.0	3.79	76
					54.0	47.8	89
Hole 583B							
1	7/11	2128	4758.7-4763.7	0-5.0	5.0	4.99	100
2	7/11	2240	4763.7-4768.7	5.0-10.0	5.0	5.20	104
3	7/11	2355	4768.7-4773.7	10.0-15.0	5.0	4.33	87
4	7/12	0150	4773.7-4778.7	15.0-20.0	5.0	5.07	101
5	7/12	0300	4778.7-4783.7	20.0-25.0	5.0	5.10	102
6	7/12	0500	4783.7-4786.7	25.0-28.0	3.0	0	0
					28.0	24.69	88
Hole 583C							
1	7/12	0925	4783.7-4788.7	25.0-30.0	5.0	0.25	5
2	7/12	1102	4788.7-4793.7	30.0-35.0	5.0	5.24	105
3	7/12	1240	4793.7-4798.7	35.0-40.0	5.0	5.17	103
4	7/12	1400	4798.7-4803.7	40.0-45.0	5.0	3.36	67
5	7/12	1540	4803.7-4807.7	45.0-49.0	4.0	3.85	96
					24.0	17.87	74
Hole 583D							
H1			4759.0-4805.8	0-46.8	Drilled		
1	7/13	2210	4805.8-4815.4	46.8-56.4	9.6	0.10	1
2	7/14	0015	4815.4-4825.0	56.4-66.0	9.6	0.01	—
3	7/14	0200	4825.0-4834.6	66.0-75.6	9.6	1.19	12
4	7/14	0610	4834.6-4844.3	75.6-85.3	9.7	1.08	11
5	7/14	0755	4844.3-4854.0	85.3-95.0	9.7	1.03	11
6	7/14	0945	4854.0-4863.7	95.0-104.7	9.7	3.98	41
7	7/14	1125	4863.7-4873.2	104.7-114.2	9.5	1.39	15
8	7/14	1330	4873.2-4882.7	114.2-123.7	9.5	1.60	17
9	7/14	1725	4882.7-4892.2	123.7-133.2	9.5	3.82	40
10	7/14	1915	4892.2-4901.9	133.2-142.9	9.7	1.08	11
11	7/14	2050	4901.9-4911.6	142.9-152.6	9.7	1.95	20
12	7/14	2240	4911.6-4921.3	152.6-162.3	9.7	3.78	39
13	7/15	0035	4921.3-4931.0	162.3-172.0	9.7	2.09	22
14	7/15	0505	4931.0-4940.7	172.0-181.7	9.7	4.93	51
15	7/15	0730	4940.7-4950.4	181.7-191.4	9.7	3.39	35
16	7/15	0925	4950.4-4960.0	191.4-201.0	9.6	4.74	49
17	7/15	1110	4960.0-4969.6	201.0-210.6	9.6	2.33	24
18	7/15	1315	4969.6-4979.2	210.6-220.2	9.6	0.39	4
19	7/15	1710	4979.2-4988.9	220.2-229.9	9.7	3.56	37
20	7/15	1930	4988.9-4998.6	229.9-239.6	9.7	0.92	9
21	7/15	2128	4998.6-5008.3	239.6-249.3	9.7	0.11	1
22	7/15	2325	5008.3-5018.0	249.3-259.0	9.7	8.10	84
23	7/16	0110	5018.0-5027.7	259.0-268.7	9.7	2.22	23
24	7/16	0330	5027.7-5037.4	268.7-278.4	9.7	8.40	87
25	7/16	0700	5037.4-5047.0	278.4-288.0	9.6	2.57	27
26	7/16	0850	5047.0-5056.6	288.0-297.6	9.6	0.02	—

Table 1. (Continued).

Core	Date (1982)	Time (L) ^a	Depth from drill floor (m)	Depth below seafloor (m)	Length cored (m)	Length recovered (m)	Percent recovered
Hole 583D (Cont.)							
27	7/16	1040	5056.6-5066.2	297.6-307.2	9.6	0	0
28	7/16	1224	5066.2-5076.9	307.2-316.9	9.7	0.44	5
29	7/16	1450	5076.9-5085.6	316.9-326.6	9.7	4.50	46
					279.8	69.7	25
Hole 583E							
H1	7/17	0635	4665.0-4815.4	0-150.4	Drilled	9.12	—
1	7/17	0840	4815.4-4825.0	150.4-160.0	9.6	0.44	5
2	7/17	1038	4825.0-4834.6	160.0-169.6	9.6	0	0
3	7/17	1225	4834.6-4844.3	169.6-179.3	9.7	0	0
4	7/17	1423	4844.3-4854.0	179.3-189.0	9.7	0	0
5	7/18	0045	4854.0-4863.7	189.0-198.7	9.7	0.55	6
					48.3	0.99	2
Hole 583F							
H1	7/18	1750	4665.0-4815.4	0-150.44	Drilled	—	—
1	7/18	1947	4815.4-4825.0	150.4-160.0	9.6	0	0
2	7/18	2230	4825.0-4834.6	160.0-169.6	9.6	0.01	0
3	7/19	0130	4834.6-4844.3	169.6-179.3	9.7	0.03	0
4	7/19	0315	4844.3-4854.0	179.3-189.0	9.7	Trace	0
5	7/19	0455	4854.0-4863.7	189.0-198.7	9.7	0	0
6	7/19	0635	4863.7-4873.2	198.7-208.2	9.5	2.99	31
7	7/19	0842	4873.2-4882.7	208.2-217.7	9.5	0.24	3
8	7/19	1250	4882.7-4892.2	217.7-227.2	9.5	0.51	5
9	7/19	1424	4892.2-4901.9	227.2-236.9	9.7	Trace	0
10	7/19	1612	4901.9-4911.6	236.9-246.6	9.7	0	0
11	7/19	1755	4911.6-4921.3	246.6-256.3	9.7	1.15	12
12	7/19	2013	4921.3-4931.0	256.3-266.0	9.7	3.52	36
13	7/20	0017	4931.0-4940.7	266.0-275.7	9.7	0.69	7
14	7/20	0215	4940.7-4950.4	275.7-285.4	9.7	2.81	29
15	7/20	0415	4950.4-4960.0	285.4-295.0	9.6	1.05	11
16	7/20	0555	4960.0-4969.6	295.0-304.6	9.6	1.99	21
17	7/20	0805	4969.6-4979.2	304.6-314.2	9.6	2.50	26
18	7/20	1030	4979.2-4988.9	314.2-323.9	9.7	4.21	43
19	7/20	1417	4988.9-4998.6	323.9-333.6	9.7	1.18	12
20	7/20	1619	4998.6-5008.3	333.6-343.3	9.7	2.66	27
21	7/20	1816	5008.3-5017.9	343.3-352.9	9.6	0.13	1
22	7/20	2005	5017.9-5027.5	352.9-362.5	9.6	2.23	23
23	7/20	2154	5027.5-5037.1	362.5-372.1	9.6	0.13	1
24	7/20	2359	5037.1-5046.8	372.1-381.8	9.7	6.56	68
25	7/21	0230	5046.8-5056.5	381.8-391.5	9.7	1.85	19
26	7/21	0430	5056.5-5066.2	391.5-401.2	9.7	4.89	50
27	7/21	0630	5066.2-5075.8	401.2-410.8	9.6	2.20	23
28	7/21	0847	5075.8-5085.4	410.8-420.4	9.6	0.82	9
29	7/21	1105	5085.4-5095.0	420.4-430.0	9.6	2.33	24
30	7/21	1315	5095.0-5104.7	430.0-439.7	9.7	Trace	—
					289.3	46.7	16
Hole 583G							
H1	7/29	0240	4663.0-4863.7	0-200.7			
H2	7/29	0500	4863.7-4892.2	200.7-229.2		0.71	
H3	7/29	0710	4892.2-4921.3	229.2-258.0		7.79	
H4	7/29	0938	4921.3-4950.4	258.0-287.4		4.76	
H5	7/29	1200	4950.4-4969.6	287.4-306.6		6.22	
1	7/29	1415	4969.6-4979.2	306.6-316.2	9.6	4.50	47
2	7/29	1650	4979.2-4988.9	316.2-325.9	9.7	5.75	59
3	7/29	2135	4988.9-4998.6	325.9-335.6	9.7	4.90	50
4	7/29	2340	4998.6-5008.3	335.6-345.3	9.7	7.00	72
5	7/30	0155	5008.3-5018.0	345.3-355.0	9.7	3.59	37
6	7/30	0445	5018.0-5027.7	355.0-364.7	9.7	5.76	59
7	7/30	0645	5027.7-5037.4	364.7-374.4	9.7	6.43	66
8	7/30	0850	5037.4-5047.1	374.4-384.1	9.7	4.88	50
9	7/30	1055	5047.1-5056.8	384.1-393.8	9.7	1.54	16
10	7/30	1330	5056.8-5066.5	393.8-403.5	9.7	6.41	66
11	7/30	1530	5066.5-5076.1	403.5-413.1	9.6	3.25	34
12	7/30	1840	5076.1-5085.7	413.1-422.7	9.6	1.41	15
13	7/30	2025	5085.7-50				

the top of the first core indicates that it is a mudline sample.

By 0130Z, 11 July, the final core (Core 11) was retrieved from a sub-bottom depth of 54 m. The thick sandy turbidite within that core probably corresponds to Core 3 of Hole 583, suggesting that we achieved at least our first objective. All six attempts to use the von Herzen heat probe in this hole were successful. After Core 11 was retrieved, results from the von Herzen probe and the Uyeda-Barnes probe were compared. For the first time during Leg 87, the pore-water sampler had correctly functioned and had obtained a high-pressure sample from a depth of 54 m. After filling Hole 583A with heavy mud, we moved on to a third HPC hole.

Hole 583B

Pulling the pipe just above the mudline, the *Glomar Challenger* moved to the south-southeast across the Site 583 beacon and offset 75 m downslope from it. The hole was originally designated to detect any hydrocarbons trapped at this structurally complex place. Upon receiving a telegram from the JOIDES Safety Panel stating their unwillingness to approve any departure from their original recommendation regarding Hole 583B, we moved to a position corresponding to SP 1795 on the Ocean Research Institute (ORI) seismic reflection Profile N55-3-1 (Fig. 39).

On the 12-kHz PDR record, bottom reflectors occur at 4677 and 4756 m (corrected depth). An attempt was made to feel the bottom at 4677 m; however, only water cores were retrieved. The mudline core finally penetrated the bottom at 1115Z, 11 July. This first core established the mudline depth and indicated a drill string length of 4749 m. After recomputation we realized that our position was at SP 1799.5 not at SP 1795, as originally planned.

Continuous 5-m stroke-coring was attempted with the HPC sampler. On several occasions, cores contained intervals of flow-in separated by intervals of normal-looking sediment. These gross layerings of the core might indicate heave of the ship caused by rougher sea conditions during the day of 11 July, when winds gusted up to 35 knots during the passage of a frontal system over the site. Perhaps as a result of the ship's heave, the core was intermittently stretched with the loss of equivalent amount of sediment from the bottom of the cored interval. It is also possible that most of the cores did not achieve full stroke, probably contributing to flow-in disturbance. The frequency of flow-in was low, however, and core recovery was perfect for the first five cores. From Core 2 downward, bedding planes dipped as much as 45°, and the drift of the hole was about 5°.

By 2000Z, 11 July, Core 6 was retrieved, and a failed connection at the bottom of shaft of HPC assembly was found. An HPC core barrel and von Herzen heat-flow unit were left in the hole. The loss may have been a result of peculiarities in the rocks at the hole, because later we took an indurated carbonate rock from the same horizon at Hole 583C.

Hole 583C

Hole 583C spudded in at the same place as Hole 583B, at a water depth of 4748.7 m at 2250Z on 11 July. After washing down to 25 m sub-bottom, the first core was retrieved from the same interval as Core 583B-6, between 25 and 30 m sub-bottom. That core contains carbonate nodules, perhaps the same lithology that refused continuous coring in Hole 583B.

After continuous coring with fairly good recovery, we retrieved Core 4 from 45 m sub-bottom. Orientations of inclined bedding planes measured in this hole, like those of Hole 583B, are consistent within each core, but inconsistent between consecutive cores, suggesting rotation of drilling pipe after recording orientation, misfire of the directional camera, or misinterpretation or lack of recognition of the information at hand. A hole angle of 3.5° was measured. The hole was terminated at 0640Z, 12 July at a depth of 49 m, in preparation for rotary drilling at the same location. Retrieval and securing of the drill string were completed on deck at 1647Z, 12 July.

Hole 583D

Hole 583D spudded in at the same place as Hole 583C at a water depth of 4749 m at 0552Z, 13 July. During the pipe trip, an inner barrel apparently did not latch, causing the barrel to float. After washing down to 46.8 m sub-bottom and recovering a wash core containing a handful of calcareous pebbles and a piece of wood, we sent down the heat-flow-pore-water-pressure measuring instrument (HF-PW-PMI) probe to check the length of the inner barrel. The probe was successfully retrieved from the bottom, and temperature and pressure data showed that the shorter barrel had latched properly into the BHA. A battery pack malfunctioned, so no pore-water sample was taken.

Cores 2 and 3 between 56 and 76 m sub-bottom are firm mud and required 40–45 minutes to cut. This slow drilling was partly due to light weight of the BHA, but apparently also due to disturbed sediments along the major thrust plane. Based on bathymetry, seismic reflection profiles, bedding-plane orientation, and a micropaleontologic datum, the fault plane is placed near 75 m sub-bottom (Fig. 3). The drift angle remained a stable 5.5° at 46, 56, and 114 m sub-bottom. The second HF-PW-PMI probe was recovered from 75.6 m sub-bottom, and, once again because of a battery-pack malfunction, no pore-water sample was obtained. Firm sand layers were encountered between 75 and 95 m sub-bottom (Cores 4 and 5), indicating a good seismic reflector. The third HF-PW-PMI probe run "scored the hat trick" at 123.7 m sub-bottom.

At 162.3 m sub-bottom, the inclination of the bedding approached nearly 60°, indicating presence of another fault plane. The hole angle slightly increased to 6° at this depth. At the same time, weather conditions worsened as a complex frontal system slowed drilling operations on the night of 14 July. Winds of up to 40 knots were recorded. Under these conditions, the fourth

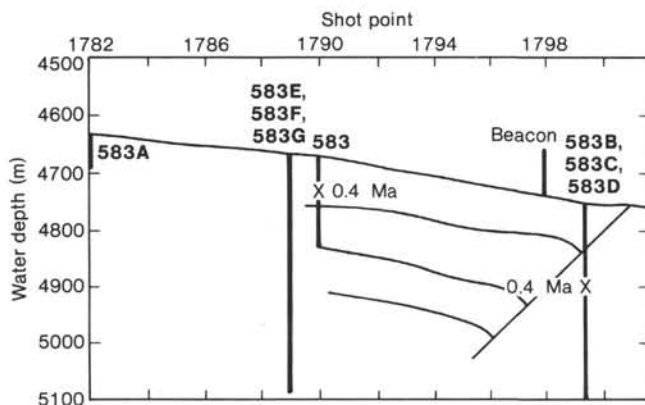


Figure 3. Simplified structural cross section based on seismic Profile N55-3-1 across Site 583.

trial of HF-PW-PMI probe was conducted successfully at a sub-bottom depth of 172 m. The pore water was, however, contaminated. The heave compensator worked perfectly with 1.5-ft. stroke on 1500 psi.

Beginning at 175 m sub-bottom, the core became firm enough to form drilling biscuits. A fifth HF-PW-PMI probe was retrieved from a depth of 220 m at 0620Z on 15 July. This time the probe measurements were taken within the drilling fill because of latching trouble. After passing through a sandy mud sequence with very low recovery, Core 22 was the first with recovery greater than 8 m. It consists of a complete muddy turbidite sequence with basal silty layers and hemipelagic sediments topping each sequence. Although no core was recovered, drilling character as observed on the rig floor indicated that Core 27 required very low torque, suggesting extremely soft sediments in the interval between 297 and 307 m sub-bottom. At Core 29, muddy and sandy turbidites were retrieved from a depth of 326.6 m sub-bottom. Intensive study of organic chemistry indicated neither quantitative nor compositional changes in the composition of gases across the fault plane visible on seismic Profile N55-3-1 (Fig. 39). Thus, our objective was accomplished.

By 1145Z on 16 July, the hole was cleaned to its bottom and cement of 15 lb./gal. was plugged in. On completion of the cementing, the pipe was firmly stuck in the hole, but after one full hour of attempts, it was finally freed. Differential sticking of the pipe may have occurred within the sandy strata. Hole 583D ended with retrieval of the drill pipe above the mudline plus four stands by 1330Z on 16 July.

After Hole 583E was spudded, a compilation of the bottom depth, fault plane position, and a nannofossil datum indicated that Holes 583B, 583C, and 583D were located at SP 1799.5 (Fig. 3).

Hole 583E

From Hole 583D, the vessel offset 446 m to 330°T from the Site 583 beacon. The new hole is situated 45 m upslope from Hole 583 and 350 m downslope from 583A. The location was selected to delineate the physical, mechanical, and chemical properties of thrust sediments. In particular, penetrating through a major thrust

plane would provide the data needed to calibrate the slip rate on the basal thrust.

The drill string spudded in at a depth of 4655 m, which is 26 m more than the PDR's value of 4629 m at 1805Z on 16 July. The site is situated at a reflection shadow zone as shown in Figure 1 and coincident with SP 1789 of the ORI Profile N55-3-1. Because of these hyperbolic reflectors, the depth given by the PDR is not true depth. Under these circumstances, we could have used a narrow-beam echo sounder to great advantage. After drilling to 150 m sub-bottom, the wash sample of 9.12 m mud was recovered. Core 1 contained 44 cm of sand, but nothing was recovered from Cores 2 and 3. The pipe drift was measured at 2.5° at 179 m sub-bottom. The HF-PW-PMI probe was run in at a depth of 189 m, but the formation was too soft to support the pipe. The probe was immediately retrieved without data. Because three cores between 160 and 189 m sub-bottom were empty, we decided to pull out of the hole. At 1545Z on 17 July, the last core was retrieved with the BHA, and it contained approximately 55 cm of sand and some barite drilling mud. We did not discover the cause for the failure of the barrels to latch.

Hole 583F

After the bit was cleaned and the hydraulic-bit release was filled with aqualube, the drill string spudded in at a depth of 4655 m at 0424Z on 18 July. Hole 583F is in the same position and at the same depth as Hole 583E. The hole was washed down to 150 m. Between 150 and 199 m, sub-bottom core recovery was almost nil. The HF-PW-PMI probe was recovered from 170 m sub-bottom, but it had not functioned properly. Core 6 was the first at Hole 583F to contain as much as three sections of core; a fissile mud with a loose sand layer of 50 cm length. Core recovery dropped again between 208 and 247 m sub-bottom, despite various efforts made to improve recovery. These attempts included the use of various combinations of core catchers and drilling parameters, but all were generally unsuccessful. HF-PW-PMI probe No. 2 was recovered from the depth of 218 m sub-bottom and worked well.

During the afternoon of 19 July, a southwesterly wind up to 45 knots aligned with the current, which forced us to move the vessel some 70 ft. Rig operations were temporarily interrupted when four engines were needed for propulsion. Subsequently, when the pipe entered a muddy turbidite facies at a depth of 256 m, the recovery ratio improved. A third HF-PW-PWI probe was run in at a sub-bottom depth of 266 m and worked well. The drift of the hole had remained stable at an angle between ½° at 218 m and 1° at 150 and 295 m sub-bottom. A fourth HF-PW-PWI probe was recovered from 324 m sub-bottom with great difficulty. Over 25,000 psi were required to pull the probe out, probably because of the accumulation of more than 4 m of drilling fill in the base of the hole. In spite of these difficulties, the probe worked well. Core 30 was retrieved with only a trace of mud from a depth of 440 m. The shoulder of the core-barrel latch finger was sheared off, indicating that the barrel was forced past the latch sleeve. The next barrel showed no

setting-pressure kick and could not be immediately retrieved. It was eventually recovered at 0615Z on 21 July with its end cut, which seemed to indicate that the bit had already been released.

Logging operations at Hole 583F started at 0815Z. The calibration and test logging sondes were installed, revealing that the hole was filled below 270 m sub-bottom. In spite of the shortened hole, the decision was made to continue logging, because it would help us to decipher the lithology of the zone between 150 and 250 m sub-bottom, an interval of very poor recovery. The sonic-induction-gamma-ray and caliper logs were lowered first and produced good induction results. The second run included the density-porosity and caliper logs and also got good results. An electric circuit failure delayed deployment of the temperature log, but finally a profile reaching down to 250 m sub-bottom was obtained. Logging operations ended at 0730Z on 22 July.

In the early afternoon of that day, cracks were found at the guide rail support padeye, requiring our immediate return to the Yokohama dock yard. The vessel departed Hole 583F heading on a course of 139° at 0031Z on 23 July, and underway gear was lowered at 0035Z. The vessel crossed the Nankai Trough and upon coming to the outer slope turned to course 58° at 0300Z on 23 July. The gear was retrieved at about 1100Z on 24 July.

Hole 583G

The *Glomar Challenger* departed Yokohama, Japan at 1133Z on 26 July after repairs on the starboard guide rail padeye were complete. On approaching Miyake Island, underway geophysical gear was streamed as the ship headed on a course of 235°T at 1000Z. Our track was generally seaward of the axis of the Nankai Trough. The underway survey was interrupted between 1016Z on 26 July and 0833 hr. on 27 July; the vessel had to steam at a reduced speed because of the failure of a motor driving the lube-oil pump of the starboard reduction gear. While we were approaching Hole 583F, the gear was retrieved at 1014Z on 28 July. We reached the Site 583 beacon at 0133Z and began running on auto-positioning at 0220Z. Because the previous 16-kHz beacon signal at Site 583 was getting weak, a new 13.5-kHz beacon was dropped at the same location. Its position is 31°50.07'N and 133°51.40'E. The BHA was made up in the same way as that used at Hole 582, with the mechanical bit release. The drill string spudded in Hole 583G at 1208Z on 28 July. The corrected PDR depth was 4627 m and the drill pipe depth was 4653 m.

After five wash cores (taken to monitor hydrocarbons), continuous coring started from 306.6 m sub-bottom. During the cutting of Core 3, the heave compensator (HC) began to leak Pydraul-fluid from the compensator piston. The hole was flushed with 40 barrels of mud, the drill pipe retrieved one stand for safety, and the HC removed from the traveling block. Core 3 washed down through 16 m of fill before cutting.

The drift angle of the hole was 1° at 335.6 m, and 1½° at 364.7 m sub-bottom. Continuous coring proceeded to 403.5 m sub-bottom (Core 10); after that hydrocarbons were monitored before each core was cut.

After Core 15 was cut, the approach of Typhoon Bess toward Kii Peninsula forced abandonment of Hole 583G by 1500Z on 30 July, before we had reached our goal of 600 m sub-bottom. This storm was the strongest of the year with 915 mbar atmospheric pressure and wind speeds of 110 knots. At 2330Z, the BHA was on deck and the *Glomar Challenger* took evasive action to east. The underway gear was streamed as the ship headed on a course of 077°. On the way to Site 584, we passed near Hachijo Jima of the Izu Ridge.

SEDIMENTOLOGY

Hydraulic-Piston-Corer Holes 583, 583A, 583B, 583C

In order to evaluate changes in both lateral and vertical facies in the uppermost sediments on the deepest part of the landward slope of the Nankai Trough, we drilled four holes with the hydraulic piston corer in three locations at Site 583. Hole 583 was the deepest, reaching 152 m sub-bottom from a starting depth, based on drill-pipe length of 4663 m. Hole 583A was spudded 405 m away, upslope at a depth of 4622 m, and penetrated 54 m. We drilled Holes 583B and 583C 475 m downslope of 583 at a water depth of 4749 m, based again on drill-pipe length. Hole 583B penetrated 30 m of sediment; Hole 583C, offset and washed down to 25 m, cored a farther 24 m to give a total penetration of 49 m. Recovery percentages are 55, 89, 88, and 74% for Holes 583, 583A, 583B, and 583C, respectively (Fig. 4). All recovered sediment is Quaternary; the only datum surfaces are found in Holes 583 and 583A in which, based on nanofossils, an age of 0.21 Ma is reached at depths of 18 and 47 m sub-bottom, respectively, and an age of 0.44 Ma is reached at 92 m in Core 583-13. No correlation between holes of beds or groups of beds on purely sedimentologic features proved possible and, although ash layers occur, no general tephrochronologic correlation could be assumed. The overall nature—lithology, composition, color, consistency of the sediments and bed thickness—of the sediments in all four holes is generally similar and thus can be regarded as part of one unit. This unit differs from Unit 1 of Site 582 in having fewer coarse sand layers and more pyrite-rich bases to the thin graded muddy sands and silts. Notwithstanding some differences which are elaborated elsewhere, the sediments recovered by piston coring at Site 583 may be collectively described as dark gray to dark olive gray hemipelagic muds with generally thin, less than 10 cm, and frequently graded sand and silt layers, the whole interrupted by sparse layers of ash and vitric sands. Plant fragments are common, locally abundant. Carbonate content is generally low, except at rare, thin carbonate-rich layers or at places where large (some up to 50 mm in length), pale yellow and sometimes hollow, authigenic calcium carbonate crystalline aggregates occur. Although some pumice pebbles are recorded and at two places hard carbonate pebbles occur, nothing resembling Unit 1 of Site 298 drilled on Leg 31 (Ingle, Karig, et al., 1975) was observed.

In Holes 583 and 583A, the layering is horizontal or nearly horizontal throughout, but in Holes 583B and

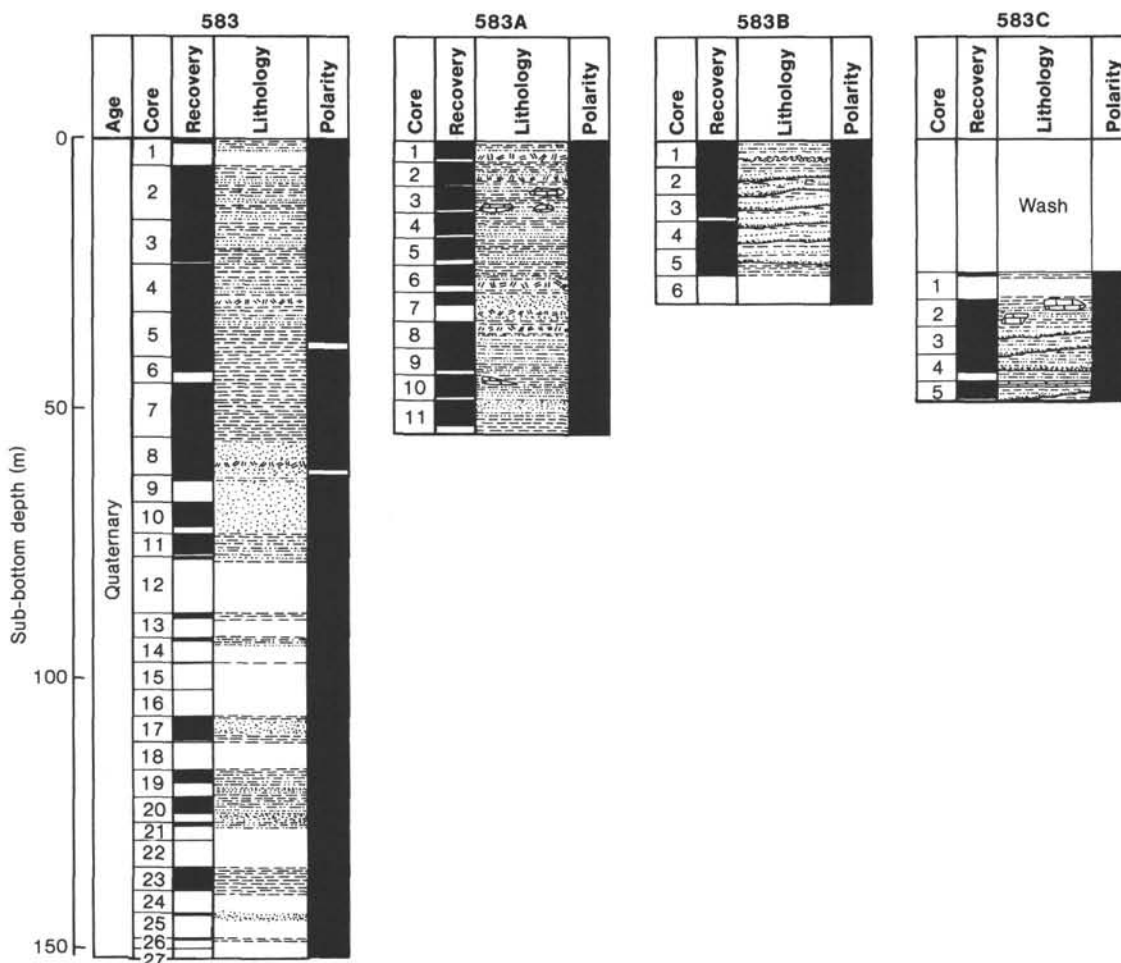


Figure 4. Summary lithologic columns for Site 583 hydraulic-piston-core holes. See Explanatory Notes chapter (this volume) for key to lithologic symbols. In polarity columns, black is normal and white is reversed polarity.

583C inclined layering is the rule; this is described and discussed in Structural Geology, this chapter.

Hole 583 (0 to 152 m sub-bottom, Cores 1 to 27)

This hemipelagic mud sequence is characterized by graded sands and silts with occasional ash layers. Plant matter occurs in association with coarser sands, and pyrite, either free or contained in lithic particles, causes the lower part of some of the graded layers to be very dark gray or black. Most of the graded layers have sharply defined, possibly erosional bases.

The topmost 16 m, to Core 3, consist of dark gray mud (5Y 4/1), free of calcareous fossils and interrupted at intervals ranging from approximately 5 to 40 cm by thin (1-to-5-cm thick), sharp-based, graded silts. Only these coarser layers contain calcareous fossils. One of these layers, capped by a calcite-aragonite layer, is shown in Figure 5. A dark gray micaceous sand (110 cm thick) at 16 m sub-bottom is just perceptibly graded and contains woody matter. Coarse and thick sands recur between 16 and 32 m sub-bottom in Cores 3 and 4. One light gray (5Y 7/1) ash layer (2.5 cm thick) occurs towards the base of this sandy interval. A predominantly clay sequence was cored from 32 to 53 m sub-bottom in Cores 5, 6, and 7. This clayey interval resembles the

shallow muddy sequence and is also interrupted by thin, very dark gray, graded silts. From 53 to 61 m, the mud becomes more silty. The clay fraction decreases gradually downhole, until from about 62 to 73 m sub-bottom (Cores 9 and 10) the sediment consists of muddy pumice-rich sand containing pumice granules, mud clasts, and woody fragments. Beneath 73 m, after 15 m of mud containing a 45-cm-thick sandy mud layer, recovery is poor to 107 m, where a 4-m interval of hemipelagic silty mud with black sandy layers is encountered (107 to 111 m sub-bottom, Core 17). A nonrecovered interval at 112 to 117 m may represent a sandy sequence, but at 117 to 130 m (Cores 19 to 21) there is more hemipelagic mud, with 5-cm-thick, very dark gray and black, graded muddy sands and silts. In Core 20 (122 to 126 m) this sequence is interrupted by a 135-cm-thick, graded, dark gray muddy sand. Beyond 130 m sub-bottom, recovery is poor to Core 25 (143 m sub-bottom) and from this point to 148 m (Core 26) consists of soupy sand and dark hemipelagic mud with silt layers. The deepest core (Core 27) reached to 152 m sub-bottom, but did not recover sediment.

Time markers occur at 18 and 92 m; their dates, based on microfossils, are 0.21 and 0.44 Ma, respectively. The derived sediment accumulation rates (uncorrected for com-

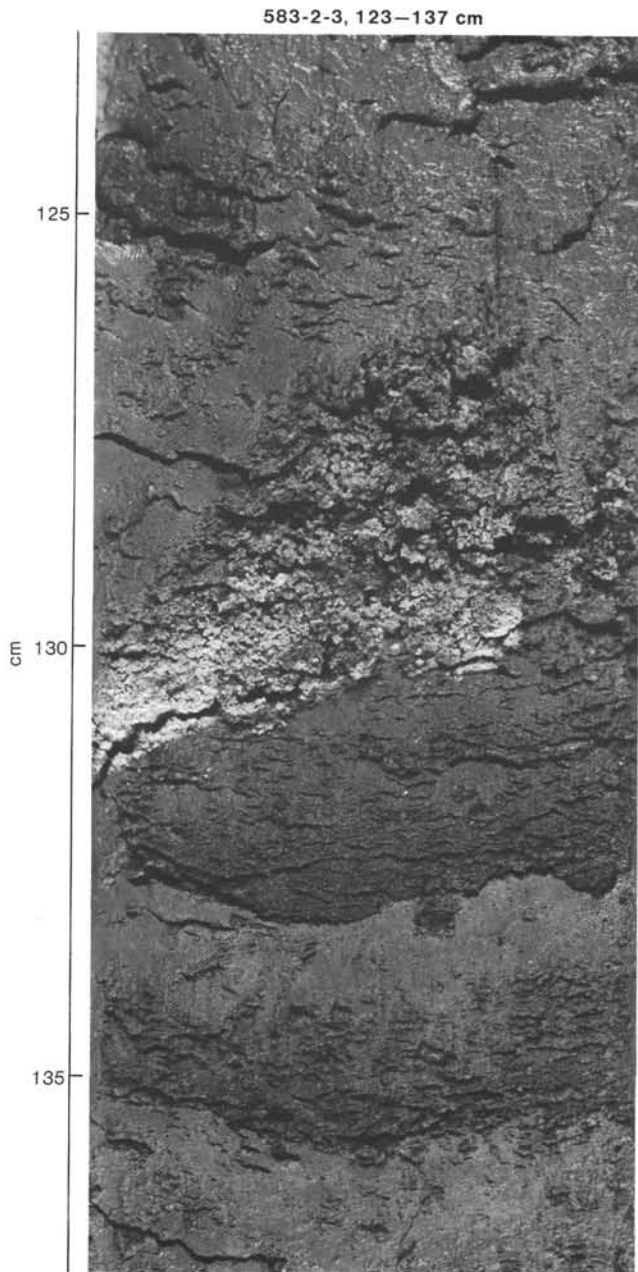


Figure 5. Coarse-grained layer capped by calcite and aragonite, Core 583-2.

paction) are about 86 m/Ma for the topmost sediments and 209 m/Ma for the lower part. The low sediment accumulation rate for the upper part may, however, be incorrect because of possible erosion or slumping of the youngest sediments from this locality. The sediment bears no indication of different rates from Hole 583A, which has a rate of 225 m/Ma.

No trace fossils, such as those found in Site 582 were observed in Hole 583, and a shallower depositional setting may be indicated than for Site 582.

Hole 583A (0 to 54 m sub-bottom, Cores 1 to 11)

This hemipelagic mud sequence is like that of Hole 583 and has common silty layers that are usually graded

and pyrite rich in the lower part and that have sharp erosional bases.

The first 14 m sub-bottom consist of dark gray, graded silty layers every 5 to 10 cm, somewhat more common than in Hole 583. The bases of these graded silts are sharp and may be erosional (Fig. 6). Towards the lower part of this first 14 m, the mud becomes darker, although it is interrupted at 4 m sub-bottom by a 55-cm-thick gray and light gray composite ash layer (Fig. 7), and at 6.6 m sub-bottom by a thin (5.0-cm) greenish gray vitric sand. Below 14 m (Core 4), graded silts are less common and those that occur have sharp, clearly erosional, bases and pyrite-rich lower portions. The pyrite occurs both as free pyrite grains, usually framboidal, and as inclusions in lithic fragments. Plant fragments are present, some muds are mottled with black, probably organic matter-rich material. At 24.3 m sub-bottom, several pebbles occur in a 4-cm-thick layer of coarse sand, and at 27 m in Core 6, a 30-cm ash layer with an apparently eroded upper surface occurs. Below 27 m, the sequence reverts to dark gray hemipelagic mud with frequent graded silt layers, black where the silts are coarsest. A thin, white ash layer is mixed with sand at 29.5 m sub-bottom in Core 7, and another ash layer occurs at 31 m sub-bottom in the same core. In Core 11 (49 m sub-bottom), the graded silts are interrupted by a muddy sand layer >1.2 m thick, containing pumice grains and (at the top) plant debris.

Pale yellow (5Y 8/3) authigenic calcium carbonate concretions or crystalline aggregates (Fig. 8), some up to 50 mm in length and occasionally hollow, occur at 8.5, 9.3, 12.7, 13.2, 13.4, 13.9, and 44.9 m sub-bottom. These are described in the Inorganic Geochemistry section of this chapter.

A paleontologically identified time marker occurs at about 47 m sub-bottom depth. This marker, dated at 0.21 Ma, yields an average sediment accumulation rate of about 225 m/Ma.

Holes 583B and 583C (0 to 49 m sub-bottom, Cores 583B-1 to 583B-6, 583C-1 to 583C-5)

Hemipelagic mud here is interrupted by graded silts with sharp erosional bases; the coarser silt, just above the base of the graded layers, is often black.

Holes 583B and 583C are at the same location and, in contrast with the layering of Holes 583 and 583A, which was nearly horizontal, the layers of Holes 583B and 583C are always inclined (Fig. 9).

The first 2.5 m sub-bottom are composed of dark bluish gray (5BG 4/1) hemipelagic mud with graded silt layers, plant debris, and pumice fragments. From 2.5 to 5.5 m, a muddy sand sequence contains abundant plant fragments, some carbonate concretions and pumice particles. With the exception of a 40-cm sandy layer at 11.5 m sub-bottom in Core 583B-3, and a 70-cm muddy silt at 20 m in Core 583B-5, hemipelagic mud with graded silts at varying intervals continues to 25 m sub-bottom. An additional 5 m penetration at Hole 583B produced no sample. Pumice grains and particles are recorded throughout the hole, and a fragment of gray limestone was recovered at 25 m.

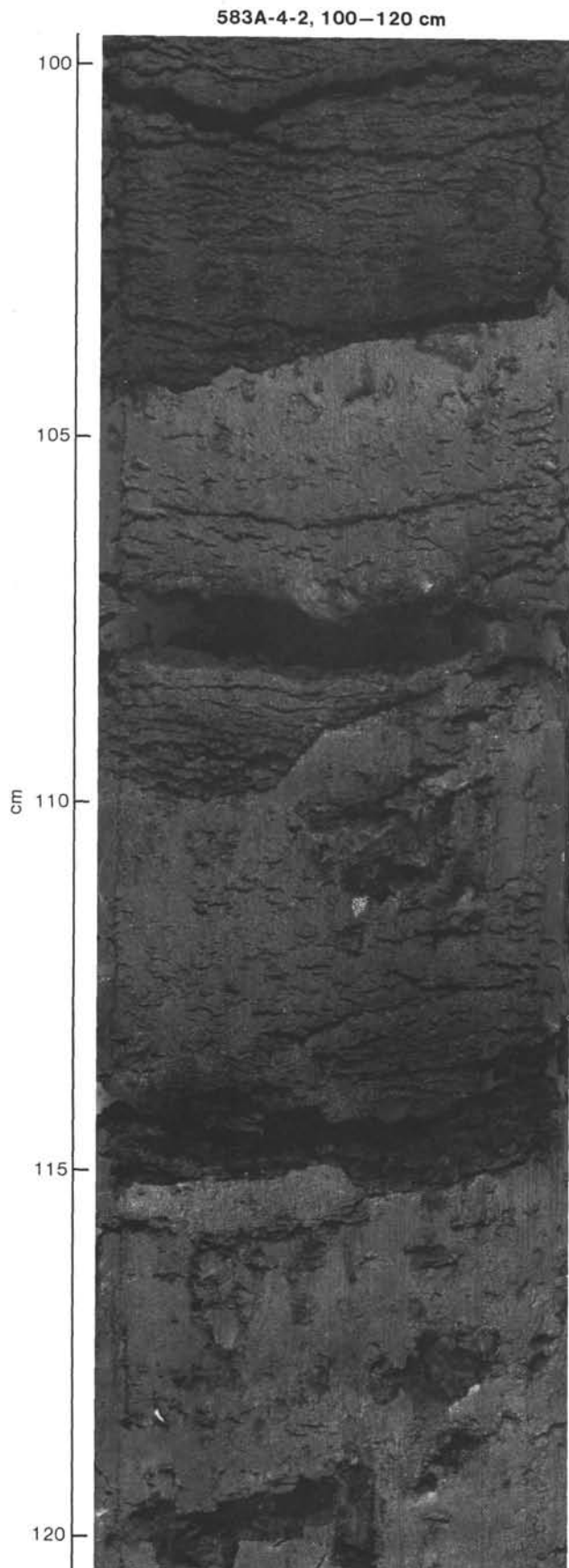


Figure 6. Graded silts in Core 583A-4.

Below 30 m there are muddy silt layers, some of which are deformed either by slumping or by drilling. These silts are up to 15 cm thick and occur at intervals of 20 to 40 cm. Most of the inclined graded silts have sharp erosional bases; the coarser parts are often black. Sands become more abundant from 36 to 40 m sub-bottom and commonly contain pumice fragments in the coarser parts. Below 40 m sands are less common down to 45 m sub-bottom where thicker, 6-to-30-cm, dark gray silts with sharp bases are common to 48 m sub-bottom. Fragments of marly limestone occur at 47 m. The last meter of this core consists of hemipelagic mud with 2-cm-thick graded silts.

Calcium carbonate crystalline aggregates similar to those described in Hole 583A occur in Core 2 at 30.5, 30.7, and 31.9 m. Yellow calcareous crystalline sands occur at 34.6, 35.0 and 35.6 m sub-bottom.

No time markers were found in Holes 583B or 583C.

Rotary-Drilled Holes 583D, 583E, 583F, and 583G

The general character of the rotary cored sediments of these holes differs from that of the HPC samples from Holes 583, 583A, 583B, and 583C. They resemble more the rotary-cored sediments from Site 582. In both rotary-cored sequences, the sandy muds are thicker (greater than 1 m); thin (10 to 30 cm) silt beds are less common; and the units of hemipelagic mud are thicker than in the HPC samples (Fig. 10). At least part of the differences must be ascribed to the change from hydraulic piston coring to rotary drilling.

Hole 583D (46 to 327 m sub-bottom, Cores 1 to 29)

This dark gray (5Y 4/1) hemipelagic mud contains some graded silts and occasional coarse sands, commonly with plant matter, but without ash layers or carbonate layers. A paleontologic time marker of 0.44 Ma occurs in Core 12.

This hole, located very close to Holes 583B and 583C, was rotary drilled rather than piston cored, and core recovery was a mere 25% (Fig. 10). From Cores 1 to 15 (46.8 to 191.4 m sub-bottom), the recovered sediment is generally hemipelagic mud with sparse silty layers and very dark gray laminations. The only exceptions are 2.1 m of uniform muddy sands in Cores 4 and 5, and 20-cm-thick graded silts in Cores 9, 11, and 13. Recovery was poor, but we cannot determine whether this was due to unrecovered sands or some other cause. Core 16 (191.4 to 201.0 m sub-bottom) contains more sand, some of it coarse to pebbly, containing mud clasts and plant fragments. Cores 17 and 18 revert to generally uniform hemipelagic mud, but in Core 19 (220.2 to 229.9 m sub-bottom) sand-rich sediments very similar to those in Core 16 occur again. Cores 20 and 21 contain muddy silt and mud, but graded bedding and burrows, including *Planolites*, occur in Core 22 (249.3 m to 259.0 m sub-bottom). Similar sediments occur in Core 583-23, with the first occurrence of *Chondrites*, a common feature in Unit 1 below Core 582-21. Core 24 has a few burrows, and, at 278.4 m (Core 25), silty mud and coarse sand with abundant plant fragments occur. Poor recovery from 288.0 to 307.2 m is followed downsection by

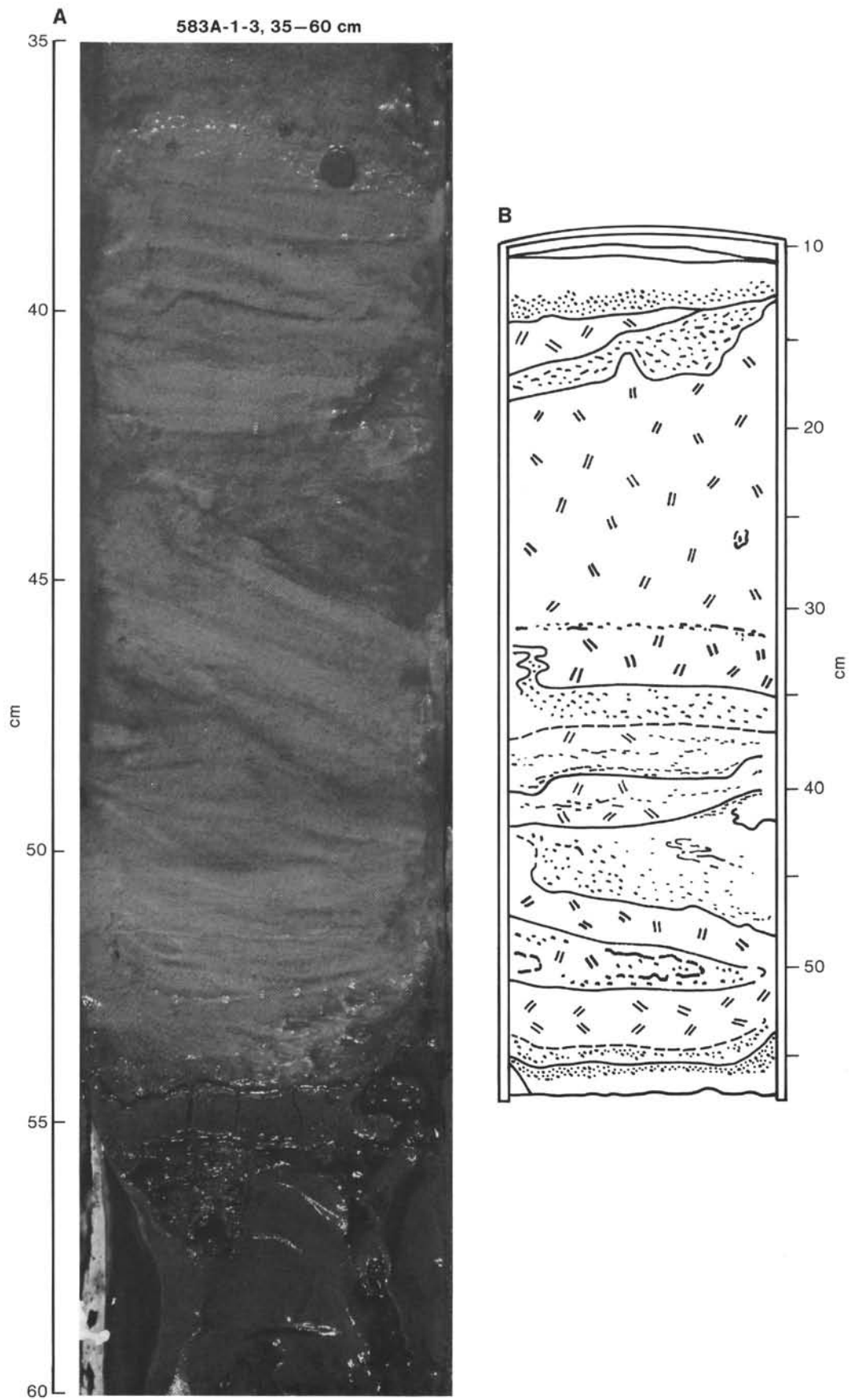


Figure 7. Composite ash layer, Core 583A-1. A. Photograph. B. Interpretive sketch.

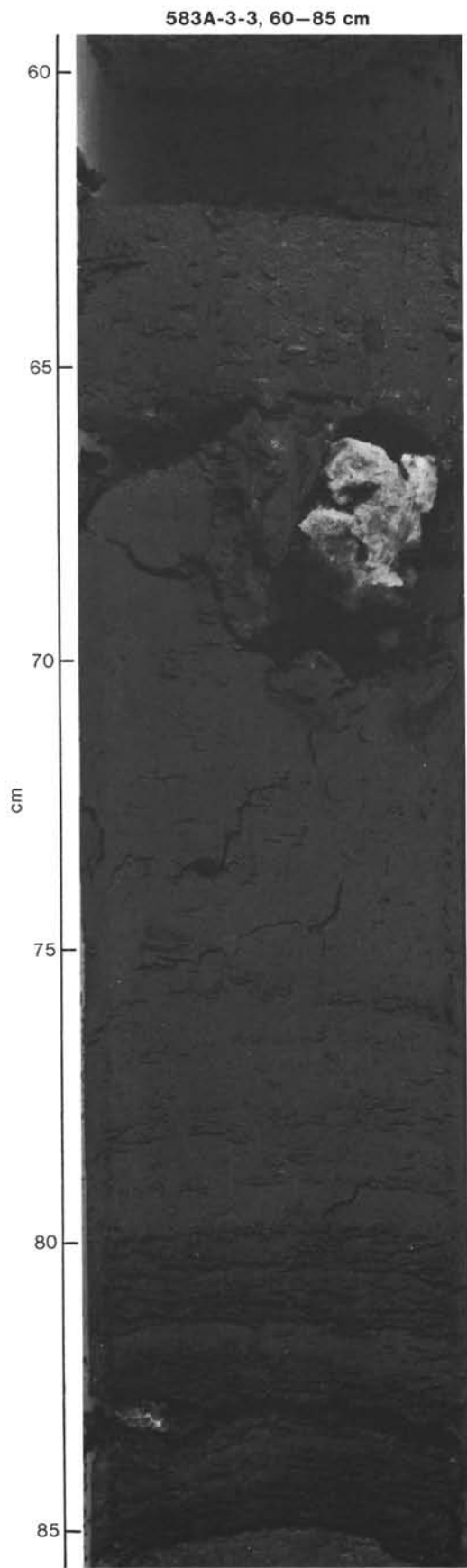


Figure 8. Authigenic calcium carbonate in Core 583A-3.

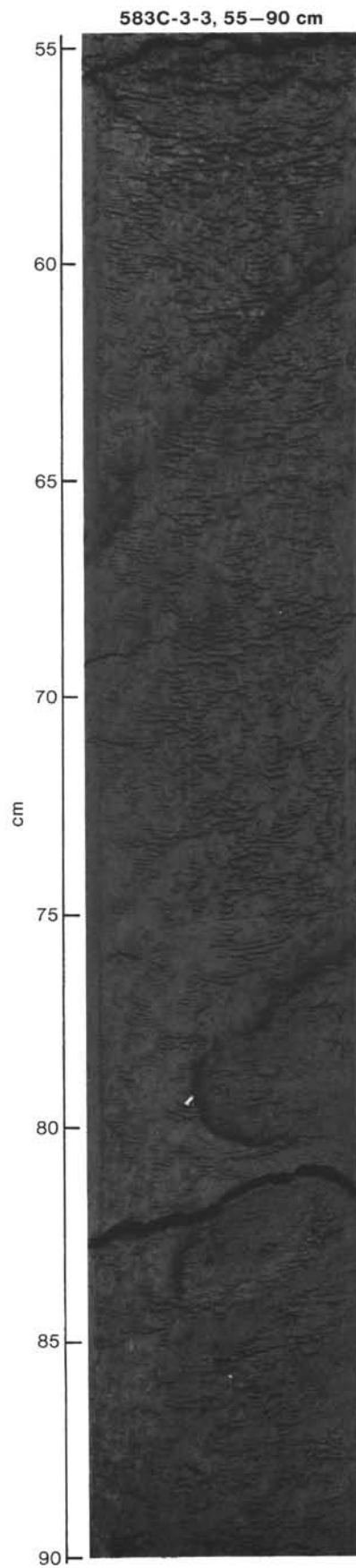


Figure 9. Inclined bedding and small slump fold in Core 583C-3.

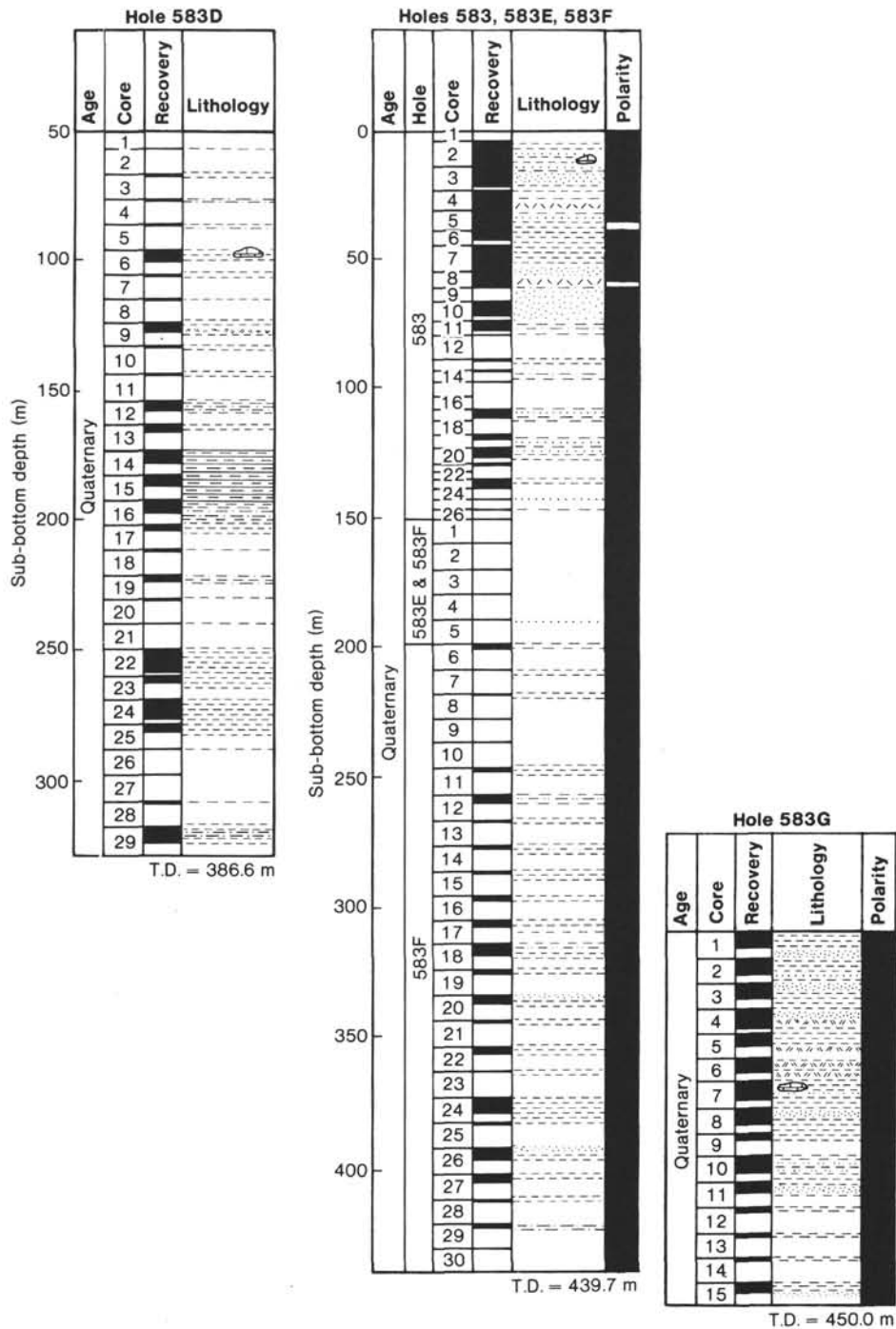


Figure 10. Summary lithologic columns for Site 583 rotary-drilled holes. For lithologic symbols, see Explanatory Notes chapter (this volume). In polarity columns, black is normal and white is reversed polarity. T.D. = total depth.

mud with plant fragments (Core 28), and at the bottom of the hole by graded silts, 30 cm thick, in bioturbated *Chondrites*-bearing mud, with scattered dark gray-green laminations (Core 29).

Hole 583D is more uniform than Holes 583, 583A, 583B, and 583C, and its lithologies resemble, towards its base, those encountered in Hole 582, Unit 1. The actual contact between lithologic units above and below a prominent landward-dipping seismic reflector was not re-

covered, nor is there a sharp contrast in lithologies that might aid in positioning it.

Hole 583E (150.4 to 198.7 m sub-bottom, Cores 1 to 5)

Characterized by extremely poor recovery (2%), this apparently hemipelagic mud sequence includes silt rich in mica and in feldspar.

This hole was positioned near to the original Hole 583. Core 1 (150.4 to 160 m sub-bottom) consists of very dark gray (5Y 4/1) hemipelagic silty mud with obvious mica grains. No further recovery was achieved until Core 5 (189 to 198 m sub-bottom) when 60 cm of hemipelagic mud with sand and a high proportion of drilling mud was recovered. The sand is arkosic (25% quartz, 35% feldspar, 22% lithic fragments, 5% volcanic glass). After this core, the hole was abandoned at total depth 198.7 m.

**Hole 583F (150.4 to 439.7 m sub-bottom,
Cores 1 to 30)**

This hole consists of dark gray (5Y 4/1) hemipelagic mud with graded silts and sands, some more than 1.0 m thick, and occasional coarse sands with pumice and plant fragments. *Chondrites* and *Planolites* occur below 257 m, and many clay portions are rich in nannofossils. The age is entirely Quaternary and greater than 0.44 Ma.

Because of poor recovery in Hole 583E, it was decided to "round-trip" and wash down to the same level; however, as in Hole 583E, Cores 1 to 5 (150.4 to 198.7 m sub-bottom) showed only trace recovery. In Core 6, starting at ~200 m sub-bottom, a coarse sandy mud more than 1.3 m thick occurs, with rounded pumice pebbles of more than 1 cm diameter; more than 25% of the grains are lithic fragments, which occupy more than half of the recovered core. The clay portion of this core is bioturbated and has a high nannofossil content (15%). From Cores 6 through 11 (208 to 256 m sub-bottom), recovery was poor; it consisted of hemipelagic mud and, on two occasions (Cores 8 and 11), drill-reworked sandy muds with some mud clasts, which may have been introduced during drilling. The recovered portion of Core 12, 3.8 out of a possible 9.7 m, consists of hemipelagic mud with several silt horizons. These silts grade upwards. They have sharp, possibly erosional bases; burrows; and darker (very dark gray, 5Y 3/1) upper portions, which contain *Chondrites* (the first seen in the hole). Each of these presumably turbidite sequences is 30 to 40 cm thick. One contains a pyrite aggregate and all show signs of bioturbation. The recovery down to Core 24 (381 m sub-bottom) is of mixed quality, but every core that is greater than 1 m in length has characteristics similar to those described for Core 12. Those with thicker graded intervals have the coarsest sands, often pumice rich and containing plant fragments. *Chondrites* occur in the finer portions and thin black and very dark gray layers occur at or near the top of the best graded layers. Olive gray laminations in Section 583F-24-5 are rich in nannofossils, and those nannofossils have thick overgrowths.

Only Core 25 shows 2.0 m of uniform, very dark gray (5Y 3/1) mud. Cores 26 and 27 (391.5 to 410.8 m sub-bottom) resemble the clays and silts of those cores above Core 25. Core 27 has a thin (6 cm) clay-free layer, which expanded considerably after cutting. This layer contains fresh zircon, glaucophane, and K-feldspar grains; lithic fragments were abundant (greater than 40%).

Core 28 (410.8 to 420.4 m sub-bottom) recovered 0.9 m of sample; it resembles Core 25, and like Core 26 it is rich in nannofossils. Core 29 contains two graded silts,

30 and 50 cm thick, separated by 50 cm of mud. Plant fragments were recovered from one of these layers. Nannofossils make up 20% of the clay portion of this core. The last core (Core 30 from 430 to 439.7 m sub-bottom) consists of only 20 cm of hemipelagic mud. Overall, sediments from Hole 583F resemble those of Site 582 and are assumed equal to Unit 1 of the latter site.

**Hole 583G (306.6 to 450 m sub-bottom,
Cores 1 to 15)**

This hole contains dark gray to dark olive gray mudstone, with thin (generally several centimeters) beds of very fine sand and silt and beds of locally coarse-grained sand (up to >80 cm thick). Below 399 m, inclined open fractures and a subhorizontal-to-inclined microfracture network of possible dewatering origin occur. Age is Quaternary and greater than 0.44 Ma.

After a port call in Yokohama, we returned to Site 583 with the objective of penetrating below the prominent thrust fault in seismic Record N55-3-1 (Fig. 39). Washing to 306.6 m sub-bottom, we began coring in hard mud and mudstone identical to that recovered in other holes at Site 583. Safety considerations necessitated our duplicating the bottom 103.1 m of Hole 583F, which we accomplished with considerably improved recovery. We deepened Site 583 by only 10.3 m before the approach of typhoon Bess forced our withdrawal.

The dominant lithology at 583G is a dark gray to dark olive gray mudstone with a variable sand and silt component. Local silt content in excess of 50 to a maximum of 60% (583G-4-2, 26 cm and 583G-6-2, 90 cm), warrants description as a silty mudstone. However, we detect no regular changes in the silt content and choose to describe the dominant lithology as mudstone throughout the core in order to avoid overcomplication.

Parallel lamination is locally manifested by pyritic concentrations (black laminations), slight mottling, and sharp changes in the hue of greenish gray. Pyrite content in the black laminations ranges up to about 7% (583G-2-2, 9 cm) and is generally about 1 to 3% of the normal mud. In some of these dark laminations, glauconite is also concentrated.

Fissility is variably developed throughout the section and becomes a prominent flaggy parting in some of the lower cores. Drilling laminations and biscuits are irregularly developed in all sections that have good recovery.

Chondrites is common throughout, varying in clarity of preservation. Local concentrations are evident (e.g., Fig. 11), but we detected no systematic pattern in the distribution of burrows with respect to sand and silt beds. They do, however, seem more abundant just below sand and silt beds in Sections 583G-8-2, 583G-8-4, 583G-10-2, and 583G-10-3. The reason for this apparent patchiness may in part be that the *Chondrites* traces are present but difficult to detect where the sediment shows incipient fissility. One hollow *Cylindrichnus* trace occurs in 583G-1-1, 50 cm (307.2 m sub-bottom).

Sand beds, irregularly distributed in the sequence, are of nongraded and graded varieties, ranging in grain size from very fine to coarse. All are recovered in a soft to soupy condition; original internal structures were oblit-

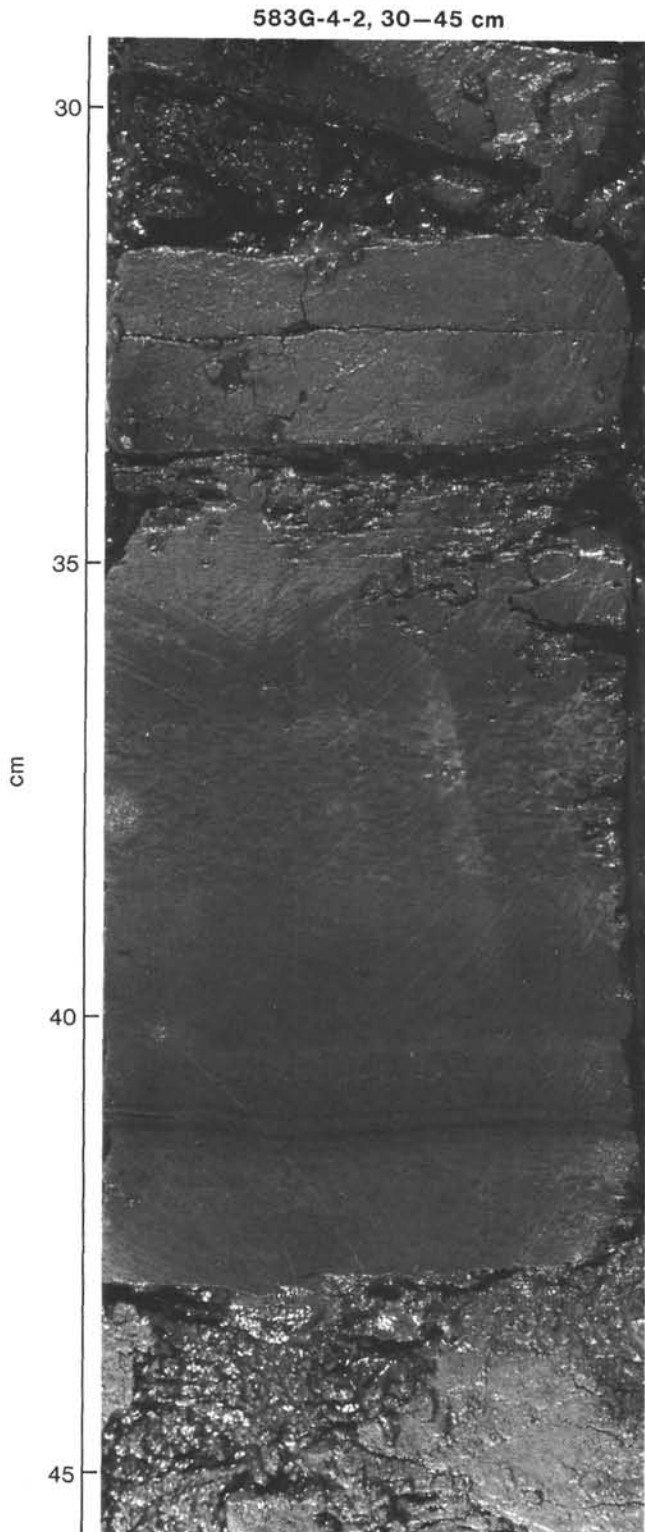


Figure 11. *Chondrites* in Core 583G-4.

erated by drilling. The thickest sand occurs at the very base of the hole, being graded over 80 cm in Section 583G-15-3 and possibly continuing up into a missing interval of core (removed as an organic geochemistry sample in Section 583G-15-2) and down into unrecovered section. A graded 60-cm fine-sand bed at 340 m (Section 583G-4-3) has a sharp, irregular base, though the

irregularity (convex up) may have been caused by mechanical erosion of the hard underlying mudstone during drilling.

Red volcanic grains and large (up to several mm) pumice clasts are noticeable components of all the coarser sand beds. Several are rich in wood, and one 20-cm bed is particularly rich in wood. This bed occurs at 583G-1-3, 60 cm; it is nongraded and packed with wood flakes including an irregular chip of 10-mm maximum dimension.

Beds (generally several centimeters thick) of silt and very fine sand occur at intervals. These are commonly darker gray (5YR 4/1); observations in previous holes at Site 583 suggest that this color and size contrast is due to pyrite concentration. Thin beds of silt and very fine sand are concentrated at 369 to 374.4 m sub-bottom (Sections 583G-7-4 and 583G-7-5).

Sporadic silty ash layers, consisting of dacitic to rhyolitic bubble wall-type glass shards, range from 0.7 cm (Section 583G-5-1) to 16 cm (Section 583G-6-1). A 1-cm ash bed in Section 583G-4-3 has ash-filled burrows below it. Volcanic glass shards are both brown and translucent. Volcanic glass content in the mudstone averages between 1 and 3%, up to a maximum of 6% in the vicinity of the two ash layers in Core 6.

Carbonate bodies occur at 343.3, 366.9, and 489.3 m sub-bottom (Sections 583G-4,CC; 583G-7-2; and 583G-14-1). The first one is circular, 4 mm in diameter, and emits a strong H₂S odor when treated with HCl. The second one, 10 cm across, is a sideritic concretion of diagenetic origin. The third one is oblong, 1 × 0.5 cm, and composed of siderite. A 2-cm dark gray brown calcareous layer of unknown affinities occurs in Sample 583G-6-4, 102–104 cm (395.5 m sub-bottom).

Inclined fractures begin at 399 m (Section 583G-10-4) and continue at intervals to the base of the hole (see Structural Geology section). At the same level, we first see the appearance of a network of parallel but slightly irregular, short open microfractures. These are not easily visible, except when the core is compressed. Most are horizontal or subhorizontal (inclined at less than 5° and parallel to bedding), but inclined healed fractures occur intermittently in Cores 7 to 15 (see Structural Geology section). A vertical set appears in the next core, where bedding is inclined at 25°.

Green to brown hornblende and biotite grains of fine-sand size to silt size are common. Blue green silt-size glaucophane grains are observed exclusively in Sections 583G-11-3 and 583G-13-1.

A Note on the Recovery and Nonrecovery of Sandy Muds and Silts from Holes 583E and 583F

In general, the coarsest sands have the highest proportion of lithic grains, pumice, and plant fragments. The lithic component includes chert and other sedimentary particles and volcanic grains; the heavy mineral portions include fresh and worn zircons, epidote, rutile, glaucophane, and other amphiboles and pyroxenes. The richest nannofossil-bearing parts are in the finest part of the clays.

The poor recovery overall in Hole 583F (16% overall, 19% when the first five cores are ignored) requires some

speculation as to the possible cause. The first five cores of Hole 583F repeated the poor performance registered at 583E, and then recovery improved. In general, cores less than 1.0 m in length contained only hemipelagic mud (only Core 583F-25 was an exception with 2.0 m of mud), whereas cores greater than 1.0 m contained silts. Cores with thick (>1.0 m) muddy sands usually had about 1 m of mud below the sand on recovery. This mud core-catcher effect implies that poor recovery at Site 583 is due at least in part to frequent sands separated by thinner muds. This obvious interpretation does not, however, seem to be supported by the seismic records or by the interpretations of those records.

Subdivision of the Sediments Recovered at Site 583 and Comparisons with the Sediments of Site 582 and Site 298 (Leg 31)

The shipboard sedimentologists gave much thought to the division of the sediments of Site 583 into separate units. They seemed much in favor of grouping the sediments of Hole 583A, the shallowest hole, and those at the top of Hole 583 into one unit. The identity of this unit would be based on the close frequency of thin graded silts with sharply defined bases, the abundance of pyrite in the lower part of these silts, the frequency of ash and vitric sand layers, and the variety of plant fragments and thick sands, the latter even when core recovery was excellent. Further, this possible unit could have its base defined by the 0.21-Ma, paleontologically defined time-marker. The establishment of this unit was, however, rejected because (1) Hole 583A was too shallow to permit us to establish a base for the unit there; (2) sediments resembling those of the proposed unit reoccurred deeper in Hole 583 (Cores 17 and 19, no sediment was recovered in Core 18); (3) similar sediments, including the carbonate aggregates so typical of Hole 583A, occur in the lower part of Hole 583B and in the deeper Hole 583C; and (4) sediments similar to those of the "type" hole (583A) occur even at Site 582.

We conclude, therefore, that the sediments of Site 583 are essentially of one unit and that the unit is equivalent to Unit 1 of Site 582. Nevertheless, we recognize that a facies characterized by pyrite-rich graded silty layers does exist and that such a facies is more common at Site 583. This facies is best seen when hydraulic piston coring is used and, unfortunately, the change in coring style hampers a better discussion of the distribution of such a facies.

The occurrence of pyrite demands comment. It occurs both as free, often framboidal, pyrite (2–5%) and, more abundantly (10–30%) as a medium cementing fine-grained particles to give the lithic fragments that occur in the graded silts. This abundance causes the dark bases of these silts. It is our view that the iron sulfide develops in basins on the inner slope. We knew from seismic records that basins of many sizes exist on the slope, and we believe that at times some of these basins become euxinic in character, thus permitting the precipitation of FeS₂. Sediment cemented by the pyrite may be subsequently eroded and redeposited as pyrite-rich lithic fragments either elsewhere on the slope or in the trough at

the foot of the slope. Their more frequent occurrence at Site 583 may be a reflection of that site's position, and the abundance in Hole 583A and the top of Hole 583 may indeed reflect *in situ* euxinic conditions or recent derivation from a nearby euxinic source. The occurrence of similar sediments elsewhere and deeper at Site 583 is an indication of the prevalence of these conditions. Further, the abundance of authigenic CaCO₃ in several forms and crystal habits may also be indicative of the occurrence of special conditions associated with the pyrite-rich sediments.

If circumstances had allowed us to piston core at Site 582, we may have been able to determine how important this slope-derived component is in the trough. Furthermore, because we could not drill at a site higher on the slope, where a slope basin was known to exist, we cannot establish whether or not truly euxinic conditions do exist on the slope. It remains clear that Site 583 does have a special facies, but we refrain from giving this facies the designation of a separate unit. We group all the sediments into one unit, which we regard as broadly similar to Unit 1 of Site 582.

The report on the sediments of Site 298 (Ingle, Karig, et al., 1975), which is situated only some 15 n. mi. away to the west-southwest and in an approximately similar slope setting, makes no reference to the presence of abundant pyrite. Site 298, however, was only spot-cored and total recovery was low.

Ingle, Karig, and others (1975) divided the sediments of Site 298 into two units. Unit 1, an upper unit reaching from 0 to 174.2 m sub-bottom, is described as a "cobble bearing clayey and silty sand and silty clay;" Unit 2, 194.2 to 611 m sub-bottom, consists of "fissile clay(stone), silt(stone), and clayey and silty sand." Some pebbles were noted at Site 583 in what is a much more complete record than that of Site 298, but, the differences are such that we refrain from trying to make any correlation with Unit 1 of Site 298. Unit 2 of Site 298 does resemble Unit 1 of Site 582 and its equivalent at Site 583.

STRUCTURAL GEOLOGY

Bedding surfaces in the upper 45 m of HPC Hole 583 show evidence of bowing by coring, and all bedding dips recorded for this interval, measured where they are nearly planar in the central portion of the cores, are probably drill induced (Fig. 12A). Bedding planes are nearly horizontal where present in cores from below 45 m sub-bottom in Hole 583, and throughout Hole 583F (Fig. 12A). No bedding dips were determinable in the poorly recovered Hole 583E. At the landwardmost location, bedding dips measured in oriented cores from Hole 583A suggest a 10 to 15° dip to the west from 20 m sub-bottom to total depth at 54 m sub-bottom (Figs. 12A and 13A).

Cores from Holes 583B and 583C show steep dips at surprisingly shallow depths, and even beds in the mud-line core (Core 583B-1; 0 to 5 m sub-bottom) dip 34 to 43° (Fig. 12B). Consistent dip angles in all cores from Holes 583B and 583C, and consistent dip azimuths within each piston core, strongly suggest that the interbed-

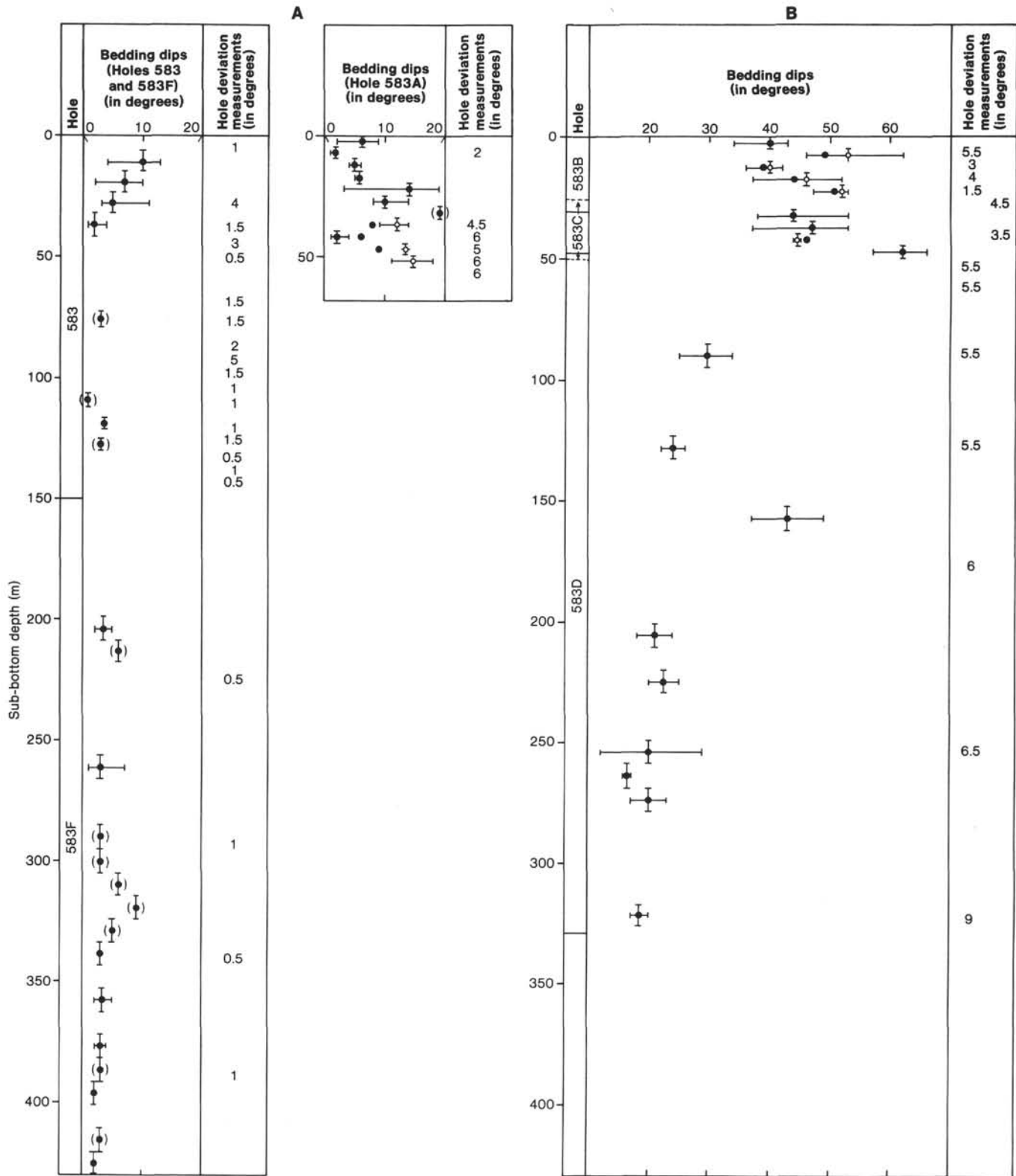


Figure 12. Bedding dips. Solid dots represent core averages of bedding dips; open circles are core averages corrected for hole deviation. Vertical bars indicate depth range of each core; horizontal bars indicate range of bedding dips measured in each core; dots in parentheses are based on only one measurement. A. Holes 583, 583A, and 583F. B. Holes 583B, 583C, and 583D.

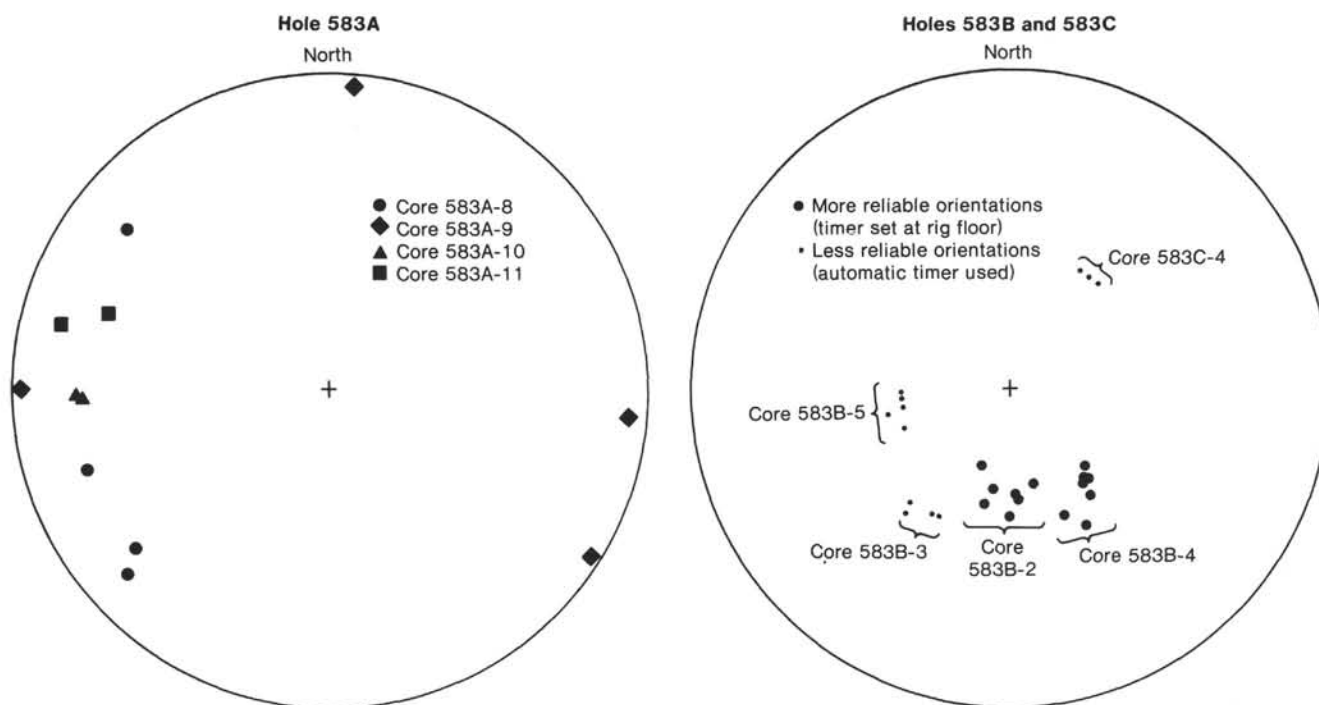


Figure 13. Oriented bedding dips, Site 583 hydraulic-piston-corer holes. Lower hemisphere projection of dip lines, corrected for drift (trend and plunge of dips plotted).

ded mud and turbiditic sands dip homoclinally, at approximately 45° (total range, 34 to 66°). Because of technical difficulties, fewer than half of the piston cores in these two holes could be oriented, and the resulting dip directions vary somewhat from core to core. Of the five oriented cores, orientation photographs from only Cores 583B-2 and 583B-4 were exposed using the reputedly more reliable timer that is set manually on the rig floor, rather than an automatic timer. By weighing more strongly the relatively consistent results from these two cores, our data suggest that the dip is to the south or south-southeast (Fig. 13B). Furthermore, an inconsistent azimuth of hole deviation recorded for Core 583B-5 suggests that dip azimuths in this core are 73° clockwise from what they should be. A 73° counterclockwise rotation of Core 583B-5 azimuths (Fig. 13B) places these dip directions squarely on the cluster of more reliable azimuths.

Deeper cores at this location, recovered by rotary-drilled Hole 583D, show much less detail than do the piston cores. Bedding dips preserved in Hole 583D cores are consistently shallower than those in Holes 583B and 583C, generally 15 to 25° , although two cores have somewhat steeper dips, averaging 30 and 43° (Fig. 12B). Assuming that Hole 583D was, in fact, drilled at the same location as Holes 583B and 583C, shallower dips at depth are significant. Graded beds throughout these holes are demonstrably upright, and the pattern of consistently steep dips over consistently shallow dips suggest a structural break at some level between 50 and 75 m sub-bottom. Unfortunately, only 1 m of sediment was recovered from this interval, and one possible explanation is that the upper portion is a slide block. The reflection profile

shows no evidence of a >50 -m thick coherent slide block, however, and does show a thrust fault that could reasonably intercept the drilled section at the appropriate depth. Our favored interpretation is that the steeply dipping beds of Holes 583B and 583C are part of the seaward flank of an anticline, located in the hanging wall of a landward-dipping thrust fault, a splay of which was penetrated at 50 to 75 m sub-bottom. The rotary cores from Hole 583D are not oriented, so the direction of dip is not directly known for the section below the presumed thrust fault. Uniformly steeper dips (37 to 49°) in Core 583D-12 at 152.6 to 162.3 m sub-bottom suggest another deformed zone, perhaps a second splay of the thrust fault. This second zone is bracketed by zones of consistently shallow bedding dip at 135 and 200 m sub-bottom.

Fissility is developed intermittently in clay-rich, non-bioturbated intervals below 210 m in Hole 583D. This depth is slightly shallower than the 254 m depth to the shallowest fissility noted at Site 582 in the Nankai Trough. The steep and consistent dips of bedding extending to the surface suggest that the uppermost part of the section at Hole 583B has been stripped off by erosion. Porosities and biostratigraphy substantiate this suggestion, and the present difference in depth to initial fissility at the two sites is probably not meaningful.

A small slump fold at 583C-3-3, 76 cm (Fig. 9) suggests the paleoslope was to 182° , assuming that bedding dips to 160° at present. A minor reverse fault in firm mud and sand at 583C-3-2, 95 cm dips 70° and shows 4 cm of stratigraphic offset (Fig. 14). The curvilinear morphology of the fault surface, the soft nature of the sediment, and especially the drawn-down features near

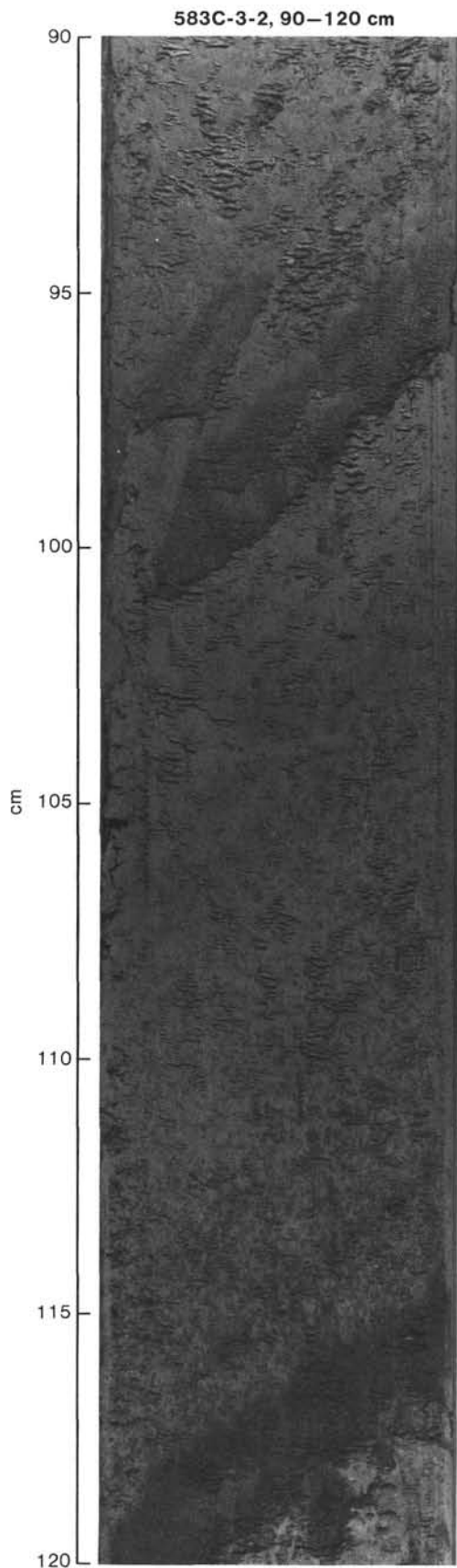


Figure 14. At 583C-3-2, 95 cm is a probably artificial reverse fault dipping 70° with ~ 4 -cm offset in firm mud and sand.

the core liner (which on one side forms an apparently artificial normal fault) suggest that this reverse fault is an artifact of coring.

Discrete open fractures cut mudstone recovered from below a sub-bottom depth of 353 m in Cores 22, 28, and 29 of Hole 583F. These discrete fractures have planar, polished slickensides, and commonly slickenlines, indicating direction of displacement. Subtle to pronounced steps on the slickensides suggest a sense of relative motion as well. Of 19 fractures judged to be potentially natural, *in situ* faults, 11 show slickenlines indicative of dip-slip motion (slickenlines rake within 20° of dip direction of fracture), 2 show evidence of strike-slip motion (slickenlines rake within 20° of strike azimuth of fracture), and 6 indicate oblique-slip motion. Steps developed on the slickensides suggest consistent senses of both dip-slip and strike-slip components of relative motion across these fractures, but a lack of consensus among structural geologists concerning the origin of such steps precludes a definitive interpretation. Assuming these steps were formed by the long risers sliding over one another, as a first impression suggests, dip-slip components are uniformly normal and strike-slip components uniformly right-lateral. This more obvious interpretation fitting a priori with the steep dips of faults is disputed, however, by experimental results (Durney and Ramsey, 1973; Hobbs et al., 1976), which suggest rather that fractures in cores from Hole 583F record reverse and left-lateral displacements.

There is no evidence that any of the open fractures in these cores were open at depth, and they may have all opened in response to drilling and recovery. Some of the open fractures in these cores are demonstrably artifacts of drilling or handling, and it is possible that some or all of the 19 fractures discussed above are artificial as well. In our selection of these fractures, however, we have dismissed as probably artificial those fractures with clearly curvilinear or hackly, nonpolished surfaces, or which bear a suspicious spatial relationship to the core liner or to the (previously vertical) core axis, or which exhibit only crudely developed slickenlines. The 19 remaining fractures are tentatively judged to be pre-drilling, *in situ* features because they were not present in cores of the same sedimentary section where it was drilled at Site 582, beyond the seismically defined deformation front. Alternatively, these fractures may form below the drill bit, in response to an *in situ* stress field affected by drill-induced loading, unloading, and torque. Whatever their origin, we note also that discrete, inclined open fractures cut cores from Site 298 as well, below 316 m sub-bottom (Core 298-8).

A penetrative secondary fabric defined by inclined dark zones is developed intermittently in mudstone in Cores 583F-24 to 583F-26 (372 to 401 m sub-bottom). These faint dark zones superficially resemble features called dewatering veins, vein structure, or spaced foliation, but in several aspects are distinctly different. They are extremely planar throughout affected intervals, occur in very parallel sets in most cases, and dip uniformly at about 60° (total range, 58 to 66°) to bedding, which in Hole 583F is virtually horizontal (Fig. 15). They lack

anastomosing or distributary patterns. In one example, a subtle internal fabric is discernible within dark zones (Fig. 15A). This fabric is defined by slightly curved, convex-outward bounding surfaces, which extend within and across the zones, producing a braided appearance. The dark zones are commonly 2 to 5 mm apart, range from less than 1 to 5 mm thick, and generally do not change thickness across the core. They do not appear to offset bedding macroscopically in the few examples recovered from near the base of Hole 583F (Fig. 15B). They are morphologically similar to less-dense sets of inclined dark zones found in cores from Site 298 (Lundberg, unpublished data), which locally resemble kink bedding. In these bands, primary features are slightly rotated in the sense of relative motion of a reverse fault. In at least one example from Hole 583F, these dark bands do rotate bedding-parallel fissility in the sense of a reverse fault (Fig. 15B).

The distribution of these "kink bands" in cores from Site 298 suggests that they are common at depths below

the section penetrated in Holes 583F and 583G. Steps developed on surfaces visible when the core breaks open along these dark bands represent intersections with bedding, bedding-parallel fissility, and in at least one case a conjugate set of "kink bands," in which offset appears to be reverse. They are distinctly steeper than the 30°-dipping thrust fault resolved seismically beneath Hole 583F. The steep kink bands may have formed earlier than the thrust fault, in a tectonic setting analogous to the prot thrust zone, in which seismically resolved 60°-dipping reverse faults mark the initial horizontal shortening in response to subduction at the Nankai Trough.

Hole 583G

Bedding in Hole 583G is essentially horizontal. Within only three very short zones does the dip exceed the maximum measured hole deviation (2.5°). In Section 583G-2-2 (318 m sub-bottom), a contact between muddy silt above and clay beneath dips approximately 40°. Bedding above and below this zone is horizontal, suggesting

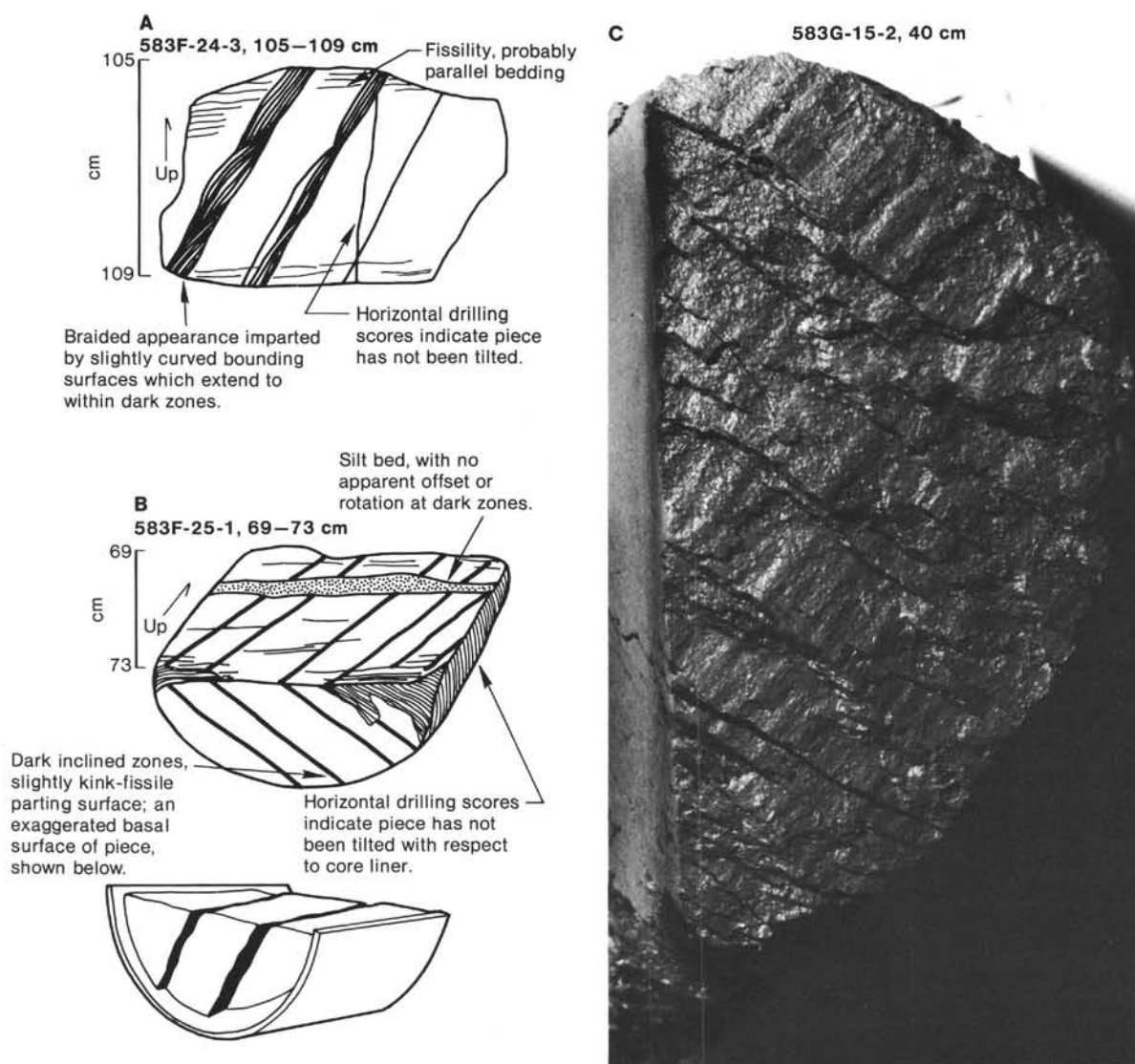


Figure 15. Penetrative secondary fabric. A. Core 583F-24. B. Core 583F-25. C. 583G-15-2, 40 cm; Steps on surface, broken along fabric, apparently formed by intersection of the bedding with conjugate fabric.

that the contact represents some form of displacement. The sense of displacement is unknown, and the interface may be induced by drilling.

Bedding over a short interval in Section 583G-7-2 (368 m sub-bottom) dips up to 30° adjacent to a 5-cm-thick piece of burrowed calcareous ooze, which could be a clast or an interbed. Bedding within the calcareous sediment also dips about 30° and shows no evidence of internal folding. This calcareous fragment occurs at the top of a sand sequence and very likely is a displaced fragment. The steep dips immediately adjacent to this fragment could be part of a small slump or features induced by introduction of the fragment.

A more clearly defined fold structure occurs in Core 10 (402 m sub-bottom) where a section of thin bedded sand and silt at least 50 cm thick dips 55°, but remains upright. Beds immediately above this section and below, in Section 583G-11-2, are horizontal, which constrains the amplitude of this structure to a few meters or less.

Core recovery became quite poor below Core 10 (400 m sub-bottom), but only horizontal bedding could be discerned in this basal interval. The low core recovery may have been a result of structural disturbance, but any structures that escaped sampling in Holes 583F and 583G must have been less than several meters in amplitude. There certainly was no room for folds greater than several meters in amplitude cored in combined Holes 583B, 583C, and 583D.

Three types of pervasive foliation occur in cores from Hole 583G: an irregular, but subparallel parting; a bedding-parallel fissility; and planar, faint “kink band” structures. Parting is most common, appearing in all cores, particularly in homogeneous clay and occasionally in burrowed hemipelagite. Where best developed, it defines a system of anastomosing cracks 1 mm or less apart that isolate lenses of clay up to 1 cm long. This pattern is clearly seen when a wetted sample is squeezed, expelling water from the partings. In most sections, the parting is subhorizontal and parallel to bedding, but in Core 583G-10, well-developed parting parallels the dominant fracture surfaces, which, as subsequently described, dip about 40°.

The cause and significance of this parting are not obvious. It might simply be attributed to compaction, except for cases where it parallels the steeply dipping fractures. It may develop as stress release cracks that vary in orientation as the local stress tensor does. If the parting exists, or is latent *in situ*, it could possibly serve as a precursor for phacoidal cleavage and/or “scaly clay.”

A second foliation is a bedding-parallel fissility, defining laminae with very planar surfaces 1 or 2 mm apart. Fissility is localized in short intervals of clay or silty clay, parallels bedding, and may coincide with very subtle lithologic discontinuities. Most likely this foliation is a result of compaction.

The third type of foliation noted for Hole 583G core samples is “kink band” surfaces similar to those described in much greater detail for Hole 583F. These features are equally subtle in Hole 583G and were first noted

in Core 10 (400 m sub-bottom). They are more extensively developed in the massive claystone of Core 15. Apparent dips, as measured on the cut core surface approached 60°. These faint, slightly darker tabular zones do not interact with other structural elements, so that their position in the developmental history of structures cannot be determined. As in Hole 583F, these zones do not offset bedding.

A well-developed fracture system, similar to that noted in Hole 583F, is first apparent in Core 583G-4 (345 m sub-bottom) and increases in intensity downward, as increasing compaction produces longer sections of sediment without drill laminae. Approximately 20 examples of fractures were measured and described, producing a very consistent pattern of orientations and characteristics. The dominant fracture dips about 40° and displays smooth grooved and striated surfaces. These lineations in most cases are oriented parallel to the dip and in no case is the rake less than 65°. The fracture surfaces are also cut by small steps, less than 1 mm high and spaced 1 cm or less apart. These steps invariably descend in the dip direction (looking down on a fracture surface) and define a nearly horizontal lineation. These steps can be shown in a number of cases to be the intersection of the parting with the fracture surface. Because of the steps, the dips of individual “trends” on the fracture surface dip a few degrees less than the gross fracture.

A second fracture set, often intersecting the first, but less persistent, dips at 20 to 40° and has identical dip-slip grooves and striae. The intersection of the two fractures in the four instances noted is horizontal. The acute angle between these fractures, which are presumed to be genetically related, is roughly horizontal, suggesting that the maximum compressive stress generating them was also subhorizontal. This orientation, the systematic nature of the fracturing down the section, and the similarity in occurrence between Holes 583F and 583G suggest that the fracture set is of tectonic origin. Paleomagnetic measurements on core sections adjacent and contiguous to these fractures indicate that the strike of both fractures and of the intersection is northeasterly, subparallel to the trend of the Nankai Trough (see Paleomagnetism section, this chapter).

Hole 583G apparently did not penetrate the targeted thrust zone, but on the basis of the reference seismic profile, it should have reached within several tens of meters of it (Fig. 16). If so, then both the profile and the core data indicate very little mesoscale folding associated with the fault plane near Hole 583G. This absence contrasts with the large fold that overlies the fault near Holes 583B, 583C, and 583D. Both these observations and the general structural configuration of the fault system as displayed on the seismic profile suggest that this is a bedding plane-step thrust. A fault ramp, dipping approximately 30°, flattens into bedding near SP 1796 at a sub-bottom depth near 300 m. A hanging-wall anticline, penetrated in Holes 583B, 583C, and 583D, has developed over this ramp corner. Balancing this structure, assuming conservation of cross-sectional area, sug-

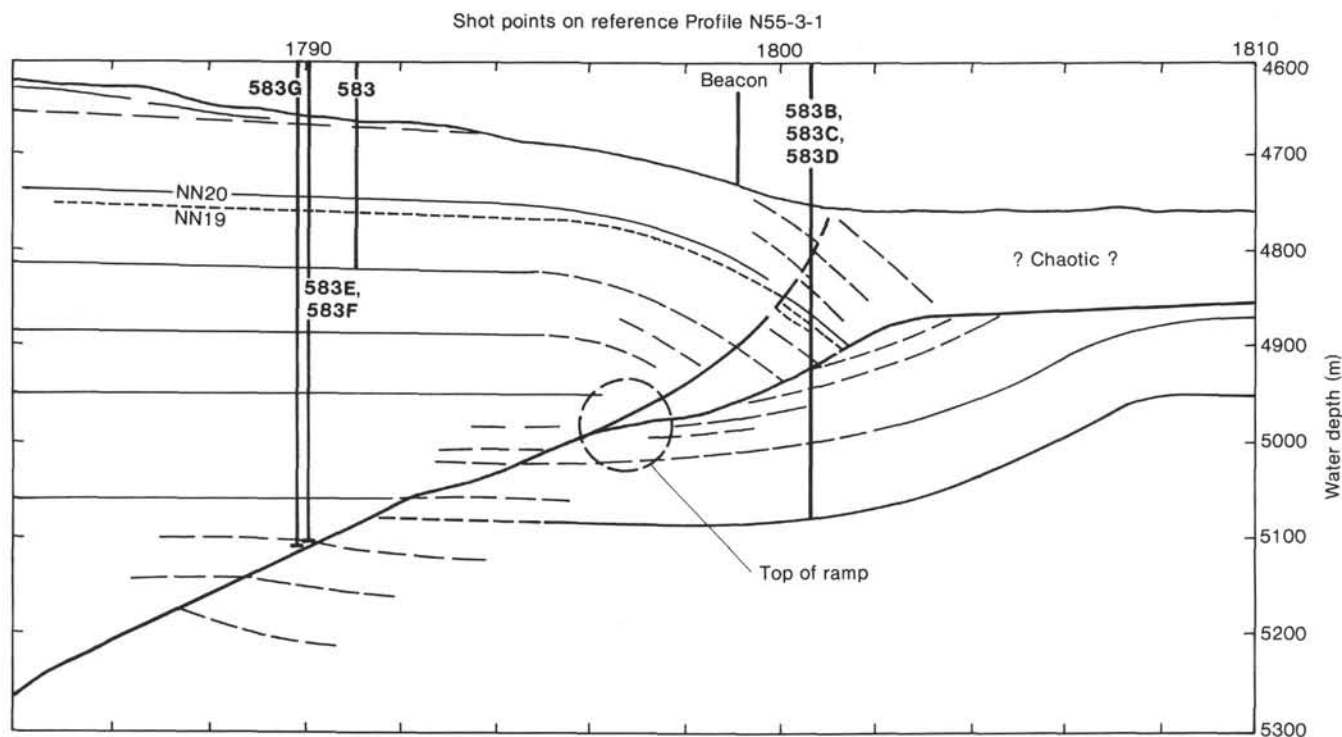


Figure 16. Structural section through Site 583 based on the reference seismic Profile N55-3-1 (Fig. 39) and drilling results. The fault is shown to be a bedding-plane step thrust with a ramp topping out near SP 1796. The hanging wall penetrated near 60 m in Holes 583B, 583C, and 583D has very little displacement. Hole deviations are not shown.

gests a total slip of at least 280 m on the fault, giving rise to 130 m of vertical throw and 245 m of horizontal offset.

BIOSTRATIGRAPHY

Radiolarians, calcareous nannofossils and foraminifers, and diatoms were found in the interbedded, hemipelagic muds and turbidite sands penetrated at the eight holes drilled at Site 583. All microfossil groups indicate that the entire section penetrated is Quaternary (Fig. 17). The biostratigraphy of the HPC and rotary core holes is described separately in the discussion below.

HPC Holes 583, 583A, 583B, and 583C

The HPC holes penetrated a composite thickness of 152 m sub-bottom in the uppermost sediments at Site 583. Microfossil distributions and preservation vary greatly from sample to sample, as at Site 582. These variations are produced by a combination of depositional and dissolution processes discussed previously in the Site 582 report.

All of the HPC sections are Quaternary in age. Calcareous nannofossils and radiolarians show that Hole 583 reached the upper lower Quaternary. All other holes retrieved upper Quaternary sediments only.

Calcareous Nannofossils

HPC samples at Site 583 contain common Quaternary calcareous nannofossils. Holes 583A, 583B, and 583C failed to penetrate sediment older than the late Quaternary *Gephyrocapsa oceanica* Zone (Martini, 1971). Hole 583, however, did reach the lower to lower upper

Quaternary *Pseudoemiliana lacunosa* Zone in Sample 583-13-1, 95–96 cm. Preservation is moderate to poor in most samples. Assemblages are generally dominated by *Gephyrocapsa oceanica*, which is commonly associated with *Helicopontosphaera kamptneri*, *G. caribbeanica*, *Calcidiscus leptoporus*, and *Coccolithus pelagicus*. Other less common forms include *Discolithina japonica*, *Ceratolithus cristatus*, *Umbilicosphaera mirabilis*, and *Rhabdosphaera clavigera*. Reworked discoasters are fewer in these sediments than in those of Site 582.

Foraminifers

Foraminifers from Holes 583, 583A, 583B, and 583C are Quaternary, Zone N22/N23 (Blow, 1969). The planktonic assemblages contain *Globorotalia truncatulinoides*, *Neogloboquadrina eggeri*, and the modern form of *G. inflata*. Associated species are a mixture of warm-water and cool-water forms, as at Site 582. The most common assemblages continue to occur in sandy turbidite layers (Fig. 18). Samples are classified as muddy or sandy based on the amount retained on the 63- μ m sieve after washing, the boundary placed at roughly 50% sand. Although a crude measure of grain size, the resultant plot of foraminiferal abundance against sediment type (Fig. 18) clearly shows the importance of rapid deposition by turbidites for preservation of calcareous foraminifers in areas at or below the calcite compensation depth (CCD).

The benthic foraminiferal faunas in these sandy samples are mixtures of deep-water species (such as *Melonis pompilioides*, *Cibicides wuellerstorfi*, *Pullenia bulloides*, and hispid to hispidocostate uvigerines) and shallow-

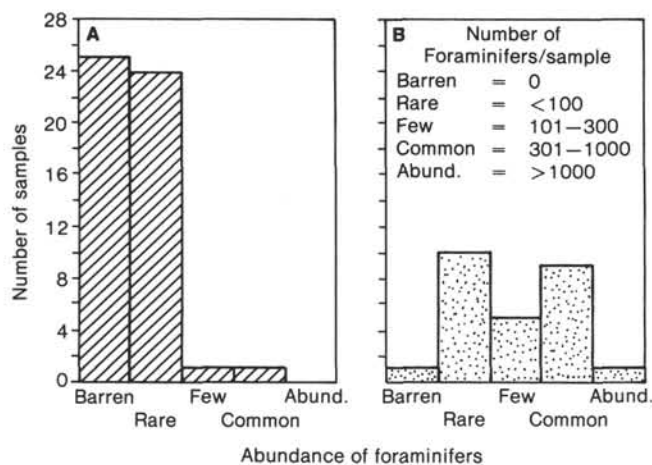


Figure 18. Variation of foraminiferal abundance with grain size in hydraulic-piston-corer holes, Site 583. A. Muddy sediments (51 samples). B. Sandy sediments (26 samples).

water species (such as *Ammonia* spp., *Elphidium* spp., and various quinqueloculines). The rare benthic foraminifers occurring in hemipelagic mud are generally deeper-water species.

Radiolarians

Radiolarians were recovered in varying abundance from Holes 583, 583A, 583B, and 583C and are poorly to moderately preserved.

Samples 583-1-1, 69–70 cm through 583-2-5, 48–49 cm are assigned to the *Buccinosphaera invaginata* Zone, uppermost Quaternary. Zonal diagnostic species are not present until Sample 583-3-3, 4–5 cm, which is assigned to the *Collosphaera tuberosa* Zone, lower upper Quaternary. The last sample that could be confidently dated is still in this zone at Core 583-9-1, 113 cm. Zonal diagnostic species were not found in any other samples except 583-13-1, 9–10 cm, which lacked tropical zonal indicators but did possess *Stylatractus universus*. This combination places that sample in the higher-latitude *S. universus* zone. No radiolarians were recovered from the core catchers of Cores 8, 19, 25, or 26 of Hole 583.

Samples from 583A are assigned to the *B. invaginata* Zone down to 583A-10-1, 110–111 cm, and the *C. tuberosa* Zone is found below that. Holes 583B and 583C do not contain sufficient radiolarians to determine zonal assignments.

When radiolarians are common, the faunas are diverse, as at Site 582. Subtropical species such as *Larospira quadrangula*, *Liriospyris reticulata*, and *Giraffospyris angulata* are mixed with cooler-water species such as *Theocalyptra davisiana*, *Spongotrochus glacialis*, and *Actinomma antarcticum*. In samples with sparse assemblages, the cool-temperate species dominate.

Diatoms

Common to rare diatoms were recovered from Holes 583, 583A, 583B, and 583C. They are poorly preserved in most samples and moderately well preserved in a few samples.

The upper Quaternary *Pseudoeunotia doliolus* Zone (0 to 0.63 Ma), based on the presence of *P. doliolus* (base; 1.8 Ma) and the absence of *Nitzschia reinholdii* (top; 0.63 Ma), is recognized from all HPC holes in the following intervals: Cores 583-1 through 583-26, 583A-1 through 583A-9, 583B-1 through 583B-2, and 583C-1 through 583C-3.

Assemblages are essentially uniform in all samples, and differences arise by different degrees of preservation. Marine planktonic species are the dominant component, with various amounts of displaced forms (namely, marine benthic and nonmarine diatoms), which are paleontologic evidence that the deposits are turbidites. Nonmarine diatoms occur throughout the holes in varying numbers. Common members among marine planktonic diatoms are *Coscinodiscus nodulifer*, *C. wailesii*, *Cyclotella striata*, *Nitzschia marina*, *Rhizosolenia bergonii*, *Thalassionema nitzschioides*, *Thalassiosira eccentrica*, and *T. lineata*. Except for *C. striata*, *Thalassionema nitzschioides*, and *Thalassiosira eccentrica*, these species are typical warm-water diatoms. Diagnostic cold-water diatoms are absent.

Reworked diatoms were recognized only in Core 583A-3, where a single specimen of *Denticulopsis hustedtii* (middle to upper Miocene) was found.

Accumulation

Calibration of zonal boundaries to radiometric time-scales allows sediment accumulation rates to be estimated for the late Quaternary at Site 583. For these calculations, the *Buccinosphaera invaginata*/*Collosphaera tuberosa* boundary is taken to be 0.21 Ma and the NN19/NN20 boundary to be 0.44 Ma. The accumulation rate for the latest Quaternary (*B. invaginata* Zone) at Hole 583A is 225 m/Ma. At Hole 583, the rate is 315 m/Ma for the interval from the NN19/NN20 boundary to the *B. invaginata*/*C. tuberosa* boundary, early late Quaternary.

Rotary-Core Holes 583D, 583E, 583F, and 583G

Three rotary-core holes penetrated to a composite depth of 450 m sub-bottom depth. The calcareous nannofossils, foraminifers, and radiolarians found in these holes are all Quaternary.

Calcareous Nannofossils

Calcareous nannofossils from these holes have a wide range of abundance and degree of preservation, and all are Quaternary, in particular the *Pseudoemiliania lacunosa* Zone (Martini, 1971). The dominant forms in these samples are species of *Gephyrocapsa*. Larger forms such as *Helicopontosphaera* and *Discolithina* are also present in essentially the same numbers as in the HPC cores. In general, most samples contain few nannofossils, and these generally show poor to moderate preservation. Several intervals are barren but a few, small intervals contain abundant, well-preserved coccoliths. The thrust fault prominent on seismic records from this site occurs in the interval above the extinction level of *P. lacunosa* and is not detectable on the basis of nannofossils.

Foraminifers

Planktonic foraminifers from these rotary-drilled holes are Quaternary, Zone N22/N23 (Blow, 1969), and include scattered *Globorotalia truncatulinoides* and rare specimens transitional to *G. tosaensis*. Assemblages, preservation, and mode of occurrence are the same as in the HPC holes; the most abundant and diverse faunas occur in sandy sediments. Benthic assemblages remain unchanged as well and consist of mixed shallow-water and deep-water species in sandy samples and deep-water species only in hemipelagic muds. Paleobathymetry for the entire section studied is lower bathyal to abyssal.

Radiolarians

Intermittent occurrences and poor to moderate preservation preclude radiolarian-based zonation of these rotary-cored holes. The fauna is primarily composed of cool-temperate species. The tropical species and zonal diagnostic species present at Site 582 and the HPC holes at 583 were not found in these greater sub-bottom depths.

Diatoms

Diatoms are common to absent, and preservation is poor in most of these rotary-cored samples. Assemblages are virtually the same as those found in the HPC samples. The *Pseudoeunotia doliolus* Zone, upper Quaternary, occurs in Cores 583D-1 down to 583D-28; 583F-H1; and 583G-H2 down to 583G-10-5, 16–18 cm. A single reworked specimen of *Denticulopsis nicobarica* (lower to lower middle Miocene) was found in 583G-10-2, 29–31 cm.

Summary

The entire section at Site 583 is Quaternary. The preservation and abundance of all microfossil groups at this site parallels that of Unit 1, Site 582. Microfossil abundance and diversity fluctuates greatly depending on lithology. In general, depositional and dissolution processes that effect biostratigraphic and paleoenvironmental resolution at Site 582 are also of prime importance at Site 583.

INORGANIC GEOCHEMISTRY

Several calcareous layers occur in the sediments recovered at HPC Holes 583, 583A, 583B, and 583C. These layers, apparently free of biogenic carbonate remains, are white to yellowish brown coarsely crystalline aggregates. These are commonly composed of euhedral crystals approximately the size of coarse sand; in cores from Holes 583A and 583C, very large crystalline lumps occur, some greater than 5 cm in length. Calcite twinning and scalenohedral terminations are commonly visible with a hand lens. Visual inspection as well as thin-section examination show that these lumps are composed almost exclusively of large, usually rhombohedral calcite crystals, some of which were clearly zoned, surrounded by a matrix of fine-grained, acicular, and occasionally hollow needles, with minor quartz inclusions. X-ray diffraction patterns confirm the identification of these minerals.

Textural relations of these phases as seen in thin section (Fig. 19) suggest that the larger calcite crystals have grown at the expense of, and perhaps in part replacement of, the needles. The size, zoning, and crystal habit of these carbonates suggest *in situ* growth, most likely the result of precipitation from upward percolating interstitial waters (see Stein and Smith, this volume).

Results of shipboard interstitial water analyses for Site 583 are listed in Table 2 and shown in standard DSDP-format plots (Fig. 20). The data for calcium, magnesium, and alkalinity are combined and replotted in Figures 21 and 22. In general, these profiles show nearly linear trends: calcium content increases slightly with depth, whereas both alkalinity and magnesium increase in the uppermost 50 m before decreasing steadily toward the bottom of Site 583 (Figs. 21 and 22). The trends defined by these data are very similar to those obtained at Sites 438 and 440 in the Japan Trench (Scientific Party, 1980). At Site 440, the dominant authigenic carbonate phases present are calcite and ankerite, frequently seen as an intimate intergrowth, perhaps not too different from the mode of occurrence of the calcareous aggregates seen in the sediments at Site 583; furthermore, a similar interpretation of the data may be used to explain carbonate diagenesis at Site 583.

The carbonate-rich zones at Site 583 occur exclusively within sandy sediments containing abundant pyrite. A high sedimentation rate probably aided in the entrapment of plant remains in the graded beds in Site 583 and in the subsequent formation of localized highly reducing environments. The higher alkalinity values in the upper part of the section are also consistent with a high organic carbon content and calcium carbonate precipitation. In such an environment, the reduction of iron (as Fe^{2+}) accompanied by sulfate reduction leads to pyrite formation, whereas Mg^{2+} is more readily deposited in the carbonate phases. This argument suggests that the calcite seen in these aggregates at Site 583 is of the high-Mg variety. The absence of ankerite as the companion phase in contrast to its presence (as reported for Site 440; Scientific Party, 1980) is somewhat questionable. One possible explanation may be that the alkalinity values reported for Site 440 are significantly higher than those obtained from the Site 583 samples and that this difference inhibits the kinetics of ankerite precipitation. Alternatively, the activity of Fe^{2+} may not have been sufficiently high for ankerite formation.

Bulk X-Ray Mineralogy of Hole 583G Sediments

Quartz, plagioclase and K-feldspar, amphibole, 7Å clays (chlorite and/or kaolinite), 10Å clays (illite), 14Å clays (chlorite and/or smectite), calcite, dolomite, and siderite were detected in Hole 583G sediments by means of a shipboard X-ray diffractometer (Fig. 23). Among these components, quartz, feldspars, amphibole, and clay minerals are detrital, as determined by the smear-slide analyses. Carbonate minerals are mostly authigenic; biogenic calcite is estimated to be less than 5%.

The relative abundance of quartz, feldspars, and 7 and 10Å clay minerals fluctuate widely and show no general trend with depth. Amphibole and 14Å clay min-

583A-3-3

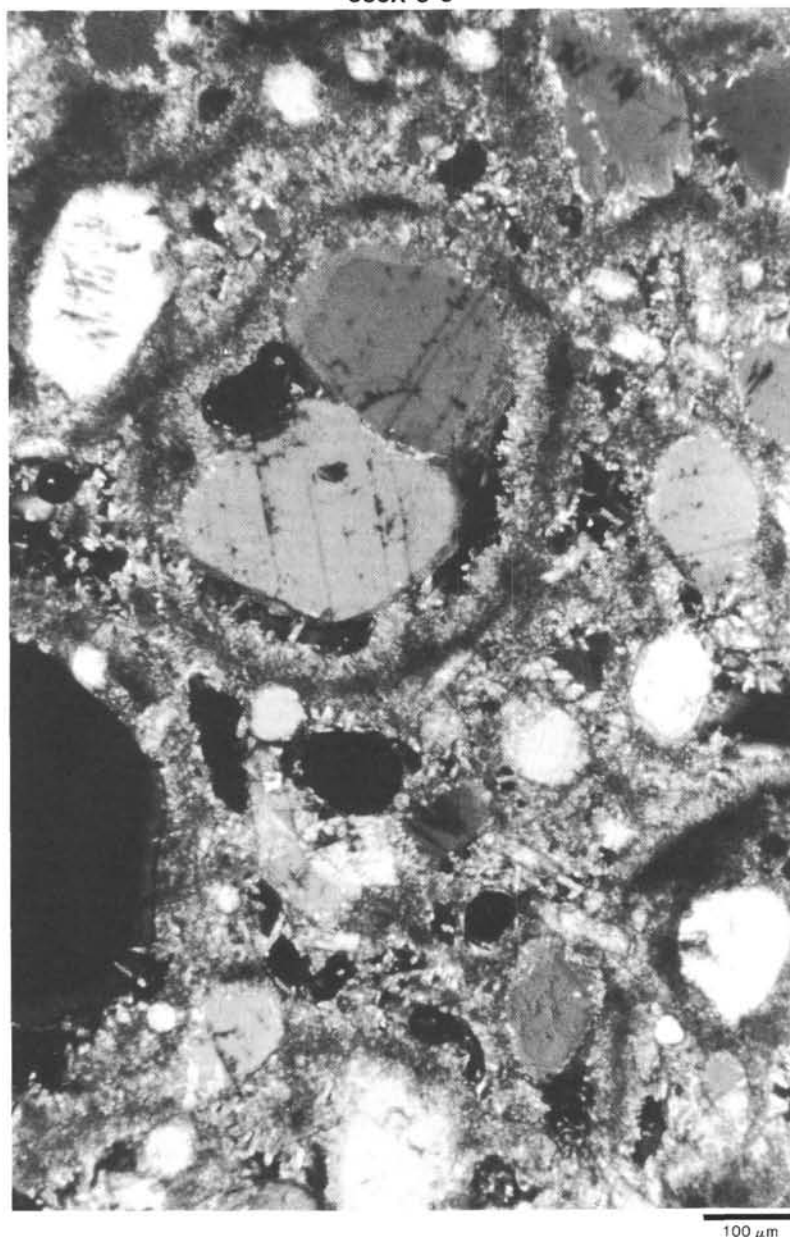


Figure 19. Thin section showing the relationship between calcite crystals and aragonite needles, Site 583, landward slope of the Nankai Trough.

erals, probably smectite, however, seem to decrease in abundance below 390 m sub-bottom. The decrease of smectite does not result from diagenetic transformation of smectite to nonexpandable clay because the temperature near 400 m sub-bottom is not sufficiently high (estimated to be about 14°C from the logging data) and because the relative abundance of nonexpandable clays does not increase. Smectite is a typical hydrothermal alteration product, and a likely source is the hydrothermal-volcanic regions of the Fossa Magna and Izu Peninsula. Decrease of amphibole and smectite in the deeper cores suggests a change in composition of sediments supplied to the basin. According to the smear-slide analysis,

glaucofanite is exclusively contained in the deeper sediments (Sections 583G-11-3 and 583G-13-1, and 583F-26-1, 583F-27-2, and 583F-29-2) and in the shallowest sediment of Section 583-4-1. Because it is present only in trace quantities, it may be more common than these chance identifications suggest. Glaucofanite, usually accompanied by illite and chlorite, is probably derived from the Sambagawa metamorphic terrain.

Siderite (identified by X-ray diffraction) occurs as a large light brownish gray nodule, 6-to-8 cm thick (583G-7-2, 49-55 cm, Fig. 24) and a small nodule 1 × 0.5 cm (583G-14-1, 57 cm), both imbedded in a matrix of hemipelagic mud. Both are composed of yellowish brown

Table 2. Shipboard analyses of interstitial water chemistry, Site 583.

Core-Section (interval in cm)	Sub-bottom depth (m)	pH	Alkalinity (meq/l)	Salinity (‰)	Calcium (mM/l)	Magnesium (mM/l)	Chlorinity (‰)
IAPSO		7.31	2.34	35.2			
Surface seawater	0.0	8.06	2.436	34.4	10.34	52.11	18.40
Hole 583							
2-5, 140-150	13.0	8.12	28.347	33.6	4.11	36.63	19.17
3-5, 140-150	22.5	7.73	25.522	34.1	4.19	34.34	19.58
4-2, 138-150	29.0	7.73	24.908	33.8	4.21	35.64	19.34
5-4, 135-150	40.0	7.70	26.194	34.1	4.15	35.04	19.75
7-3, 135-150	50.4	7.80	25.737	34.4	3.85	35.70	18.70
17 ^a -2, 130-150	110.0	7.86	31.816	34.6	4.53	42.65	20.05
23 ^a -3, 135-150	139.5	7.77	17.777	34.4	6.64	44.12	18.81
Hole 583A							
5-3, 135-150	23.5	8.01	35.442	34.4	6.51	37.41	19.24
10-3, 140-150	48.5	7.75	27.368	34.4	5.15	34.46	19.81
	54	7.70	22.744	34.4	6.61	41.35	19.31
Hole 583B							
2-3, 140-150	7.5	7.73	33.98	34.4	3.15	44.99	20.04
4-1, 135-150	16.5	7.82	35.27	34.4	2.51	46.10	19.07
5-2, 135-150	23.0	7.78	35.11	34.9	3.82	46.58	19.11
Hole 583C							
2-3, 135-150	34.5	8.01	50.366	35.2	3.44	46.62	17.76
4-2, 135-150	46.0	8.06	45.782	34.9	1.32	52.66	19.11
Hole 583D							
	123.5	7.66	40.618	34.9	4.84	49.92	19.04
9-2, 135-150	126.7	7.67	33.702	34.1	6.18	42.32	19.41
12-2, 140-150	155.6	7.76	26.368	34.1	6.74	40.20	19.17
	172.0	7.80	38.866	35.2	7.64	46.10	19.78
14-2, 135-150	175.0	7.71	29.252	34.4	6.34	39.65	19.34
	220.2	7.69	28.060	35.2	8.55	48.48	18.90
19-1, 135-150	221.7	7.70	32.690	34.9	7.83	40.19	19.45
22-4, 135-150	255.3	7.66	26.218	33.8	6.30	34.68	19.34
	278.4	7.52	17.010	34.1	8.21	43.86	19.45
29-2, 135-150	319.9	7.75	22.480	33.6	5.27	34.38	18.70
	326.6	7.52	15.080	34.4	7.40	44.26	15.11
Hole 583F							
	169.9	7.75	33.668	35.5	7.89	44.83	19.84
6-2, 135-150	201.7	7.60	25.508	33.8	6.34	38.22	19.48
	217.7	7.61	8.136	34.1	9.47	49.57	18.67
12-1, 140-150	257.8	7.79	20.782	37.1	5.96	32.63	19.34
14-1, 135-150	227.2	7.80	19.780	34.4	6.34	30.94	19.71
17-1, 135-150	306.1	7.84	14.542	30.5	7.04	27.97	17.16
18-3, 135-150	318.7	7.95	15.498	34.6	8.13	30.82	20.39
	323.9	7.63	15.032	34.4	9.74	37.38	19.04
20-1, 135-150	335.1	7.76	14.066	34.4	8.93	29.72	19.85
24-3, 135-150	376.6	7.67	12.704	34.4	9.53	28.53	19.54
29-1, 135-150	421.9	7.96	11.744	34.1	9.14	24.92	19.81
Hole 583G							
Surface seawater	0.0	8.08	2.704	35.2	10.27	52.71	18.81
3-3, 135-150	330.4	7.75	16.882	34.4	8.29	33.50	20.37
7-4, 135-150	370.7	7.90	13.606	34.4	8.96	27.44	20.27
12-1, 135-150	414.6	7.80	9.662	34.1	9.00	24.40	20.27
14-2, 0-15	433.8	7.82	10.722	33.8	8.33	20.82	20.20

Note: Samples with no sample number, only sub-bottom depth indicated, are *in situ* samples.

^a May have been contaminated with drilling water. Sample from Core 583-17 looked like marble cake; sample from Core 583-23 was muck.

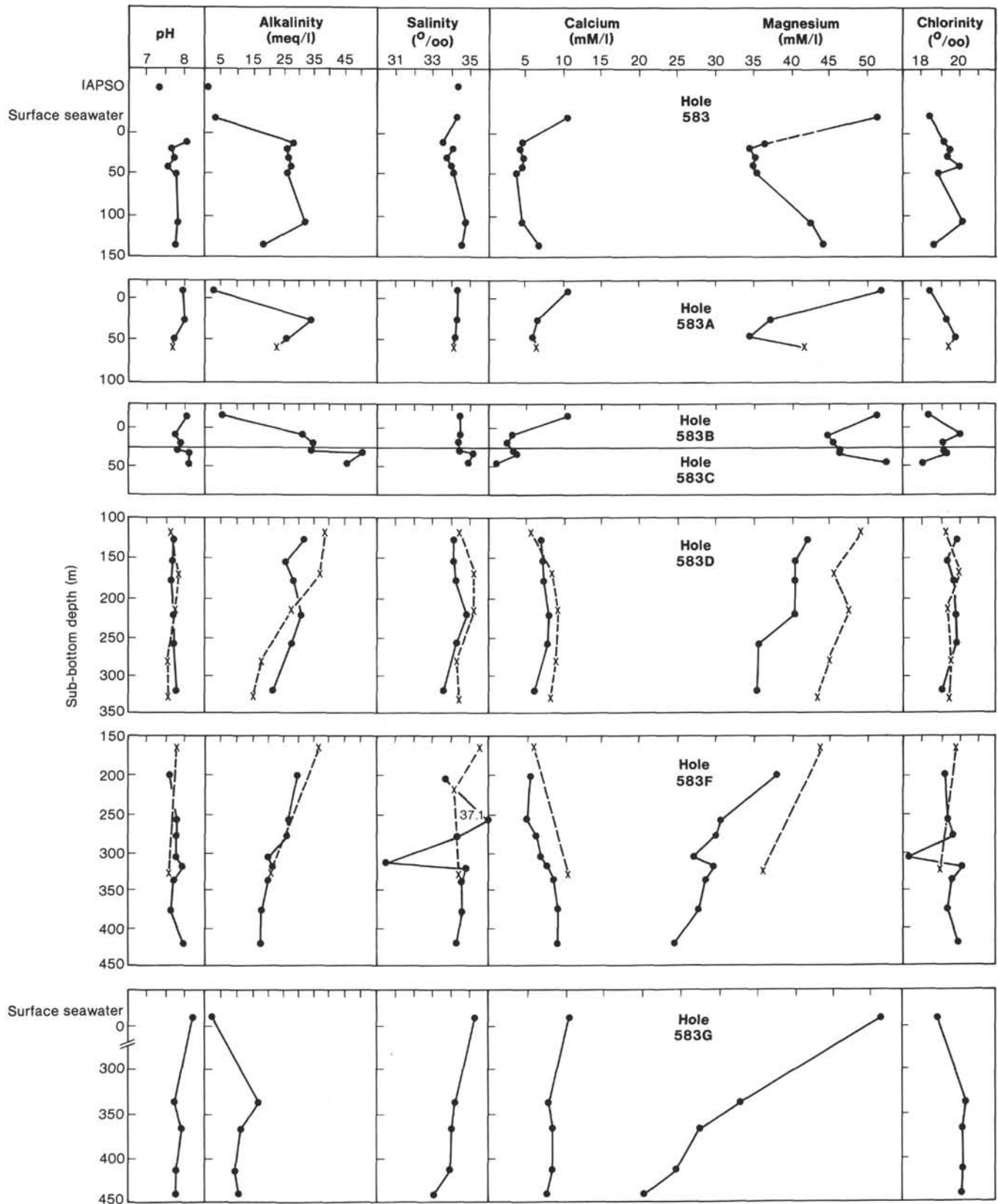


Figure 20. Shipboard analyses of interstitial water chemistry. Closed circles indicate interstitial water squeezed results (except where labeled IAPSO or Surface seawater); crosses indicate *in situ* results.

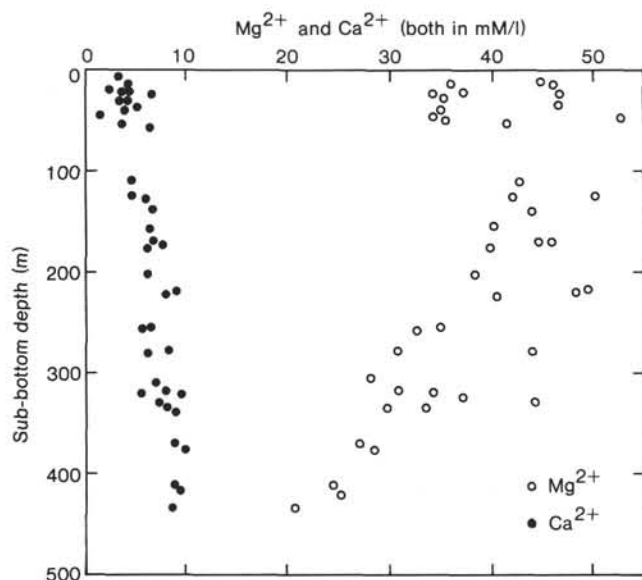


Figure 21. Concentrations of magnesium and calcium versus sub-bottom depth at Site 583.

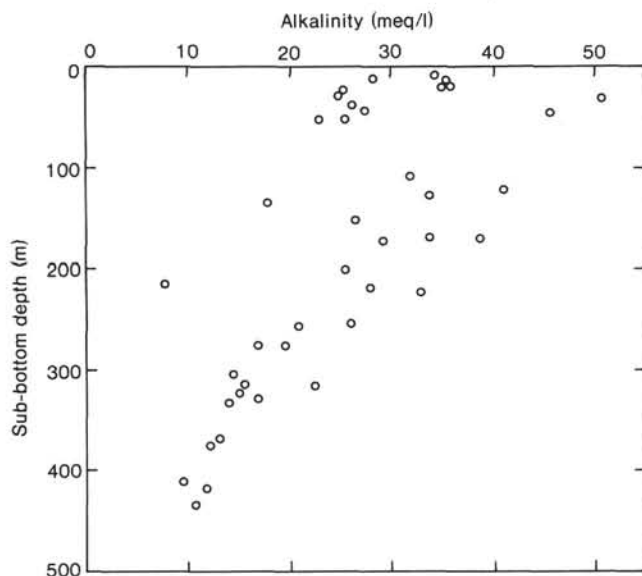


Figure 22. Alkalinity versus sub-bottom depth at Site 583.

rhombohedral to subhedral silt-size grains of siderite. The surrounding mudstone layers contain disseminated siderite approximately the size of silt to fine sand.

ORGANIC GEOCHEMISTRY

Introduction

For the shipboard organic geochemists, the main objective of this site was to detect and to analyze gas hydrates, and to monitor any vertical migration of these light hydrocarbon gases along the thrust plane shown in the JAPEX seismic Profile N55-3-1 (Fig. 39). A round-the-clock gas-analysis program was carried out for safety purposes and included almost all cores, wherever the core liner contained gases. In view of the contamination of some of the vacutainers (as discussed in a following sec-

tion), we took the gas samples directly by 10-ml syringes after punching the core liner by the normal vacutainer sampling procedure. In some instances, we noticed gases bubbling from the core liner. In most cases, gases were trapped as pockets between blocks of sediment within the core liner. Methods followed for the light hydrocarbon gas analysis are the same as described for the Organic Geochemistry section of site chapter, Site 582 (this volume).

Apart from monitoring the gases, we analyzed nine samples from Holes 583 and 583F for total and organic carbon.

Contamination of Vacutainers

We analyzed empty vacutainers, by injecting helium gas into them before gas samples were taken. Three batch numbers of vacutainer were analyzed (1) Lot No. 815487 (Becton-Dickinson), (2) Lot No. OF-127 (Becton-Dickinson), and (3) Lot No. 9M-116 (Becton-Dickinson). Lot 1 is an old batch, and Lots 2 and 3 are new. The contamination in the old batch of vacutainers is minor compared to the new sets (Table 3 and Fig. 25). Because most of our analyzed sample contains minor amounts of C_{2+} hydrocarbons, we reevacuated each vacutainer for 1 minute before taking each new gas sample from the core liner. At Hole 583D, we analyzed both the vacutainer sample and a direct gas sample, the latter by the 1000- μ l syringe. For future gas analyses, we suggest evacuating the vacutainers as described above. In addition to the contamination cited by us, the contamination of vacutainers by C_{6+} hydrocarbons is already well known.

Gas Analysis

We monitored the light hydrocarbon gases from almost all cores wherever gases were present in the six holes of Site 583. Tables 4 and 5 show the concentration of C_1 , C_2 , C_3 , C_4 , and C_5 alkanes. The ratios of C_1/C_2 against sub-bottom depth (m) are shown in Figure 26.

The details of our gas analysis of each hole are given below.

Hole 583

Using the old batch of vacutainers, we analyzed 14 gas samples from this hole. The concentrations of methane show almost no change from 0 to 139 m sub-bottom. The low content of methane in some cores may be due to air contamination resulting from poor core recovery. Up to Core 5 (~40 m sub-bottom), punched core liners emitted a strong smell of H_2S , and gases bubbled out along with a mixture of sediment and water. In spite of this display, only trace quantities of H_2S were detected (Table 4). We did detect gases up to isobutane, however. The quantity of C_2 to isobutane is very low (0.10 to 3.9 ppm). Except in Sections 583-9-1, 583-10-3, 583-20-1, and 583-23-2, all gas compositions show higher propane than ethane. The C_1/C_2 ratio is always beyond 10^5 and varies between 101,500 to 530,600 (Fig. 26).

Hole 583A

Gases are present throughout the cored interval, except for the first core. Cores 2 and 3 are somewhat different from the other cores (Fig. 27), because they con-

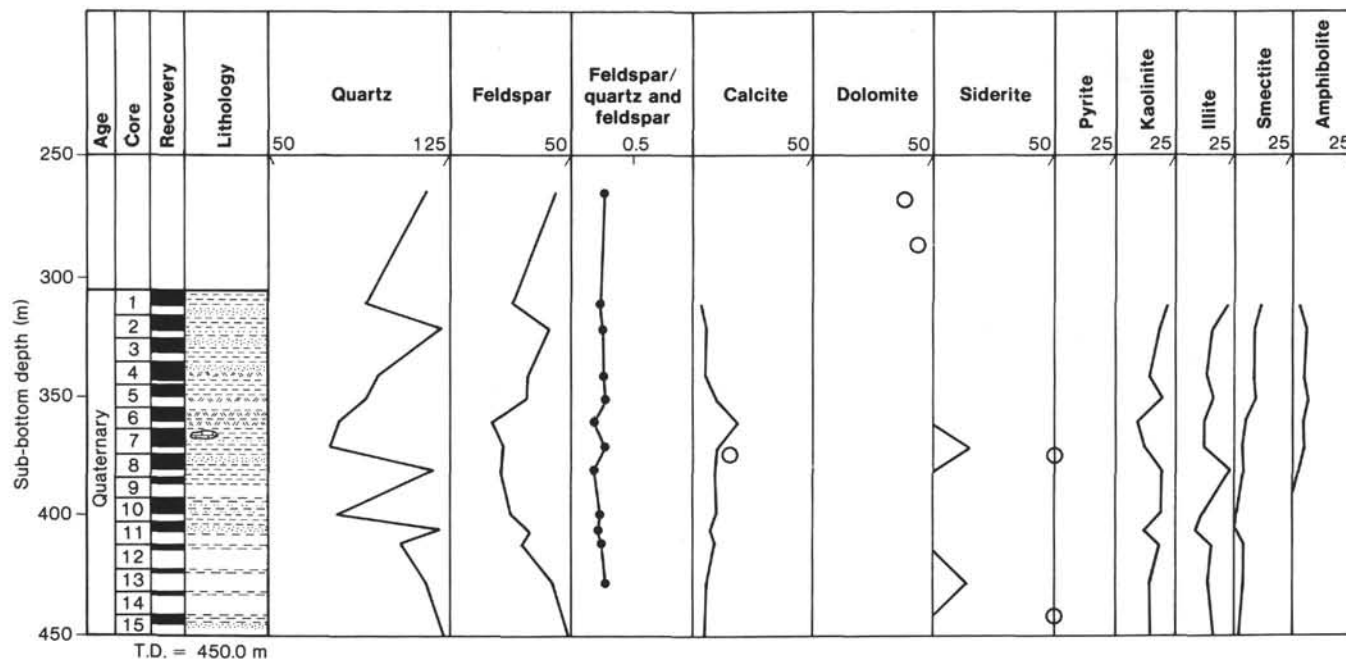


Figure 23. Summary of X-ray mineralogy for Hole 583G. X-ray intensity is expressed in arbitrary units. Large open circles are X-ray intensities measured on nodules.

tain relatively high concentrations of normal butane and normal pentane. In general, C_1 varies from 57 to 70% of the gas volume. C_2 , C_3 , C_4 , and C_5 alkanes are very low and never exceed 4 ppm. Except in Section 583A-9-2, propane (C_3) is always higher than ethane (C_2). Most of the sediments contain C_2 , C_3 , isobutane, normal butane, and pentane. No neopentane or isopentane was detected. The C_1/C_2 ratio is similar to that recorded for Hole 583, except in some cases it is slightly higher. The CO_2 content varies from 0.6 to 2.3%.

Holes 583B and 583C

The gas composition shows no detectable normal butane or normal pentane. Otherwise, compositions ranging from C_1 to $i-C_4$ and C_1/C_2 ratios are similar to those recorded for Holes 583 and 583A. We analyzed six samples from these two holes. In most of the cores, propane is higher than ethane.

Hole 583D

This well was drilled to satisfy the JOIDES Safety Panel requirements for monitoring the amount and composition of hydrocarbons across the thrust plane shown in seismic reflection Profile N55-3-1 (Fig. 39). It was drilled from 47 to 327 m sub-bottom. We analyzed 20 cores, out of which we took 10 direct gas samples by syringe after punching the core liner. In most cases, the direct samples showed higher gas volumes in air (greater than 80%). Both the direct and vacutainer samples show that the C_1/C_2 ratios exceed 10^5 (Fig. 26). Nearly all of the cores contain ethane, propane, and isobutane. Isopentane appeared beneath Section 583D-10-1 (142 m sub-bottom). Normal butane and neopentane were present only in trace quantities in some cores. A typical example

of n -alkane distribution from Section 583D-16-2 is shown in Figure 28. As in the other holes, propane is generally more abundant than ethane and at Hole 583D is mainly restricted to sandy and silty layers. The concentration of ethane and propane is higher than at the Site 583 HPC holes.

Hole 583F

Sediments were cored in this hole between 200 to 440 m sub-bottom. In general, methane content (percent in air volume) is very high, reaching a maximum of 96%. Downhole to Section 583F-16-2, light hydrocarbon gases up to $i-C_4$ were detected. Between Sections 583F-16-2 and 583F-29-2 (last core analyzed), gases up to isopentane were detected, and the amounts of C_2+ hydrocarbons in this interval are generally the highest among all the holes. In Section 583F-27-1 ethane content is 41.6 ppm. The C_1/C_2 ratios vary from 21,100 to 261,900 (Table 4, Fig. 26). Down to Section 583F-16-2, the amount of propane exceeds ethane, particularly in sandy and silty layers, but below that section, the amount of propane is variable, and after Section 583F-26-1, the concentration of ethane is higher than that of propane. This is the only hole where C_1/C_2 ratios show progressive decrease as depth increases (Fig. 26).

Carbon Chemistry

Nine samples were analyzed for amounts of total carbon and organic carbon (Table 6). In Hole 583, organic carbon content is variable (0.43 to 0.75%), and total carbon varies according to organic carbon. In Hole 583F, organic carbon content is more than 0.5%, the minimum level of organic carbon needed for a clastic source rock to generate appreciable amount of hydrocarbon.

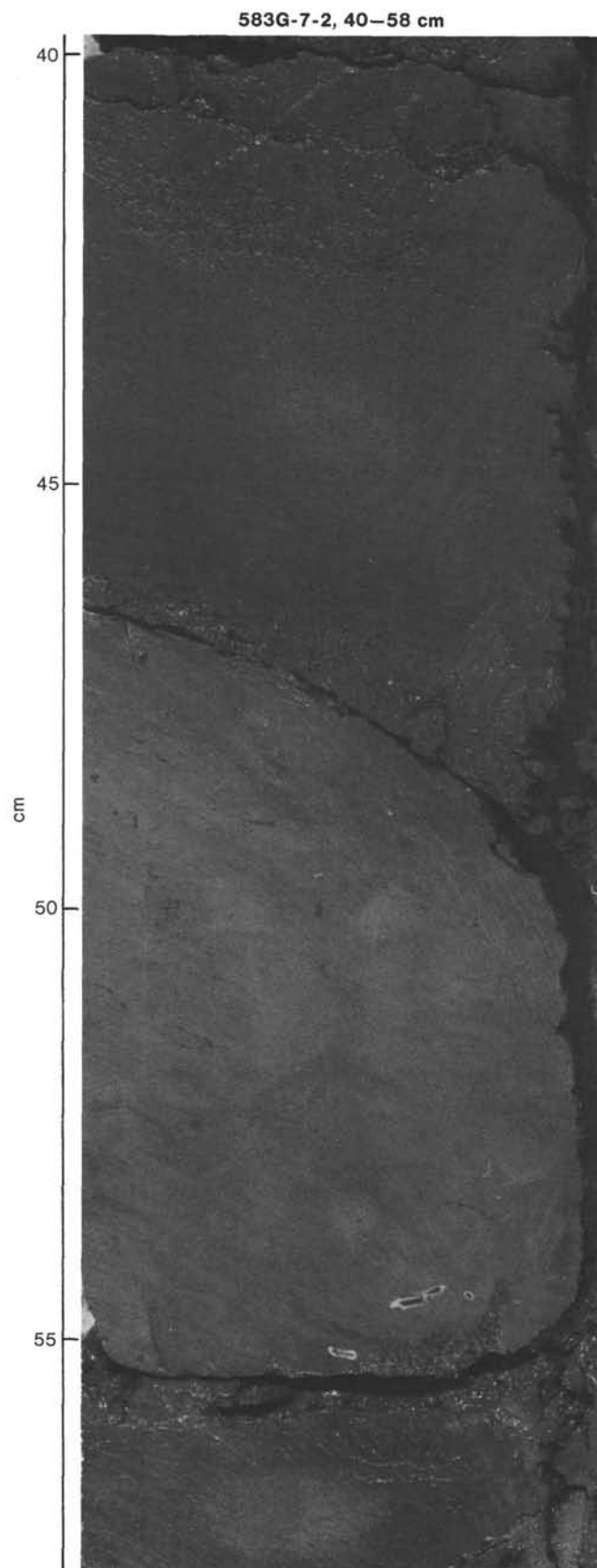


Figure 24. Siderite nodule in Core 583G-7.

Table 3. Composition of gases in the three batches of empty vacutainers (He-gas from Becton-Dickinson) available during Leg 87.

Lot number	C ₂	C ₃	i-C ₄	C ₄	neo-C ₅	i-C ₅	C ₅
8105487	Trace	0.45		0.22			0.21
OF-127	4.38	1.19	1.12	1.03	0.41	0.31	0.10
9M-116	3.78	1.08	0.92	0.79	0.40	0.10	0.10

Note: See Table 5 for definitions of C₂-C₅.

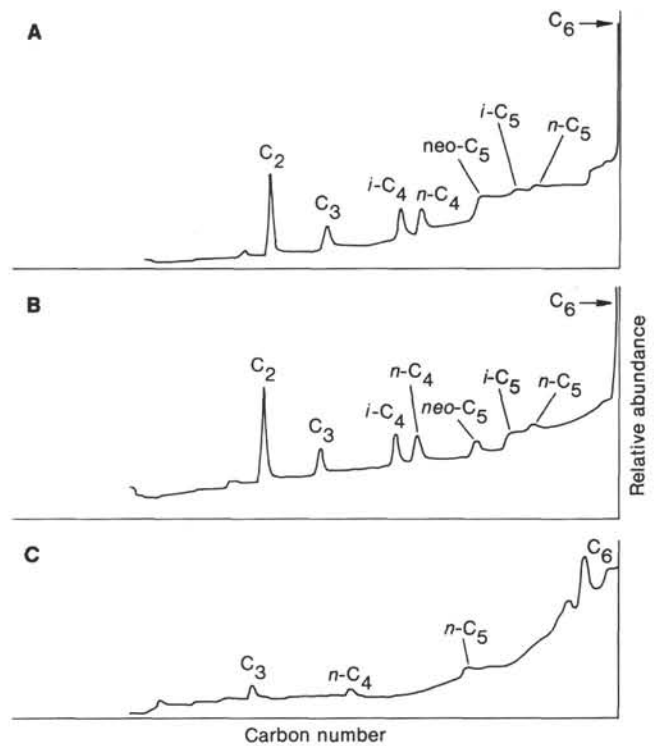


Figure 25. Chromatograms for the three sets of empty vacutainers available during Leg 87. A. Vacutainer blank run, Lot No. 9M-116. B. Vacutainer blank run, Lot No. OF-127. C. Vacutainer blank run, Lot No. 8105487.

Gas Hydrate

Neither solid hydrate nor high gas pressure were encountered at Site 583. Gas hydrates are mainly crystalline compounds in which the ice lattice of water expands to form cages that contain gas molecules up to i-C₄ (Hunt, 1979). Pentane and n-butanes are too large for this cage. Near the gas-hydrate zone, salinity is greatly reduced and alkalinity increases. At the pressure-temperature stability field for the great water depths beneath the oceans, gas hydrates can form at temperatures as high as 27°C (Hunt, 1979). The geothermal gradient, about 5°C/100 m, indicates that gas hydrate could form anywhere at Site 583; however, we never observed any frozen icelike material in the core liner, and the salinity is not low enough to indicate the presence of gas hydrates in any of these cores. Considering the absence of higher hydrocarbons beyond i-C₄, the uniformity of gas composition, and the high alkalinity, we assume that if

Table 4. Carle gas data from Site 583.

Hole	Core-Section	Method	Methane (C ₁ in vol.%)	C ₁ /C ₂ (× 10 ⁻³)	CO ₂ (%)	H ₂ S
583	2-5		73.45	253.300	0.72	Trace
	3-6		70.91	270.600	1.11	Trace
	4-6		63.44	360.500	1.77	Trace
	5-5		72.10	397.400	1.13	Trace
	7-6		67.04	392.400	1.16	None
	8-4		55.07	432.200	0.93	None
	9-1		30.12	101.500	0.12	None
	10-3		32.95	116.400	0.17	None
	13-1		45.34	362.700	0.33	None
	14-1		48.97	362.700	0.94	
	17-1		65.16	513.100	1.21	
	19-1		60.73	530.600	1.98	
	20-1		62.08	395.400	1.08	
	23-2		56.64	207.100	0.51	
583A	2-3		62.99	346.100	0.634	
	3-3		68.35	427.200	0.804	
	4-3		70.12	547.800	1.02	
	5-2		65.00	625.000	1.00	
	6-2	Vacutainer	66.95	619.900	0.755	
	7-1		64.72	492.900	1.10	
	8-1		70.76	735.800	0.692	
	9-2		62.34	167.600	0.998	
	10-2		70.57	664.900	0.950	
	11-2		57.45	407.446	2.342	
	2-2		66.3	383.200	0.599	
	3-2		66.65	396.600	1.359	
	4-2	74.03	417.900	1.241		
	5-3	76.78	673.500	0.934		
583C	2-1	70.45	448.700	1.07		
3-2	57.06	538.300	0.864			
583D	3-1	48.75	455.600	1.65		
	6-2	63.50	466.900	1.34		
	7-1	36.10	229.600	0.87		
	8-1	58.64	333.200	1.42		
	9-3	68.92	133.000	0.76		
	10-1	50.09	218.700	1.10		
	11-1	47.16	354.600	1.14		
	12-1	Direct	94.05	427.500	1.58	
	12-1	Vacutainer	60.58	275.400	1.39	
	13-1	Direct	87.83	675.600	1.69	
	13-1	Vacutainer	37.63	287.200	1.15	
	14-2	Direct	91.68	377.300	1.38	
	14-2	Vacutainer	65.22	268.400	0.99	
	15-2	Vacutainer	63.07	123.400	1.06	
16-2	Vacutainer	57.49	112.900	1.44		
17-2	Vacutainer	61.78	172.600	0.87		
19-2	Direct	89.93	228.500	2.02		
20-1	Direct	23.72	539.100	0.39		
22-1	Direct	96.36	319.100	1.16		
23-1	Direct	94.95	404.000	0.97		
23-1	Vacutainer	54.52	232.000	0.69		
24-4	Direct	93.67	255.200	0.001		
24-4	Vacutainer	74.48	202.900	0.61		
25-2	Direct	83.99	171.200	1.06		
29-1	Direct	96.60	185.800	0.40		
29-1	Vacutainer	60.10	241.400	0.83		
583F	6-2	Vacutainer	76.01	212.900	0.884	
	12-1	Direct	96.17	182.500	0.440	
	12-1	Vacutainer	70.18	133.200	0.334	
	13-1	Direct	8.13	165.900	0.143	
	13-1	Vacutainer	9.33	189.200	0.098	
	14-2	Direct	87.72	261.900	0.854	
	14-2	Vacutainer	80.35	239.900	0.349	
	16-2	Direct	93.02	155.200	0.392	
	16-2	Vacutainer	78.51	130.900	0.380	
	17-1	Direct	78.46	75.930	0.760	
	18-1	Vacutainer	84.75	141.700	0.504	
	19-1	Direct	59.08	113.600	1.013	
	19-1	Vacutainer	68.75	132.200	0.931	
	20-1	Direct	94.79	62.360	0.333	
	20-1	Vacutainer	28.57	53.500	0.235	
	24-1	Direct	89.52	68.340	0.314	
	25-2	Direct	88.72	96.960	0.930	
	26-1	Direct	95.55	71.250	0.605	
26-1	Vacutainer	84.14	62.800	0.483		
27-1	Direct	93.96	22.570	0.218		
27-1	Vacutainer	87.79	21.100	0.272		
29-1	Vacutainer	28.02	33.042	0.158		

Note: See Table 5 for ethane (C₂) values.

gas hydrate is present at all in Holes 583B and 583C, it is in a dispersed form.

Summary

Light hydrocarbon gases at Site 583 are mainly methane with variable amounts of alkanes up to isopentanes, the latter in very low concentration. Gases up to pentane in a very shallow core in Hole 583A may indicate a change of kerogen type and organic facies.

The C₁/C₂ and C₁/C₂₊ ratios generally exceed 10⁵, and a change with depth occurs only in Hole 583F. These ratios generally decrease with increasing depth. This trend may indicate either the migration of light hydrocarbon gases from the thrust plane or a normal maturation profile with increasing organic carbon level.

The origin of these gases is difficult to predict because of the higher concentration of propane over ethane, but high methane content and presence of H₂S and CO₂ with low concentrations of C₂₊ hydrocarbon indicate a biogenic or early diagenetic origin. The relative prevalence of propane over ethane is still an enigma. We assume that this is due to uneven pressure release of dispersed solid or liquid gas hydrates into a gaseous state at normal conditions of pressure and temperature.

Organic carbon content is, in general, higher than 0.5% in the deeper sediment.

Hydrocarbons at Hole 583G³

The purpose of organic geochemical sampling at this site was primarily twofold: (1) to monitor light hydrocarbon gases for satisfaction of JOIDES Safety Panel requirements, and (2) to detect possible hydrocarbon migration along the thrust fault plane underlying this site.

Sampling of gases was performed according to the procedure previously described. Initially we used vacutainers that had been evacuated for 3 minutes by a vacuum pump; later we switched to flushing the vacutainers briefly with helium and evacuating several times using a large syringe. Neither technique proved to be wholly satisfactory, as spurious peaks in the C₆₊ range continued to appear in the chromatograms and are attributed to the vacutainer contamination described for the previous Site 583 analyses. In an effort to circumvent this problem as much as possible, cores below the wash-down zone (i.e., beginning around 315 m sub-bottom) were sampled both by the vacutainer method and also directly through the core liner with a 10-ml syringe. These samples were then used for the methane and the C₂-C₂₊ determinations, respectively. The standards used for chromatograph calibration and calculation of the response factors are the Scott analyzed gases; methods for gas analyses using the Carle and Hewlett-Packard chromatographs are as previously described. Because of lack of time and experience on the part of the analyst, no or-

³ Editor's note: *Glomar Challenger* returned to Site 583 unexpectedly, after Leg 87A scientists had disembarked at Yokohama. The organic geochemists were among those that had left. Because the JOIDES Safety Panel required continuous monitoring of light hydrocarbons at Site 583, a replacement for Drs. Machihara and Mukhopadhyay had to be found. Dr. Carol Stein offered to perform the necessary analyses and interpretations. Her findings regarding hydrocarbons at Hole 583G offer an interesting cross-check and confirmation of the results obtained by the Leg 87A team.

Table 5. Composition of gases in samples from Site 583—Hewlett-Packard gas data.

Hole	Core-Section	Method	Ethane (C ₂)	Propane (C ₃)	Isobutane (i-C ₄)	Butane (C ₄)	Neopentane (neo-C ₅)	Isopentane (i-C ₅)	Pentane (C ₅)	
583	2-5		2.90	3.33	N.D.					
	3-6		2.62	2.64	0.29	N.D.	N.D.	N.D.	N.D.	
	4-6		1.76	3.04	0.45					
	5-5		1.81	2.86	0.29					
	7-6		1.80	3.92	0.30					
	8-4		1.28	2.63	0.22					
	9-1		2.97	1.20	0.22					
	10-3		2.83	0.52	Trace					
	13-1		1.25	1.82	0.11					
	14-1		1.35	2.02	0.12					
	17-3		1.27	2.08	0.20					
	19-1		1.14	2.57	0.20					
	20-1		1.57	1.40	0.10					
	23-2		2.73	1.30	Trace					
583A	2-3		1.82	3.52	0.67	2.36	N.D.	N.D.	2.35	
	3-3		1.60	3.03	0.45	0.59			0.97	
	4-3		1.28	2.26	0.36	0.36			0.96	
	5-2		1.04	1.90	0.34	0.56			0.49	
	6-2		1.08	2.00	0.22	0.18			0.21	
	7-1		1.31	2.04	0.25	Trace			0.17	
	8-1		0.96	2.38	0.16				Trace	
	9-2		3.72	1.54	0.11					
	10-2		1.06	2.10	0.16				Trace	
	11-2		1.41	2.37	0.31	Trace			Trace	
	583B		2-3	Vacutainer	1.72	1.73	0.17			
3-2		1.98	1.68		0.13					
4-2		1.77	1.83		0.17					
5-3		1.14	1.88		0.11					
583C	2-1		1.57	1.97	0.13					
	3-2		1.06	1.69	0.10					
583D	3-1		1.07	2.33	0.18	N.D.	N.D.	N.D.	N.D.	
	6-2		1.36	2.15	0.21					
	7-1		1.57	1.74	0.21					
	8-1		1.76	2.67	0.40					
	9-3		5.18	1.90	0.38					
	10-1		2.29	2.08	0.36			Trace		
	11-1		1.33	1.68	0.34			0.14		
	12-1		2.20	4.36	0.62			0.27		
	13-1		1.31	1.86	0.38			0.15		
	14-2		2.43	2.44	0.29					
	15-2		5.11	4.47	0.71			0.18		
	16-2		5.10	6.02	1.23	Trace	Trace	0.36		
	17-2		3.58	7.38	1.21	Trace	Trace	0.36		
	19-2		3.93	6.57	0.81			0.11		
	20-1		0.44	0.62						
	22-1		3.02	4.37	0.75			0.18		
	23-1		2.35	3.78	0.71			0.45		
	24-4		3.67	5.49	0.78			0.27		
	25-2		4.91	6.54	0.43			0.36		
583F	29-1		5.20	4.30	0.41		Trace	Trace		
	6-2		Vacutainer	3.57	5.20	0.20	N.D.	N.D.	N.D.	N.D.
	12-1		Direct	5.27	4.90	0.42				
	13-1		Vacutainer	0.49	0.67					
	14-2		Vacutainer	3.35	5.60	0.63				
	16-2		Vacutainer	6.00	5.10	0.51				
	17-1		Direct	10.33	5.03	0.60			0.17	
	18-1		Vacutainer	5.98	7.25	0.86	Trace		0.10	
	19-1		Vacutainer	5.20	8.62	1.87	0.18		0.20	
	20-1		Direct	15.20	4.04	0.20			Trace	
	24-1		Direct	13.1	2.04	0.15			Trace	
	25-2		Direct	9.15	11.80	3.35	0.36	0.17	0.53	
	26-1		Vacutainer	13.4	7.27	2.04	0.32	0.13	0.90	
27-1	Vacutainer	41.6	3.21	0.36			0.33			
29-1	Vacutainer	8.48	2.32	0.47	0.34		0.33			

Note: N.D.: <0.1 ppm.

ganic carbon measurements were made on material from Hole 583G.

The C₁/C₂ (and C₁/C₂₊) ratios from the analyses at Hole 583G are virtually identical to those obtained at Hole 583F (Fig. 26). Because Hole 583G did not extend into previously unsampled horizons, no new trends were seen; it is not possible to draw any new conclusions from the hydrocarbon analyses at this hole other than to state

that the close agreement of the data confirms the data of the previous investigators and possibly their interpretations as well.

PHYSICAL PROPERTIES

Physical properties measured on board for samples from Site 583 include wet-bulk density, water content, porosity, shear strength, and sonic velocity (Appendix at

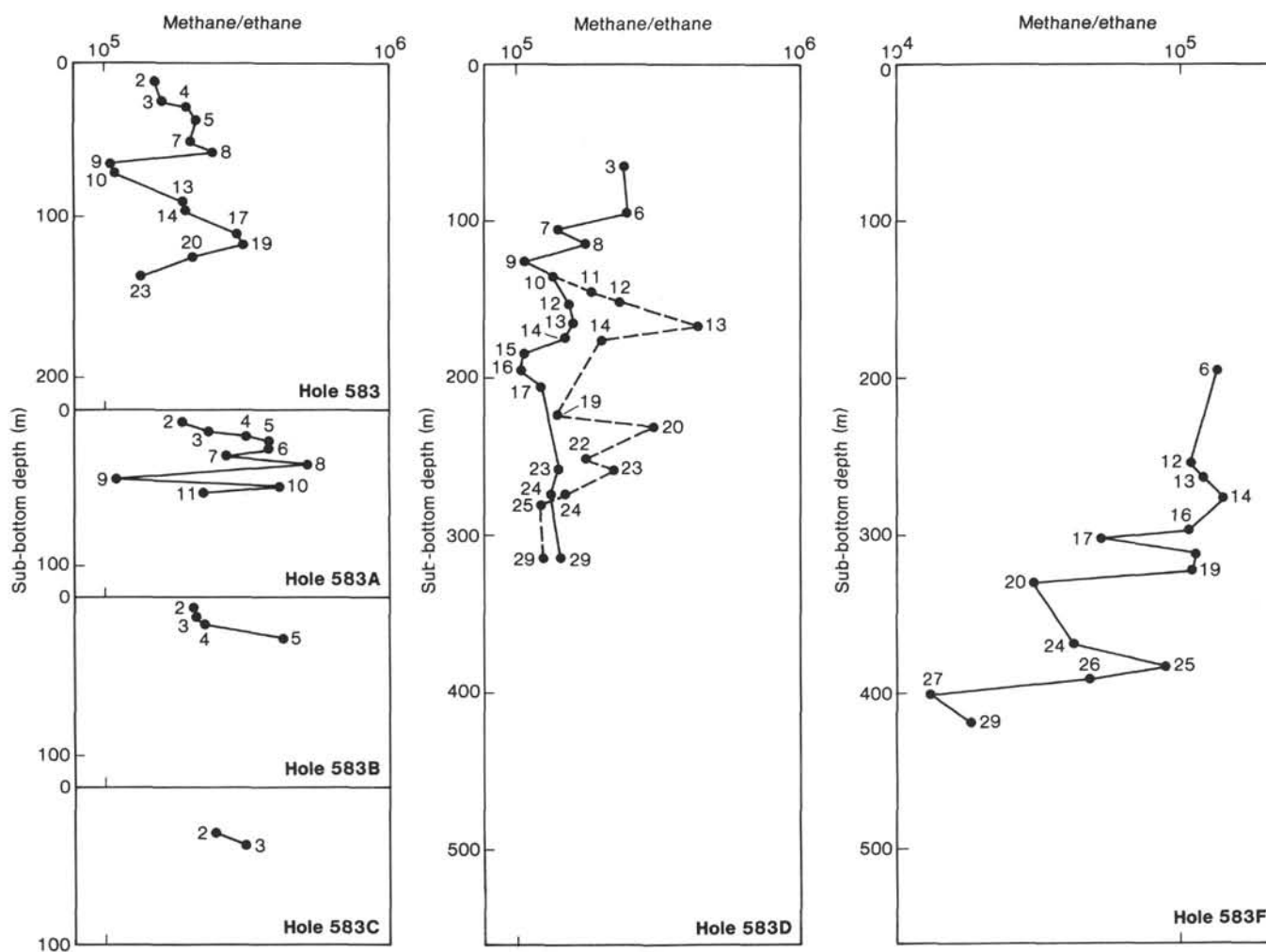


Figure 26. Methane/ethane (C_1/C_2) ratios versus sub-bottom depth at Site 583. Numbers indicate cores from where gas analysis was done. "Direct" measurements are connected with dashed lines; all others are vacutainer measurements.

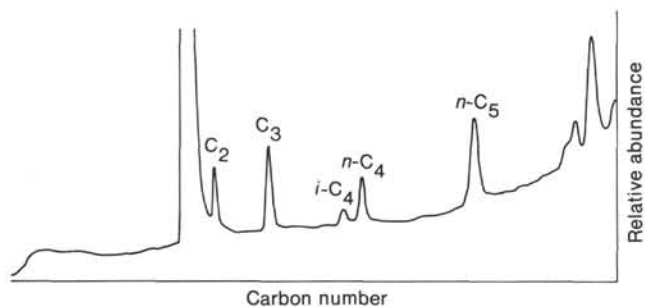


Figure 27. Gas chromatogram for Section 583A-2-3.

the end of this volume). Grain densities of representative samples were measured postcruise. The data from these eight holes are presented in four composite sections (arranged in order from the most seaward to the most landward). Sampling frequency in each of the holes depended on recovery rate, coring disturbance, sample cracking, and volume increase caused by gas expansion upon pressure release during the coring process. Care was taken to sample only the most undisturbed inter-

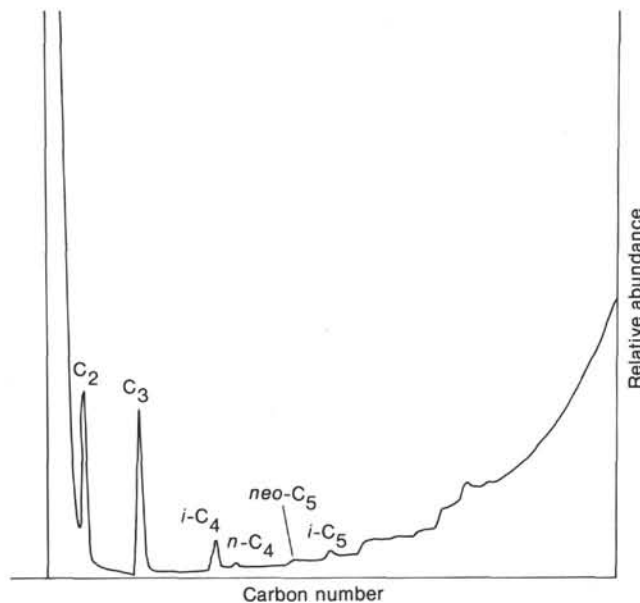


Figure 28. Gas chromatogram for Section 583D-16-2.

Table 6. Organic carbon analysis, Site 583.

Hole-Core-Section (interval in cm)	Total carbon (%)	Organic carbon (%)
583-2-3, 109-111	0.83	0.46
583-7-2, 5-7	1.18	0.75
583-11-3, 0-2	0.72	0.55
583-14-1, 5-7	0.58	0.43
583F-12-1, 54-55	0.65	0.62
583F-16-1, 65-67	1.57	0.70
583F-20-2, 1-3	1.01	0.69
583F-25-1, 80-82	1.15	0.95
583F-29-2, 14-16	1.31	0.77

vals. Additional plots and discussions of the data are included in Bray and Karig (this volume).

Holes 583B, 583C, and 583D

Holes 583B, 583C, and 583D, located on the lower slope of the Nankai Trough, penetrated to a total depth of 326.6 m sub-bottom. Excellent physical property data were anticipated from the relatively undisturbed hydraulic piston cores of Holes 583B and 583C. Unfortunately, gas expansion caused significant alteration of *in situ* sediment fabric and structure.

All the physical properties samples from Holes 583B and 583C were taken in Boyce cylinders. Boyce cylinders were used for Cores 583D-3 through 583D-19. Chunk specimens from Cores 22 through 29 of Hole 583D were cut and trimmed with a razor blade. A rock saw was not required for sampling in this composite hole. When the condition of the sample permitted, the same sample was used for 2-minute GRAPE, water content, and sonic velocity measurements.

Cracking and volume increase caused by gas expansion upon pressure release during sampling adversely affected wet-bulk densities determined from the continuous analog GRAPE records. As a result, only the maximum sustained wet-bulk densities from the continuous GRAPE are considered reliable. In this composite hole, maximum sustained wet-bulk densities increase down-hole from 1.80 Mg/m³ at the sediment/water interface to 1.92 Mg/m³. Wet-bulk densities determined from special 2-minute GRAPE counts on 64 Boyce-Cylinder and chunk-type samples increase from an average of 1.65 Mg/m³ at the sediment/water interface to about 1.95 Mg/m³ at 326.6 m sub-bottom.

Water content (percentage wet weight) was determined for all Boyce cylinder and chunk samples used previously for the special 2-minute GRAPE measurements. Water content decreases from approximately 35% at the sediment-water interface to about 23% at the base of the section.

Sediment porosities were calculated from the maximum sustained GRAPE wet-bulk densities, 2-minute GRAPE wet-bulk densities, and water content measurements (see Appendix at the end of this volume). In spite of the difficulties of accurate weighing at sea, the porosities calculated from water contents are considered to be least affected by gas expansion and most representative of *in situ* conditions. Porosity decreases rapidly within the two HPC holes from a maximum of about 60% to

about 50% by 50 m sub-bottom (Fig. 29). Below 95 m, porosity decreases at a decreasing rate, reaching a minimum of about 43% at the base of the drilled section. Because of the lack of recovery, no data are available for the interval from 50 to 95 m. This zone apparently consists of sediments too stiff to penetrate with the hydraulic piston corer, yet too soft to drill without severe deformation. A coarse sand unit could also account for lack of recovery. Alternatively, the seismic reflection Profile N55-3-1 (Fig. 39) indicates a potential zone of thrusting, which could be a contributing factor to poor recovery. Regardless of the cause, poor recovery in this zone prevents correlation of the data sets from hydraulic piston cores and rotary cores.

A second thrust zone near 155 m sub-bottom was also a zone of poor recovery. Although limited by recovery, the data suggest no anomalous physical properties for this zone.

Because of gas expansion, only 13 vane shear tests are considered reliable and those are from the upper 40 m of Hole 583B. Surface cracks developed before shear failure in all the vane shear tests of Hole 583D. The rate of increase in shear strength with depth, as determined by the maximum obtained value, is about 3.0 kPa/m (Fig. 29). Sensitivity (ratio of undisturbed to remolded shear strength) ranges from 2.5 to 5.1 and averages 3.7. The pocket penetrometer was a useful means of measuring shear strength in the upper 220 m of the section. Below this depth, valid tests were difficult because of surface cracking. The shear strengths measured with the Torvane are considerably lower than those measured with the other two methods. Excessive scatter in the data obscures any relation that might exist between strength and depth.

Only two compressional-wave and shear-wave velocity measurements were possible in the 50-m length of HPC sample because of high energy attenuation resulting from gas and associated expansion cracks. Compressional-wave velocities are 1.64 and 1.60 km/s and corresponding shear-wave velocities are 0.51 and 0.50 km/s. In the rotary-drilled Hole 583D, a complete sequence of measurements were taken. Compressional-wave velocities increase with depth from 1.58 km/s at 67 m to 1.64 km/s at 278.5 m sub-bottom. Shear velocities at the same depths are both 0.36 km/s.

Holes 583, 583E, and 583F

Holes 583, 583E, and 583F, located 475 m upslope from Holes 583B, 583C, and 583D, combine to form the second composite hole for Site 583. At Hole 583, the upper 152 m of the section were piston cored but as in Holes 583B and 583C, high gas content altered the structure of the hemipelagic mud and thus its physical properties. Rotary coring in Hole 583E yielded only one interval with measurable physical properties. Recovery was limited at rotary core Hole 583F, but was sufficient to allow collection of good samples for wet-bulk density water content, porosity, and sonic velocity measurements.

Maximum sustained wet-bulk densities, as measured by the continuous GRAPE in Hole 583, range from 1.61 to 1.99 Mg/m³ with no apparent increase with depth. In Hole 583F, maximum sustained wet-bulk densities in-

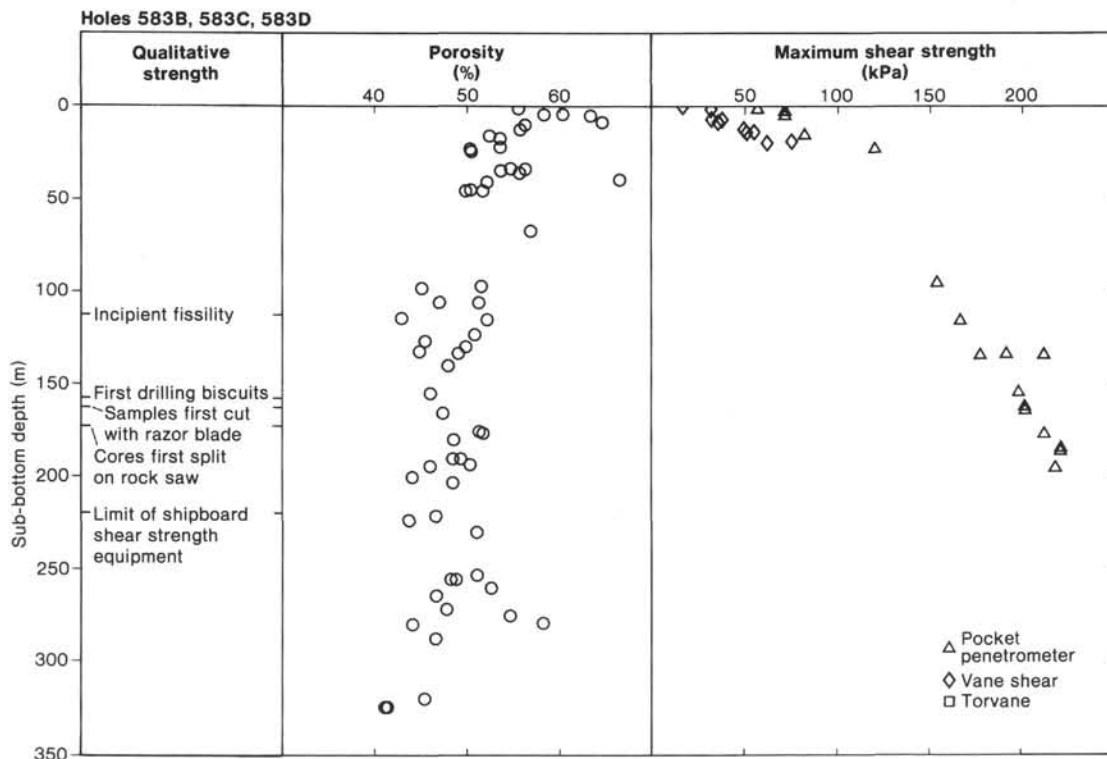


Figure 29. Porosity and maximum shear strength versus sub-bottom depth for composite Holes 583B, 583C, and 583D. Porosities are calculated from water contents using grain densities listed in the Appendix at the end of this volume.

crease gradually and sporadically from about 1.85 Mg/m^3 at 200 m to about 1.95 Mg/m^3 at 420 m sub-bottom. Special 2-minute GRAPE wet-bulk densities increase from 1.62 to 1.85 Mg/m^3 with depth through the entire 152-m interval cored at Hole 583. The wet-bulk density of the only sample from Hole 583E is 1.92 Mg/m^3 . In Hole 583F, wet-bulk densities, as measured with special 2-minute GRAPE counts, vary from 1.75 to 2.06 Mg/m^3 , again with no significant increase with depth.

Water contents (percentage wet weight) in this composite hole initially decrease with depth, but below 250 m remain constant.

As expected, because of the gassy and disturbed nature of the entire assemblage, the porosities determined from water contents in Hole 583 are consistently lower than those from the 2-minute GRAPE samples. Porosities decrease continuously with depth from $\sim 62\%$ at 0 m to $\sim 45\%$ at 150 m sub-bottom (Fig. 30). The porosity in Hole 583E at 160 m is 43% . Because of the paucity of data from Hole 583E and the upper 100 m of Hole 583F, the porosity value is unclear between 140 and 300 m sub-bottom. From 300 m to the bottom of Hole 583F at 439.7 m, the porosity remains nearly constant at 42 to 43% . As in Holes 583B, 583C, and 583D, the nature of the transition between the zone of rapid porosity decrease and that of nearly constant porosity is unknown because of limited recovery. This section of nonrecovery again lies at the transition from hydraulic piston coring to rotary coring.

Valid shear-strength measurements were obtained only through Core 20 at 124 m in Hole 583. Maximum vane shear strengths indicate an increase of shear strength

of about 0.6 kPa/m (Fig. 30). The sensitivity of the sediment in the top 30 m ranges from 1.6 to 5.2 with an average of 3.4. Shear strengths, as measured by the Soiltest Torvane on clay and silty clay intervals in the upper 30 m, increase in strength at the rate of 1.2 kPa/m . The maximum pocket penetrometer shear strengths plotted in Figure 30 agree well with the vane shear and Torvane data and show a 1.0 kPa/m increase in strength with depth. Sediments of Hole 583E were too disturbed to warrant measurement for shear strength. The shear strength of all "undisturbed" sediments and rocks of Hole 583F exceeds the capacity of both the vane shear and torvane equipment. Pocket penetrometer tests were attempted, although the brittle and fissile nature of the samples often caused surface cracking. The deepest valid maximum shear-strength measurement is a pocket penetrometer value of 202 kPa at 201.5 m sub-bottom.

Sonic velocities were obtained in the gassy sediments of Hole 583, but as before yielded compressional velocities less than or barely higher than that of pure seawater (1.38 to 1.77 km/s) and correspondingly low shear velocities (0.29 to 0.52 km/s). Although the sediments recovered from Hole 583F are more coherent and less gassy than those in Hole 583, measured sonic velocities are still low and variable. Compressional velocities range from 1.23 to 1.86 km/s . Shear-wave velocities vary randomly from 0.26 to 0.53 km/s .

Hole 583G

Hole 583G is adjacent to composite Hole 583-583E-583F (Figs. 3, 10). Wash Cores H1 to H5 from Hole 583G contain relatively undisturbed sections and are in-

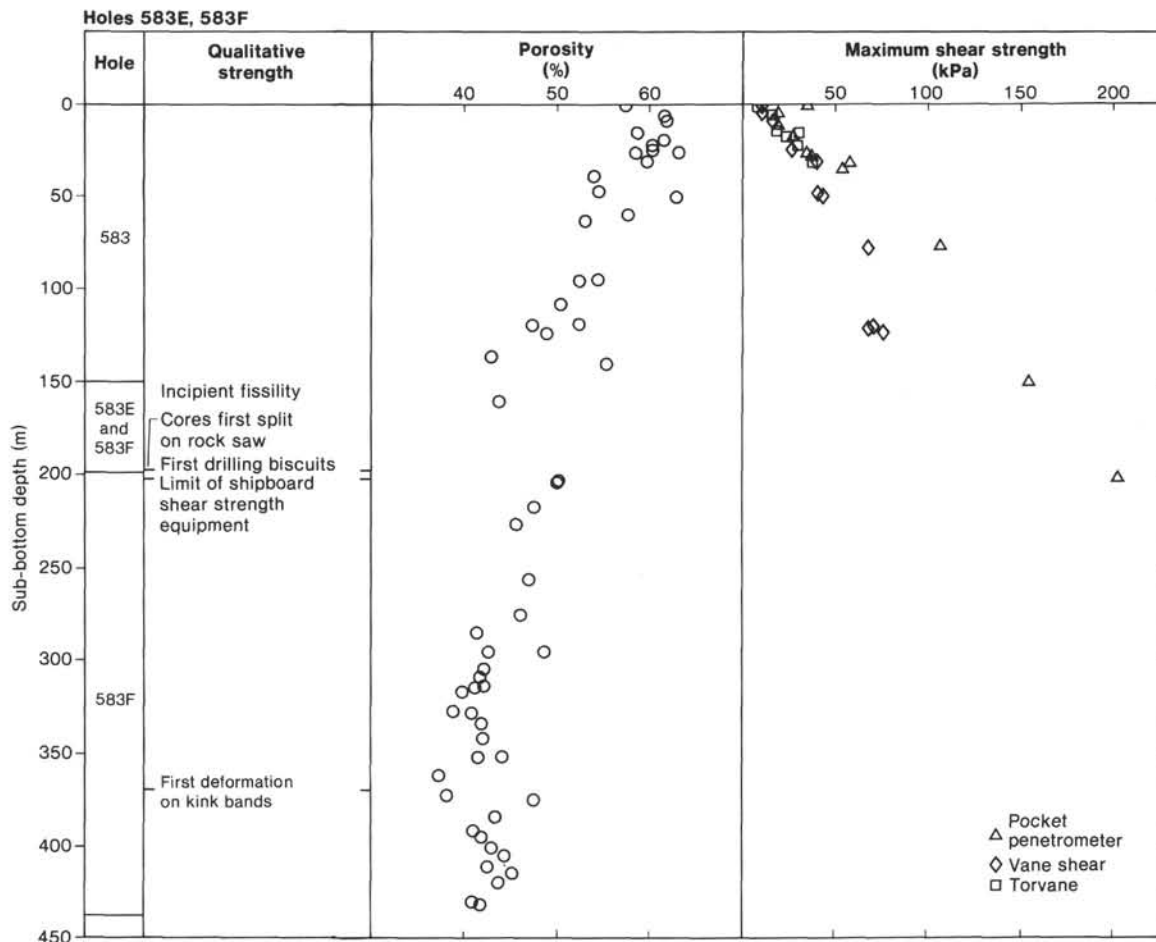


Figure 30. Porosity and maximum shear strength versus sub-bottom depth for composite Holes 583, 583E, and 583F. Porosities are calculated as in Figure 29.

cluded in the data set along with measurements from the continuously cored portion.

Maximum sustained wet-bulk densities in Hole 583G, as measured by the continuous GRAPE, range from 1.73 to 2.07 Mg/m³ and generally increase with sub-bottom depth. Special 2-minute GRAPE wet-bulk densities from Boyce-Cylinder, chunk, and minicore samples vary from a minimum of 1.85 Mg/m³ in Core 8 to a maximum of 2.27 Mg/m³ in a sandy unit of Core 4. The intermediate wet-bulk densities are scattered and increase slightly with sub-bottom depth.

Water contents (percentage wet weight), determined from the special 2-minute GRAPE samples, show a minimum value of 13.7% in the sand of Core 583G-7. Throughout the remainder of the section, porosities varied from 20.2 to 26.2%.

Throughout the wash and continuous cored sections, the porosity was nearly constant at ~40% (Fig. 31). Again, the only exception to the trend was the sand recovered in Core 7 which has a porosity of 28.9%.

The vane shear and Torvane shear equipment were not used at Hole 583G, because the shear strength of all "undisturbed" sediments exceeded the equipment operating capacity. Only five pocket penetrometer measure-

ments were successfully performed without surface cracking, before the capacity of the probe was exceeded at 306 m sub-bottom. Shear strengths are lower in the Hole 583G samples than in those from equivalent depths at Hole 583F (Fig. 31). Perhaps Cores 583G-H1 to 583G-H5 were more disturbed than anticipated. No estimate of rate of increase in strength with depth is made based on this low-quality data.

Sonic velocities were measured for samples from the interval between 361 and 444 m sub-bottom. Compressional-wave velocities vary from 1.61 to 1.76 km/s. Corresponding shear-wave velocities range from 0.38 to 0.42 km/s.

Hole 583A

As at the other HPC holes, recovery at Hole 583A was very good, and sampling disturbance minimal, but gas expansion below a depth of about 10 m degraded the quality of the physical properties data.

Continuous GRAPE maximum sustained wet-bulk densities are very scattered with the maximum value of 1.82 Mg/m³ occurring in Core 1. Loss of coherent sediment structure caused by gas expansion has apparently masked any real changes in sediment wet-bulk density.

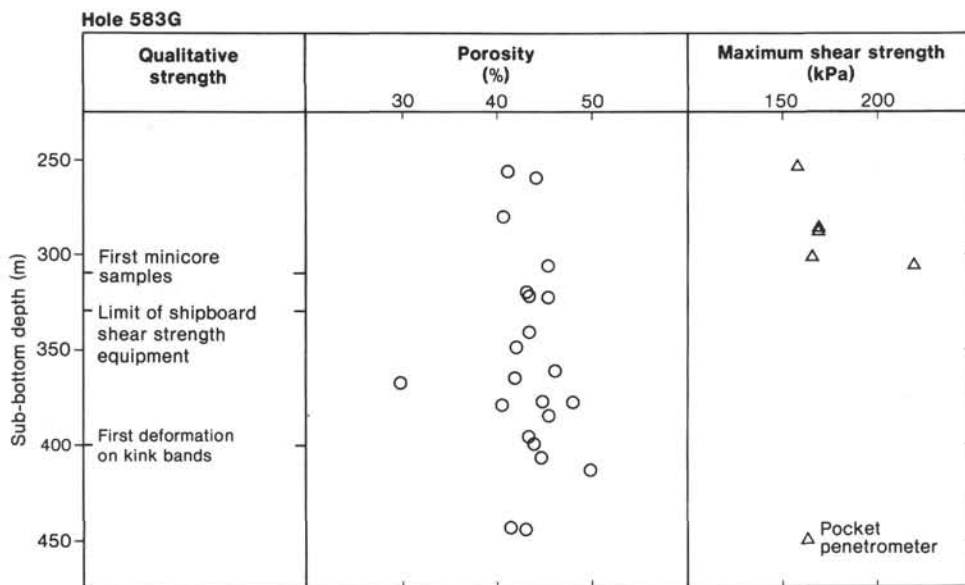


Figure 31. Porosity and maximum shear strength versus sub-bottom depth for Hole 583G. Porosities are calculated as in Figure 29.

Special 2-minute GRAPE counts on Boyce-Cylinder samples showed wet-bulk densities that range from 1.463 to 1.795 Mg/m³, also with little discernible pattern.

The sediment porosities calculated from continuous GRAPE, 2-minute GRAPE, and water content measurements generally agree, but vary about ± 5% at any given depth. The porosity at the sediment/water interface is ~ 63 and decreases to 57% at 54 m.

Only five vane shear tests were successful in causing shear failure on a cylindrical surface before the core surface developed horizontal surface cracks. These tests indicate an apparent increase in shear strength of about 0.5 kPa/m (Fig. 32). Sensitivity, as measured in these five tests, ranges from 2.61 to 8.50 and averages 4.69. Successful Torvane shear-strength measurements show an increase of shear strength of about 0.7 kPa/m. The pocket penetrometer data agree with the other two shear-strength data sets, the maxima (Fig. 32) indicate roughly an increase of 0.5 kPa/m with depth.

Sonic velocities in Hole 583A show no apparent trend with depth. Compressional-wave velocities vary from 1.54 to 1.91 km/s, whereas shear-wave velocities range from 0.40 to 0.58 km/s.

Conclusions

A comparison of porosity and shear-strength distributions in the three composite holes of Site 583 yields the following observations and conclusions. In each of the porosity versus depth curves, porosity decreases rapidly through the top 25 to 125 m of Quaternary sediment, then decreases at a lesser rate to the base of the hole. The zone of rapid decrease increases in thickness with increasing distance of each composite hole from the trench axis. At the same time the rate of porosity reduction with depth decreases upslope. At a given depth, the shear strength decreases landward from the trench axis. The rate of increase in shear strength with depth decreases in successive upslope holes. Two explanations may be suggested. Tectonically induced dewatering and consolidation is perhaps more active at the deformation front than at positions slightly landward. Alternatively, biostratigraphic and structural control suggest that thrust-related slumping or erosion at Holes 583B, 583C, and 583D may have removed the upper 10 to 50 m of the section, resulting in the accelerated consolidation and rapid dewatering of the upper section.

Vitally important to the understanding of the mechanisms of deformation and dewatering at convergent margins is a comparison of the physical properties at various stages of deformation. Site 582, located seaward of the deformation front, and Site 583, on the first structural plateau on the lower trench slope, provide an excellent opportunity for such a comparison. Except for minor fluctuations, the porosity distributions with depth are nearly identical for these two sites. No significant

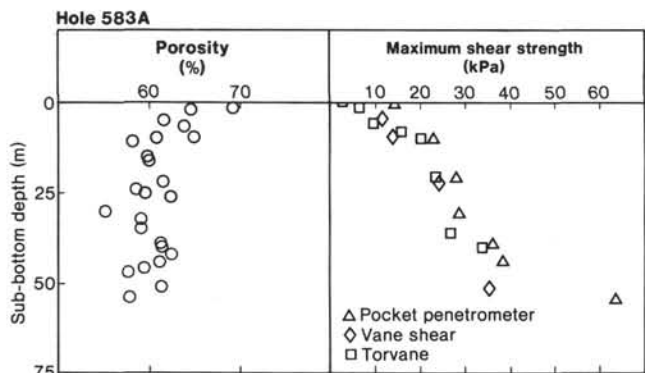


Figure 32. Porosity and maximum shear strength versus sub-bottom depth for Hole 583A. Porosities are calculated as in Figure 29.

difference in porosity was measured between deformed and undeformed sediments at equivalent depths, as suggested by the modeling experiments of Carson and Berglund (in prep.).⁴

The rate of shear-strength increase with depth at Site 583 is 2 to 10 times greater than at Site 582. The reason for the observed increase in shear strength without loss of water remains uncertain, but tectonically induced re-orientation of fragile clay fabrics and structures may be responsible.

PALEOMAGNETICS

Site 583 samples were measured for magnetostratigraphy and orientation of bedding and fault planes. Selected samples were examined for their character of remanent magnetization using a stepwise alternating field (AF) demagnetization method; no significant changes in direction of remanent magnetization were found above the 15-mT step of AF demagnetization. For these samples, the fluctuation for AF demagnetization is small and the inclination is consistent with that of normal polarity of the axial dipole field after bedding correction, indicating that the direction of remanent magnetization after 150-Oe AF demagnetization is reliable for paleomagnetic studies.

All samples were examined routinely for natural remanent magnetization (NRM) and remanent magnetization after 15-mT AF demagnetization. The intensity of the measured samples after demagnetization is 1×10^{-3} to $\sim 4 \times 10^{-1}$ A/m, strong compared with the noise level of the shipboard magnetometer (4×10^{-4} A/m). The relative intensity after demagnetization is 0.715 ± 0.189 versus NRM. The uppermost part of Hole 583 shows weaker magnetization. This pattern is also observed in Hole 582, suggesting a change in provenance of supplied sediments.

Horizontally bedded sediments were drilled in Holes 583, 583A, 583F, and 583G. Most sediments have positive inclination, which indicates normal polarity of the geomagnetic field, and these are correlative with the Brunhes Epoch. Some horizons in the sediments have negative inclination, indicating reversed polarity (Fig. 4). The short reversed polarity horizons match those of the Brunhes Epoch and possibly correlate with similar events observed at Site 582.

We drilled dipping strata in Holes 583C and 583D, and in addition to these, a limited number of paleomagnetic samples were also collected from the same sediments investigated for structural studies (see Structural Geology section, this chapter). In the case of those with positive inclination, the sediments are magnetized to normal polarity, so magnetic declination should be toward the north. Using the declination data to orient the dip direction of bedding planes, we see that their strike is almost constant and is parallel to the axis of the Nankai Trough, but that the dip direction changes 180° across

140 m sub-bottom. For the other samples from Holes 583C and 583D, only apparent inclination before bedding correction is shown. The apparent inclination is significantly shallower above 150 m sub-bottom depth, meaning that in upper interval the bedding planes dip toward the southeast.

Negative inclination occurs in three horizons. In the upper two, the negative inclinations are derived from the steep dips of the bedding plane, as mentioned above. In contrast, the negative inclination of the lower horizon cannot be explained by bedding plane dip because the amount of the apparent inclination is comparable to the positive inclinations, both above and below the horizon. The best explanation is, therefore, that the negative inclination represents a short time interval of reversed polarity.

In Hole 583G, horizontally bedded sediments were drilled, except for the inclined beds in Core 583G-10. Based on declinations, dip-direction of bedding planes are oriented and agree with those from the upper portions of Holes 583C and 583D. The directions are perpendicular to the axis of the Nankai Trough.

HEAT FLOW

Of the 20 heat flow measurements made in Holes 583 through 583F, 15 were successful. Five runs were unsuccessful, probably in part because of the mechanical failure of the latching mechanism in the bottom-hole assembly. The tempered steel composing the latching teeth was evidently of insufficient strength to make a firm latch. Although this possibility was immediately apparent after retrieval of rotary drilling system, doubts were readily raised by the temperature variations sensed by the heat flow probe during operations. In addition, the pressure gage attached to the Barnes *in situ* water sampler and deployed along with the heat flow tool indicated, in some cases, that the tool was hanging in water or in the soft bottom-fill of the hole. In all these cases, the heat flow data were considered to be unreliable (see footnote, Table 7). Eighty-three individual samples were measured for the thermal conductivity with the needle probe (Table 8).

Coincidence of measurements between the two types of heat flow probes, the Tokyo University and the Woods Hole-type tools, is good when the two are used simultaneously. We had an opportunity to do a cross-check run at a sub-bottom depth of 54 m in Hole 583A. The test run was performed by attaching the HPC cutting-shoe tip to the bottom end of the Barnes *in situ* water sampler bulkhead. The arrangement of the tools is: a thermister-sheathing nose about 15 cm long seated in the leading edge of the core barrel, followed by the HPC cutting-shoe tip immediately after the sheathing nose and right around the intake-filter tip of the water sampler (Fig. 33).

The results of the test run for the Woods Hole tool and for the Tokyo University tool show that temperature increased noticeably about 50 minutes after the start of operation of the Tokyo University probe (Fig. 34). Later, the cause of this jump was found to be a loose wiring connection in the electronics circuit, further weakened

⁴ Carson, B., and Berglund, P. L., in prep. Sediment dewatering associated with subduction-accretion: experimental results. A modified viewpoint of these data, which concludes that a small but systematic reduction of porosity takes place at equivalent depth between Sites 582 and 583, is presented in Bray and Karig (1985).

Table 7. Bottom-hole formation temperature, Site 583.

Sub-bottom depth (m)	Temperature (°C) for Hole				
	583	583A	583B	583D	583F
9.0		4.0			
10.0			5.0		
19.0		3.8			
29.0		4.4			
32.5	2.3				
40.9	4.7				
46.2				4.6	
54.2		4.6 ^a			
54.2		4.0 ^b			
76.5				6.1	
121.7				8.3	
135.0	5.5				
148.0	9.7				
172.0				10.4	
219.7					6.7 ^c
220.2				6.0 ^c	
266.0					6.8 ^c
278.4				7.0 ^c	
322.6					11.3 ^c
326.6				8.7 ^c	

Note: No temperature measurements were made in Holes 583C, 583E, or 583G. Assumed bottom-water temperature is 1.75°C.

^a Woods Hole tool temperature.

^b Tokyo University tool temperature.

^c Apparently incomplete emplacement of tools in mud caused by the mechanical failure of a latching tool.

Table 8. Average thermal conductivity values of recovered cores, Site 583.

Hole	Number of measurements	Average value ($\times 10^{-3}$ cal/(cm·deg·s))	Standard deviation ($\times 10^{-3}$ cal/(cm·deg·s))
583	21	3.16	0.38
583A	31	3.39	0.70
583B	0		
583C	0		
583D	15	2.90	0.90
583E	0		
583F	16	3.04	0.48
Site 583	83	3.17	0.61

Note: Heat flow = $1.59 \pm 0.34 \times 10^{-6}$ cal/(cm²·s). (See detailed discussion in the text.)

by a jerking motion of the tool when it latched in. The temperature reading of the Tokyo University tool was, therefore, corrected in reference to the mudline temperature, which in most of the good runs was about 1.8°C. The trend and the difference in the temperature variations recorded by both of the tools are in the sense expected. The temperature variation registered by the Woods Hole tool suggests that it penetrated only a short distance into the bottom mud. Probably because of the poor settling of tools, the temperature could not reach steady state even after 40 minutes of measurements in the mud. No further attempts to run cross-checking tests were made because of shortage of drilling time.

The average temperature gradient is 50.0°C/km (Fig. 35). The heat flow is estimated as 1.59 HFU at this site.⁵

⁵ HFU = heat flow units = $\times 10^{-6}$ cal/(cm²·s).

This value is in good correlation with the regional heat flow value distribution of the area (Fig. 36).

LOGGING

A comprehensive logging program was planned for Sites 582 and 583 in order to detect the changes in physical properties accompanying subduction-related deformation as well as to aid in the lithologic correlation between these two sites. Unfortunately, the bit failed to unlatch at the base of Hole 582B, and it inadvertently unlatched in Hole 583F at a depth of 429 m. Because of the open-ended pipe in Hole 583F, the decision was made to log, despite the discovery that the hole had bridged near 260 m sub-bottom and the requirement to suspend about 90 m of pipe below the mudline.

Four logs were acquired using three different tool configurations (Fig. 37). The first logging run included borehole-compensated sonic, self-potential (SP), dual-induction, gamma-ray (GR), and caliper tools. This array was lowered across the logged interval a second time to acquire sonic-wave-form data. The second tool configuration included GR, compensated-neutron-log (CNL), formation-density (compensated), and caliper tools. This array was run over the loggable interval twice. The third lowering utilized only a borehole temperature log. For all the logs, the hole was filled and conditioned with fresh-water barite gel mud with a density of 1.438 g/cm³ (12 lbs./gal.). The entire logging operation took 26 hr., from the time the hole was conditioned with mud until the rig floor was cleared of logging gear.

The logs are of fair to good quality; in part because the calm seas minimized cable oscillation. Hole conditions degraded log continuity, especially of those measurements most affected by borehole rugosity and large washouts. Over 80% of the hole logged had a diameter greater than the caliper capacity (33.7 cm or 13.25 in.). In the upper section, the hole enlargement appeared to be more regular so that the eccentricized tools could maintain wall contact reasonably well, but large washouts of the less cohesive sands and constricted zones of claystone in the lower part of the logged interval (below about 160 m sub-bottom) led to much poorer log continuity.

Interpretation

Despite the abbreviated logging program, several useful objectives still could be defined. One of the most important of these was to determine the lithostratigraphy over the logged interval and to compare this interpretive section with that inferred from the sparse core recovery. In this way we hoped to understand how well the cores represented the total stratigraphy. The logs also were intended to supply the parameters with which the section could be correlated with the seismic profile. Another important objective was the determination of *in situ* physical properties, their comparison with values measured in the laboratory, and their gradients over the logged interval. Finally, the temperature log was run specifically to test for possible flows of low-temperature water into the borehole within the logged interval.

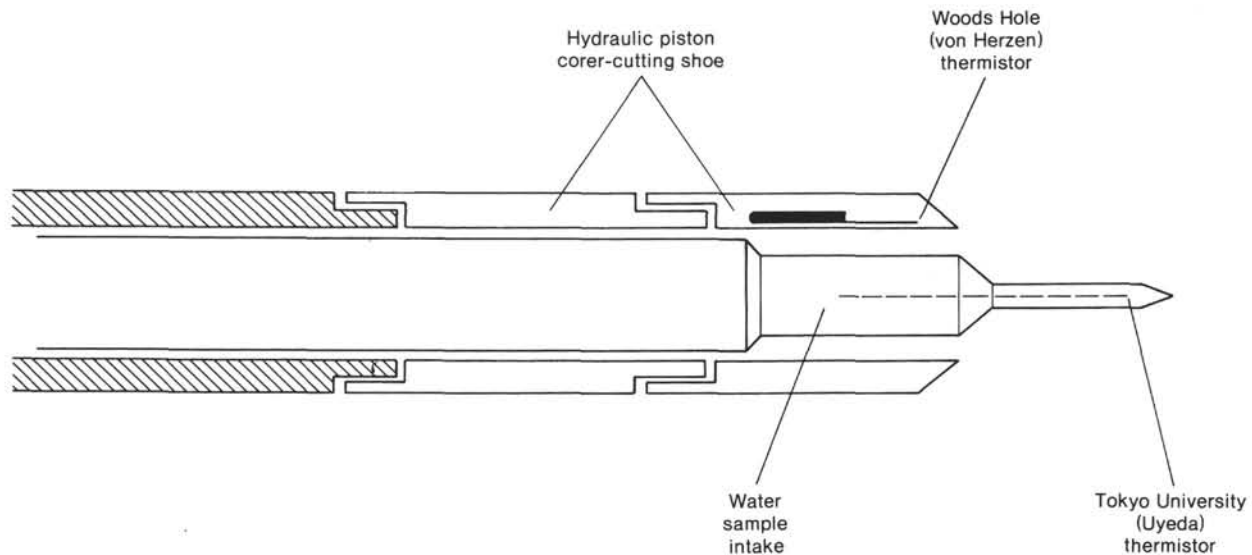


Figure 33. Lateral view of the arrangement of the head portion of the heat flow tool used for the temperature comparison run.

General Background

Values and variations in formation porosity, density, lithology, sonic velocity (V_p and V_s), and borehole temperature were of primary interest in our logging program. Borehole temperature interpretation, assuming proper calibration of the tool, is straightforward and showed a nearly linear gradient of $0.028^\circ\text{C}/\text{m}$ and a maximum temperature of 9°C at 255 m sub-bottom. This value represents a minimum temperature gradient.

Sonic velocities (Table 9) are derived both from transit times (first arrivals of compressional waves) and from the full-wave forms recorded every 6 in. (Fig. 37, Transit time column). Transit times are insensitive to variations in borehole diameter unless the borehole diameter is so large that the wave front through the mud is the first arrival. Transit times that inverted to velocities below about 1.65 km/s and that are correlatable with "washouts" are attributable to first arrivals through the mud. This masking probably completely obscures the slower V_s wave through the formation. For these reasons, the recorded velocities must be interpreted very cautiously.

Lithologies were interpreted from a combination of gamma-ray, porosity, and density logs, assuming that the sediment ranges between clay and sand end members. Gamma-ray curves are perhaps the simplest measure of sand-shale ratio because the clay fraction produces nearly all the natural radiation in this setting and because this log is relatively insensitive to borehole diameter. Clayey sediments also tend to register higher porosities than sands on the compensated neutron log. Porosity values on the neutron log are generally higher than those calculated from the formation-density log, because hydrogen in bound water as well as in pore water is sensed by the neutron log and because borehole diameters often became too large to be corrected or compensated for. The formation-density log appears to provide the best measure of density and, assuming a grain density, of porosity. Also this log is automatically corrected for borehole rugosity, and in this case the magnitude of the correc-

tion is recorded and can be analyzed. Except in certain "overcorrected" situations, densities given by the formation-density log are minimal, because they are reduced by the amount of borehole mud along the measuring path. Porosities are also calculated from sonic logs but these values are not as reliable as those from the formation-density log because the assumptions used in the conversion becomes invalid at high porosities.

SP logs rely on the contrast between the salinity of that volume of the formation invaded by the drilling fluid and the salinity of connate pore water. Because salt water was used as a drilling fluid, this contrast was very small in the hole. The fresh-water mud emplaced in the hole before logging apparently did not invade the formation to any great extent, because the SP curve is effectively featureless. The induction and spherically focused logs measure electrical resistivity, which is a function both of formation porosity and the salinity of the pore fluid. Some separation in signal trends from the different induction logs result from differing resistivities produced by partial invasion of the most permeable zones. These departures proved of limited correlative value, because they only confirmed other evidence for the occurrence of major sand intervals.

Interpretation of Lithologies

With the assumption that sand and clay are the lithologic end members, we can reconstruct the stratigraphy of the logged interval (Table 9; Fig. 38). Sand content increases downward from about 175 m sub-bottom to the bottom of the logged interval. From 88 to about 140 m sub-bottom in a series of units, each 2 to 4 m thick, clay content and porosity increase uphole as density and sonic velocity decrease upward. These units could be single, graded turbidite sequences or amalgamated fining-upward sets of turbidites. From 140 to about 175 m sub-bottom, there is a clay-rich sequence with several sand layers. A rapid increase in the amount of sand below 175 m is marked by large negative gamma-ray excursions and many "washout" intervals. Scattered thin clay

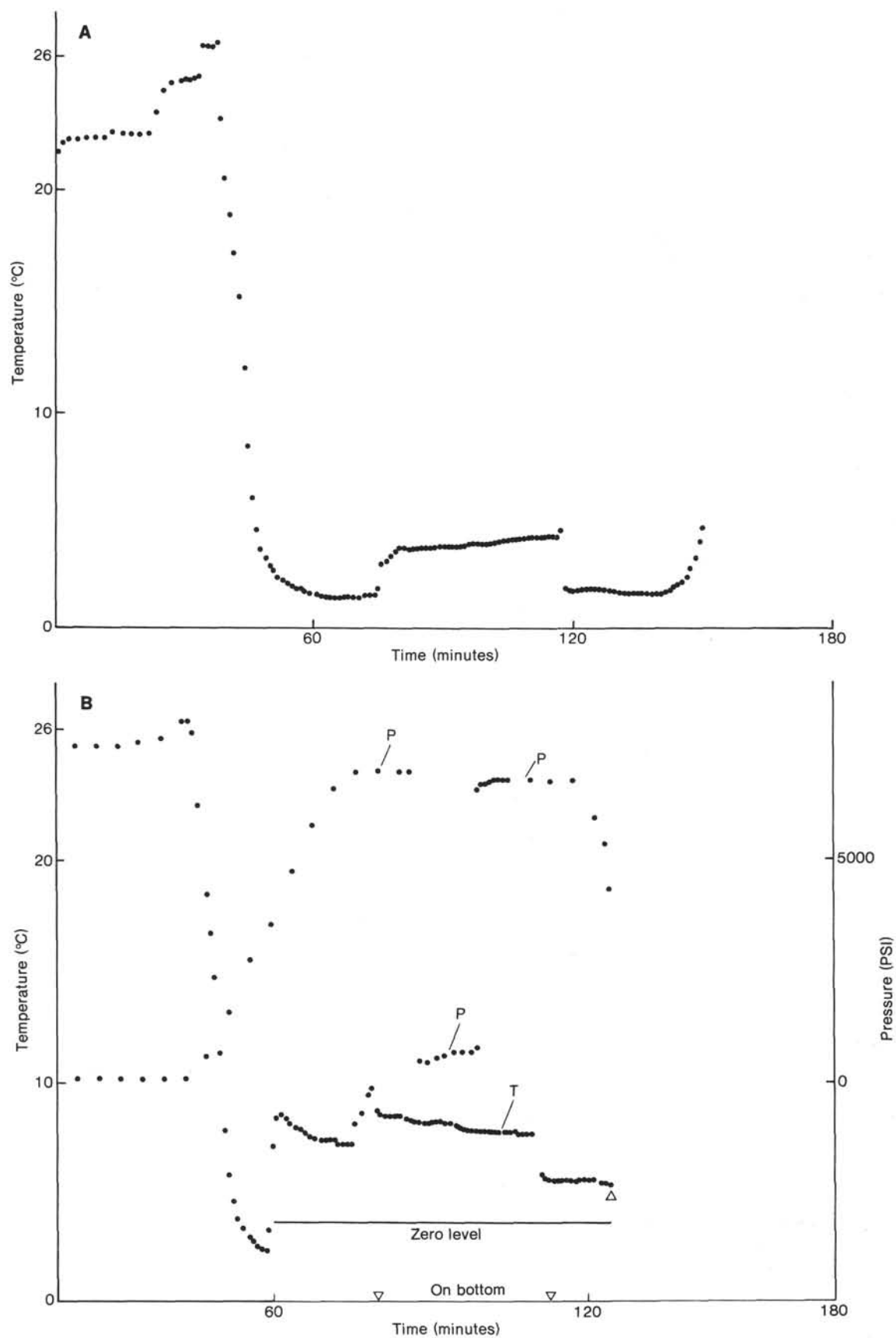


Figure 34. A. An example record of a bottom-hole temperature run using the Woods Hole tool. Hole 583A, sub-bottom depth 54 m. B. Plots of Tokyo University tool data (Barnes Uyeda device). Zero level jump at 50 minutes was eliminated by referring mudline temperature obtained by the tool on return to the ship's deck. P = pressure; T = temperature.

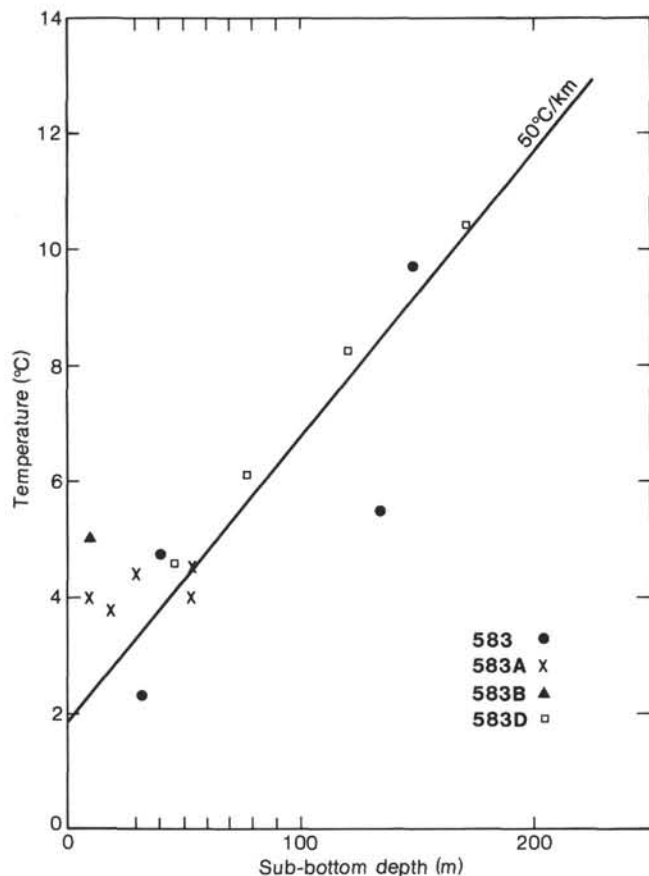


Figure 35. Temperature versus sub-bottom depth around Site 583.

or clayey silt layers in the lower section caused borehole constrictions, one of which (at 247 m) caused temporary bridging. Several thin (<1 m) intervals are characterized by high sonic velocities (≥ 2.2 km/s), moderate to high bulk densities (> 2.1 g/cm³), a moderate gamma-ray spike, and often high resistivities as well as by constricted hole diameters. These thin intervals generally lie between clay-rich and sand-rich units and may be poorly sorted, highly compacted clay-rich silts or fine-grained sands.

Correlation with Cores

The logged interval was sampled by the hydraulic piston cores of Hole 583 to a depth of 152 m, and by the rotary cores of Hole 583F below 150.4 m (Fig. 38). The primary and clearest observation drawn from the correlation between log and core lithologies is that coring selectively recovers the clay-rich parts of the stratigraphic section. This result is not surprising, but the misleading impression of the stratigraphy provided by the cores is alarming. Both massive or thick sands and much siltier sections are missed in the cores. Thus, even the identification of intervals without recovery as sand underestimates the occurrence of coarse-grained horizons.

Physical Properties

Because the raw log values of porosity, density, and velocity are so strongly affected by the borehole condi-

tions, an adequate or even approximate idea of the physical properties cannot be obtained by averaging log values. A better, if somewhat less quantitative, approach is to determine the physical properties for short intervals that appear to best represent the end-member clay and sand lithologies. These values can then be applied to the interpretation of lithologic section, remembering that physical properties vary with both sub-bottom depth and lithology.

The clay-rich sections, identified by high gamma-ray counts, low borehole diameters, and generally lower densities, have physical properties that correlate in an expected manner with laboratory measured values. Porosities decrease downward from near 50% above 100 m sub-bottom to about 40% at 150 m sub-bottom (Table 9; Fig. 38). Below 150 m sub-bottom the clay intervals are not adequately developed, but appear to develop porosities between 35 and 40%. These *in situ* values compare with the decrease in porosities derived from water-content measurement from 52 to 54% at 100 m sub-bottom to about 47% at 150 m sub-bottom and 44 to 46% at 260 m sub-bottom (see Physical Properties section, this chapter). The higher laboratory values, attributable to rebound upon reduction of stress and to porosity differences (4 to 7%), are of the expected magnitude (Hamilton, 1976; Shepard et al., 1982).

Sonic compressional-velocities (V_p) in these same clay-rich sections increase systematically downward from 1.72 km/s at 88 m to 1.80 km/s at 151 m (Table 9; Fig. 38). Below 150 m, clay-rich sections are not well represented, but sonic velocities in the least sandy intervals increase to about 1.85 km/s at 240 m sub-bottom. Substantially higher velocities (up to 2.3 km/s) were recorded opposite the hard thin intervals suspected to represent clay-rich silts or fine sands. Gas expansion precluded or degraded laboratory measurements of sonic velocities; the few samples measured produced velocities far below the *in situ* values. Comparison with interval velocities measured or deduced from the seismic reference profile are deferred to the Seismic Stratigraphy section (this chapter).

The *in situ* physical properties of the sand end member were initially surprising, but, in retrospect, could have been expected. Porosities calculated from the formation-density log averaged about 29% (Fig. 38) and are significantly lower than values measured by laboratory methods. Moreover, sand porosities do not change noticeably with depth. These porosities are reasonable, although on the low side, for moderately compacted, poorly sorted sands (Clark, 1966). Sands are probably well packed at this depth but should not undergo much further compaction until grain boundary geometries begin to change, through pressure solution, comminution, or cementation.

Several reasons can be offered for the lack of recognition of these low porosities (and high bulk densities) in our laboratory measurements. The first of these is the paucity of recovered sands. However, densities even in the few recovered sands, are much lower than *in situ* densities, the values probably reflecting the reduction of density caused both by unloading and drilling disturbance of these noncohesive sediments.

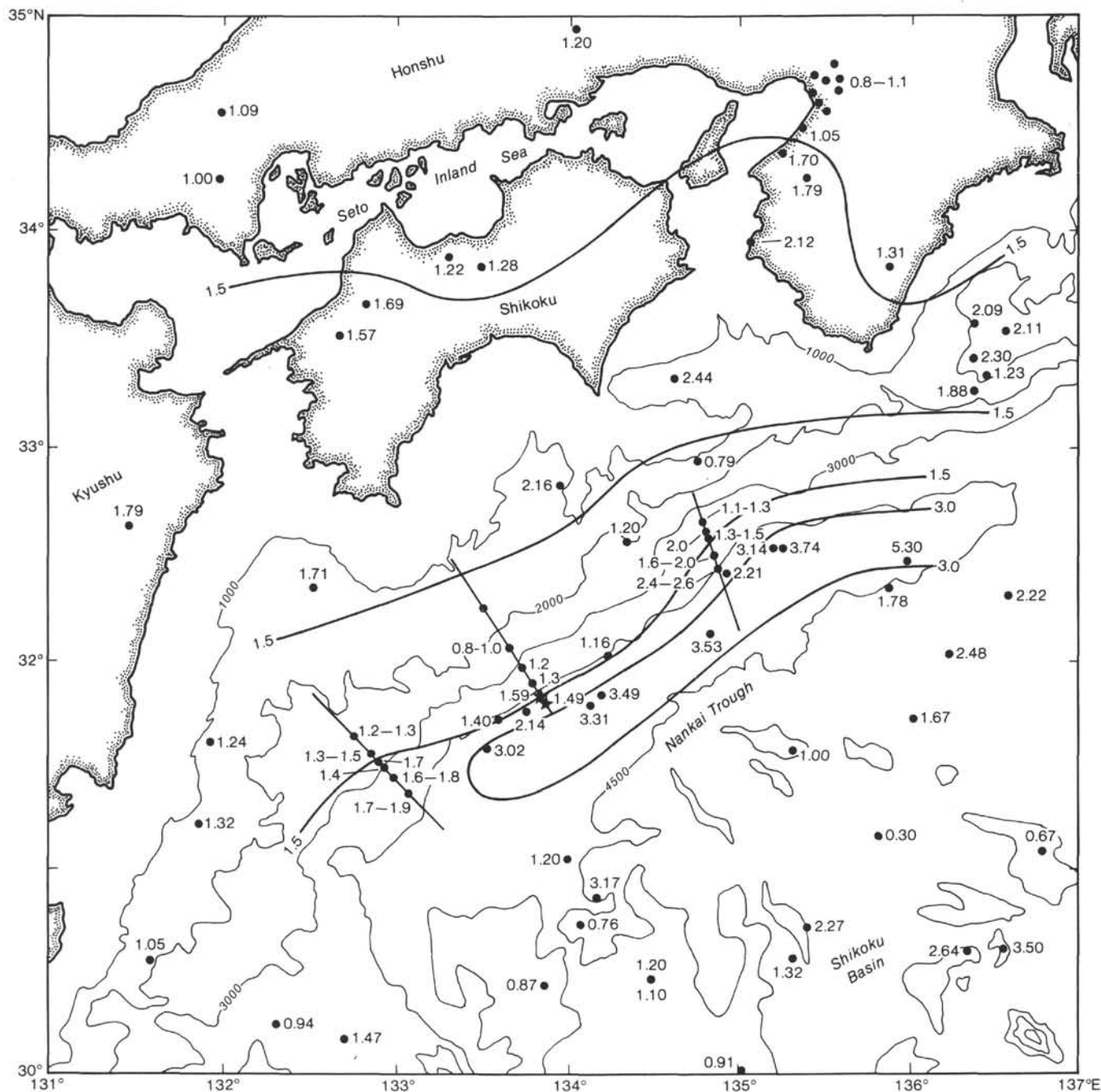


Figure 36. Regional distribution of heat flow, Nankai Trough. Asterisks indicate locations of Sites 582 and 583.

Compressional velocities in the sand-rich lithologies show a lack of trend with depth, paralleling the porosity response, and varying between about 1.9 and 2.1 km/s (Table 9; Fig. 38). Again, these values are much higher than the few laboratory velocities, which did not include any sands. The sands have a considerably higher *in situ* compressional velocity than clay at the shallower end of the logged section, but this difference decreases with increasing depth.

Correlation with Seismic Reflectors

It is difficult to make on-board correlations between logging results and the reference seismic reflection pro-

file for several reasons. First, sonic velocity (V_p) and bulk density, used to determine impedance contrasts and reflection coefficients, cannot be picked directly from the logs over many intervals, but must be indirectly determined, as previously described. Secondly, the character of a constructed or synthetic seismogram is a function of the frequency distribution of the seismic signal assumed and requires a convolution of this signal with the impedance curve.

Despite these difficulties, a strong reflector at about 0.16 s sub-bottom should fall within the logged interval, and it is tempting to search for a lithologic cause. With an interval velocity of 1.93 km/s (see Seismic Stratigra-

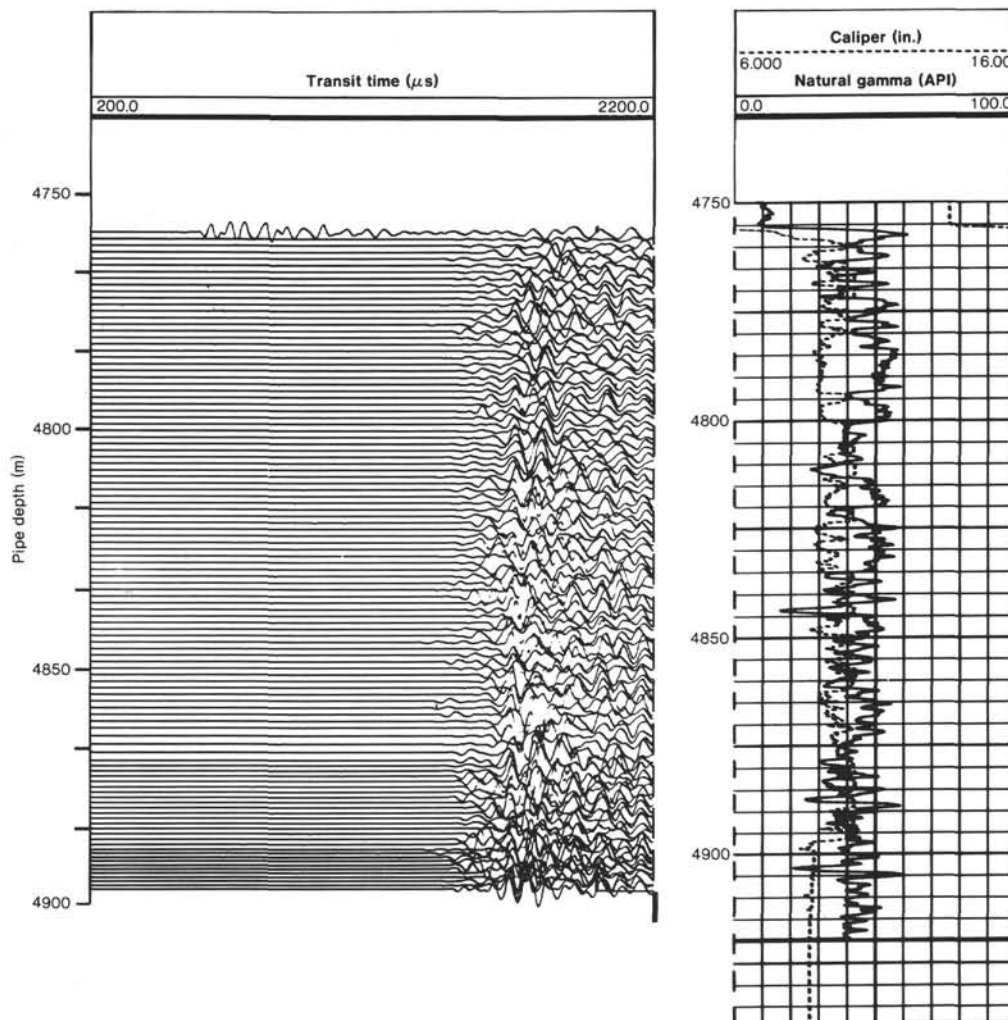


Figure 37. Composite logging results for Hole 583F. Depths are in feet of drill pipe.

phy section, this chapter), which, if anything, ought to be high for this very shallow part of the seismic interval, the depth to the reflector should be near 160 m sub-bottom (4825 m log depth). This position lies near the base of a substantial clay-rich section and the top of the strongly alternating sands and clays (Fig. 38). A second reflector at about 240 m sub-bottom (see Seismic Stratigraphy section, this chapter) corresponds to a log depth of 4905 m, but the poor quality of the logs at these depths and the fact that this is very close to the bottom of the logged interval make it inadvisable to attempt a correlation.

SEISMIC STRATIGRAPHY

One of the purposes of this site was to clarify the origin and the mechanism for the formation of the wedge at the northwest side of the Nankai Trough. Particularly important is definition of geologic contrasts across a major thrust fault shown on the reference seismic Line N55-3-1 (Fig. 39). At two locations, Holes 583D and 583F, drilling almost achieved that goal. Penetration of the fault at these points would have helped us to correlate seismic reflectors across the fault and to develop a structural interpretation of the overlying prism.

Seismic reflectors at Holes 583B, 583C, and 583D are shown in Table 10. The hole encountered faults at 76 and at 172 m sub-bottom, but these offsets were not revealed on the seismic record because a strong acoustic impedance contrast is lacking at this shallow depth. An interval velocity of 1.93 km/s was used for calculation of depths for the entire column at Holes 583B, 583C, and 583D (Fig. 40). This velocity is chosen because the sediment is younger than we expected—deeper, therefore older, horizons were not encountered at shallow sub-bottom depths—and because acoustic impedance does not change across the faults. Depths to seismic horizons drilled are listed in Table 11. The positions anticipated for reflectors from faults recognized by the study of the structural geology (Structural Geology section, this chapter) are estimated at 6.37 and at 6.46 s, but these are not evident on the profile (Fig. 39). Reflectors do occur at 6.40 and at 6.42 s and we expect a lithologic contrast at a corresponding sub-bottom depth. Subtle lithologic changes occur at 104 and 123 m sub-bottom, but their relation to the seismic profile is problematic. A faint reflector at 6.5 s corresponds to one of the sandy intervals above the *Chondrites*-bearing muddy turbidites and may be Horizon B, also identified at Site 582. The reflector is not

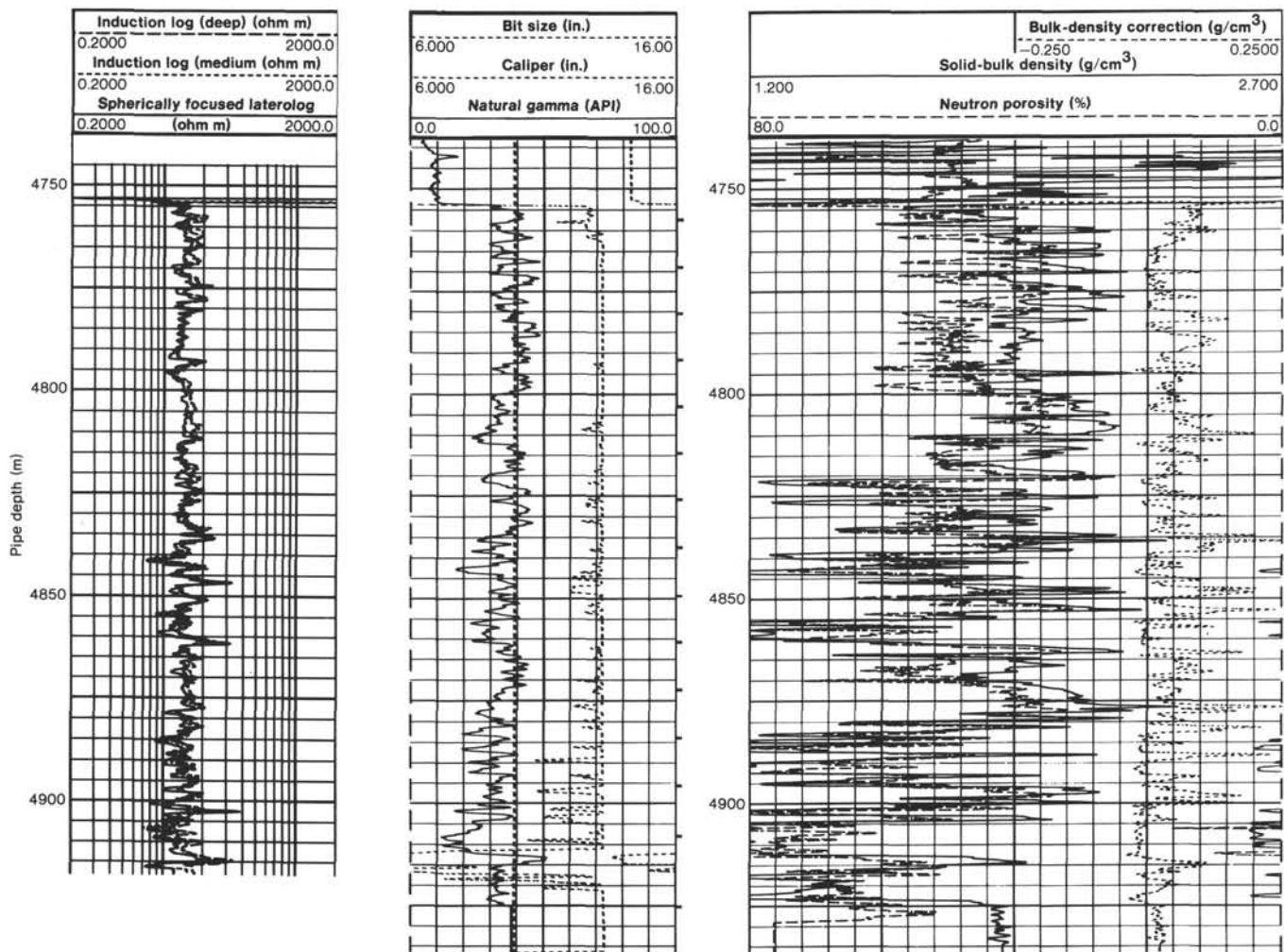


Figure 37. (Continued).

specifically defined either by micropaleontologic evidence or by seismic correlation. The interval between Horizons A and B shown on seismic Profile N55-3-1 is thinner at Site 583 than at 582, therefore Horizon B is possibly located at the shallower level at Site 583 and is obscured in the process of thrust faulting. A reflector at 6.62 s was not penetrated, but this horizon is easily traced from Site 582 and is identified as Horizon C. In comparison with Site 582, the thickness between Reflectors C and B increases because of the intercalation of sand layers, which unfortunately could not be sampled by rotary drilling. By seismic stratigraphy, the section at Site 583B, 583C, and 583D is divided into three units. Unit 1-2 (the lower part of Unit 1) is apparently duplicated by faults. The fault may also truncate the upper part of Unit 2. Unit 3 consists of three sequential lithologies: sandy, muddy, and then sandy turbidites; their calculated interval velocities are considered reasonable.

Six seismic reflectors are recognized at Hole 583 (Table 11). A moderately strong, irregular reflector at 6.215 s suggests rough topography, perhaps a hiatus at the base of so-called slope sediment, picked up seismically between the sand layers of Cores 3 and 4. Because it is an irregular feature, seismically defined Unit 1 is divided

into two subunits, the upper is called Unit 1-1 and the lower is 1-2. A strong reflector at 6.285 s separates an upper interval of dominantly sandy turbidites from a lower interval of dominantly muddy turbidites. The nanofossil datum of 0.44 Ma occurs slightly above this horizon, allowing correlation with a 6.6 s reflector at Site 582. At Hole 583, therefore, this reflector is designated as Horizon A.

A strong reflector at 6.355 s was not reached at Hole 583, but was penetrated at Holes 583E and 583F (Table 11). Unfortunately, no cores were recovered and its sub-bottom depth could not be refined. The reflector is identified as Horizon B, and is tentatively placed at 170 m sub-bottom at Hole 583, where dominantly muddy turbidites overlie the predominantly sandy turbidites of Unit 3. Drilling continued at Hole 583F, where the sandy interval is so thick and homogeneous that it forms another strong reflector at the bottom of the interval at 247 m sub-bottom. This level is a boundary from sandy intervals above to muddy *Chondrites*-bearing intervals below. A moderate reflector at 6.50 s correlates with Core 583F-17 at 314 m sub-bottom where, as at Site 582, coarse turbidite sands including scattered pumice grains (a few millimeters in diameter) occur. On the basis of

Table 9. Physical properties for end member lithologies from logged intervals in Hole 583F.

Depth of pipe (m)	Sub-bottom depth (m)	Density (g/cm ³)	Porosity (%)	V_p (km/s)
Clay-rich sediments				
4761 to 4762	99 to 100	1.88	47	1.72
4767	105	1.88	47	1.73
4770 to 4771	108 to 109	1.76	56	
4782 to 4784	120 to 122	1.94	43	1.77
4789 to 4792	127 to 130	1.94	43	1.75
4797	135	1.84	50	
4813 to 4816	148 to 151	2.02	39	1.79
4824	160			1.85
4827	144			1.81
4881	219			1.89
4884	222			1.88
4888	226			1.87
Sand-rich sediments				
4759	97	2.18	29	
4763 to 4764	101 to 102	2.26	24	1.99
4766	104	2.33	21	
4770	108	2.40	15	2.18
4776	114	2.25	25	2.06
4779	117			2.03
4794	132	2.19	28	1.93
4801	139	2.13	32	
4803	141	2.17	30	
4804	142	2.20	28	
4807	145	2.20	28	
4820	158	2.19	28	1.98
4852	190	2.18	29	
4862	200	2.17	30	
Clay-rich silt or fine sand intervals				
4810				2.35
4828	166			2.15
4848	186			2.29
4863	201			2.28
4867	205			2.31
4871	209			2.28
4901	239			2.23

Note: V_p : compressional-wave velocity.

these data, we concluded that reflector is Horizon C. Coring ended after penetrating the next strong reflector (tentatively called C1) below Horizon C. Horizon B was identified neither by stratigraphic nor by paleontologic methods; however, the horizon is marked on logging profiles. Sonic and density logs register a clear spike at this horizon (see Logging section, this chapter).

Our correlation of the seismic horizons to those at Site 298 uses the reference cross Line N55-A-1 (Fig. 41). Line N55-A-1 crosses Line N55-3-1 (Fig. 39) at approximately SP 1730, where Horizon C is recognized at approximately 0.5 s below the seafloor. At that point, Horizon E is at 0.9 s below the seafloor. When these reflectors are traced to Site 298, located on the Profile N55-A-1, Horizon C is recognized at approximately 0.34 s below the seafloor and Horizon E is at approximately 0.6 s (Table 12). The apparent thinning of formations above Horizon C could be explained by topography (Fig. 2B). Because Site 298 was situated near the Ashizuri Canyon axis, thinning of the section above Horizon C might arise either from nondeposition or from erosion. Profile N55-A-1 gives the impression that the general stratification at Site 298 is similar to Sites 582 and 583, despite extensive thrust faulting along this margin.

Correlation of seismic horizons between Sites 583 and 582 is established across the major fault and is shown on the reflection profile (Fig. 39). The variation of sediment thickness, the location of the major thrust fault, an arch-shaped structure, and the protothrust zone are clearly shown. The vertical offset along the major thrust fault is measured at 40 to 50 m for the interval below Horizon C, and 70 to 90 m above Horizon C. Large values in the upper part are perhaps related to the angle of the thrust: 25° below Horizon C and 45° above Horizon C. The real movement or slip rate along the fault plane may be the same, indicating that the entire slip movement occurred simultaneously. The upper fault plane does not appear on the seismic profile, it was recognized only on the basis of studies of the structural geology (Fig. 3). This 30° fault plays a role in the relative uplift of a block of subhorizontal formations approximately 5 km in length (Aoki et al., 1982; Kagami et al., 1982).

The arch-shaped structure next to the fault has several features (SP 1800 to 1820, Fig. 39). The arcuate curvature is smaller in the upper part and almost flat at the bottom. Horizons A and B are not recognized seismically within this area, but cores at Holes 583B, 583C, and 583D contain indications of both horizons. A 60° thrust fault cuts the arch on its seaward side. This kind of fault is well developed in the protothrust zone, which will be discussed next. Across the arch, the variation of sediment thickness was calculated using corrected interval velocities (Fig. 42). Because Horizon C was identified throughout the area, it is drawn as straight line on the figure. The basin-shaped strata between Horizons C and E are upper Pleistocene turbidites and have a depositional center around SP 1840. On the contrary, the wedge-shaped sediment column between Horizons B and C thickens landward, a result of either tectonic thickening (Moore et al., 1982) or a shift of depositional center (Coulbourn and Moberly, 1977). The association of sand layers with the thickening of the strata at Hole 583F suggests a main channel facies. The sediment column above Horizon A decreases in thickness on the arch at SP 1840. The arch may have formed after the deposition of Horizon A, when the major thrust fault became active.

Thrust faults dipping landward at approximately 60° are common in the protothrust zone (SP 1800 to 1910, Fig. 39) and are a characteristic feature of the western Nankai Trough (Kagami et al., 1982); they contribute to regional uplift relative to the trough floor. It is surprising that the seismic reflectors do not show any evidence of the 60° fault, after incorporation into the "uplifted" block by the 30° fault shown in seismic reflection profile. Perhaps they are preserved as dewatering veins (Lundberg and Karig, this volume). Because this type of the protothrust zone is only observed at the western Nankai Trough, their origin may be related to the oblique subduction that Seno (1977) has computed for this part of the Philippine Plate.

Correlation of seismic horizons in cores drilled at Hole 583G was carried out by using the same important lithologic characteristics previously described (Table 11). Horizon C is placed within Section 583G-3-2 and, as before, is defined by turbidite sands with pumice grains averaging a few millimeters in diameter. Plant debris in

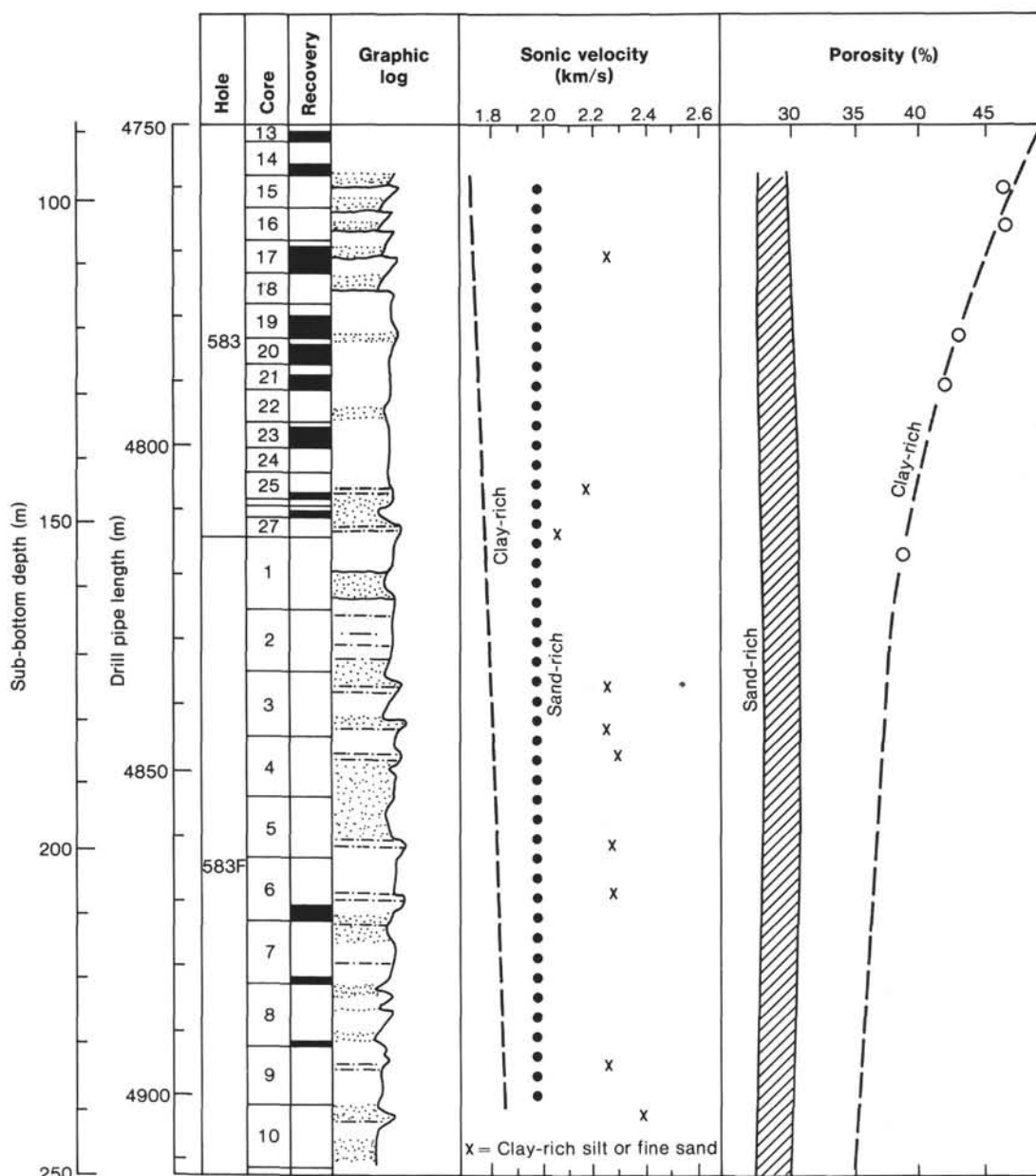


Figure 38. Summary interpretive section over logged interval in Hole 583F. For the uppermost 27 hydraulic-piston-corer cores, the correspondence with drill pipe length is approximate. Porosity is from the formation-density log.

Section 583G-1-3 form a 10-cm marker horizon, which corresponds to similar plant-rich intervals occurring in Section 583F-14-2 and in the pumice-bearing sand of Section 583F-17-2. These horizons are 20 to 30 m shallower than their counterparts in Hole 583G, even though Hole 583F is situated 2 m deeper.

Correlation of Horizon C1 with the observed stratigraphic succession is tentative; it is placed at the bottom of Core 583G-11. The boundary separates muddy turbidites above from sandy turbidites below. Again, this depth is about 20 m deeper than at Hole 583F. The reason for this discrepancy is not fully understood.

Two slump folds occur within seismic Unit 4 (see Paleomagnetism section, this chapter), and these appear clearly on the seismic profile (Fig. 39). The seaward-dipping, foreset-bedding type reflectors occur between Ho-

rizons C and C1. Apparently, they develop steeper dips toward the major thrust fault, indicating that the slump fold may be formed during uplifting of the thrust block. No other reflectors like these are identified on the seismic profile. The lower part of seismic Unit 4 is rather flat. The major thrust fault expected at 463 m sub-bottom was never penetrated because of premature abandonment of the site.

SUMMARY AND CONCLUSIONS

Despite the failure to achieve our primary objective at Site 583, the four HPC holes and the four rotary-cored holes drilled over a distance of almost 900 m across the basal structural terrace of the Nankai Trough provide several interesting insights to the problems of subduction. Some of these insights stem from the absence

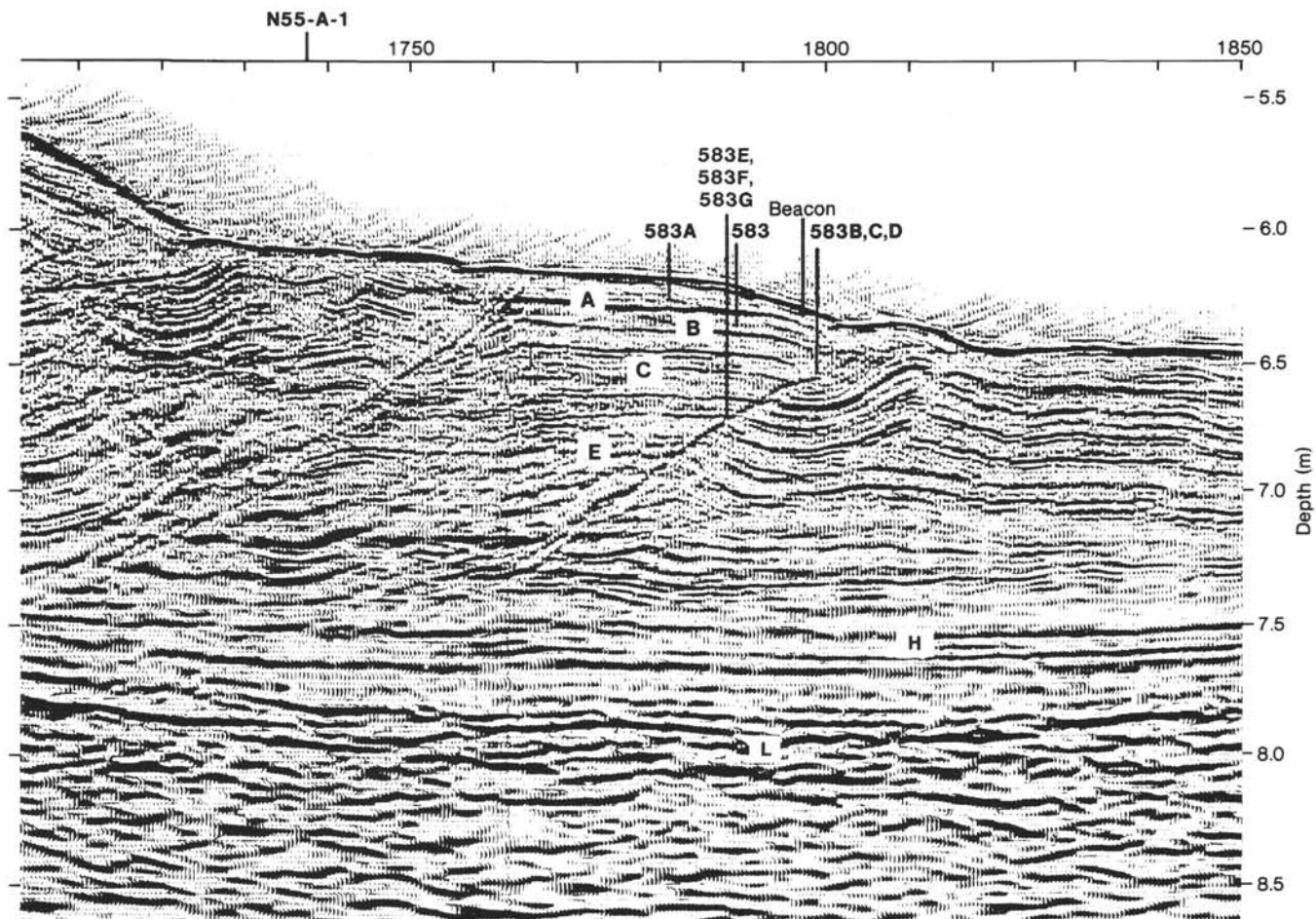


Figure 39. Reference seismic reflection Profile N55-3-1 showing location of holes drilled at Site 583. SP = shot point. Letters A through L identify seismic reflectors discussed in text.

Table 10. Seismic reflectors at Holes 583B, 583C, and 583D.

Reflection time (s)	Velocity assumed (km/s)	Calculated sub-bottom depth (m)	Remarks
6.29	1.51	0	Seafloor (4749 m)
6.37	1.93	77	Estimated fault
6.40		106	Faint
6.42		125	Moderate
6.465		169	Estimated fault
6.50		202	Faint, Horizon B?
6.54		241	Moderate
6.585		285	Moderate
6.60		299	Moderate
6.62		318	Strong, Horizon C

of evidence for features that would have been expected. Drilling results also helped to calibrate and qualify the stratigraphic and structural relations displayed by the reference seismic Profile N55-3-1 (Fig. 39).

HPC Hole 583, together with rotary Holes 583D, 583E, 583F, and 583G, constituted the major attempt to penetrate the thrust fault that bounds and apparently uplifts the terrace on which we drilled. HPC Hole 583A was offset 100 m further to the north from Hole 583 in order to sample the uppermost sediment section that was

missing or condensed in Hole 583. HPC Holes 583B and 583C and rotary Hole 583D constitute a single location 475 m south-southeast from Hole 583, further down the frontal slope of the terrace.

Structures

Holes 583B, 583C, and 583D, were drilled to test the quantity and nature of hydrocarbons that might have migrated up the fault from deeper zones of greater organic maturation. This combined hole did penetrate the basal thrust, as well as a shallower fault splay, but with inconclusive results. Structural and paleomagnetic data, combined with the reference seismic profile, suggest that the steep splay intersected the hole near 60 m sub-bottom and that the major fault lay near a depth of 155 m (Fig. 16). These intersections and the nature of the physical properties in the sediments near the fault zones could not be resolved more closely because of poor core recovery and strong drilling disturbance of these relatively shallow and uncompacted sediments.

Dips of sediments in Hole 583D, oriented by a Kuster device in piston cores above 50 m sub-bottom and by paleomagnetic declinations below that depth, define a south-facing homoclinal sequence to about 150 m sub-bottom and a north-dipping sequence beneath that depth. Although structures of this scale are near the limit of

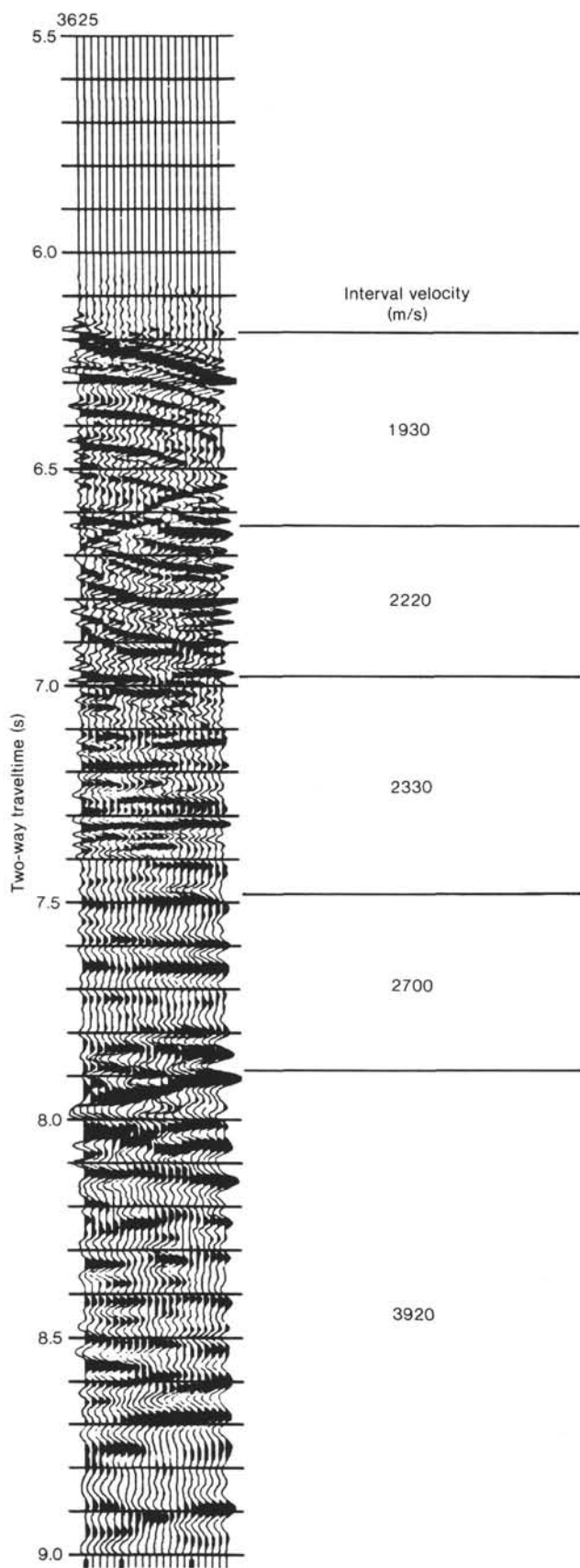


Figure 40. Interval velocities used to calculate depths to seismic reflectors. Common depth point number 3625 = Shot Point 1789.

resolution and migration techniques on the reference seismic profile, the upper homoclinal sequence clearly was part of an anticline above the fault surface. The north-dipping beds in the footwall can be interpreted as belonging to the south flank of a syncline, which is displayed on the reference profile (Fig. 39).

This hanging-wall anticline is not present at the location of Holes 583E, 583F, and 583G, where bedding was still nearly horizontal to the total drilled depth of 450 m. At Hole 583G, a dipping reflector near 460 m sub-bottom is interpreted as a thrust and was apparently closely approached but not reached.

Core recovery in Holes 583F and 583G was relatively poor, so that we cannot say whether or not small folds or splay faults exist in the unrecovered intervals, but space for the large-scale hanging-wall fold defined at Holes 583B, 583C, and 583D is lacking. The disappearance of the fold with depth, associated with a flattening of the thrust surface into the bedding near 300 m sub-bottom (Fig. 39), may have developed over the top of a ramp along a bedding-plane step thrust (see Structural Geology section, this chapter). It is remarkable that such a structure, usually associated with highly lithified sequences that have mechanically heterogeneous properties, would develop in these relatively unlithified Quaternary strata.

Small-scale secondary structures in the strata at Site 583 were remarkably subdued and limited in diversity. Below a depth of 345 m in both Holes 583F and 583G, a single conjugate set of unhealed fractures had developed. Both elements dip approximately 40° , and the slip surfaces have well-developed dip-slip grooves and striae. The horizontal intersection lineation of this fracture pair that trends about 210° , a horizontal acute angle between the fractures, and the spatial association of fracturing with the thrust all help to identify these fractures as compressional structures. A more steeply dipping system of faint dark surfaces occurs with the fractures and may be incipient dewatering phenomena or, alternatively, kink bands. No extensional structures, like those of the Japan Trench (site chapter, Site 584, this volume) occur at this site.

Physical Properties and Logging

Previous deep-sea drilling and other geologic inferences have suggested that zones of deformation beneath inner trench slopes are associated with dewatering and abnormally high pore pressures (Shepard et al., 1982). However, porosity gradients do not indicate any anomalous dewatering in the section at Holes 583F and 583G compared to porosities at Site 582. This similarity corroborates our previous conclusion that Site 582, located on the floor of the Nankai Trough and Site 298, located on the landward slope, have similar porosity versus depth characteristics (see Physical Properties section, this chapter; site chapter, Site 582, this volume; and Ingle, Karig, et al., 1975). Porosities are low at shallow depths in Holes 583B, 583C, and 583D, but these values could be explained by the removal of several tens of meters of sediment from the sloping surface in this area. No porosity anomalies occur at the intersection of Hole 583D

Table 11. Seismic reflectors and correlation of seismic horizons drilled at Site 583.

Reflection time (s) and reflectivity	Velocity assumed (km/s)	Calculated sub-bottom depth (m)	Drilled sub-bottom depth (m)	Calculated average velocity (km/s)	Calculated internal velocity (km/s)	Marker horizon	Seismic unit
Holes 583 and 583A							
6.190		Seafloor (4673 m)	0				
	1.93			1.84	1.84		1-1
6.215 (moderate)		24	23	1.83	1.82	Hiatus	
6.250 (faint)		58	55	2.40	2.40		1-2
6.285 (strong)		92	97	2.06	2.10	A	
6.325 (moderate)		130	139	2.09	2.06		2
6.355 (strong)		159	170 ^a			B	
Holes 583B, 583C, and 583D							
6.29		Seafloor (4673 m)	0				1-1
				1.90	1.90		1-2
6.37		24	76	1.90	1.87	Fault	
6.40		58	104	1.89	1.90		1-2
6.42		130	123	1.89	2.18		
6.465		159	172	2.00	2.17	Fault	2
6.50			210	1.99	1.95	(B?)	
6.54			249	1.95	1.73		
6.584			288	1.98	2.50		3
6.60			307	(2.00)	(2.30)		
6.62			(330)			C	
Holes 583E and 583F							
6.18		Seafloor (4666 m)	0				
				1.94	1.94		1
6.28 (strong)	1.93	97	97	2.00	2.09	A	2
6.35 (strong)		164	170	1.98	1.92	B	
6.43 (strong)		241	247	1.96	1.91		3
6.50 (moderate)		309	314	1.86	1.56	C	
6.60 (strong)		405	392	(1.93)	(2.60)		4
6.64	2.22	444	(444)	(2.22)	(2.22)	Fault	4
6.97 (strong)	2.33	810	(810)			E	
Hole 583G							
6.18		Seafloor (4663 m)	0				
6.28			(97)			A	
6.35			(170)			B	
				2.04	(2.08)		3
6.50			326	1.94	1.74	C	
6.60			413	(1.93)	(1.67)	C1	4
6.66			(463)			Fault	

Note: Parentheses: not drilled.
^a Data from sonic log.

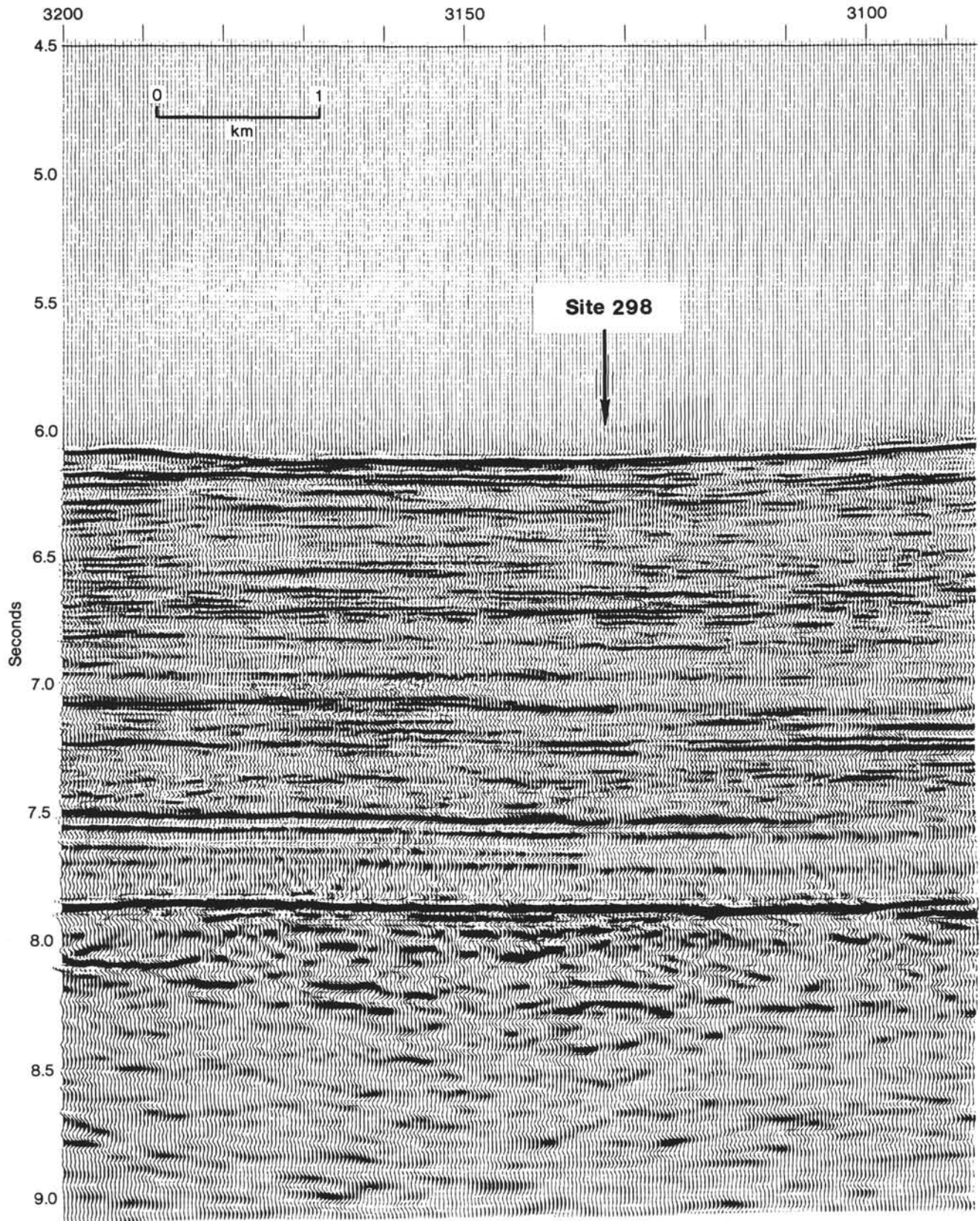


Figure 41. Multichannel seismic Profile N55-A-1.

Table 12. Seismic reflectors at Site 298.

Reflection time (s)	Velocity assumed (km/s)	Calculated sub-bottom depth (m)	Marker horizon
6.11		0	
6.45	1.80	306	Approx. C
6.64	2.28	523	
6.71		602	Approx. E
6.88	2.33	800	
7.10	2.60	956	
7.55	2.80	1586	H
7.90		2076	L

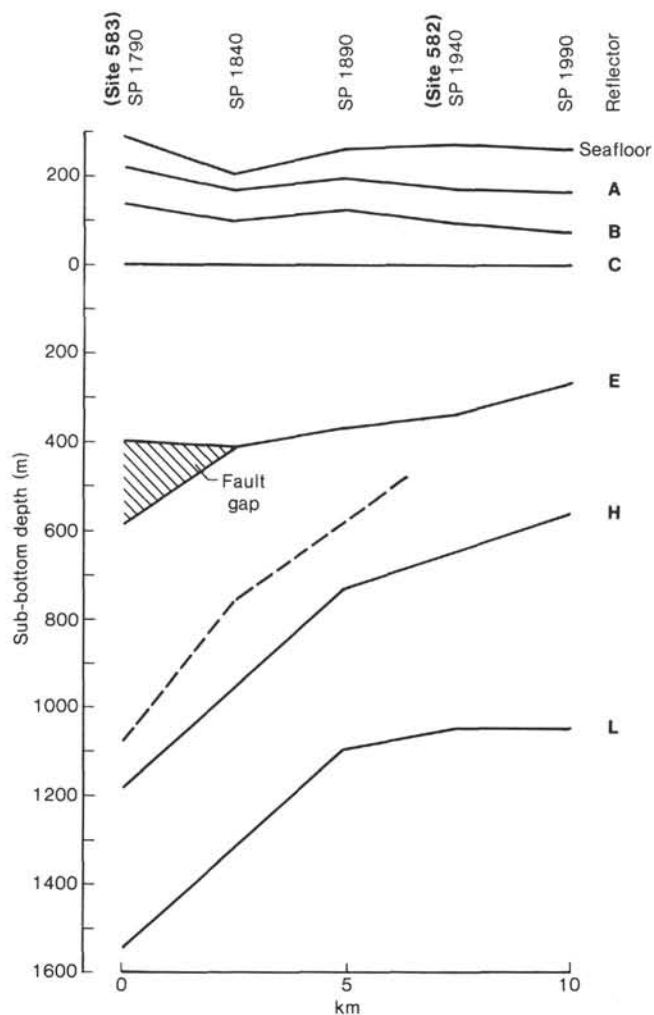


Figure 42. Interval thickness along Profile N55-3-1. SP = shot point. Broken line shows a décollement.

with faults shown in the seismic profile (Fig. 39), although poor recovery and core disturbance probably masked any local or subtle anomalies.

Shear-strength gradients in the holes of Site 583 are steeper than those in the similar sediments of Site 582. The explanation for this difference, as well as for the earlier noted lack of correlation between porosity and shear strength at Site 582, continues to elude us.

Laboratory determination of physical properties in cores were augmented by logging, although unfortunately this was accomplished only over a short section (88 to 260 m) of Hole 583F. Nevertheless, the comparison of logging and core data clearly show that the lithologic section recovered by coring in turbidite sequences drastically underestimates the proportion of sandy and silty units. Furthermore, because sand-rich units have higher *in situ* bulk density and sonic velocities than indicated by laboratory values, or than do the clay-rich units, the velocities and densities of the total section are also underestimated.

Heat Flow

The heat flow values deduced from temperature gradients and conductivities measured at Site 583 averaged 1.59 HFU, very similar to the recalculated value for Site 582 and lower than that previously suggested for this setting by near-surface instruments.

Lithology

The strata penetrated at Site 583 were not divided into separate lithologic units, although the upper few tens of meters probably constitute a slope deposit. The cores recovered a suite of clastic sediments from coarse sand to bioturbated hemipelagic mud. As at Site 582, bioturbated clay intervals appear to increase downsection, but thick, coarse sands persist to the base of Hole 583G (450 m). Logging of a section of Hole 583F confirmed the inference that lack of recovery was caused by sandier intervals and suggests that the section was quite sand rich over the entire cored interval.

Thin, graded silt units were recovered in a relatively undisturbed condition, but the few thick sands recovered showed little sedimentary structure, other than a general grading. Drilling probably destroyed any internal structure in the sands. Logging revealed stratal units 1.5 to 4 m thick (each of which changed upward from very sand rich to clay rich) and, with the resolution of the logs, very sharp basal contacts. These units could be single graded turbidites or fining-upward sequences of thinner turbidites of the decimeter thickness noted in many cores.

The sand mineralogy, determined optically as well as by X-ray diffraction, was also similar to that at Site 582. Amphibole and smectite decrease below 390 m in Hole 583G, possibly indicating a change in provenance. With the low core recovery, however, other indicators of changing provenance could easily go undetected. Authigenic nodules of calcium carbonate, primarily as calcite, occur in the shallower strata of all the HPC holes (see Inorganic Geochemistry section, this chapter). The exclusive association of these nodules with pyrite-rich sands is attributed to locally reducing environments and associated with higher alkalinities in the interstitial waters.

In the four rotary holes drilled at Site 583, core recovery was poor, turbidites repetitive, and chronologic horizons few; therefore, good lithologic correlation of beds was not expected. In the three HPC locations, however, such correlations should have been easier. Despite the

relatively good HPC recovery, stratigraphic correlation could not be made between even these holes, possibly because of the progressive southward loss of the uppermost section toward the terrace edge. Loss of shallow reflectors was noted on the 3.5-kHz profiles and substantiated by the shallower sub-bottom depth to the base of the *Collosphaera tuberosa* radiolarian Zone in Hole 583 than in Hole 583A, and by the complete absence of this zone in Hole 583B. The occurrence of steeply dipping beds in Core 1 of Hole 583B and the truncated reflectors on the 3.5-kHz profile strongly suggest that the inferred loss of surface sediment is due to slumping and erosion.

Correlation of Seismic and Lithologic Sections

Correlation of strata between Sites 582 and 583 is quite difficult but is of great importance for the interpretation of deformation, especially for the amount of slip on the terrace-bounding thrust. Seismic reflectors, tied to lithologic horizons at Site 582, can easily be traced northward on the reference profile to the thrust fault, but correlation of these reflectors across the fault is less obvious.

One correlation scheme, discussed in the section on Seismic Stratigraphy (this chapter), fits the seismic pattern reasonably well and suggests a relatively small (40 to 50 m) vertical component of slip on the thrust fault. On the other hand, this correlation is difficult to reconcile with the purely structural analysis of the fault. If the cross-sectional area through the fault and fold is balanced, preferably but not necessarily as a bedding-plane step thrust with a hanging-wall anticline, a vertical component of slip well over 100 m is required. More than 100 m of relief of the NN19/NN20 nannofossil datum between Holes 583 and 583D, and the observation that a uniform 45° dip of a homocline for a minimum length of dipping section of only 100 m will produce that 100 m of relief, support this estimate of relative uplift.

Sedimentation and erosion are occurring simultaneously in different parts of the system, and estimates of deformation will differ accordingly. Nondeposition or erosion has been occurring over the prot thrust zone for all or most of the past 0.4 Ma, whereas sedimentation on the structural terrace has been much more continuous. The units in the uppermost part of the stratigraphic section are not now continuous and may never have been, rendering correlation of deeper reflectors based on the uppermost part of the section hazardous.

The problem of the nature of sedimentation near the base of the trench slope has broader importance because this setting is generally believed to be the locus of the most intense subduction-related deformation. Studies of several other subduction zones suggest a relatively sharp upward transition from coarse trench turbidites to slope hemipelagic sediments with an associated rapid decrease in the amount of deformation. Data from Site 583 and from the several profiles permit some discussion and speculation concerning this topic.

Our combined drilling and geophysical data set demonstrates that deformation and sedimentation are not uniform across the base of the inner trench slope; there-

fore the contact relationship between trench and slope sediments may also be variable. The sediment fill of the Nankai Trough is incorporated into the base of the inner slope in thrust-bound slabs about 5 km wide. Deformation is more intense in the area in front of the slab-bounding thrusts and in the underlying prot thrust zone than it is behind the thrust faults. The least deformed section of the thrust slabs seems to be near the leading edge, where Holes 583 and 583A were drilled.

If the present trench floor is a key to the nature of the next older thrust slab, the area near the leading edge of these units should also be the locus of most continuous sedimentation, at least during the earliest phases of deformation. As thrusting and uplift proceed, our data suggest that strong erosion of the thrust toe takes place and that maximum accumulation shifts to the rear of the structural terraces, at the foot of the thrust scarps.

The slope sediments also vary in character across the base of the trench slope. In addition to the hemipelagic muds and silts that typify lower trench slopes, recycled sediment and rock are slumped or eroded from the active thrust scarps where poorly consolidated trench-fill sediments are exposed. Such a thrust scarp, with more than 400 m of relief, lies only 3 to 4 km north of Site 583 and may be responsible for both the northward thickening of the youngest part of the section and for the sandier components of the strata. Because the sands in these slope strata might be recycled trench sediments, they could be identical to those from the deeper part of the drilled sections. Larger-scale sedimentary features might be able to distinguish slope from trench sediments at Site 583, but with poorly recovered cores, we are unable to do so.

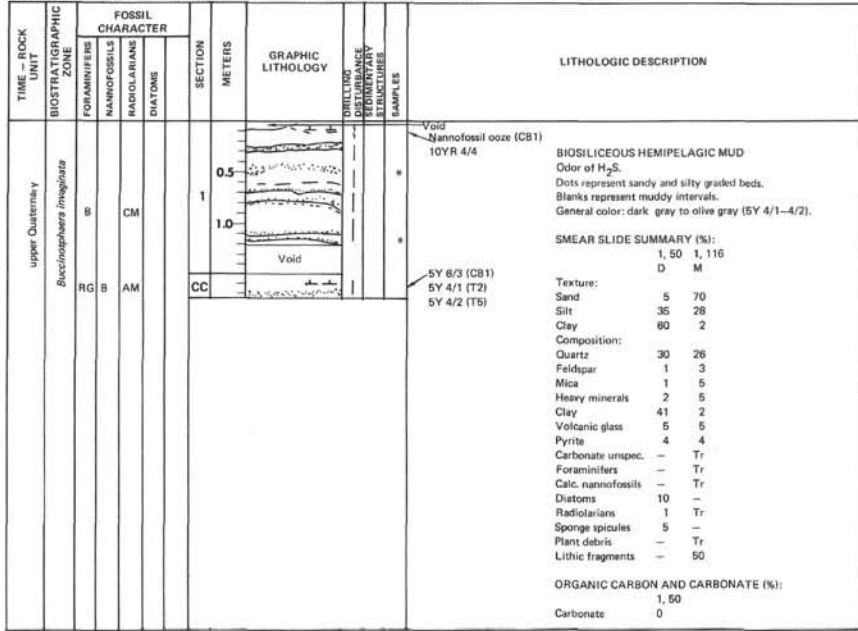
In DSDP Site 298, drilled less than 2 km from the same large thrust scarp, a 100-m-thick slope unit including pebbly mudstone was interpreted from very sparse and poorly preserved cores (Ingle, Karig, et al., 1975). The validity of this interpretation is questionable, but probably more proximal deposits from a slump were sampled at this location, somewhat closer to the scarp.

REFERENCES

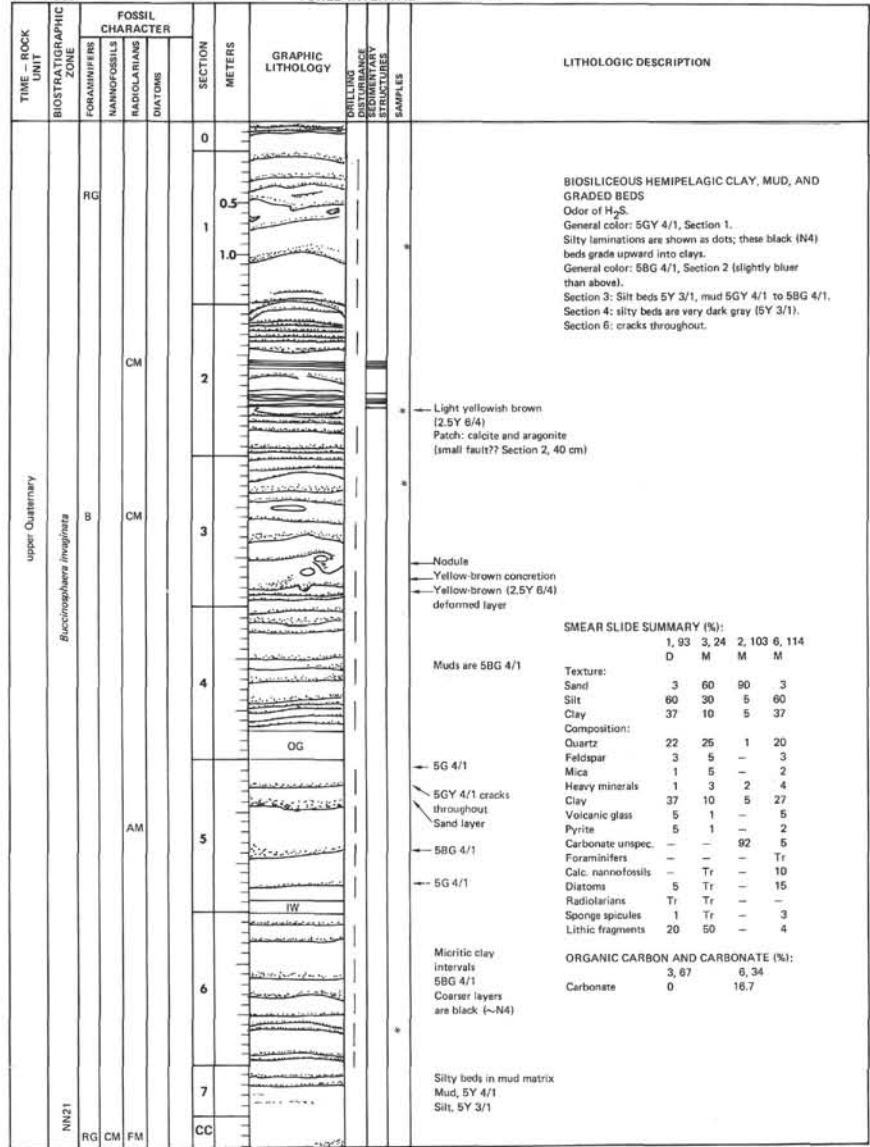
- Aoki, Y., Tamano, T., and Kato, S., 1982. Detailed structure of the Nankai Trough from migrated seismic sections. In Watkins, J. S., and Drake, C. L. (Eds.), *Studies in Continental Margin Geology: Tulsa (Am. Assoc. Petrol. Geol. Mem.)*, 34:309-322.
- Blow, W. H., 1969. Late middle Eocene to Recent planktonic foraminiferal biostratigraphy. In Brönnimann, P., and Renz, H. H. (Eds.), *Proc. First Int. Conf. Plankt. Microfossils: Leiden (E. J. Brill)*, 1: 199-421.
- Bray, C. J., and Karig, D. E., 1985. Porosity in sediments in accretionary prisms and some implications for dewatering processes. *J. Geophys. Res.*, 90:768-778.
- Clark, S. P., Jr. (Ed.), 1966. *Handbook of Physical Constants: Boulder, Colorado (Geol. Soc. Am. Mem.)*, 97.
- Coulbourn, W. T., and Moberly, R., 1977. Structural evidence of the evolution of fore-arc basins off South America. *Can. J. Earth Sci.*, 14:102-116.
- Durney, D. W., and Ramsey, J. G., 1973. Incremental strains measured by syntectonic crystal growths. In De Jong, K. A., and Scholten, R. (Eds.), *Gravity and Tectonics: New York (John Wiley and Sons)*, pp. 67-96.
- Hamilton, E. L., 1976. Variations of density and porosity in deep-sea sediments. *J. Sediment. Petrol.*, 46:280-300.

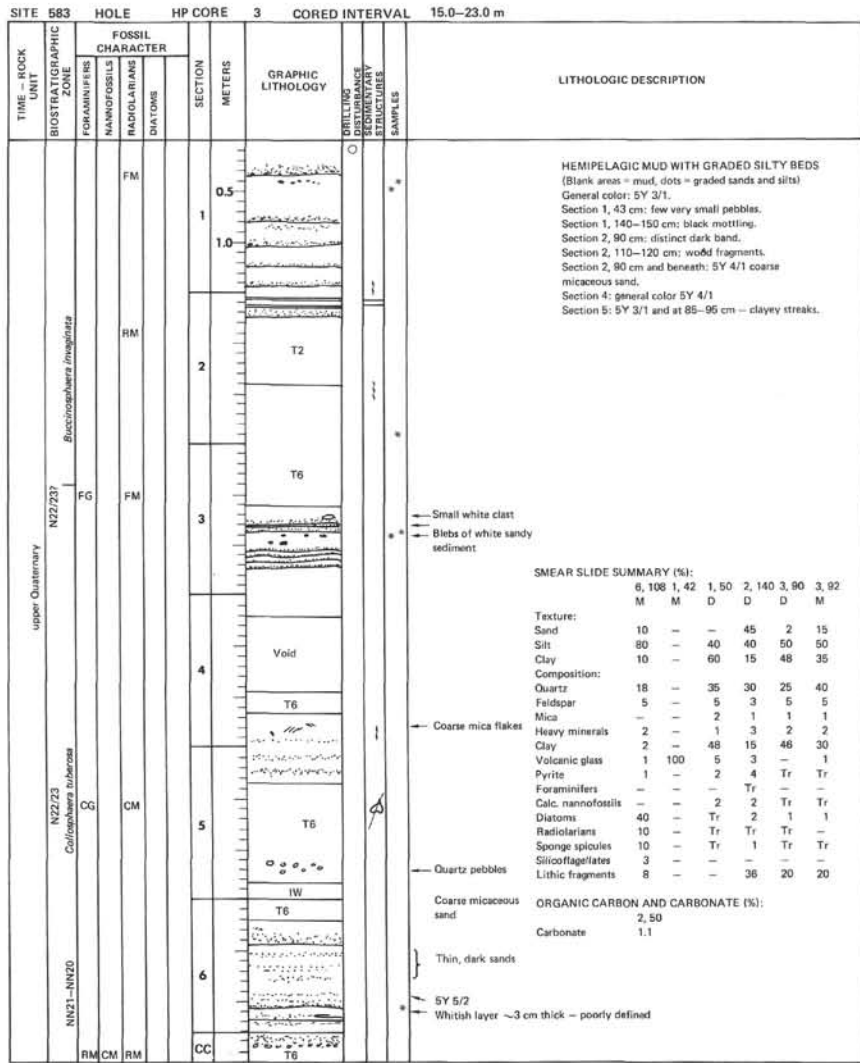
- Hobbs, B. E., Means, W. D., and Williams, P. F., 1976. *An Outline of Structural Geology*: New York (John Wiley and Sons).
- Hunt, J. M., 1979. *Petroleum Geochemistry and Geology*: San Francisco (W. H. Freeman and Company).
- Ingle, J. C., Jr., Karig, D. E., and Shipboard Scientific Party, 1975. Site 298. In Karig, D. E., Ingle, J. C., Jr., et al., *Init. Repts. DSDP*, 31: Washington (U.S. Govt. Printing Office), 317-350.
- Kagami, H., Tokuyama, H., Kong, E., Igarashi, C., and Nasu, N., 1982. Multichannel seismic reflection survey in the Nankai Trough. *Kaiyo-Kagaku*, 14(6):351-357.
- Martini, E., 1971. Standard Tertiary and Quaternary calcareous nanoplankton zonation. In Farinacci, A. (Ed.), *Proc. II Plankt. Conf. Roma*: Rome (Edizioni Tecnoscienza), 2:739-785.
- Moore, J. C., Watkins, J. S., and Shipley, T. H., 1982. Summary of accretionary processes, Deep Sea Drilling Project Leg 66: offscraping, underplating, and deformation of the slope apron. In Watkins, J. S., Moore, J. C., et al., *Init. Repts. DSDP*, 66: Washington (U.S. Govt. Printing Office), 825-836.
- Scientific Party, 1980. *Init. Repts. DSDP*, 56, 57: Washington (U.S. Govt. Printing Office).
- Seno, T., 1977. The instantaneous rotation vector of the Philippine Sea plate relative to the Eurasian plate. *Tectonophysics*, 42:209-226.
- Shephard, L. E., Bryant, W. R., and Chiou, W. A., 1982. Geotechnical properties of Middle America Trench sediments, Deep Sea Drilling Project Leg 66. In Watkins, J. S., Moore, J. C., et al., *Init. Repts. DSDP*, 66: Washington (U.S. Govt. Printing Office), 475-504.

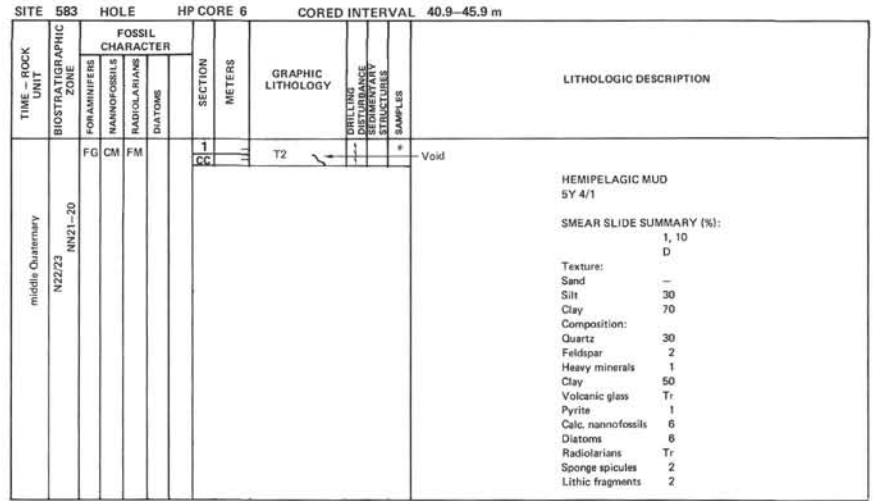
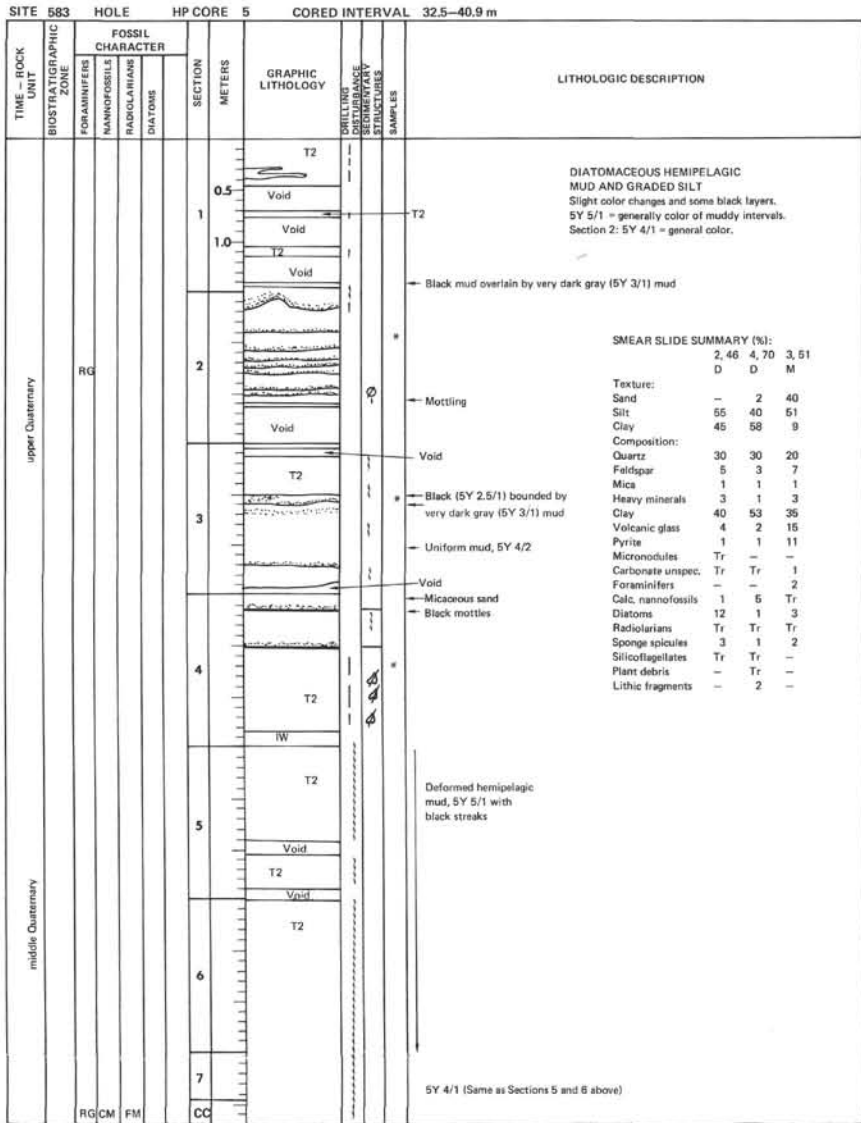
SITE 583 HOLE HP CORE 1 CORED INTERVAL 0.0-5.5 m

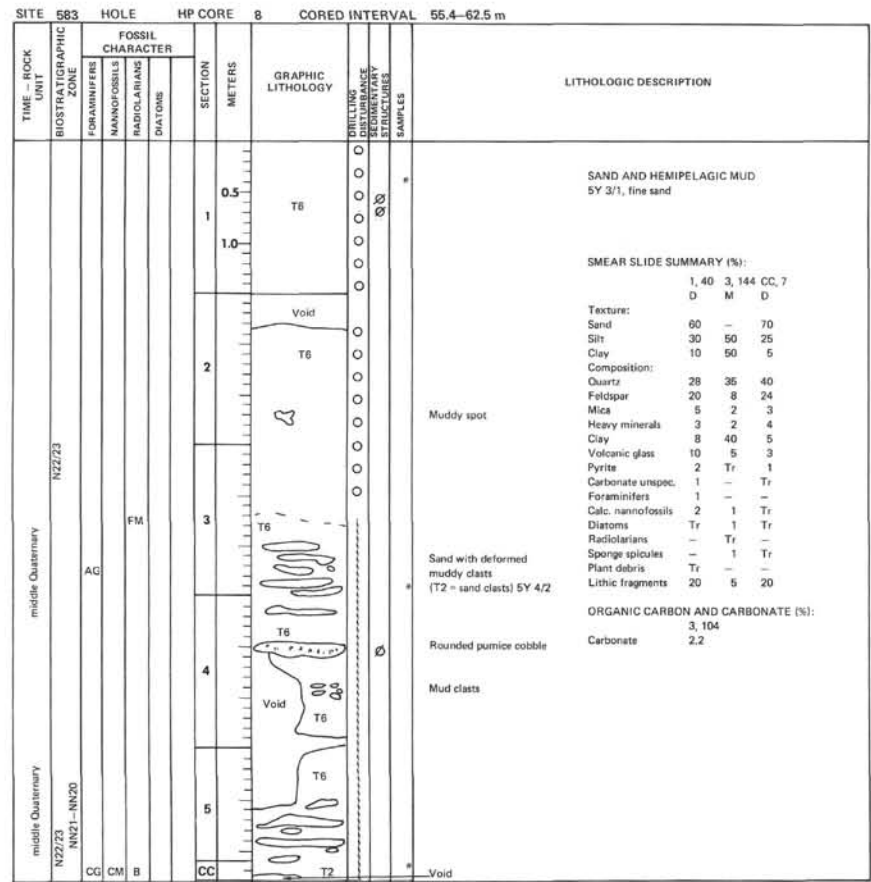
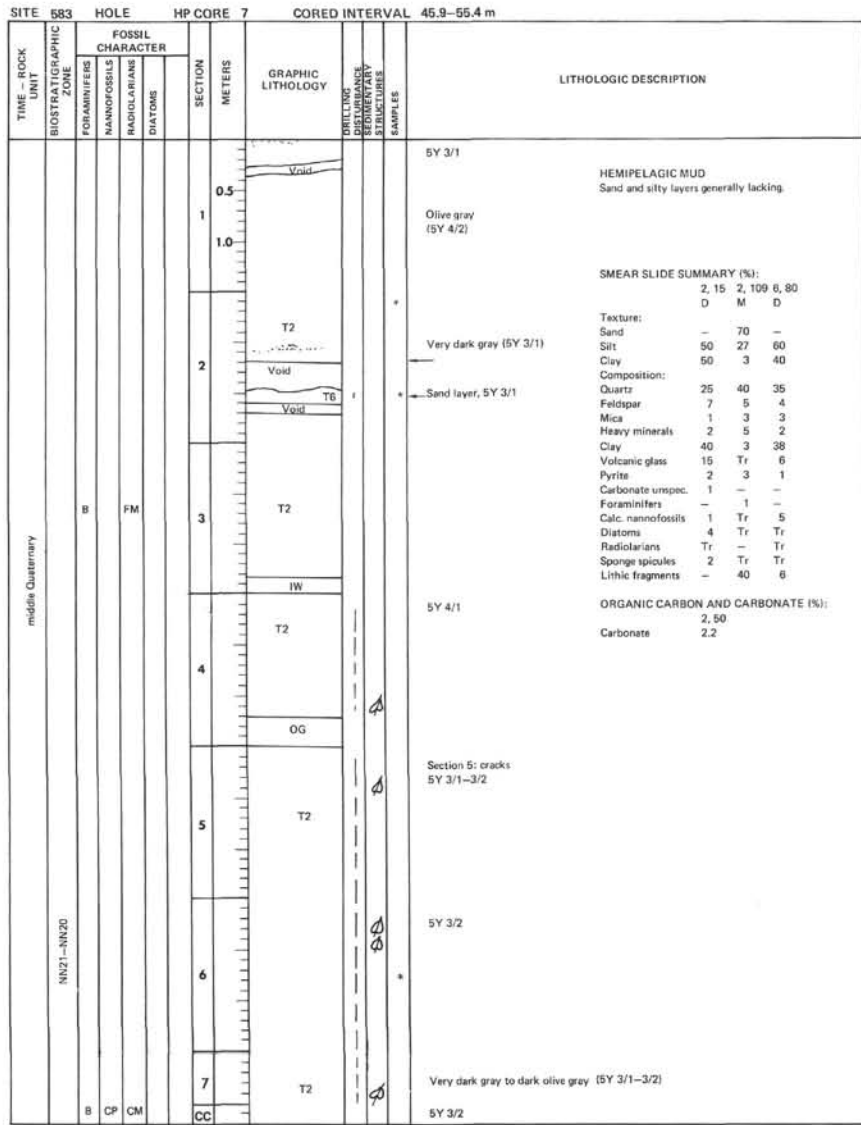


SITE 583 HOLE HP CORE 2 CORED INTERVAL 5.5-15.0 m

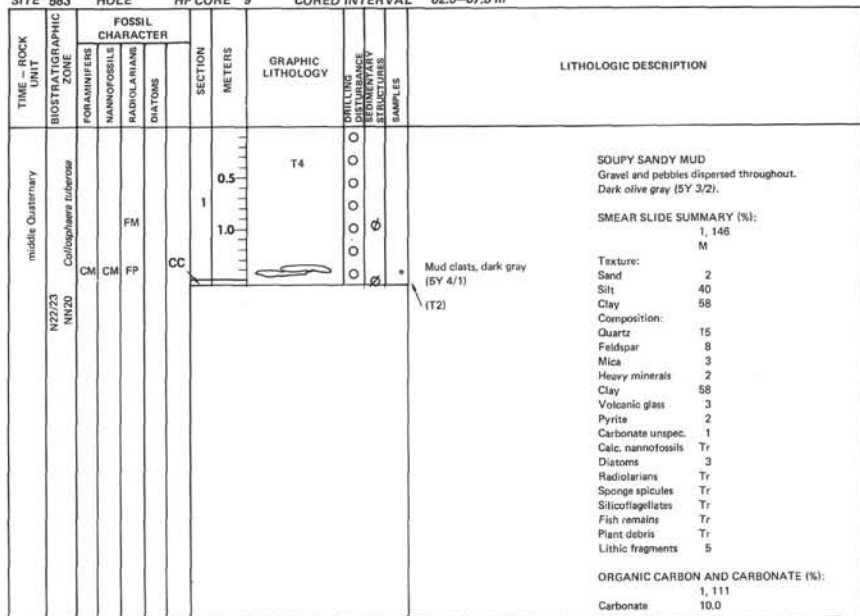




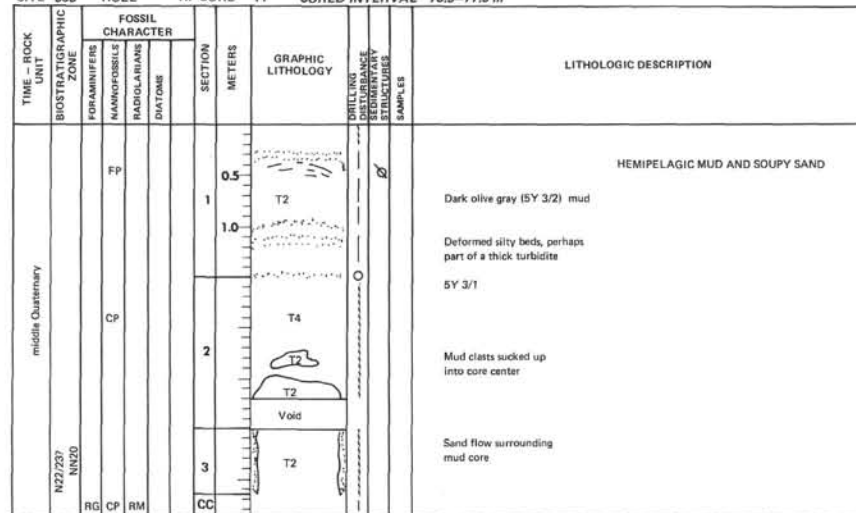




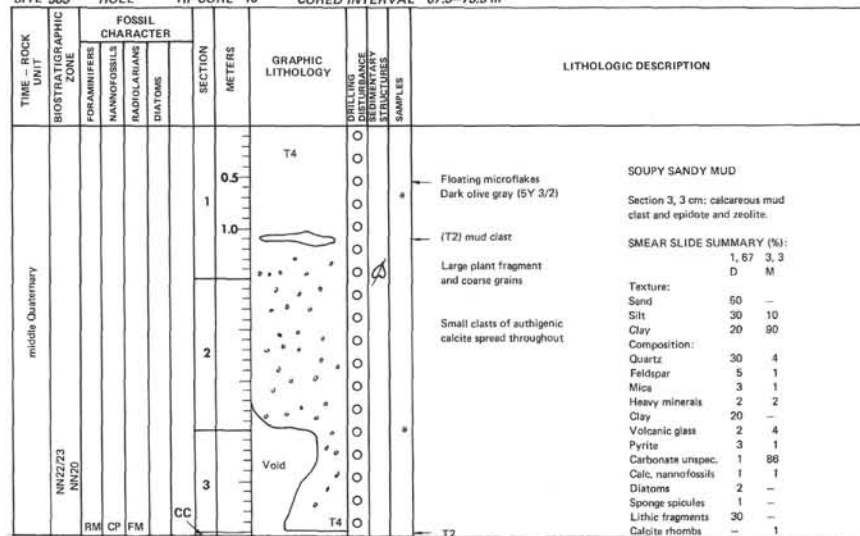
SITE 583 HOLE HP CORE 9 CORED INTERVAL 62.5-67.5 m



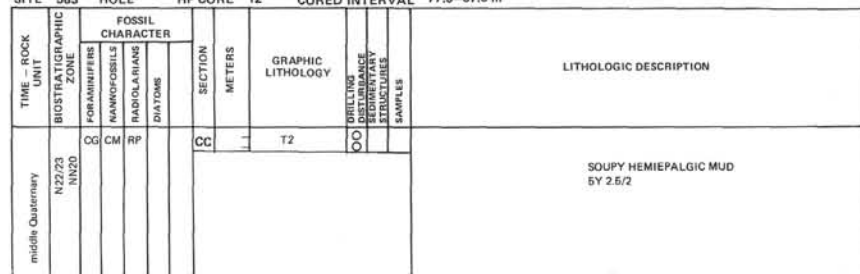
SITE 583 HOLE HP CORE 11 CORED INTERVAL 73.5-77.5 m

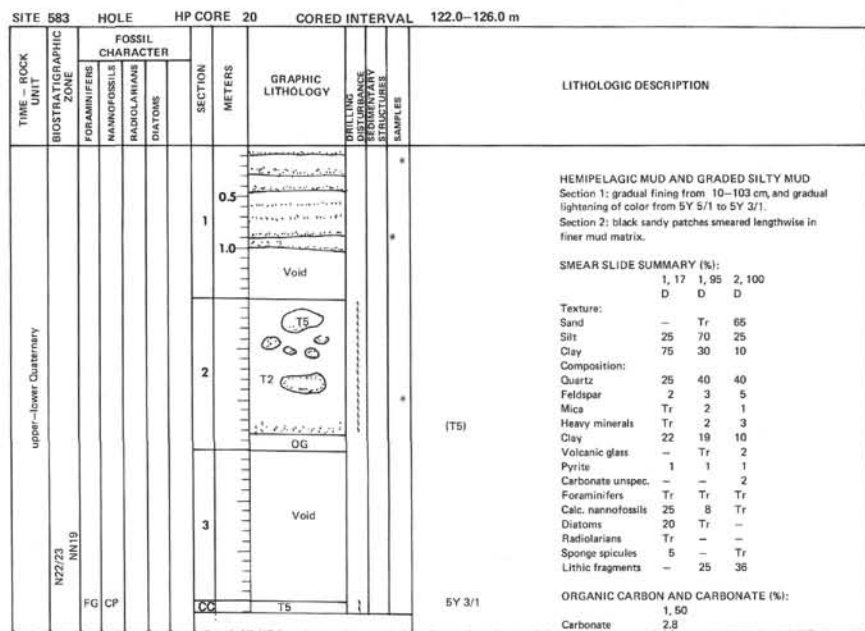
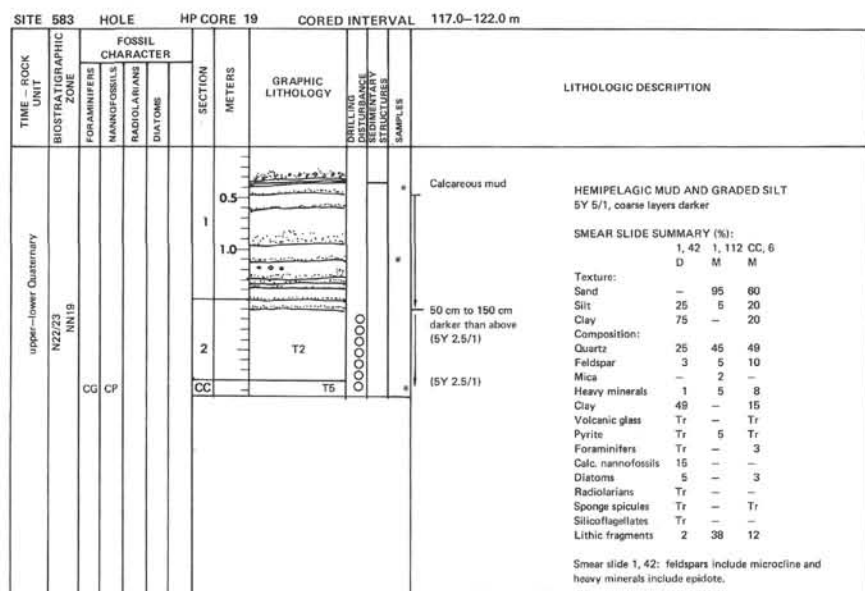
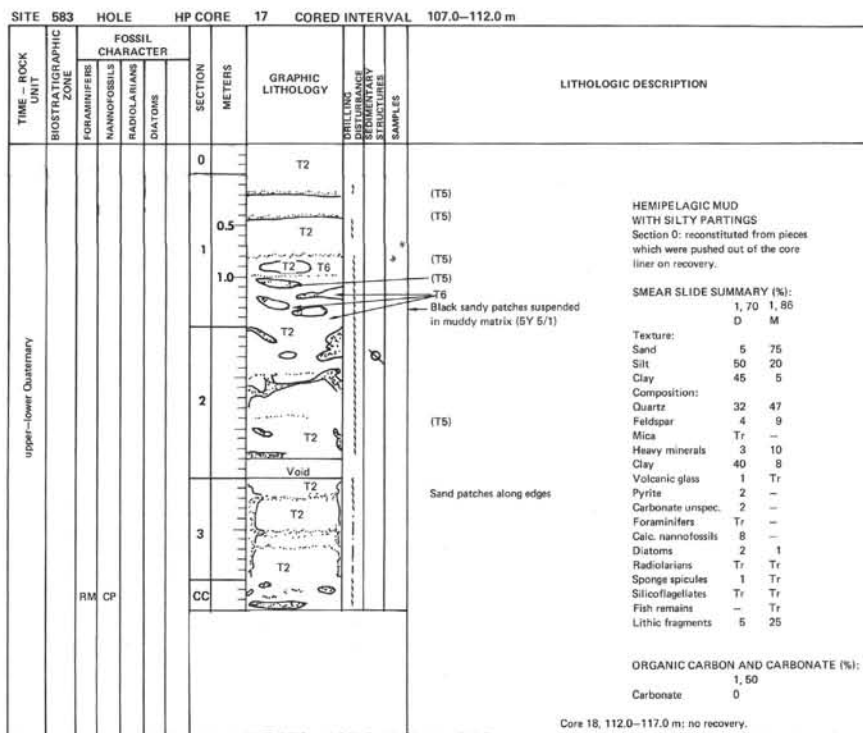


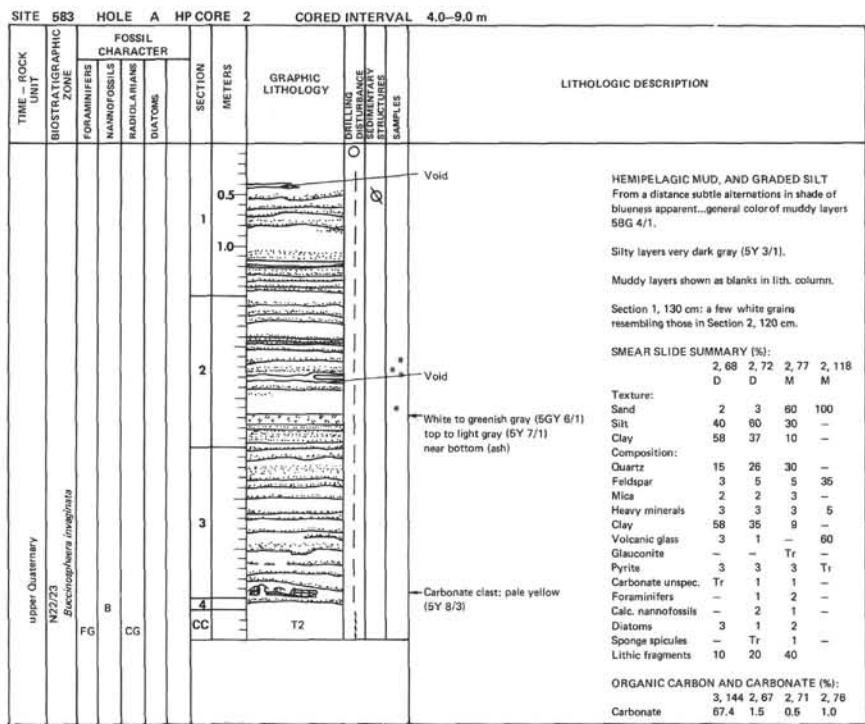
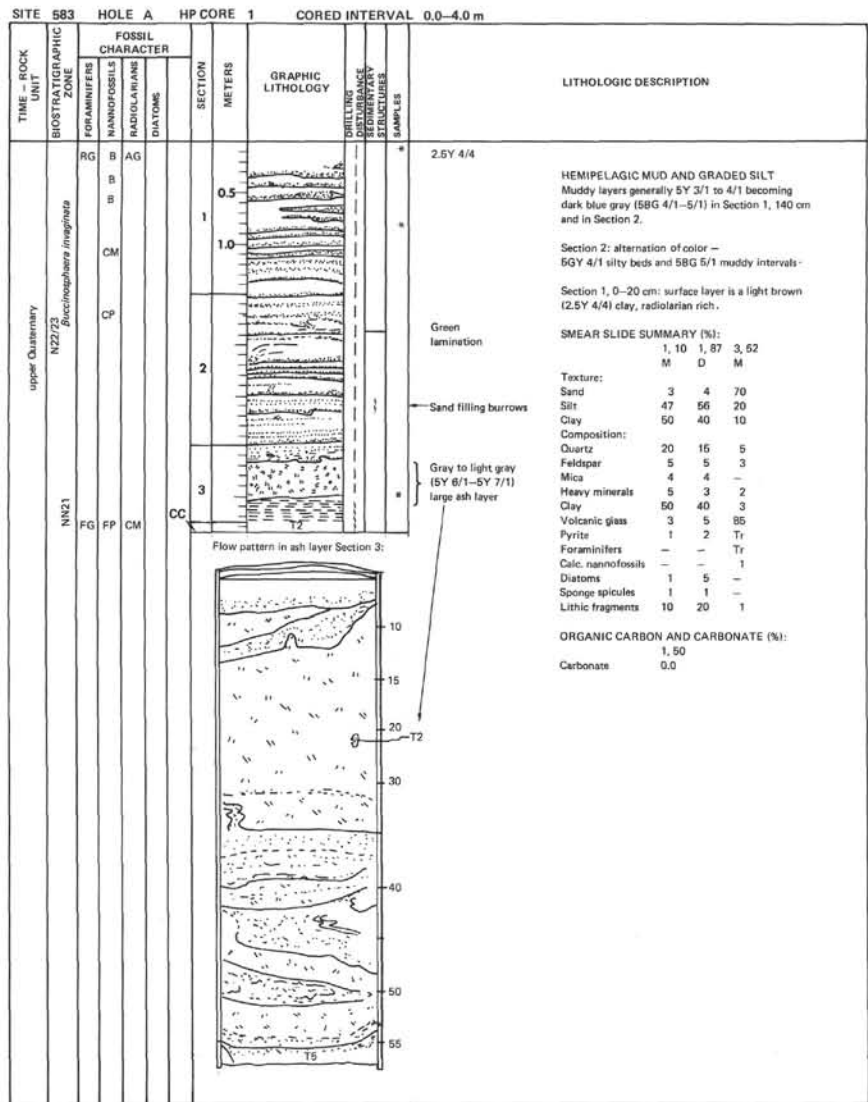
SITE 583 HOLE HP CORE 10 CORED INTERVAL 67.5-73.5 m

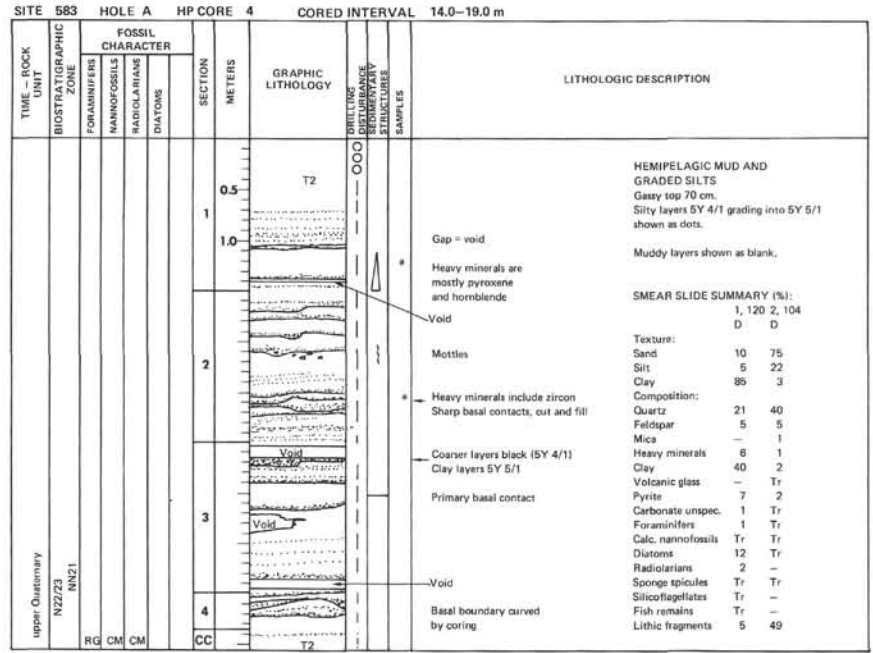
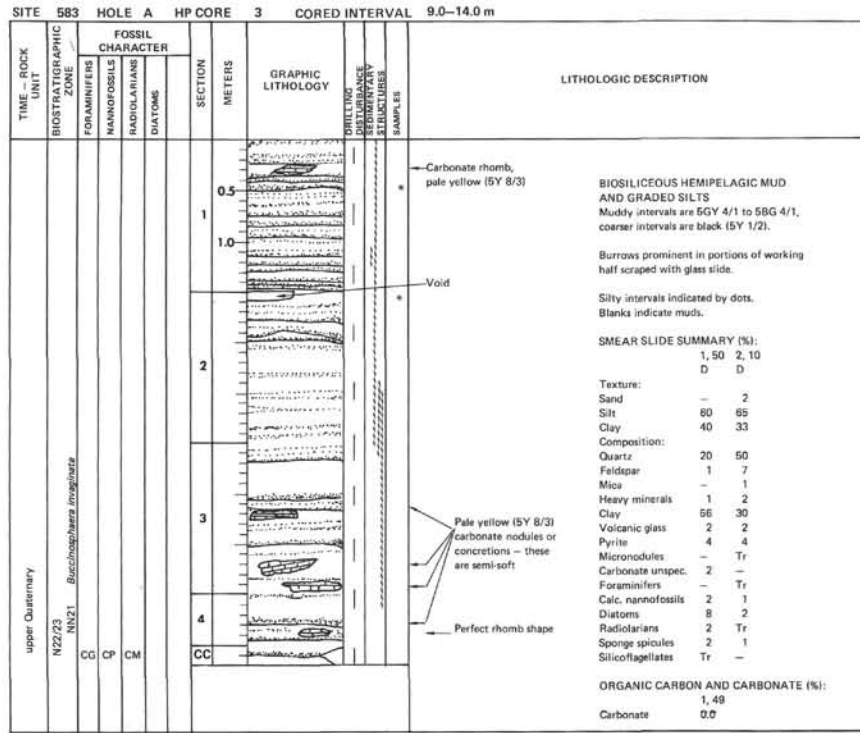


SITE 583 HOLE HP CORE 12 CORED INTERVAL 77.5-87.0 m



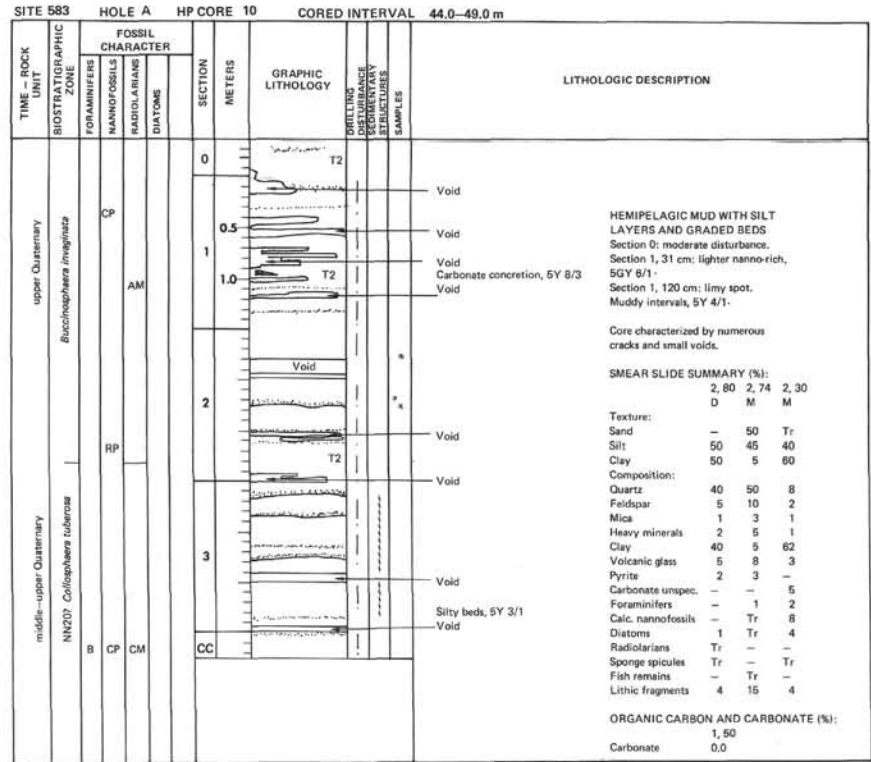
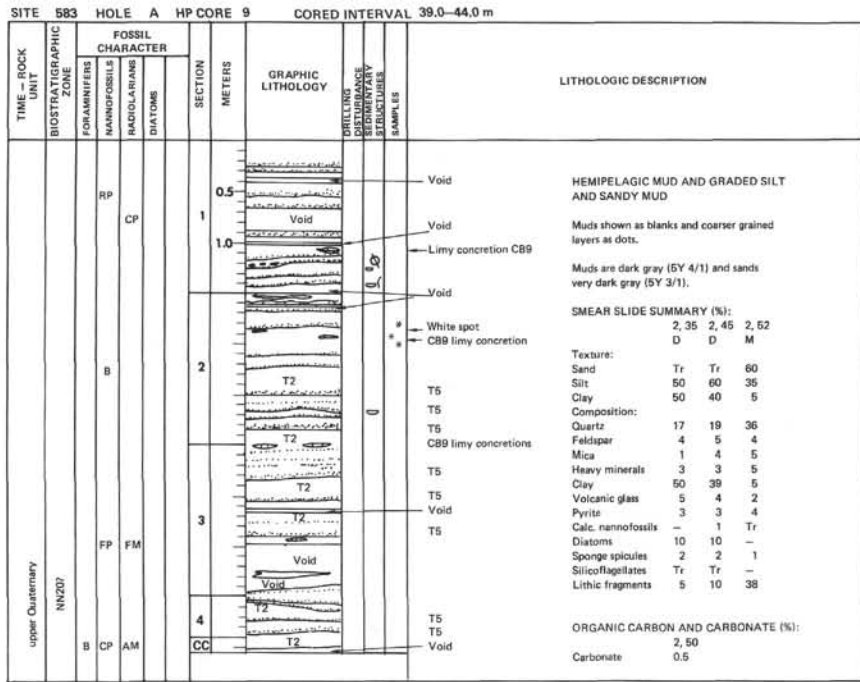






SITE 583		HOLE A		HP CORE 7		CORED INTERVAL 29.0-34.0 m																																		
TIME - ROCK UNIT	BIOSTRATIGRAPHIC ZONE	FOSSIL CHARACTER			SECTION METERS	GRAPHIC LITHOLOGY	LITHOLOGIC DESCRIPTION																																	
		FORAMINIFERS	NANNOFOSSILS	RADIOLARIANS				DIATOMS																																
upper Quaternary	N22/23 NN2/NN3 <i>Buccellastrina fragilata</i>	RM	CP	CM	1		Sand, 5Y 5/1 T8 SANDY BEDS, ASH, GRADED BEDS, AND HEMIPELAGIC MUD Sandy mud, 5Y 4/1 T4 SMEAR SLIDE SUMMARY (%): Sand, 5Y 5/1 <table border="1"> <tr> <td></td> <td>1,40</td> <td>1,70</td> <td>1,147</td> <td>2,10</td> <td>2,42</td> </tr> <tr> <td></td> <td>D</td> <td>D</td> <td>D</td> <td>M</td> <td>D</td> </tr> </table> Thin section Silty mud, 5Y 6/1 <table border="1"> <tr> <td>Texture:</td> <td>Sand</td> <td>98</td> <td>2</td> <td>2</td> <td>55</td> <td>Tr</td> </tr> <tr> <td></td> <td>Silt</td> <td>2</td> <td>68</td> <td>68</td> <td>40</td> <td>60</td> </tr> <tr> <td></td> <td>Clay</td> <td>30</td> <td>30</td> <td>5</td> <td>40</td> <td></td> </tr> </table> Composition: Quartz 5 48 50 60 45 Feldspar 10 11 6 5 Mica Tr 1 1 2 Tr Heavy minerals 2 2 5 2 Clay 25 25 4 30 Volcanic glass 95 5 2 9 10 Pyrite Tr 2 1 2 1 Micronodules Tr Tr Tr Tr Foraminifers Tr Tr Tr Tr Calc. nannofossils Tr 1 1 1 Diatoms 3 2 1 3 Radiolarians Tr Tr Tr Tr Sponge spicules Tr 1 Tr 1 Silicoflagellates Tr Tr Tr Tr Lithic fragments 3 4 10 3		1,40	1,70	1,147	2,10	2,42		D	D	D	M	D	Texture:	Sand	98	2	2	55	Tr		Silt	2	68	68	40	60		Clay	30	30	5	40	
			1,40	1,70				1,147	2,10	2,42																														
	D	D	D	M	D																																			
Texture:	Sand	98	2	2	55	Tr																																		
	Silt	2	68	68	40	60																																		
	Clay	30	30	5	40																																			
					2		Burrows show as black specks or mortles																																	
				CC			ORGANIC CARBON AND CARBONATE (%): Carbonate 1.0																																	

SITE 583		HOLE A		HP CORE 8		CORED INTERVAL 34.0-39.0 m	
TIME - ROCK UNIT	BIOSTRATIGRAPHIC ZONE	FOSSIL CHARACTER			SECTION METERS	GRAPHIC LITHOLOGY	LITHOLOGIC DESCRIPTION
		FORAMINIFERS	NANNOFOSSILS	RADIOLARIANS			
upper Quaternary	N22/23 NN2/NN3 <i>Buccellastrina fragilata</i>	RM	CP	CM	1		Void 5Y 5/2 HEMIPELAGIC MUD AND GRADED SILT AND SANDY MUD Silty layers black and shown in dot pattern... the coarser the grain size, the darker the color. Muddy layers are dark olive gray (5Y 3/2) and are shown by blanks.
					3		Ash layer Ash layer Silty layers...5Y 5/1 ORGANIC CARBON AND CARBONATE (%): Carbonate 2,80 Carbonate 0,5
				CC			ORGANIC CARBON AND CARBONATE (%): Carbonate 2,80 Carbonate 0,5



TIME - ROCK UNIT		SITE 583		HOLE A		HP CORE 11		CORED INTERVAL 49.0-54.0 m	
BIOSTRA TI GRAPHIC ZONE	FOSSIL CHARACTER			SECTION METERS	GRAPHIC LITHOLOGY	DRILLING DISTURBANCE	STRUCTURE	SAMPLES	LITHOLOGIC DESCRIPTION
	FORAMINIFERS	NANNOFOSSILS	RADIOLARIANS						
middle-upper Quaternary NN N22/237 NN20					0	T4			HEMIPELAGIC MUD, SILT, AND SAND Section 0: disturbed hemipelagic mud, 5Y 4/1. SMEAR SLIDE SUMMARY (%): 1, 145 1, 100 2, 64 D M M Texture: Sand 1 60 55 Silt 35 35 40 Clay 64 5 5 Composition: Quartz 12 65 50 Feldspar 1 4 7 Mica Tr 2 2 Heavy minerals Tr 2 3 Clay 54 5 5 Volcanic glass 3 4 8 Pyrite 1 2 1 Carbonate unsp. 1 - - Foraminifers - 1 Tr Calc. nanofossils 10 Tr Tr Diatoms 15 Tr 4 Radiolarians 1 Tr Tr Sponge spicules 2 Tr Tr Silicoflagellates Tr - - Plant debris Tr - - Lithic fragments - 15 20 ORGANIC CARBON AND CARBONATE (%): 2, 70 Carbonate 2.0
				0.5	T6				
				1	Void				
				1.0	T6			SY 3/1-5Y 2.5/1	
				2	T4			SY 4/1-5GY 4/1 Coring deformation Black (5Y 2.5/1) spots	
				3	T2			SY 3/2	
				CC				SY 3/1	

SITE 583 HOLE B HP CORE 1 CORED INTERVAL 0.0-5.0 m

TIME - ROCK UNIT	BIOSTRATIGRAPHIC ZONE	FOSSIL CHARACTER			SECTION METERS	GRAPHIC LITHOLOGY	DRILLING DISTURBANCE	REWORKED STRUCTURES	SAMPLES	LITHOLOGIC DESCRIPTION			
		FORAMINIFERS	NANNOFOSSILS	RADIOLARIANS							DIATOMS		
upper Quaternary	NN21-NN20	B	RP	FM	0.5	T4				Deformed HEMIPELAGIC MUD AND SILTY MUD Dark gray (5Y 4/1) muddy silt and 5BG 4/1-5Y 4/1 mud Strong H ₂ S odor. No orientation available.			
					1.0								
					2								
					3	SR6	T4						Pumice Layer very rich in plant fragments
4					T2				5Y 4/1				
					CC								

SMEAR SLIDE SUMMARY (%):

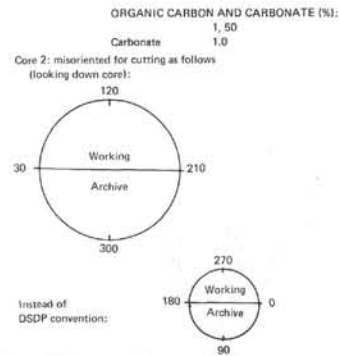
2, 80
D
Texture:
Sand 5
Silt 60
Clay 35
Composition:
Quartz 29
Feldspar 3
Mica 5
Heavy minerals 2
Clay 35
Volcanic glass 2
Glaucconite Tr
Pyrite 5
Carbonate unsp. 1
Foraminifers Tr
Calc. nannofossils Tr
Diatoms 10
Radiolarians Tr
Sponge spicules 2
Plant debris 1
Lithic fragments 5

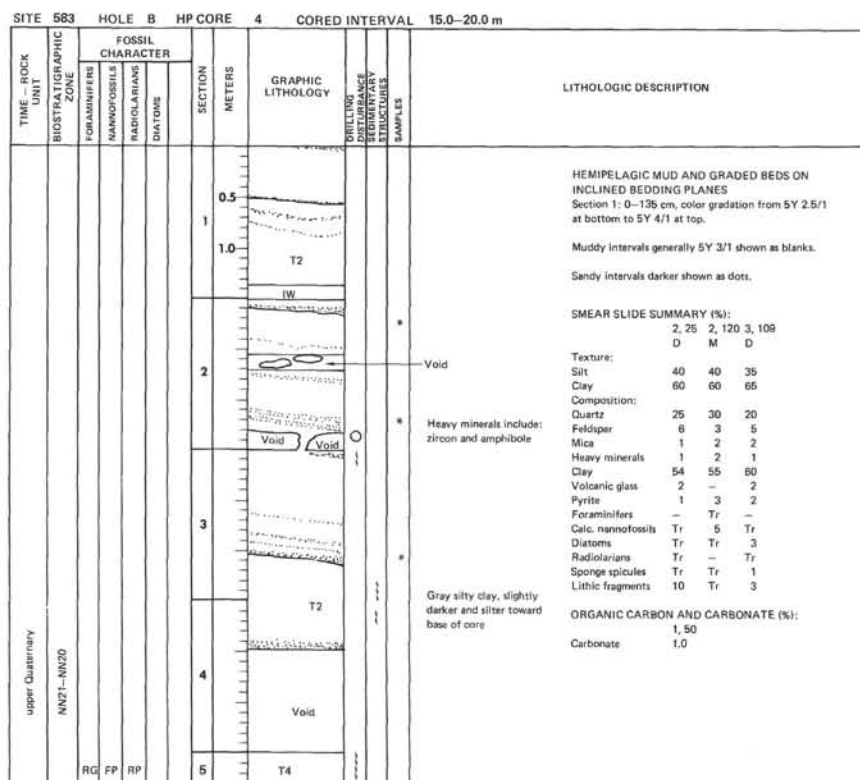
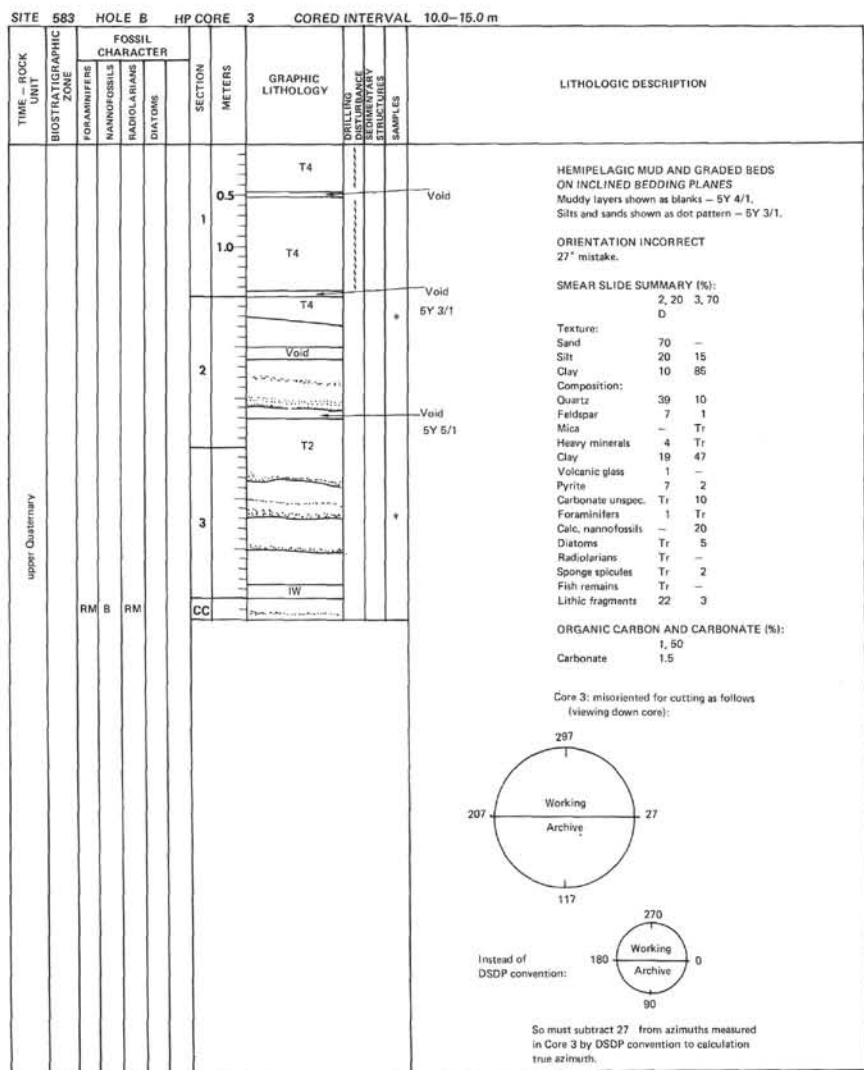
SITE 583 HOLE B HP CORE 2 CORED INTERVAL 5.0-10.0 m

TIME - ROCK UNIT	BIOSTRATIGRAPHIC ZONE	FOSSIL CHARACTER			SECTION METERS	GRAPHIC LITHOLOGY	DRILLING DISTURBANCE	REWORKED STRUCTURES	SAMPLES	LITHOLOGIC DESCRIPTION			
		FORAMINIFERS	NANNOFOSSILS	RADIOLARIANS							DIATOMS		
upper Quaternary	NN21	B	CM	RP	0.5	T6				HEMIPELAGIC MUD AND GRADED SILT ON INCLINED BEDDING PLANES Murky layers 5BG 4/1 to 5Y 4/1, 5Y 3/1 color of silt beds			
					1.0								
					2								ORIENTATION INCORRECT Drawing copies cut-core/archive half (reversing structures by 180° will give approximate correct orientation).
					3								SMEAR SLIDE SUMMARY (%):
4									ORGANIC CARBON AND CARBONATE (%):				

SMEAR SLIDE SUMMARY (%):

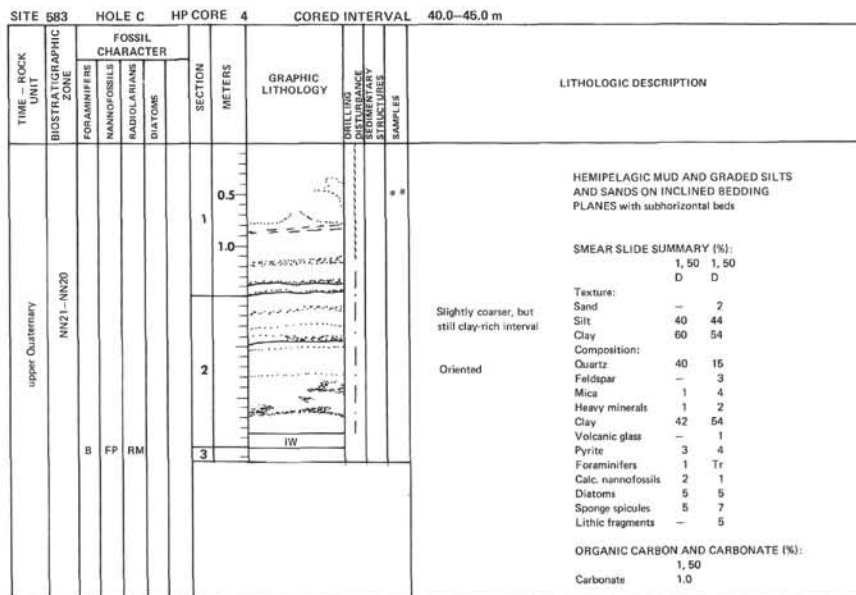
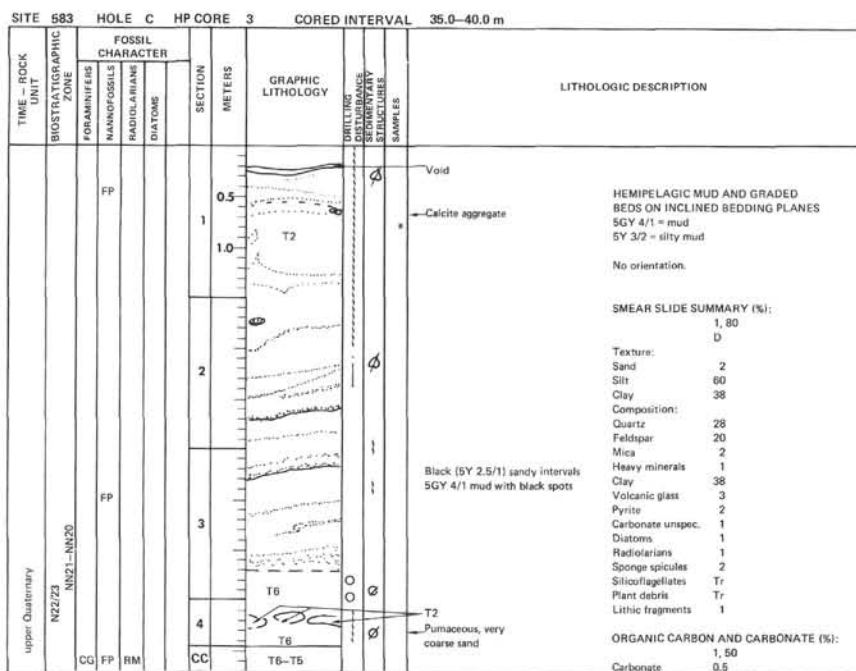
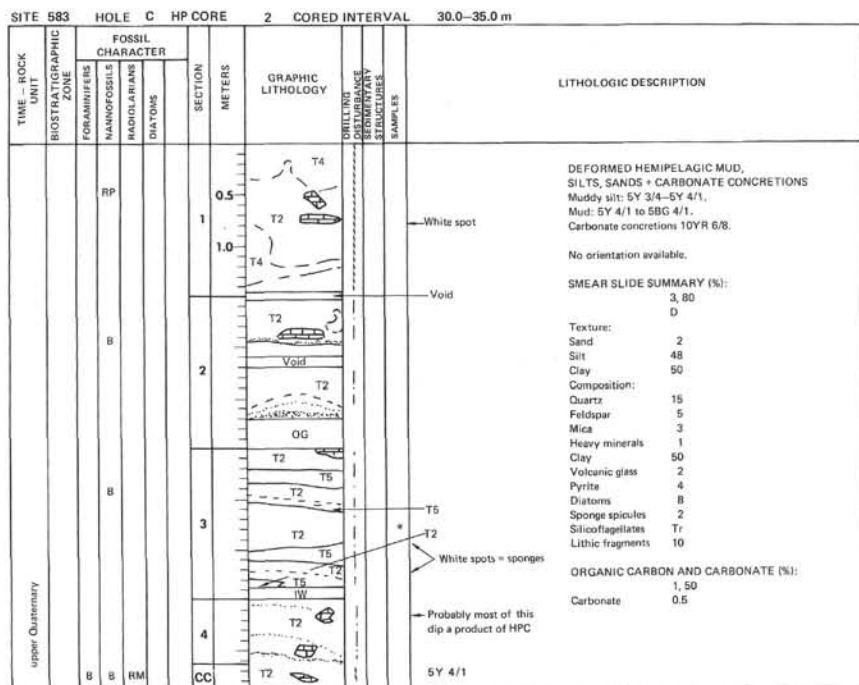
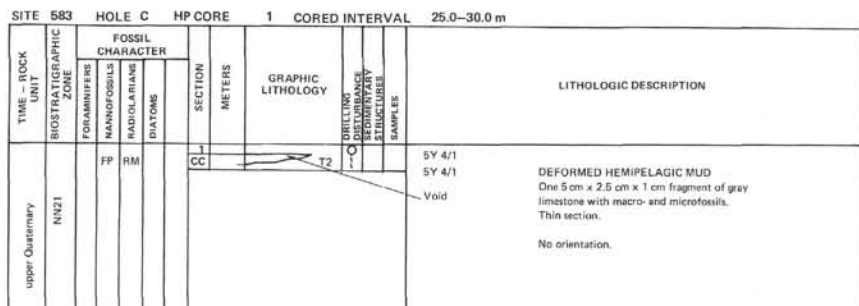
1, 50
1, 50
3, 78
D
Texture:
Sand 25
Silt 40
Clay 35
Composition:
Quartz 30
Feldspar 30
Mica 5
Heavy minerals 2
Clay 30
Volcanic glass 30
Glaucconite 1
Palagonite 1
Pyrite 1
Carbonate unsp. 2
Foraminifers 5
Calc. nannofossils 21
Diatoms 1
Radiolarians 20
Sponge spicules 5
Silicoflagellates 1
Plant debris 3
Lithic fragments 20





SITE 583 HOLE B HP CORE 5 CORED INTERVAL 20.0-25.0 m

TIME - ROCK UNIT	BIOSTRATIGRAPHIC ZONE	FOSSIL CHARACTER			SECTION METERS	GRAPHIC LITHOLOGY	CORRELATION DISTURBANCE	LABORATORY SAMPLES	LITHOLOGIC DESCRIPTION																																																																						
		FORAMIFERS	NANNOFOSSILS	RADIOLARIANS						DIATOMS																																																																					
upper Quaternary	N22/23 NN21	RG	FM	FM	0.5	Void			<p>HEMIPELAGIC MUD AND GRADED SILTY BEDS Black spots, mottles, in muddy layers. 5Y 3/2 = mud color, coarser intervals are darker and shown as dot patterns.</p> <p>Section 3: lots of cracks.</p> <p>ORIENTATION SUSPECT BECAUSE HOLE DEVIATION DIFFERS FROM PREVIOUS</p> <p>SMEAR SLIDE SUMMARY (%):</p> <table border="1"> <thead> <tr> <th></th> <th>1, 40</th> <th>3, 10</th> </tr> <tr> <th>M</th> <th>D</th> <th></th> </tr> </thead> <tbody> <tr> <td>Texture:</td> <td></td> <td></td> </tr> <tr> <td>Sand</td> <td>60</td> <td>-</td> </tr> <tr> <td>Silt</td> <td>35</td> <td>30</td> </tr> <tr> <td>Clay</td> <td>5</td> <td>70</td> </tr> <tr> <td>Composition:</td> <td></td> <td></td> </tr> <tr> <td>Quartz</td> <td>15</td> <td>20</td> </tr> <tr> <td>Feldspar</td> <td>8</td> <td>5</td> </tr> <tr> <td>Mica</td> <td>4</td> <td>1</td> </tr> <tr> <td>Heavy minerals</td> <td>2</td> <td>1</td> </tr> <tr> <td>Clay</td> <td>5</td> <td>63</td> </tr> <tr> <td>Volcanic glass</td> <td>8</td> <td>-</td> </tr> <tr> <td>Pyrite</td> <td>2</td> <td>1</td> </tr> <tr> <td>Carbonate unsp. spec.</td> <td>2</td> <td>-</td> </tr> <tr> <td>Foraminifers</td> <td>1</td> <td>-</td> </tr> <tr> <td>Calc. nannofossils</td> <td>1</td> <td>Tr</td> </tr> <tr> <td>Diatoms</td> <td>5</td> <td>5</td> </tr> <tr> <td>Radiolarians</td> <td>Tr</td> <td>Tr</td> </tr> <tr> <td>Sponge spicules</td> <td>2</td> <td>1</td> </tr> <tr> <td>Silicoflagellates</td> <td>-</td> <td>Tr</td> </tr> <tr> <td>Lithic fragments</td> <td>45</td> <td>2</td> </tr> </tbody> </table> <p>ORGANIC CARBON AND CARBONATE (%):</p> <table border="1"> <tbody> <tr> <td>Carbon</td> <td>1.50</td> </tr> <tr> <td>Carbonate</td> <td>1.5</td> </tr> </tbody> </table> <p>Core 5, 25.0-30.0 m: no recovery.</p>		1, 40	3, 10	M	D		Texture:			Sand	60	-	Silt	35	30	Clay	5	70	Composition:			Quartz	15	20	Feldspar	8	5	Mica	4	1	Heavy minerals	2	1	Clay	5	63	Volcanic glass	8	-	Pyrite	2	1	Carbonate unsp. spec.	2	-	Foraminifers	1	-	Calc. nannofossils	1	Tr	Diatoms	5	5	Radiolarians	Tr	Tr	Sponge spicules	2	1	Silicoflagellates	-	Tr	Lithic fragments	45	2	Carbon	1.50	Carbonate	1.5
						1, 40	3, 10																																																																								
					M	D																																																																									
					Texture:																																																																										
Sand	60	-																																																																													
Silt	35	30																																																																													
Clay	5	70																																																																													
Composition:																																																																															
Quartz	15	20																																																																													
Feldspar	8	5																																																																													
Mica	4	1																																																																													
Heavy minerals	2	1																																																																													
Clay	5	63																																																																													
Volcanic glass	8	-																																																																													
Pyrite	2	1																																																																													
Carbonate unsp. spec.	2	-																																																																													
Foraminifers	1	-																																																																													
Calc. nannofossils	1	Tr																																																																													
Diatoms	5	5																																																																													
Radiolarians	Tr	Tr																																																																													
Sponge spicules	2	1																																																																													
Silicoflagellates	-	Tr																																																																													
Lithic fragments	45	2																																																																													
Carbon	1.50																																																																														
Carbonate	1.5																																																																														
1																																																																															
2					T2			Black and micaceous, sandy mud																																																																							
					IW																																																																										
3					T2			Void																																																																							
4								5Y 4/1: color of mud in Section 4																																																																							
CC					T2																																																																										



SITE 583 HOLE C HP CORE 5 CORED INTERVAL 45.0-49.0 m

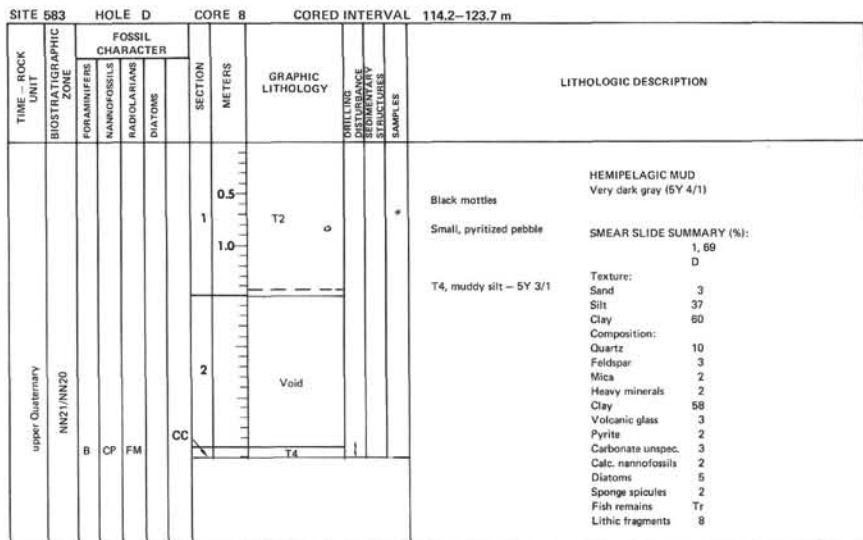
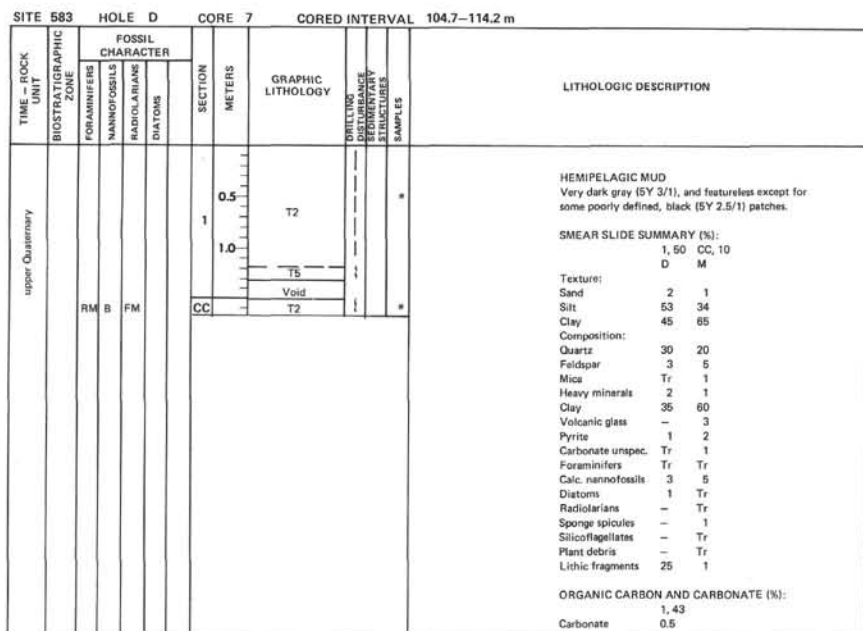
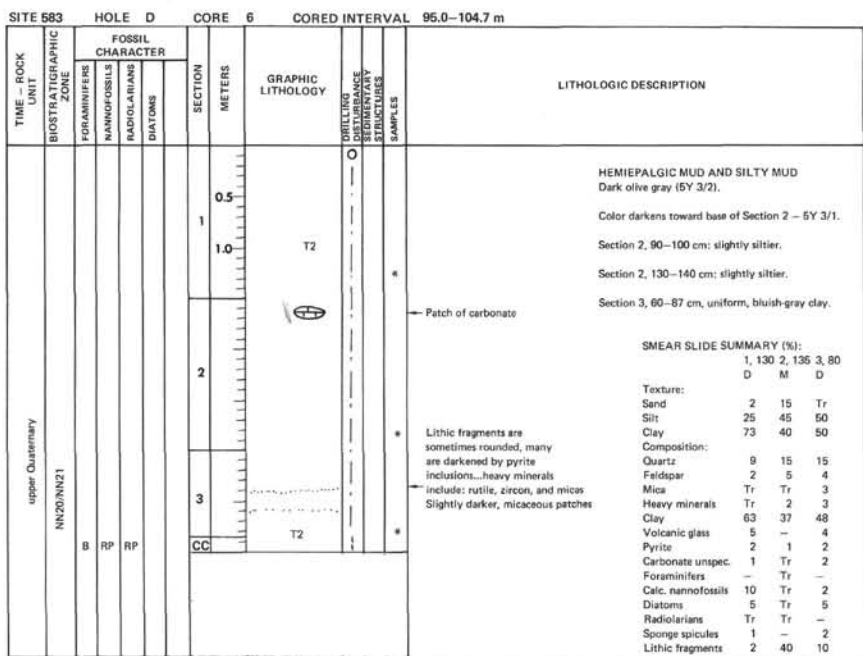
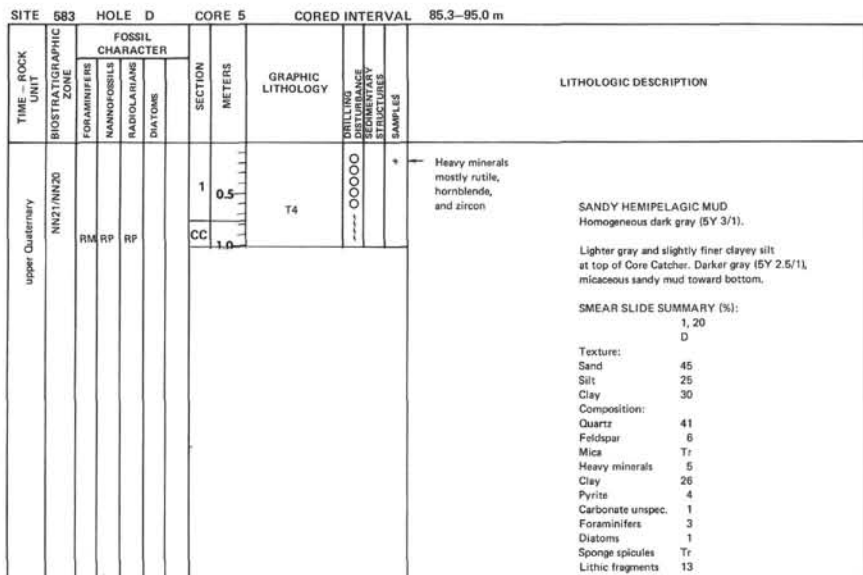
TIME - ROCK UNIT	BIOSTRATIGRAPHIC ZONE	FOSSIL CHARACTER			SECTION METERS	GRAPHIC LITHOLOGY	DRILLING DELIVERANCE SAMPLES	LITHOLOGIC DESCRIPTION
		FORAMINIFERS	NANNOFOSSILS	RADIOLARIANS				
upper Quaternary	NN21-NN20							<p>5Y 3/1 = sand and 5Y 4/1 = mud</p> <p>Brecciated marly limestone olive gray (5Y 5/2) Foraminifer bearing limestone</p> <p>Heavy minerals include: amphibole and epidote Mud = 5GY 4/1</p> <p>HEMPELAGIC MUD GRADED SILTS AND SANDS ON INCLINED BEDDING PLANES - no orientation.</p> <p>SMEAR SLIDE SUMMARY (%): 1, 110 2, 65 D M</p> <p>Texture: Sand - 3 Silt 40 60 Clay 60 37</p> <p>Composition: Quartz 30 25 Feldspar 5 5 Mica 2 5 Heavy minerals 2 3 Clay 55 35 Volcanic glass 1 1 Pyrite 1 5 Carbonate unspec. - 1 Foraminifers - 1 Calc. nannofossils Tr 2 Diatoms 1 1 Radiolarians Tr - Sponge spicules Tr 1 Lithic fragments 3 15</p> <p>ORGANIC CARBON AND CARBONATE (%): 1, 50 Carbonate 0.0</p>
	B	FP	RM		0.5 1 1.0 2 3	T2 T2 T2 Void	CC	5BG 4/1

SITE 583		HOLE D		CORE 1		CORED INTERVAL: 46.8-56.4 m	
TIME - ROCK UNIT	BIOSTRATIGRAPHIC ZONE	FOSSIL CHARACTER			SECTION METERS	GRAPHIC LITHOLOGY	LITHOLOGIC DESCRIPTION
		FORAMINIFERS	NANNOFOSSILS	RADIOLARIANS			
upper Quaternary	NN21	RM	CM	FM			HEMIPELAGIC MUD 5GY 4/1
					CC	T2	SMEAR SLIDE SUMMARY (%): CC, 6 D
							Texture: Sand 5 Silt 50 Clay 45 Composition: Quartz 15 Feldspar 3 Mica 4 Heavy minerals 3 Clay 44 Volcanic glass 2 Pyrite 3 Carbonate unspec. 1 Foraminifers 1 Calc. nannofossils 1 Diatoms 2 Sponge spicules 1 Lithic fragments 20

SITE 583		HOLE D		CORE 2		CORED INTERVAL: 56.4-66.0 m	
TIME - ROCK UNIT	BIOSTRATIGRAPHIC ZONE	FOSSIL CHARACTER			SECTION METERS	GRAPHIC LITHOLOGY	LITHOLOGIC DESCRIPTION
		FORAMINIFERS	NANNOFOSSILS	RADIOLARIANS			
upper Quaternary	NN21	B	B	FM			TRACE RECOVERY 5GY 4/1 hemipelagic mud Σ ~40 cc vol. to paleontologists.
					1		

SITE 583		HOLE D		CORE 3		CORED INTERVAL: 66.0-75.6 m	
TIME - ROCK UNIT	BIOSTRATIGRAPHIC ZONE	FOSSIL CHARACTER			SECTION METERS	GRAPHIC LITHOLOGY	LITHOLOGIC DESCRIPTION
		FORAMINIFERS	NANNOFOSSILS	RADIOLARIANS			
upper Quaternary	N22/23 NN21	RM	AG	FM			NANNOFOSSIL-RICH HEMIPELAGIC MUD Very dark gray (5Y 4/1) at the top to olive (5Y 5/2) near 100 cm.
					1	T2	SMEAR SLIDE SUMMARY (%): 1, 50 1, 110 D
							Texture: Sand - 5 Silt 5 5 Clay 95 90 Composition: Quartz 10 14 Feldspar - 1 Heavy minerals 1 1 Clay 55 24 Pyrite 1 5 Carbonate unspec. - 3 Foraminifers 5 7 Calc. nannofossils 20 20 Diatoms 5 8 Radiolarians Tr 6 Sponge spicules 3 7 Lithic fragments - 4
							* 100 cm to 110 cm contaminated by pipe-scale The piece may originally have belonged to the working half.

SITE 583		HOLE D		CORE 4		CORED INTERVAL: 75.6-85.3 m	
TIME - ROCK UNIT	BIOSTRATIGRAPHIC ZONE	FOSSIL CHARACTER			SECTION METERS	GRAPHIC LITHOLOGY	LITHOLOGIC DESCRIPTION
		FORAMINIFERS	NANNOFOSSILS	RADIOLARIANS			
upper Quaternary	N22/23 NN21	CG	FP	B			HEMIPELAGIC MUD AND SANDY MUD Color: 5Y 4/1
					1	T4	SMEAR SLIDE SUMMARY (%): 1, 30 D
							Texture: Sand 55 Silt 35 Clay 10 Composition: Quartz 20 Feldspar 8 Mica Tr Heavy minerals 3 Clay 10 Volcanic glass 2 Pyrite 2 Carbonate unspec. 1 Calc. nannofossils 1 Sponge spicules Tr Lithic fragments 53
							40-65 cm looks slightly gasier than above or below - more cracks, otherwise, entirely uniform lithology, driller described core as "through sand until new bottom"



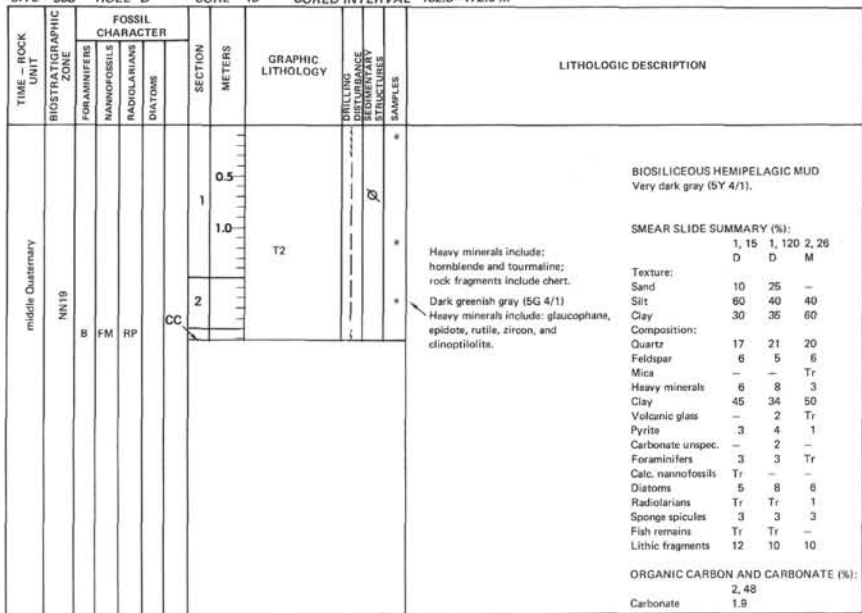
SITE 583		HOLE D		CORE 9		CORED INTERVAL 123.7-133.2 m	
TIME - ROCK UNIT	BIOSTRATIGRAPHIC ZONE	FOSSIL CHARACTER			SECTION METERS	GRAPHIC LITHOLOGY	LITHOLOGIC DESCRIPTION
		FORAMINIFERS	NANNOFOSSILS	RADIOLARIANS			
upper Quaternary	NN21/NN20	RM	CM	RM	0.5	T2	HEMPELAGIC MUD AND SILTY LAYERS Mud = very dark gray (5Y 4/1). SMEAR SLIDE SUMMARY (%): 1, 90 2, 55 3, 140 M D M Texture: Sand - 5 50 Silt 40 35 25 Clay 60 60 25 Composition: Quartz 30 25 8 Feldspar 2 5 Tr Mica 1 - - Heavy minerals 1 6 2 Clay 35 20 5 Volcanic glass - - 85 Pyrite 1 8 - Carbonate unspec. Tr - - Foraminifers Tr - - Calc. nanofossils 10 Tr - Diatoms 15 25 - Radiolarians Tr 4 - Sponge spicules 3 Tr - Silicoflagellates Tr Tr - Lithic fragments 2 7 -
					1.0	T2	
					2	T2	
					3	T2	Ashy sand Void 60 cm: white spot 5GY 4/1 mud Ashy sand Ash layer in the middle of Core Catcher

SITE 583		HOLE D		CORE 10		CORED INTERVAL 133.2-142.9 m	
TIME - ROCK UNIT	BIOSTRATIGRAPHIC ZONE	FOSSIL CHARACTER			SECTION METERS	GRAPHIC LITHOLOGY	LITHOLOGIC DESCRIPTION
		FORAMINIFERS	NANNOFOSSILS	RADIOLARIANS			
upper Quaternary	NN21/NN20	B	CM	FM	0.5	T2	HEMPELAGIC MUD Very dark gray (5Y 3/1) and featureless. SMEAR SLIDE SUMMARY (%): 1, 70 D Texture: Sand 5 Silt 50 Clay 45 Composition: Quartz 18 Feldspar 6 Mica 1 Heavy minerals 1 Clay 35 Volcanic glass 2 Pyrite 3 Carbonate unspec. 2 Foraminifers Tr Calc. nanofossils 10 Diatoms 20 Radiolarians Tr Sponge spicules 1 Silicoflagellates Tr Plant debris Tr Other 1
					1.0	T2	
					1.0	Void	ORGANIC CARBON AND CARBONATE (%): Carbonate 1.36 1.0

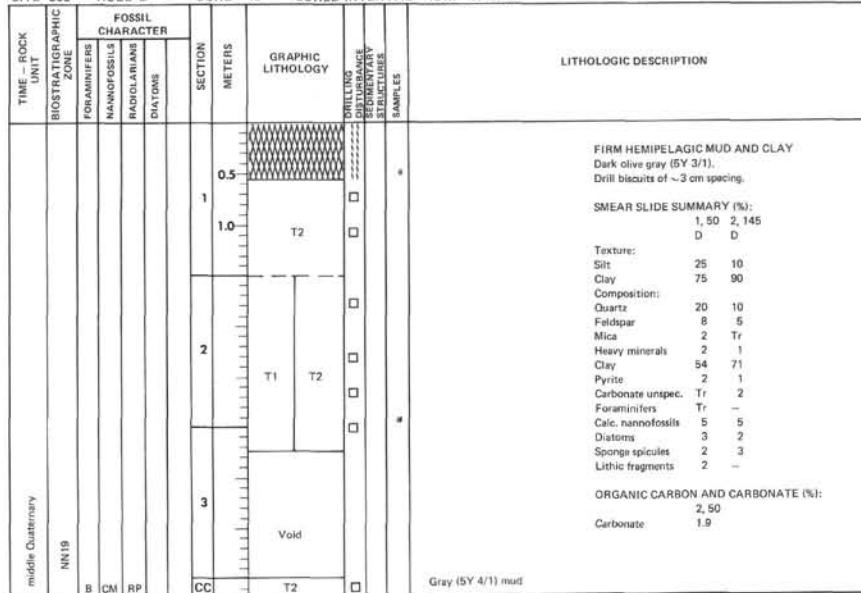
SITE 583		HOLE D		CORE 11		CORED INTERVAL 142.9-152.6 m	
TIME - ROCK UNIT	BIOSTRATIGRAPHIC ZONE	FOSSIL CHARACTER			SECTION METERS	GRAPHIC LITHOLOGY	LITHOLOGIC DESCRIPTION
		FORAMINIFERS	NANNOFOSSILS	RADIOLARIANS			
upper Quaternary	NN21/NN20	B	CP	RM	0.5	T2	DIATOMACEOUS HEMPELAGIC MUD 20-30 cm, black mottles Dark gray (5G 4/1). SMEAR SLIDE SUMMARY (%): 1, 30 1, 122 M D Texture: Sand Tr 5 Silt 51 35 Clay 49 60 Composition: Quartz 7 8 Feldspar 5 3 Mica 2 1 Heavy minerals 3 1 Clay 47 55 Volcanic glass 5 3 Pyrite 2 3 Carbonate unspec. 2 2 Foraminifers Tr Tr Calc. nanofossils 2 5 Diatoms 15 15 Radiolarians Tr Tr Sponge spicules 5 2 Silicoflagellates Tr Tr Plant debris 1 - Lithic fragments 4 2
					1.0	T2	
					2	T2	
					2	CC	ORGANIC CARBON AND CARBONATE (%): Carbonate 1.50 1.4

SITE 583		HOLE D		CORE 12		CORED INTERVAL 152.6-162.3 m	
TIME - ROCK UNIT	BIOSTRATIGRAPHIC ZONE	FOSSIL CHARACTER			SECTION METERS	GRAPHIC LITHOLOGY	LITHOLOGIC DESCRIPTION
		FORAMINIFERS	NANNOFOSSILS	RADIOLARIANS			
middle Quaternary	NN19	B	CM	RP	0.5	T2	HEMPELAGIC MUD Dark gray (5Y 4/1). Section 1, 110-120 cm: bedding defined by slight color changes. SMEAR SLIDE SUMMARY (%): 1, 45 3, 34 D M Texture: Sand - 30 Silt 60 50 Clay 40 20 Composition: Quartz 50 25 Feldspar 5 4 Mica 1 2 Heavy minerals 3 8 Clay 30 20 Volcanic glass 3 2 Pyrite 1 1 Micronodules Tr Tr Carbonate unspec. - 2 Foraminifers - Tr Calc. nanofossils 2 Tr Diatoms 2 Tr Radiolarians Tr - Sponge spicules 1 1 Lithic fragments 2 36
					1.0	T2	
					2	T2	
					3	Void	Sandy patches have been swirled and mixed with the muddier matrix. ORGANIC CARBON AND CARBONATE (%): Carbonate 1.53 1.4

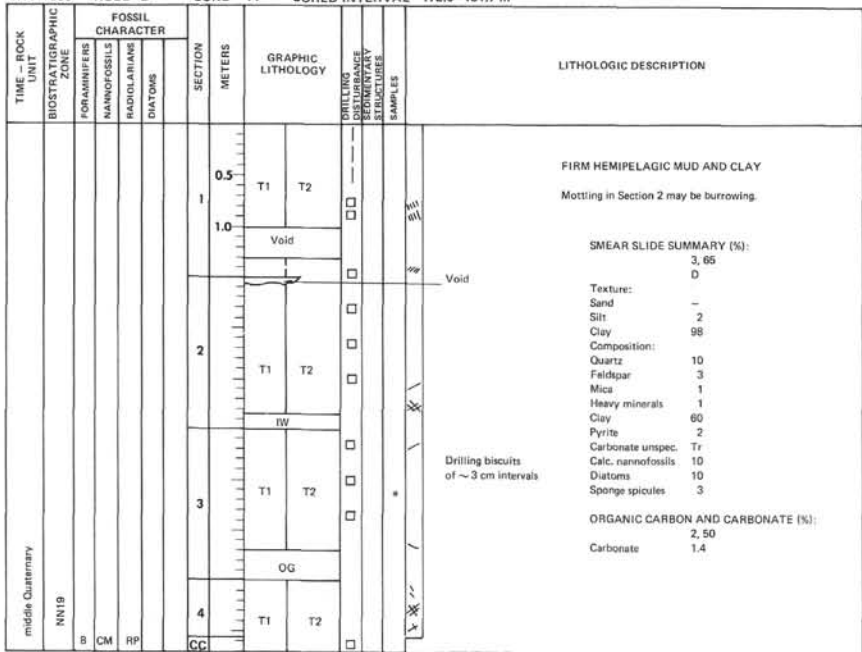
SITE 583 HOLE D CORE 13 CORED INTERVAL 162.3-172.0 m

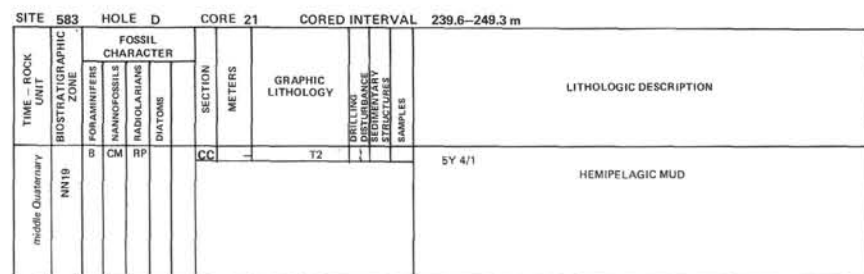
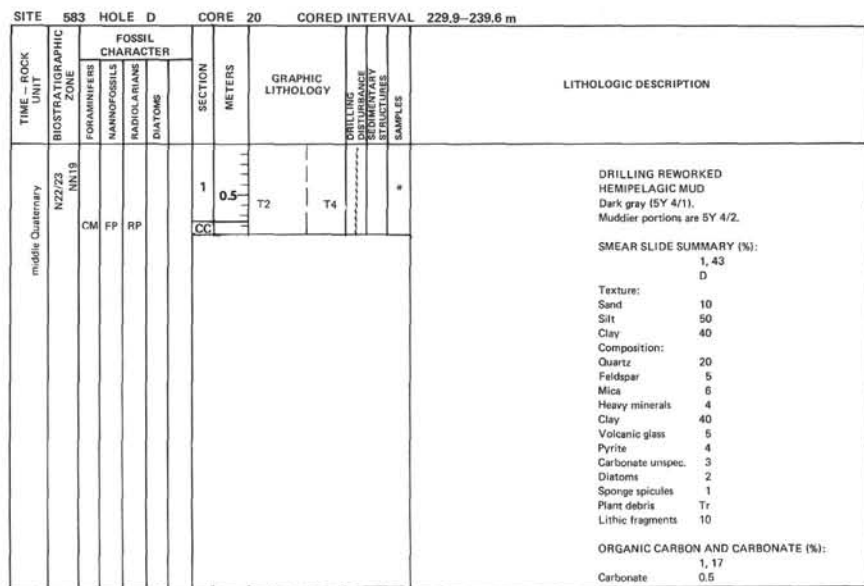
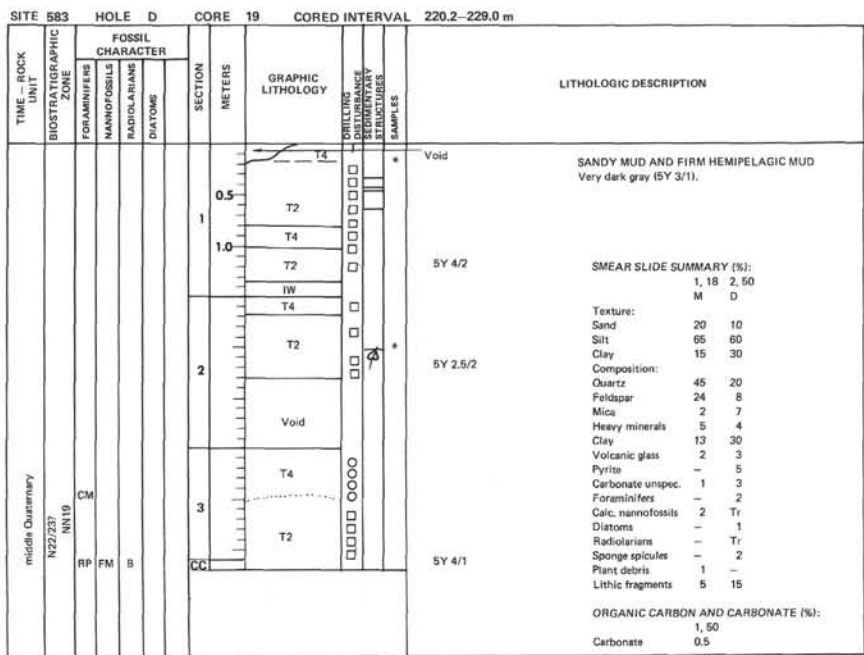


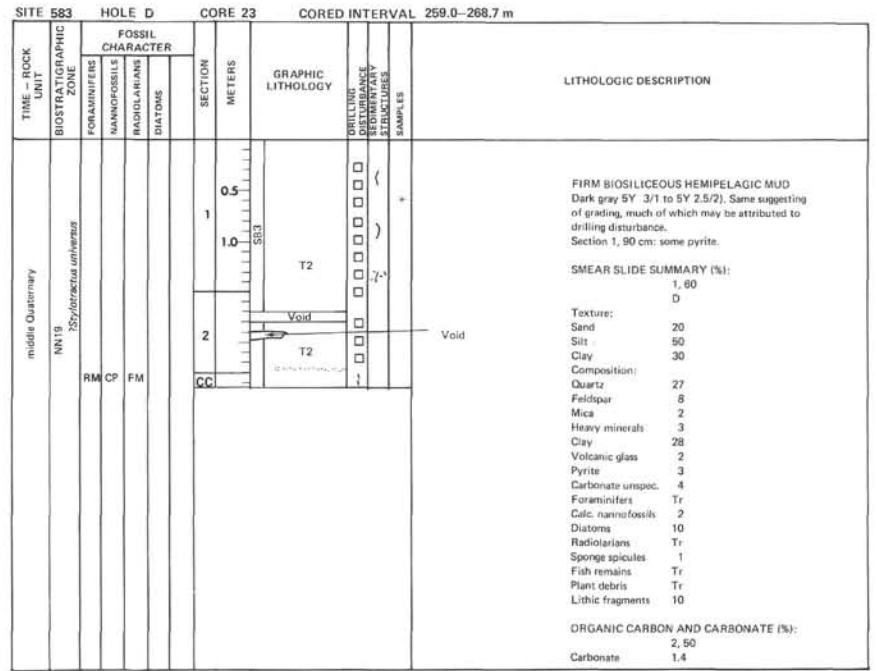
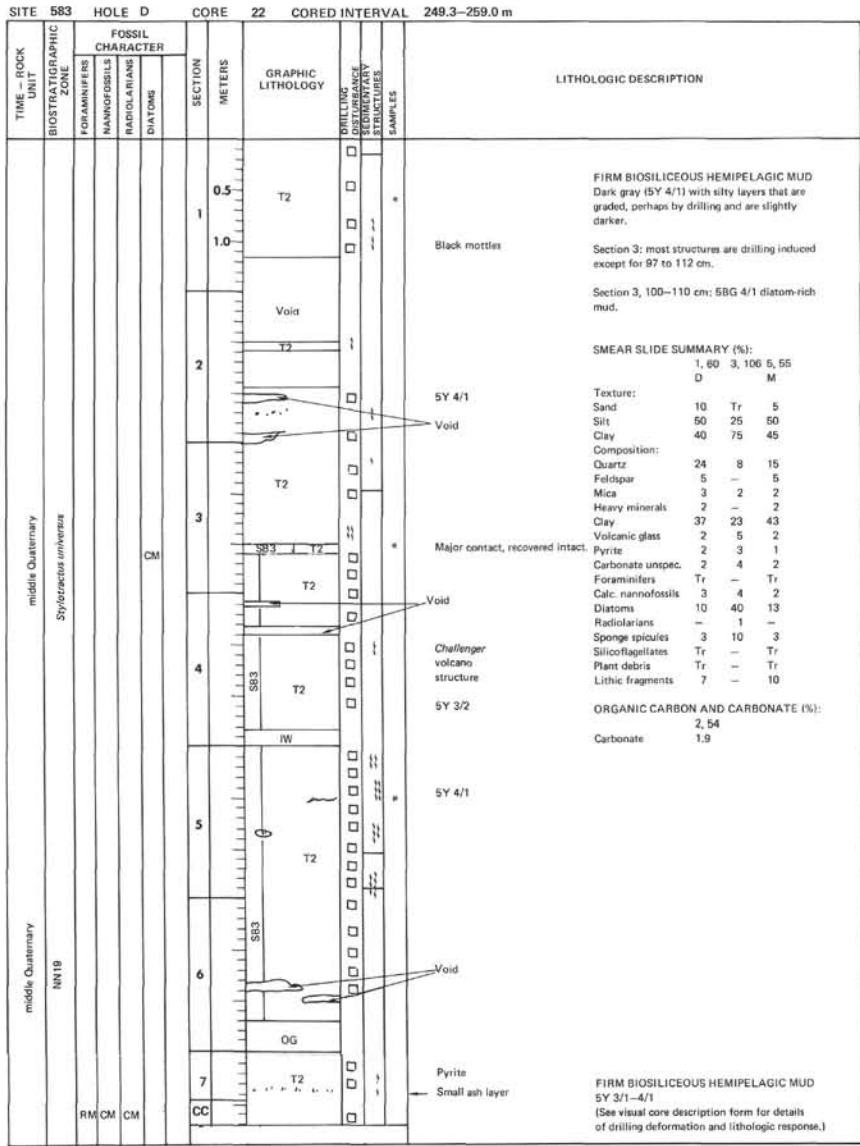
SITE 583 HOLE D CORE 15 CORED INTERVAL 181.7-191.4 m



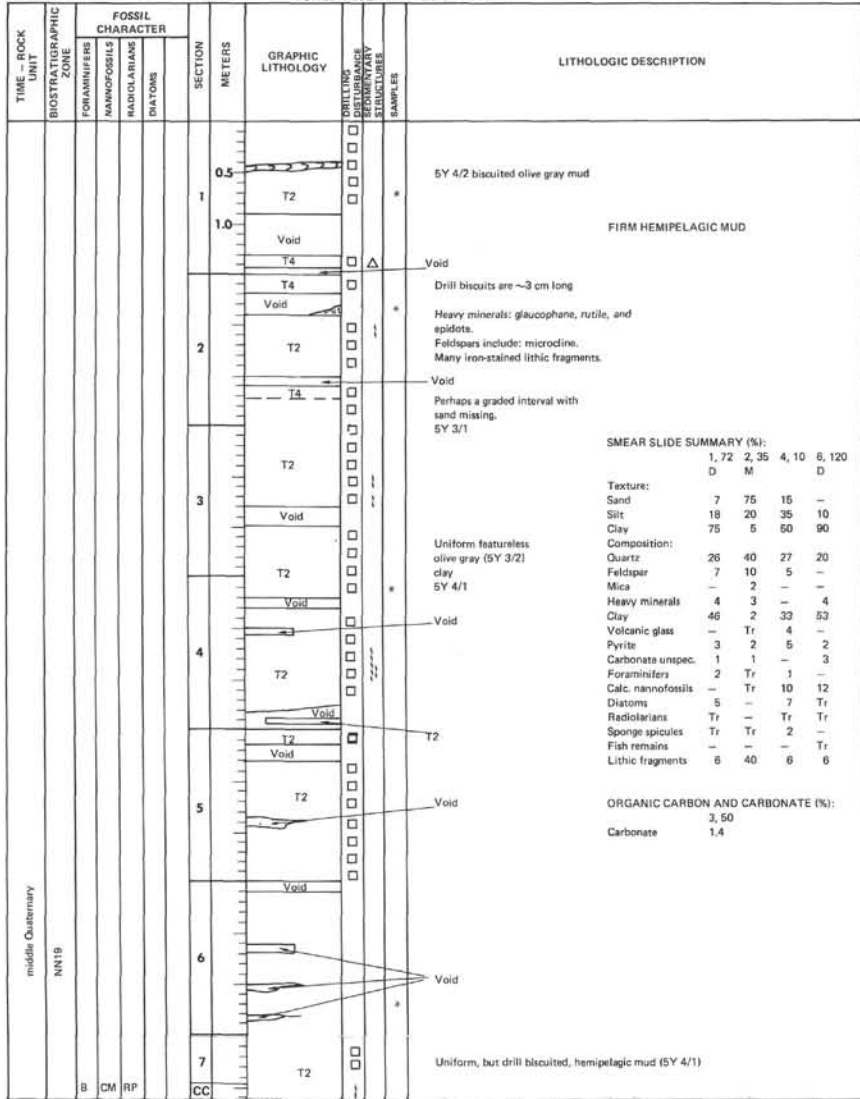
SITE 583 HOLE D CORE 14 CORED INTERVAL 172.0-181.7 m



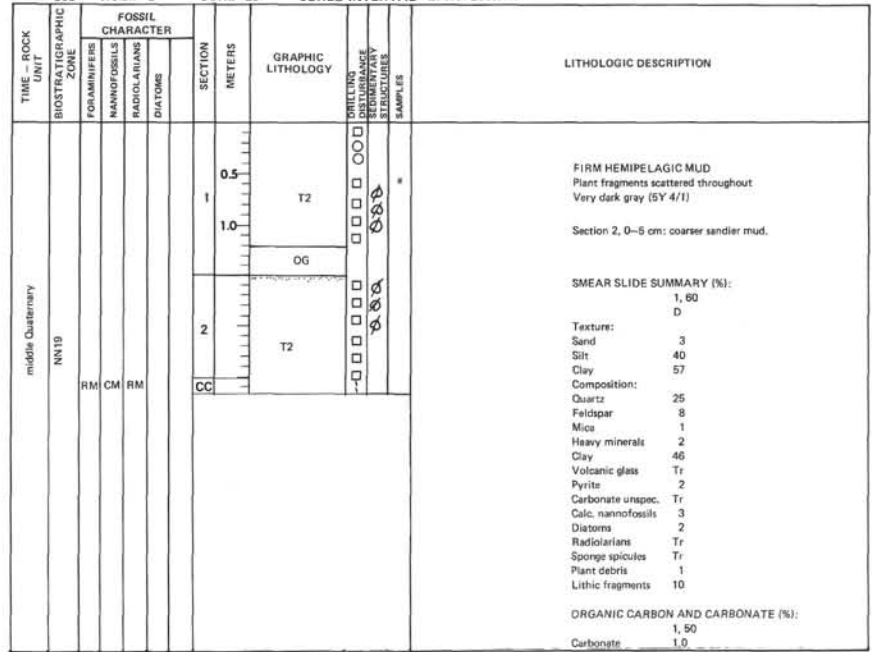




SITE 583 HOLE D CORE 24 CORED INTERVAL 268.7-278.4 m



SITE 583 HOLE D CORE 25 CORED INTERVAL 278.4-288.0 m



SITE 583 HOLE E CORE H1 CORED INTERVAL 0.0-150.4 m

TIME - ROCK UNIT	BIOSTRATIGRAPHIC ZONE	FOSSIL CHARACTER				SECTION METERS	GRAPHIC LITHOLOGY	LITHOLOGIC DESCRIPTION
		FORAMINIFERS	NANNOFOSSILS	RADIOLARIANS	DIATOMS			
							WASH CORE Color 5Y 4/1 with olive (5Y 4/4) patches.	
					0.5			
					1.0			
					2		Minor lith., color 5Y 4/4.	
					3	T2		
					4			
					5			
					6			
					CC		130 cm	

SMEAR SLIDE SUMMARY (%):

	2	29	3	130	5	47
	M	D	M			
Texture:						
Sand	30	-	40			
Silt	50	30	55			
Clay	20	70	5			
Composition:						
Quartz	15	15	20			
Feldspar	10	10	10			
Mica	1	2	2			
Heavy minerals	2	1	3			
Clay	27	57	2			
Volcanic glass	5	Tr	Tr			
Pyrite	Tr	2	Tr			
Carbonate unsp. c.	Tr	-	Tr			
Foraminifera	-	-	Tr			
Calc. nannofossils	-	-	Tr			
Diatoms	-	5	-			
Radiolarians	5	Tr	Tr			
Sponge spicules	Tr	3	-			
Silicoflagellates	Tr	Tr	-			
Lithic fragments	35	5	63			

SITE 583 HOLE E CORE 1 CORED INTERVAL 150.4-160.0 m

TIME - ROCK UNIT	BIOSTRATIGRAPHIC ZONE	FOSSIL CHARACTER				SECTION METERS	GRAPHIC LITHOLOGY	LITHOLOGIC DESCRIPTION
		FORAMINIFERS	NANNOFOSSILS	RADIOLARIANS	DIATOMS			
							HEMIPELAGIC MUD White spot of 25 cm = ash?	
					0.5			
					1.0	Void		
					CC			

SMEAR SLIDE SUMMARY (%):

	1	25	CC	8
	M	D		
Texture:				
Sand	45	10		
Silt	30	30		
Clay	25	60		
Composition:				
Quartz	48	28		
Feldspar	5	8		
Mica	-	1		
Heavy minerals	6	4		
Clay	28	50		
Volcanic glass	6	-		
Pyrite	3	2		
Carbonate unsp. c.	1	-		
Diatoms	Tr	Tr		
Radiolarians	1	-		
Sponge spicules	-	2		
Lithic fragments	4	5		

Micaceous silty mud (5Y 4/2)

Core 2, 160.0-166.6 m: no recovery.
Core 3, 169.6-179.3 m: no recovery.
Core 4, 179.3-188.0 m: no recovery.

SITE 583 HOLE E CORE 5 CORED INTERVAL 189.0-198.7 m

TIME - ROCK UNIT	BIOSTRATIGRAPHIC ZONE	FOSSIL CHARACTER				SECTION METERS	GRAPHIC LITHOLOGY	LITHOLOGIC DESCRIPTION
		FORAMINIFERS	NANNOFOSSILS	RADIOLARIANS	DIATOMS			
							DRILL MUD, HEMIPELAGIC MUD AND SAND Dark gray (5GY 5/1-4/1)	
					0.5			
					1.0	Void		
					CC	Void T6		

SMEAR SLIDE SUMMARY (%):

	1	9	1	7	1	49
	D		M			
Texture:						
Sand	65	-	85			
Silt	25	60	10			
Clay	10	40	5			
Composition:						
Quartz (+ barite)	68	40	25			
Feldspar	10	25	35			
Mica	-	1	2			
Heavy minerals	2	1	8			
Clay	5	30	5			
Volcanic glass	-	2	3			
Pyrite	5	1	-			
Calc. nannofossils	Tr	-	-			
Radiolarians	-	Tr	-			
Sponge spicules	Tr	Tr	-			
Lithic fragments	10	-	22			

Medium to coarse grained sand 58G 4/1

SITE 583		HOLE F		CORE 6		CORED INTERVAL 198.7-208.2 m	
TIME - ROCK UNIT	BIOSTRATIGRAPHIC ZONE	FOSSIL CHARACTER			SECTION METERS	GRAPHIC LITHOLOGY	LITHOLOGIC DESCRIPTION
		FORAMINIFERS	NANNOFOSSILS	RADIOLARIANS			
lower Quaternary	N22/23						
		RP					
		FM RP					
	1						
	2	FM RP					
	3	B AM FM					
	CC						

GRAPHIC LITHOLOGY: T2, Void, T8, T2, T2, IW, T2
 DRILLING DISTURBANCE STRUCTURES: *
 SAMPLES: *

LITHOLOGIC DESCRIPTION:
 FIRM HEMPELAGIC MUD AND DISTURBED SILT AND SAND
 Fidelity = ?partings, etc., especially 65 to 68 cm.
 Void space (Section 1) occupied in small part by 5Y 4/1 sandy mud with rounded pumice pebbles.
 Section 2, 137 cm: contact in IW sample... mud above...coarse black silt beneath.
 Drilling-formed contact Sand wedged between drill bitsouts
 Mottling frequent
 Uniform 5Y 4/1
 Very dark gray, 5Y 4/1

SMEAR SLIDE SUMMARY (%):
 1, 60 2, 45 2, 80
 D M D
 Texture: Sand 5 40 15, Silt 25 30 20, Clay 70 30 65
 Composition: Quartz 4 25 26, Feldspar 1 8 3, Mica 2 1 -, Heavy minerals 2 3 6, Clay 65 33 49, Volcanic glass - - Tr, Pyrite - 2 5, Carbonate unspec. Tr - -, Foraminifers Tr - Tr, Calc. nannofossils 15 3 Tr, Diatoms 5 Tr 5, Radiolarians Tr - 1, Sponge spicules 1 Tr Tr, Lithic fragments 5 25 5

SITE 583		HOLE F		CORE 7		CORED INTERVAL 208.2-217.7 m	
TIME - ROCK UNIT	BIOSTRATIGRAPHIC ZONE	FOSSIL CHARACTER			SECTION METERS	GRAPHIC LITHOLOGY	LITHOLOGIC DESCRIPTION
		FORAMINIFERS	NANNOFOSSILS	RADIOLARIANS			
lower Quaternary	NN19	B	B	CM			
	CC						

GRAPHIC LITHOLOGY: T2
 DRILLING DISTURBANCE STRUCTURES: *
 SAMPLES: *

LITHOLOGIC DESCRIPTION:
 HEMPELAGIC MUD, BADLY DISTURBED BY DRILLING
 5Y 3/1
SMEAR SLIDE SUMMARY (%):
 CC, 10
 D
 Texture: Sand -, Silt 36, Clay 65
 Composition: Quartz 29, Feldspar 1, Heavy minerals 6, Clay 47, Volcanic glass 3, Pyrite 3, Calc. nannofossils 1, Diatoms 2, Radiolarians 1, Sponge spicules Tr, Lithic fragments 7

SITE 583		HOLE F		CORE 8		CORED INTERVAL 217.7-227.2 m	
TIME - ROCK UNIT	BIOSTRATIGRAPHIC ZONE	FOSSIL CHARACTER			SECTION METERS	GRAPHIC LITHOLOGY	LITHOLOGIC DESCRIPTION
		FORAMINIFERS	NANNOFOSSILS	RADIOLARIANS			
lower Quaternary	B	FP	RP				
	1						
	CC						

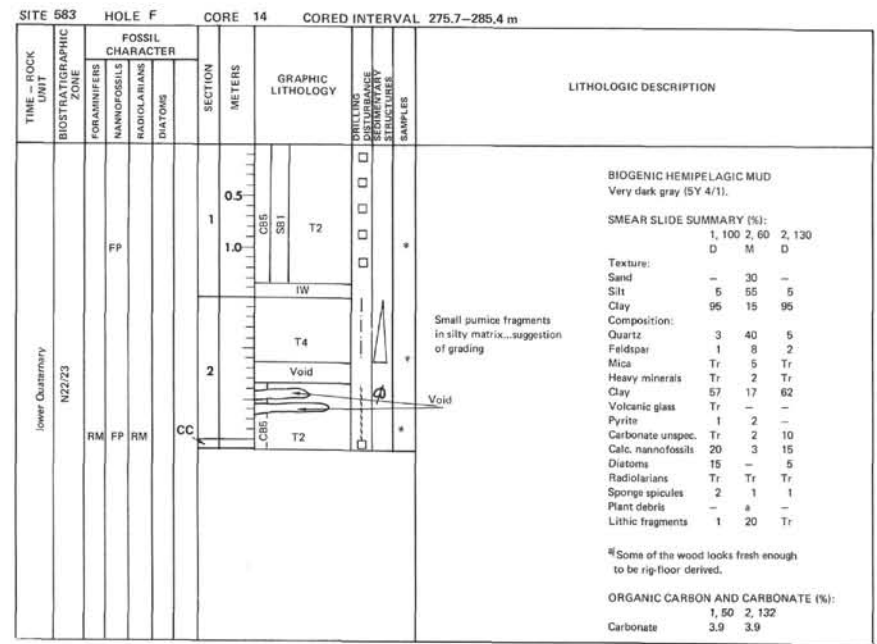
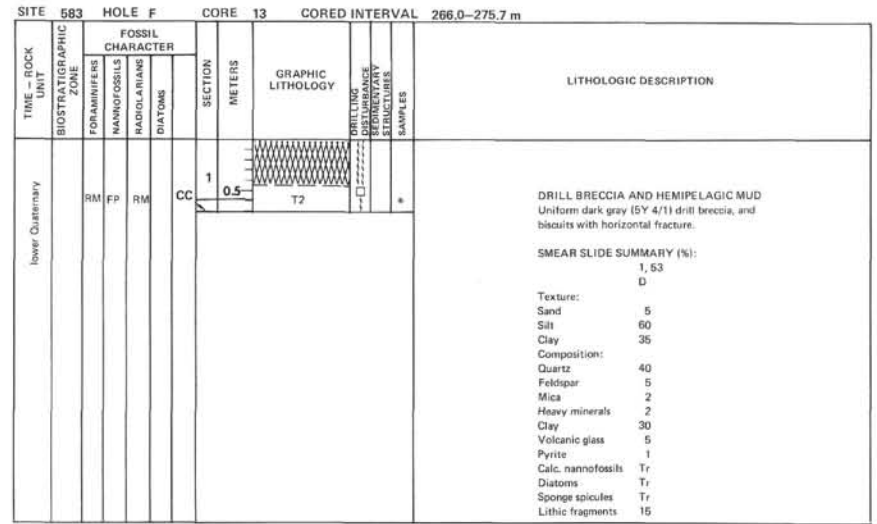
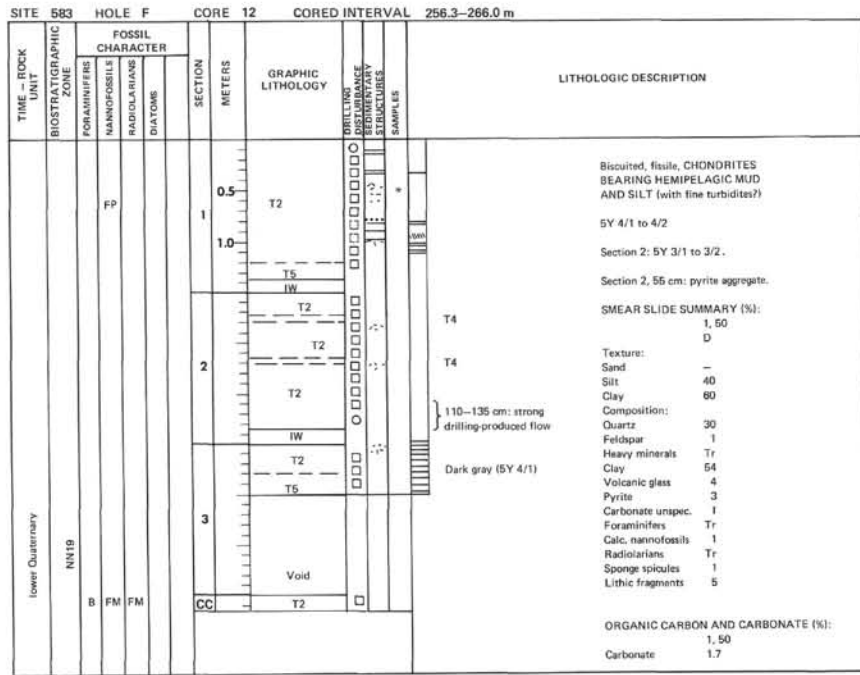
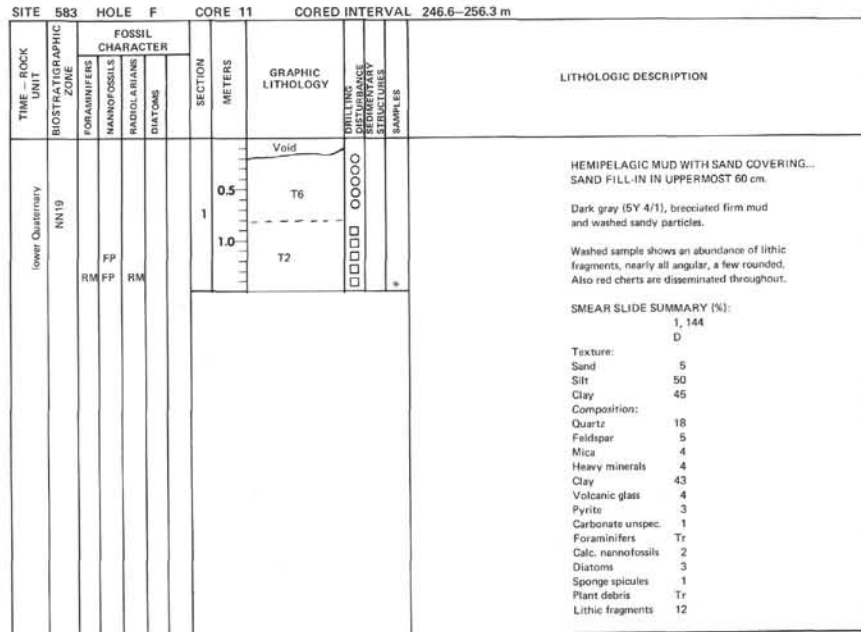
GRAPHIC LITHOLOGY: T2
 DRILLING DISTURBANCE STRUCTURES: *
 SAMPLES: *

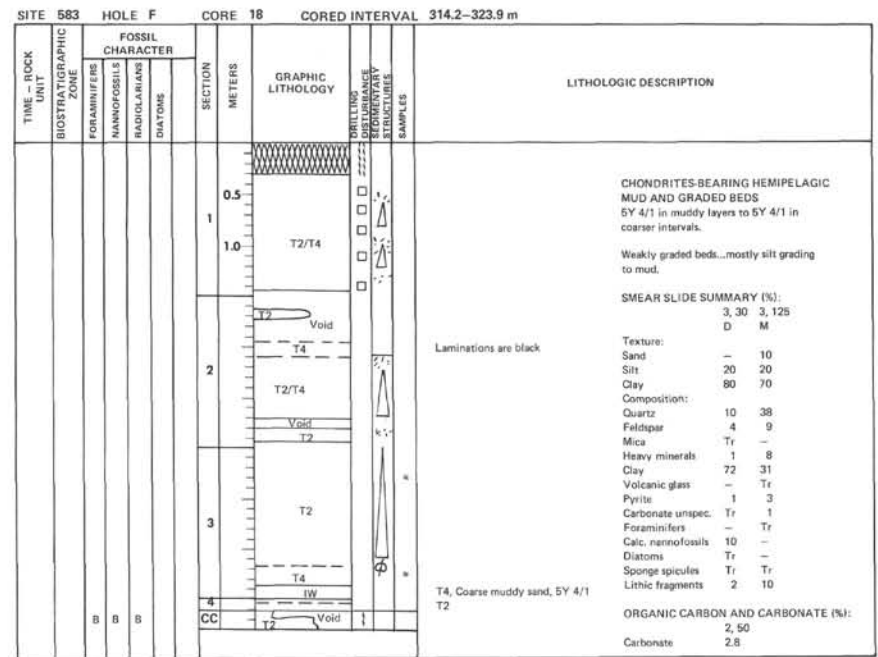
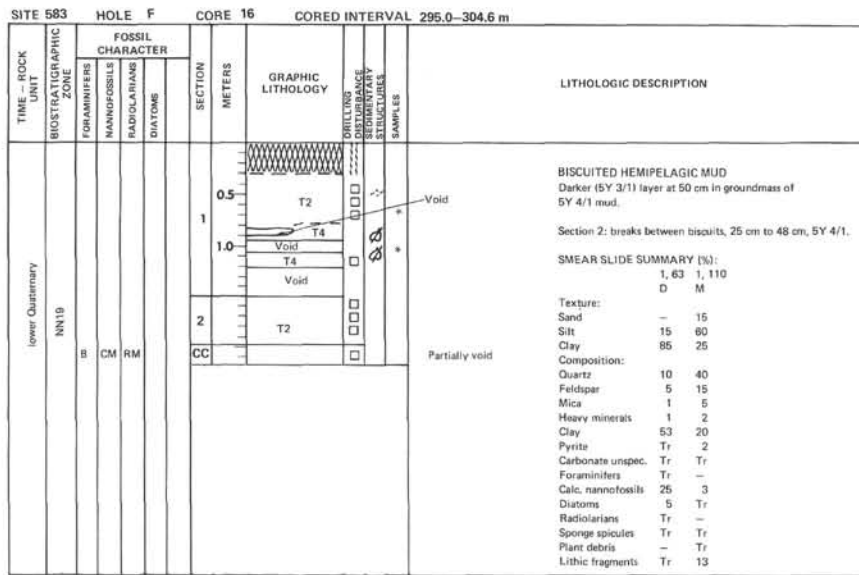
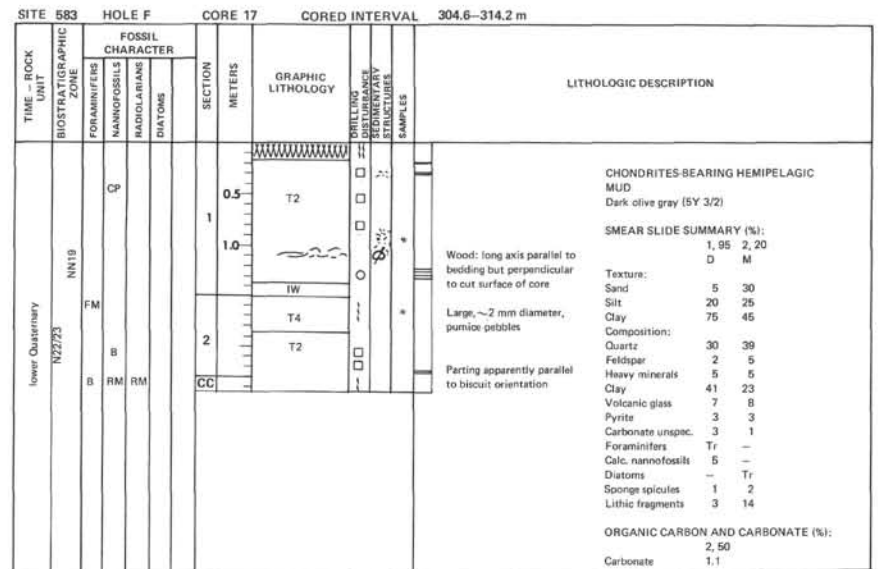
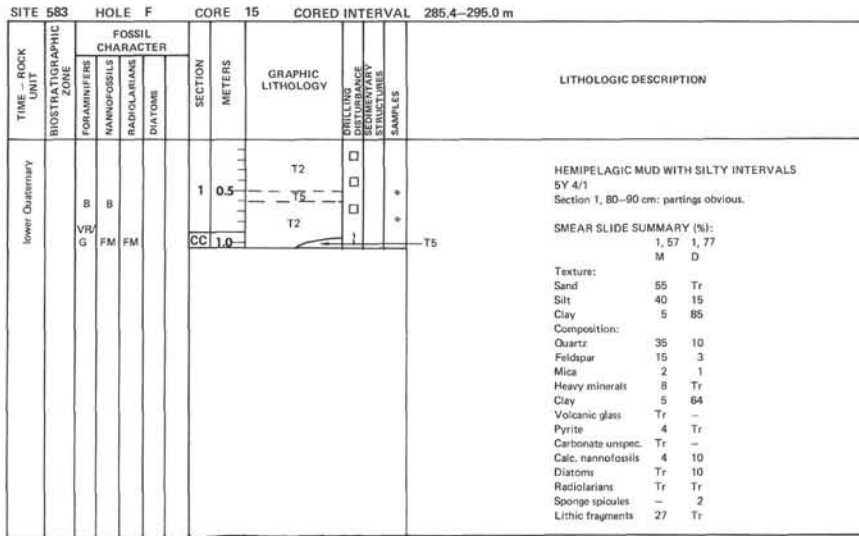
LITHOLOGIC DESCRIPTION:
 FIRM HEMPELAGIC MUD
 Dark gray (5Y 4/1) to dark olive gray (5Y 4/2)
 Section 1, 30 cm: washed sand-size grains... drill deposit.
SMEAR SLIDE SUMMARY (%):
 CC, 3
 D
 Texture: Sand 5, Silt 55, Clay 40
 Composition: Quartz 21, Feldspar 5, Mica 8, Heavy minerals 5, Clay 38, Volcanic glass 2, Pyrite 4, Carbonate unspec. 2, Foraminifers Tr, Calc. nannofossils 2, Diatoms Tr, Sponge spicules 2, Plant debris Tr, Lithic fragments 11

SITE 583		HOLE F		CORE 9		CORED INTERVAL 227.2-236.9 m	
TIME - ROCK UNIT	BIOSTRATIGRAPHIC ZONE	FOSSIL CHARACTER			SECTION METERS	GRAPHIC LITHOLOGY	LITHOLOGIC DESCRIPTION
		FORAMINIFERS	NANNOFOSSILS	RADIOLARIANS			
lower Quaternary	NN19	FM	RP				
	CC						

GRAPHIC LITHOLOGY: *
 DRILLING DISTURBANCE STRUCTURES: *
 SAMPLES: *

LITHOLOGIC DESCRIPTION:
 Trace recovery.
 Core 10, 236.9-246.6 m: no recovery.





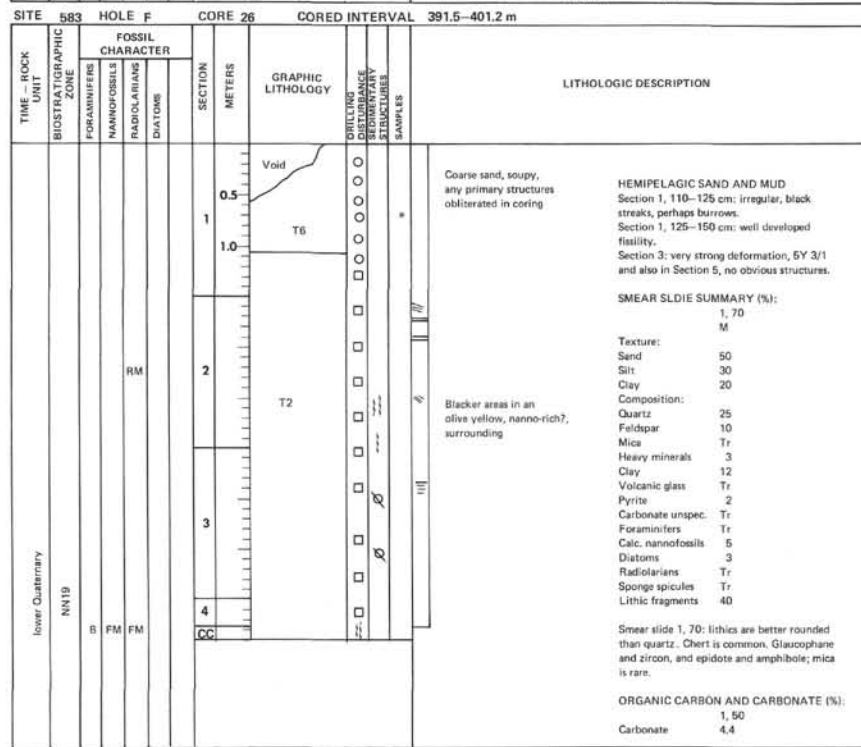
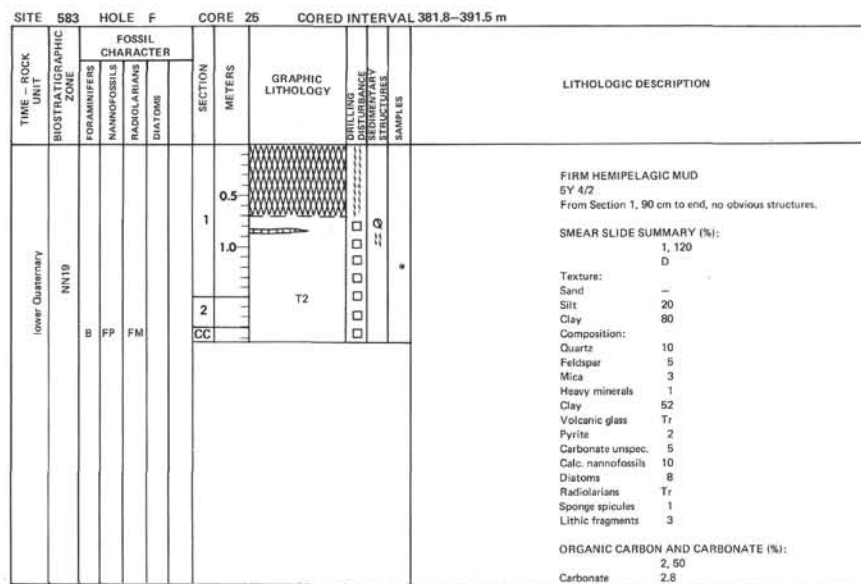
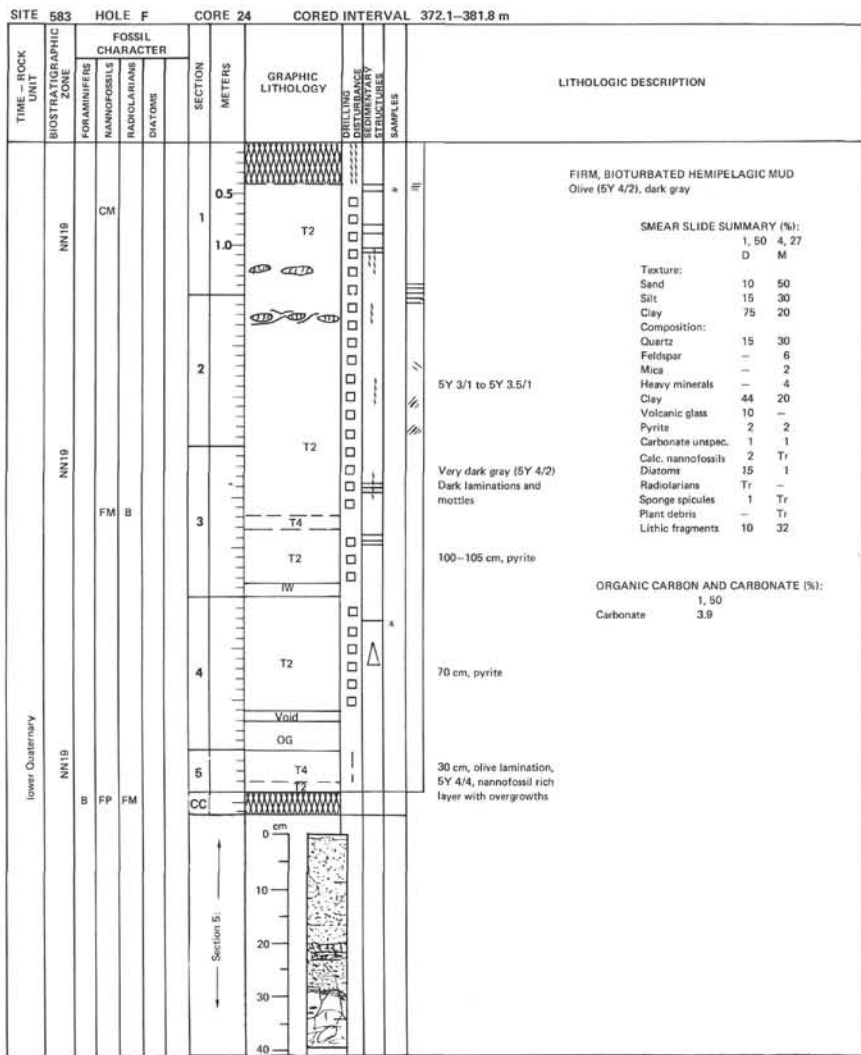
SITE 583		HOLE F		CORE 19		CORED INTERVAL 323.9–333.6 m	
TIME – ROCK UNIT	BIOSTRATIGRAPHIC ZONE	FOSSIL CHARACTER			SECTION METERS	GRAPHIC LITHOLOGY	LITHOLOGIC DESCRIPTION
		FORAMINIFERS	NANNOFOSSILS	RADIOLARIANS			
lower Quaternary	NN19	B	FM	RP	0.5 1.0		<p>FIRM, CHONDRITES-BEARING HEMIPELAGIC MUD</p> <p>Dark green laminations Dark gray (SY 4/1)</p> <p>SMEAR SLIDE SUMMARY (%):</p> <p>1, 50 D</p> <p>Texture:</p> <p>Sand – Silt 40 Clay 60</p> <p>Composition:</p> <p>Quartz 10 Feldspar Tr Heavy minerals 1 Clay 68 Volcanic glass 3 Glauconite 1 Micronodules 2 Calc. nannofossils Tr Lithic fragments 15</p>
					CC		<p>Sandy mud with pumice dark gray (SY 4/1)</p>

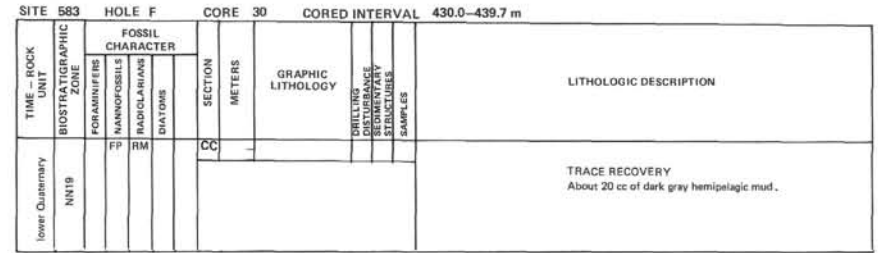
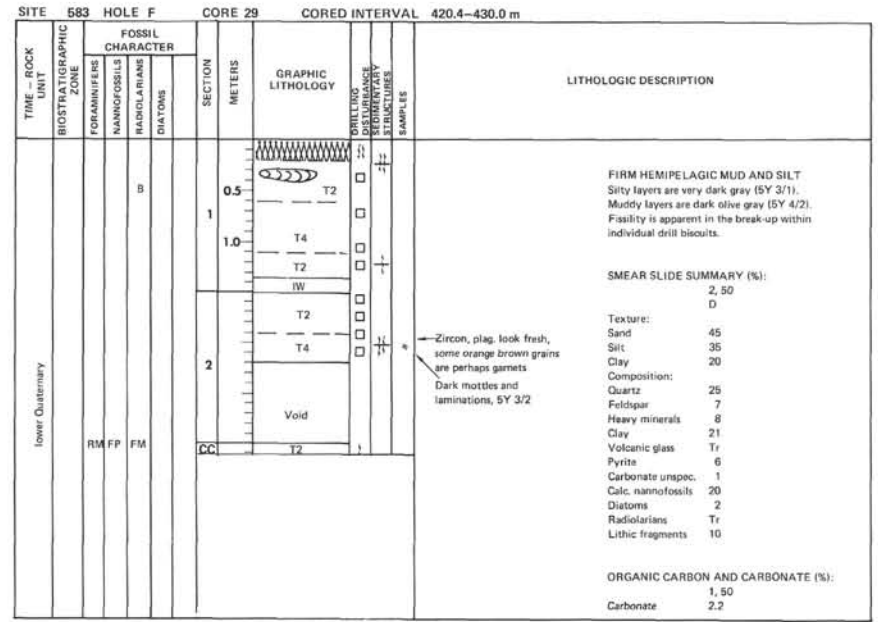
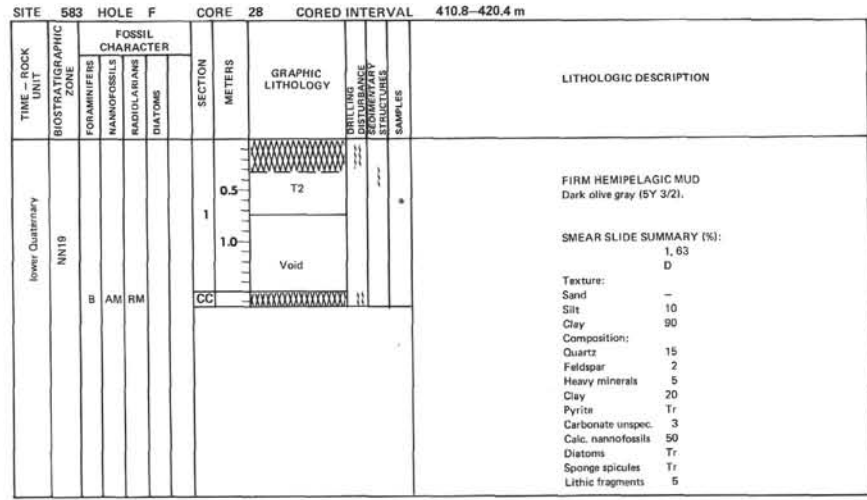
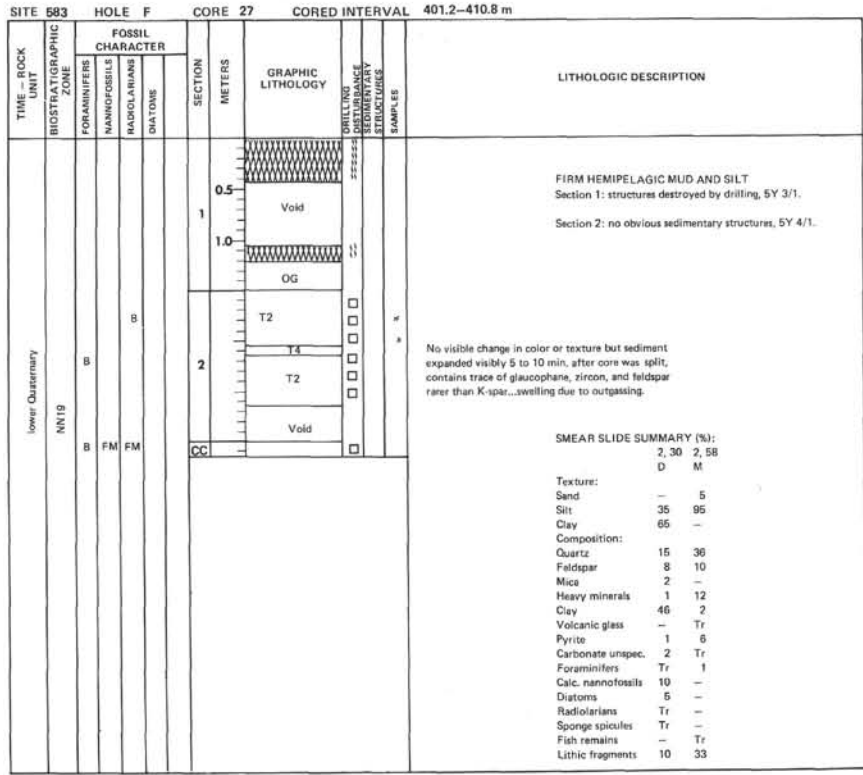
SITE 583		HOLE F		CORE 20		CORED INTERVAL 333.6–343.3 m	
TIME – ROCK UNIT	BIOSTRATIGRAPHIC ZONE	FOSSIL CHARACTER			SECTION METERS	GRAPHIC LITHOLOGY	LITHOLOGIC DESCRIPTION
		FORAMINIFERS	NANNOFOSSILS	RADIOLARIANS			
lower Quaternary	NN2/23	RM			0.5 1.0		<p>Muddy sand SY 4/1–3/1 with white pumice spots</p> <p>Void</p> <p>Very dark gray (SY 3/1)</p> <p>SMEAR SLIDE SUMMARY (%):</p> <p>1, 115 1, 50 D D</p> <p>Texture:</p> <p>Sand 1 30 Silt 39 30 Clay 60 40</p> <p>Composition:</p> <p>Quartz 26 30 Feldspar 5 4 Mica Tr – Heavy minerals 1 8 Clay 59 43 Volcanic glass 1 Tr Pyrite 2 3 Carbonate unsp. 1 1 Calc. nannofossils 1 – Diatoms – Tr Sponge spicules 1 1 Plant debris 1 – Lithic fragments – 10</p> <p>ORGANIC CARBON AND CARBONATE (%):</p> <p>1, 50 Carbonate 1.7</p>
					2		<p>5Y 4/1 fine grained silty mud</p> <p>5Y 3/2</p>

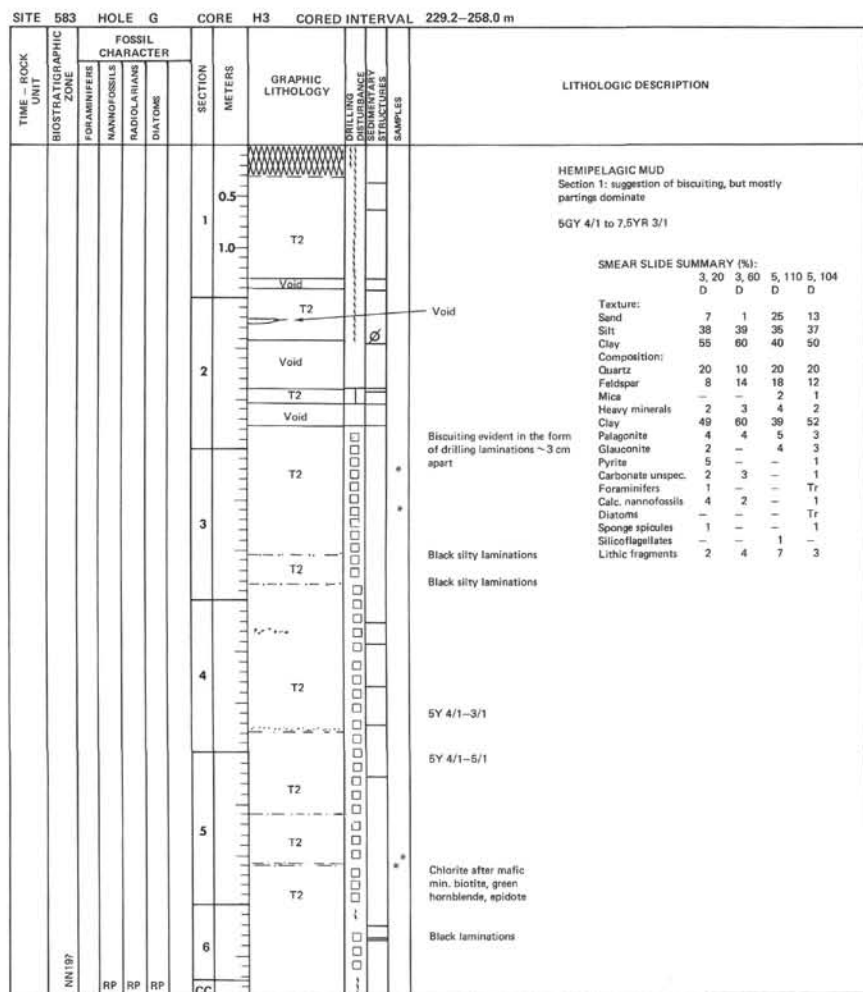
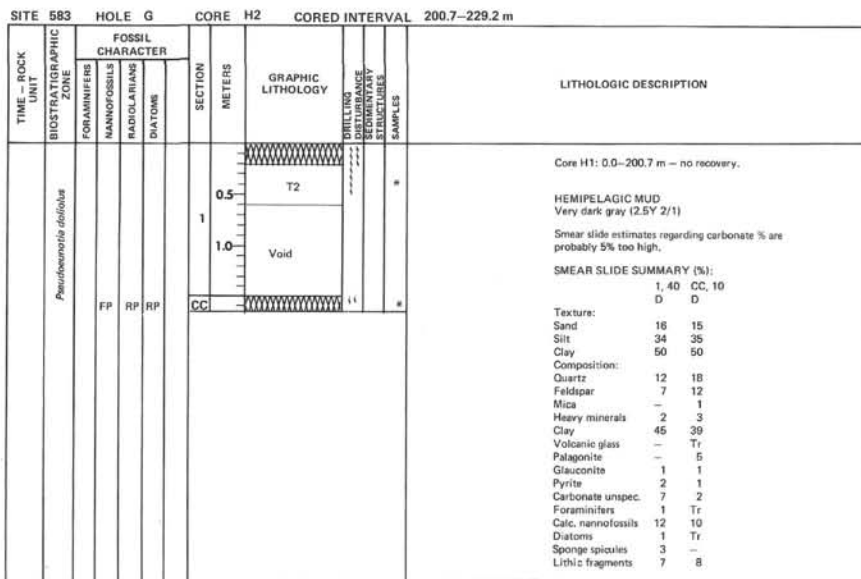
SITE 583		HOLE F		CORE 21		CORED INTERVAL 343.3–352.0 m	
TIME – ROCK UNIT	BIOSTRATIGRAPHIC ZONE	FOSSIL CHARACTER			SECTION METERS	GRAPHIC LITHOLOGY	LITHOLOGIC DESCRIPTION
		FORAMINIFERS	NANNOFOSSILS	RADIOLARIANS			
					CC		<p>HEMIPELAGIC MUD</p> <p>Dark gray (SY 4/1).</p>

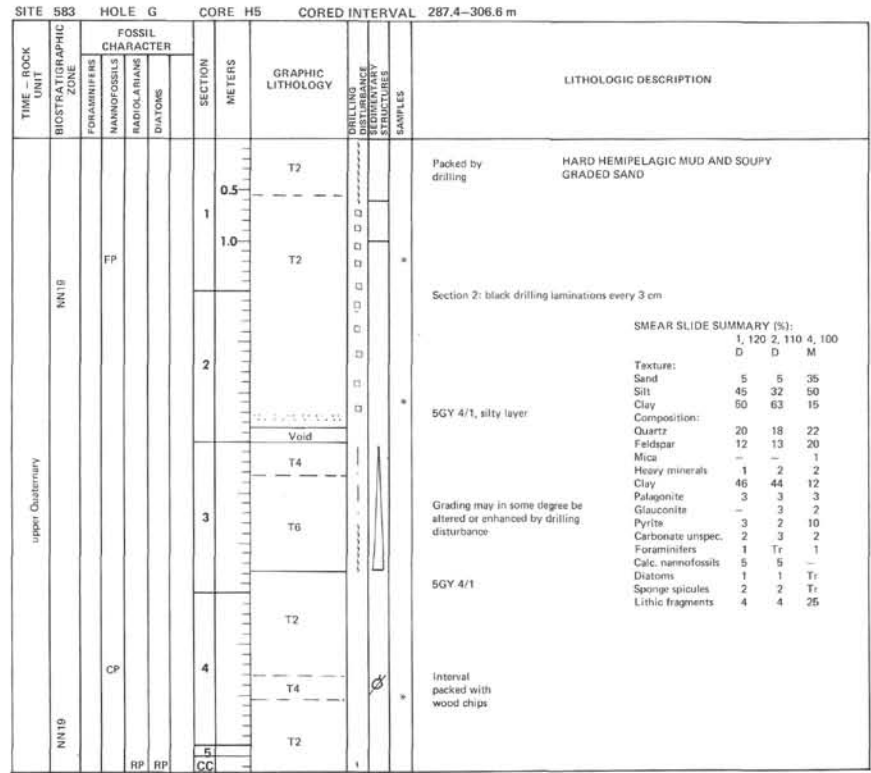
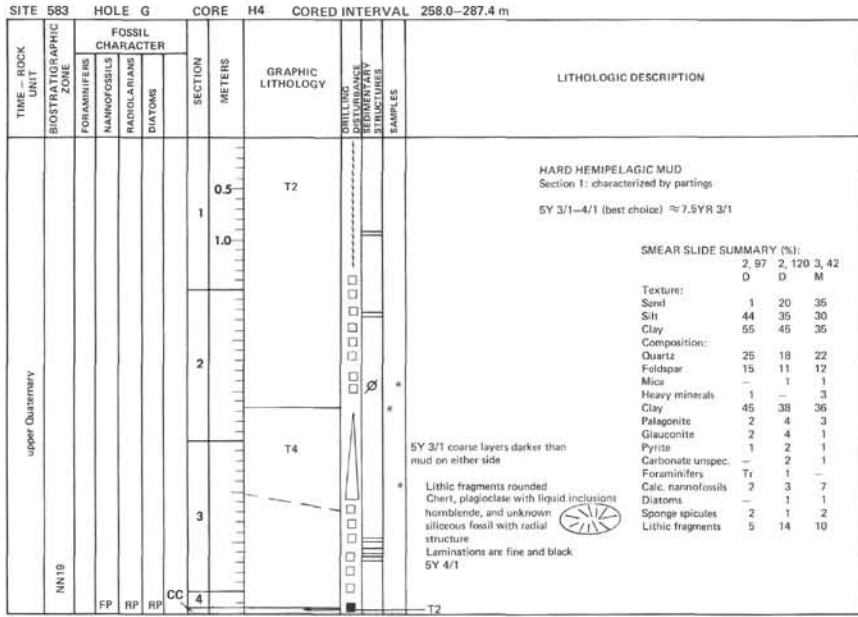
SITE 583		HOLE F		CORE 22		CORED INTERVAL 352.9–362.5 m	
TIME – ROCK UNIT	BIOSTRATIGRAPHIC ZONE	FOSSIL CHARACTER			SECTION METERS	GRAPHIC LITHOLOGY	LITHOLOGIC DESCRIPTION
		FORAMINIFERS	NANNOFOSSILS	RADIOLARIANS			
lower Quaternary	NN19	B	FM	B	0.5 1.0 2		<p>FIRM HEMIPELAGIC MUD AND FINE-GRAINED TURBIDITES</p> <p>Gray (SY 4/1 to 5/1) laminations are dark green to black.</p> <p>Planolites</p> <p>5Y 4/1 muddy silt</p> <p>SMEAR SLIDE SUMMARY (%):</p> <p>1, 107 D</p> <p>Texture:</p> <p>Sand 5 Silt 40 Clay 55</p> <p>Composition:</p> <p>Quartz 20 Feldspar 5 Mica 4 Heavy minerals 3 Clay 54 Volcanic glass 2 Pyrite 1 Carbonate unsp. 1 Calc. nannofossils 1 Sponge spicules 1 Lithic fragments 8</p> <p>ORGANIC CARBON AND CARBONATE (%):</p> <p>1, 50 Carbonate 3.3</p>

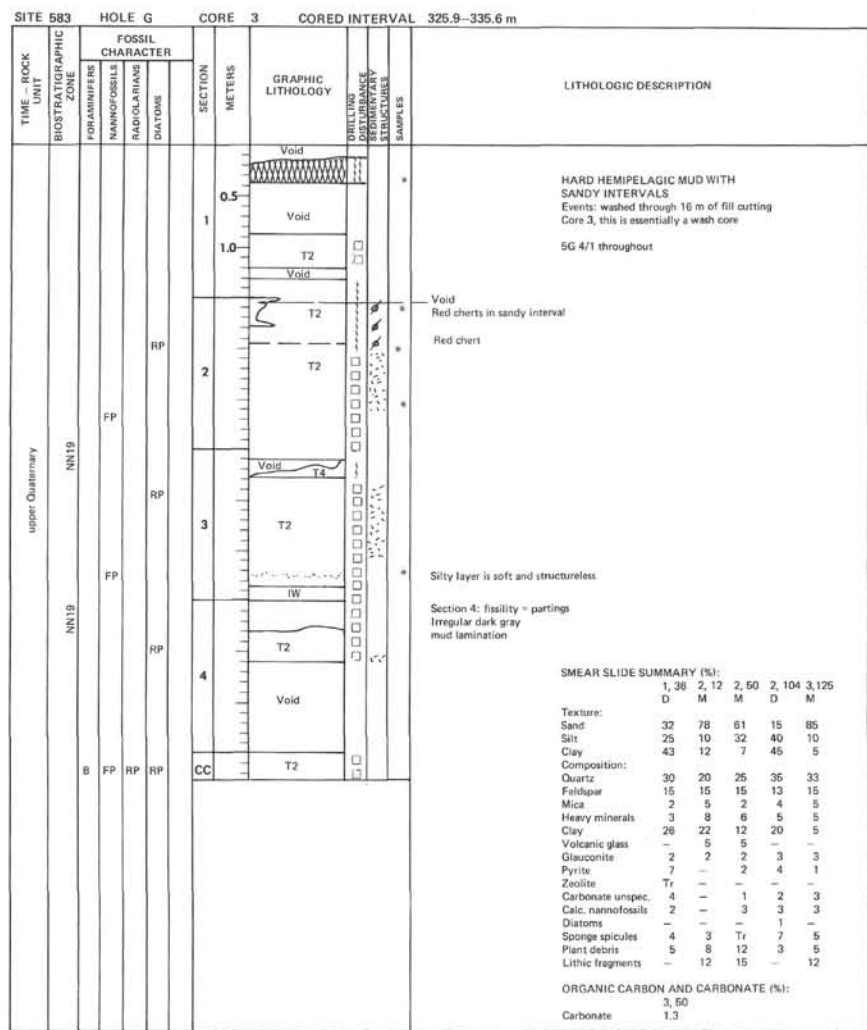
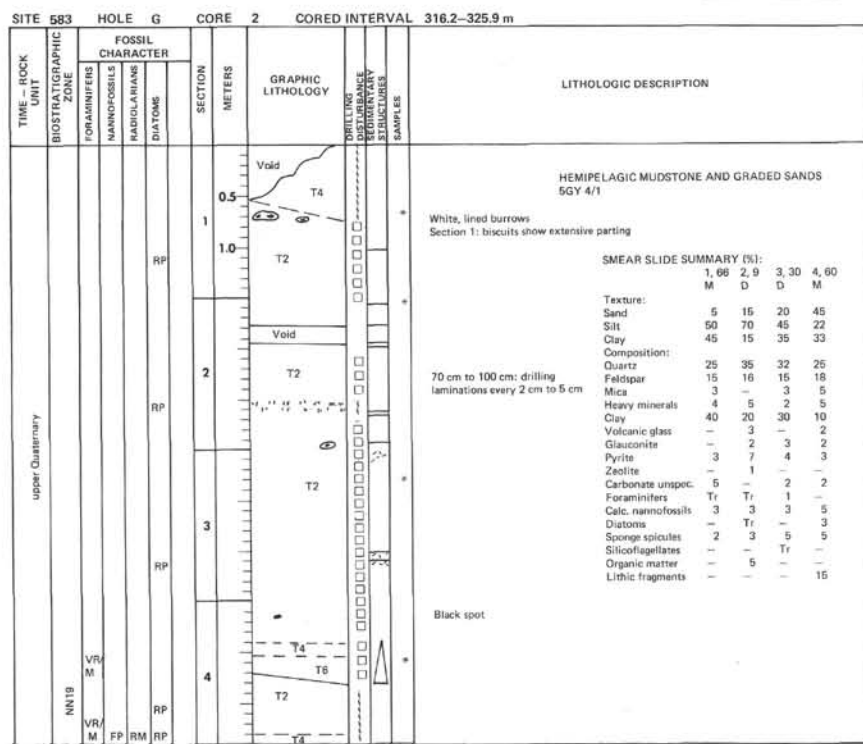
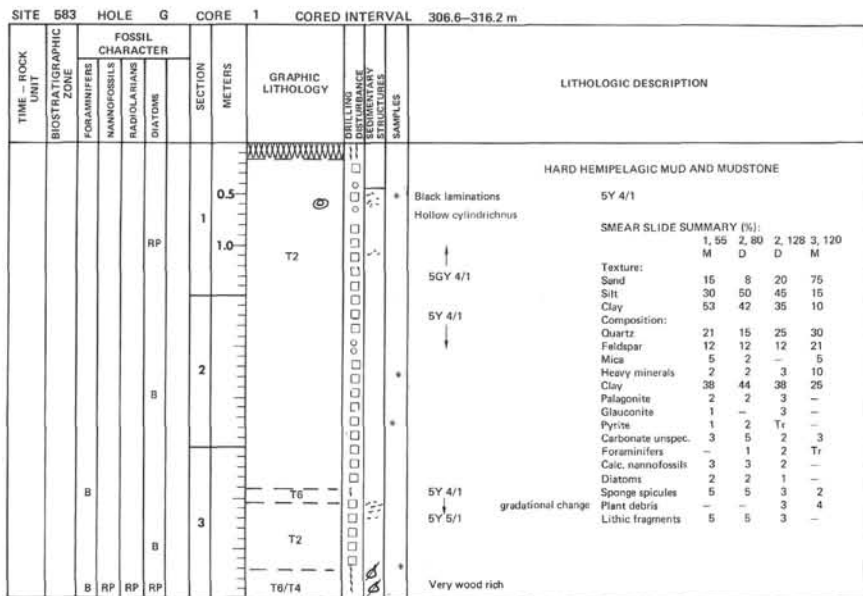
SITE 583		HOLE F		CORE 23		CORED INTERVAL 362.5–372.1 m	
TIME – ROCK UNIT	BIOSTRATIGRAPHIC ZONE	FOSSIL CHARACTER			SECTION METERS	GRAPHIC LITHOLOGY	LITHOLOGIC DESCRIPTION
		FORAMINIFERS	NANNOFOSSILS	RADIOLARIANS			
lower Quaternary	NN19	B	CP	B	CC		<p>HEMIPELAGIC MUD</p> <p>SY 4/1</p> <p>No discernible structure other than drilling deformation.</p>

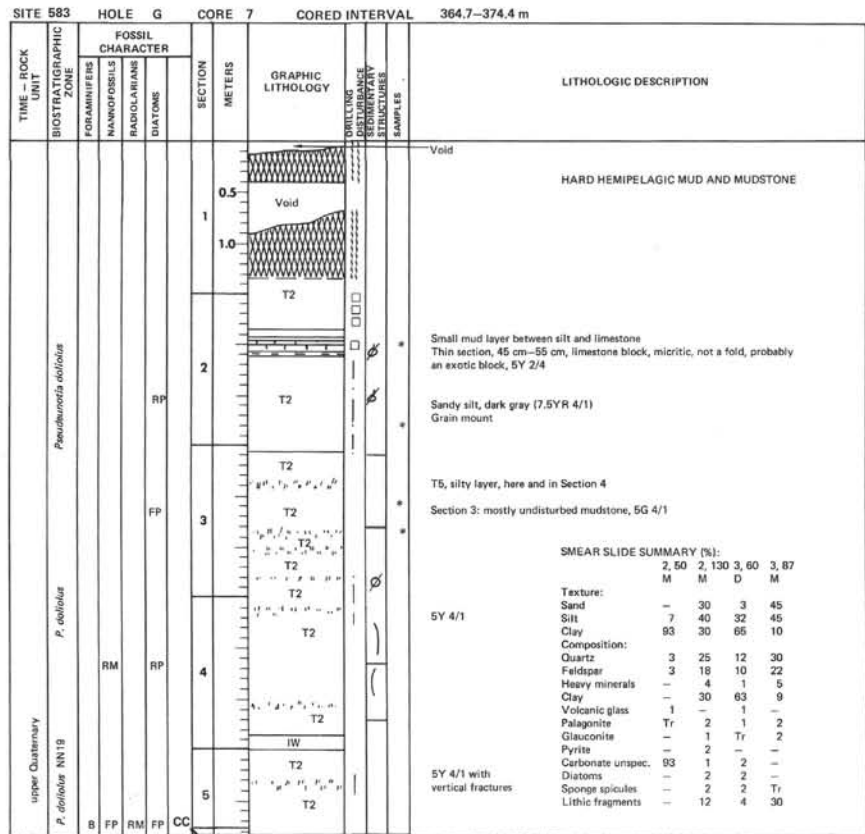
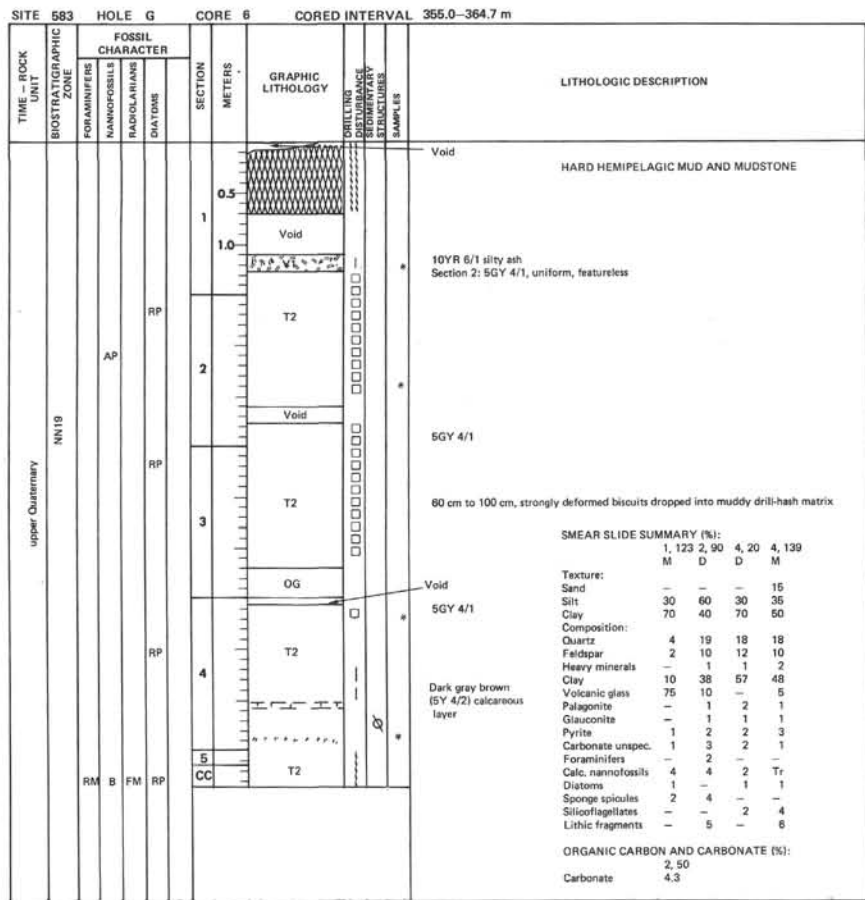


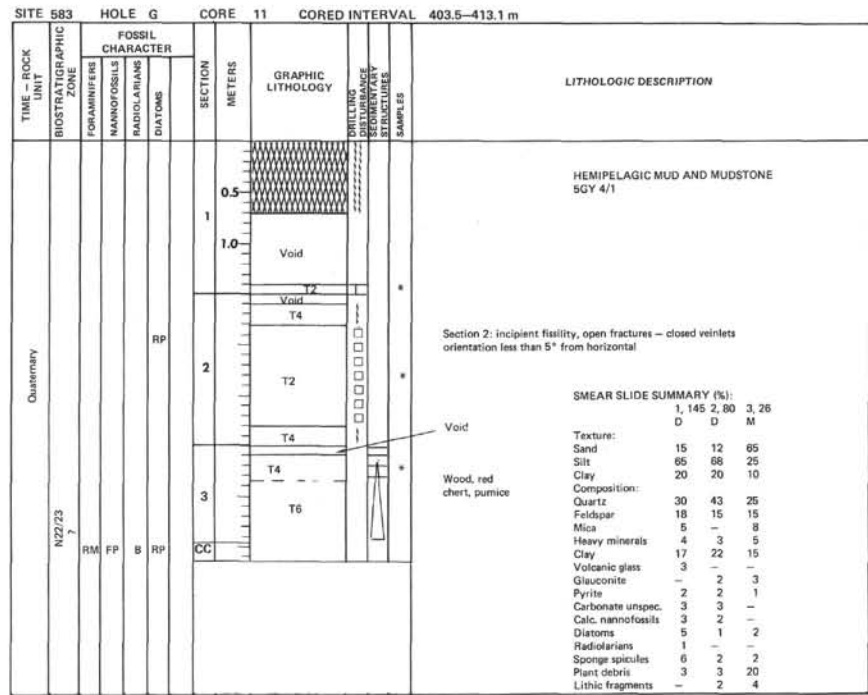
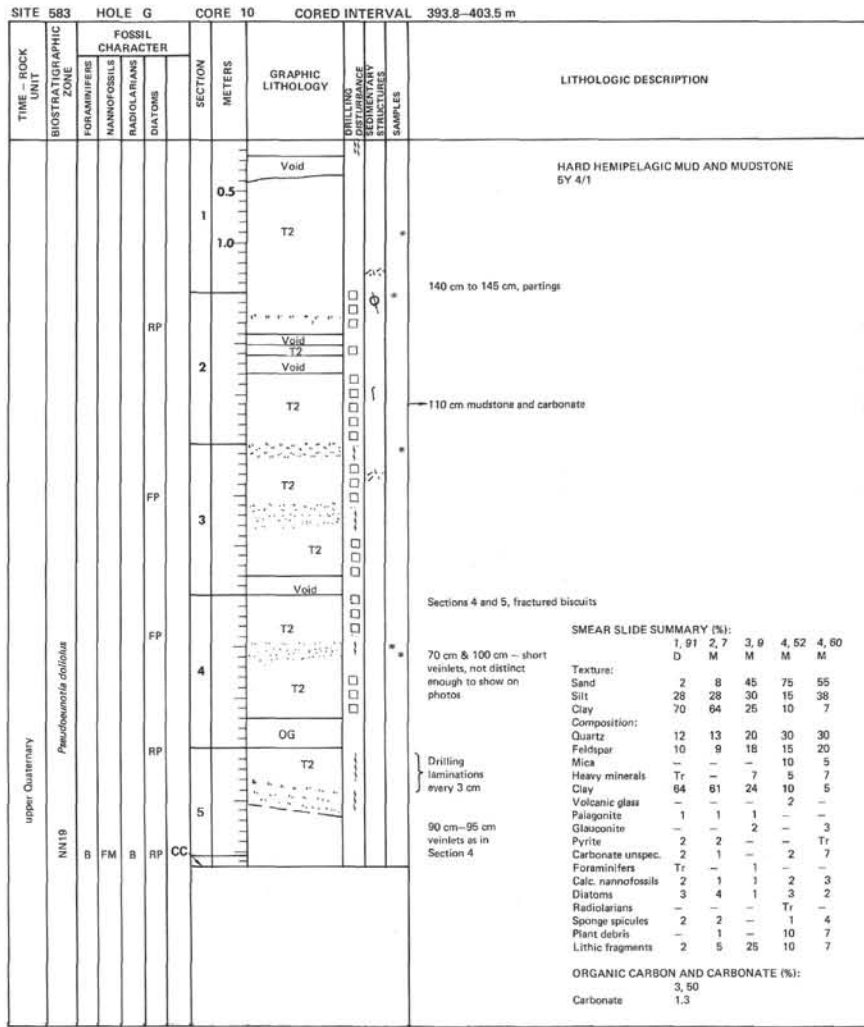












SITE 583		HOLE G		CORE 12		CORED INTERVAL 413.1–422.7 m	
TIME – ROCK UNIT	BIOSTRATIGRAPHIC ZONE	FOSSIL CHARACTER			SECTION METERS	GRAPHIC LITHOLOGY	LITHOLOGIC DESCRIPTION
		FORAMINIFERS	NANNOFOSSILS	RADIOLARIANS			
upper Quaternary	NN19				1		DRILL BRECCIA 5Y 4/1 Typhoon BESS fabric SMEAR SLIDE SUMMARY (%): 1, 54 D Texture: Sand 20 Silt 45 Clay 35 Composition: Quartz 35 Feldspar 15 Mica 2 Heavy minerals 5 Clay 10 Volcanic glass 3 Palagonite 1 Glaucinite 1 Pyrite 1 Carbonate unspec. 4 Foraminifera 1 Calc. nannofossils 2 Sponge spicules 2 Plant debris 6 Lithic fragments 10
		B	F/PM	RP	CC		Chert and green hornblende Void

SITE 583		HOLE G		CORE 13		CORED INTERVAL 422.7–432.3 m	
TIME – ROCK UNIT	BIOSTRATIGRAPHIC ZONE	FOSSIL CHARACTER			SECTION METERS	GRAPHIC LITHOLOGY	LITHOLOGIC DESCRIPTION
		FORAMINIFERS	NANNOFOSSILS	RADIOLARIANS			
upper Quaternary	NN19				1		DRILL BRECCIA – HEMIPELAGIC MUD AND MUDSTONE 5GY 4/1 Flat veinlets/incipient fissility SMEAR SLIDE SUMMARY (%): 1, 93 1, 110 D D Texture: Sand 25 45 Silt 40 36 Clay 35 20 Composition: Quartz 32 40 Feldspar 12 15 Mica 4 3 Heavy minerals 5 5 Clay 23 15 Glaucinite 1 1 Pyrite 1 2 Carbonate unspec. 4 2 Foraminifera 1 1 Calc. nannofossils 2 8 Diatoms 2 2 Radiolarians 1 2 Sponge spicules 2 2 Plant debris 7 3 Lithic fragments 5 1
		B	AM B	RP	CC		

SITE 583		HOLE G		CORE 14		CORED INTERVAL 432.3–442.0 m	
TIME – ROCK UNIT	BIOSTRATIGRAPHIC ZONE	FOSSIL CHARACTER			SECTION METERS	GRAPHIC LITHOLOGY	LITHOLOGIC DESCRIPTION
		FORAMINIFERS	NANNOFOSSILS	RADIOLARIANS			
upper Quaternary	NN19				1		DRILL BRECCIA Argiata typhoon BESS
		B	FM	B	RP	CC	

SITE 583		HOLE G		CORE 15		CORED INTERVAL 442.0–450.0 m	
TIME – ROCK UNIT	BIOSTRATIGRAPHIC ZONE	FOSSIL CHARACTER			SECTION METERS	GRAPHIC LITHOLOGY	LITHOLOGIC DESCRIPTION
		FORAMINIFERS	NANNOFOSSILS	RADIOLARIANS			
Quaternary	N22/23				1		HEMIPELAGIC MUDSTONE 5G 4/1 to 58G 4/1 Dark gray Section 1: 49 cm, nanno-rich layer 50–58 cm strongly bioturbated, burrows show as faint black (these are not Chondrites) Section 3: graded sand, cycle probably extends upward to OG sample. Numerous gas bubbles, mica, black lithic fragments, pumice. Contains some barite?
		FM	RP	B	RP		

